

In compliance with the
Canadian Privacy Legislation
some supporting forms
may have been removed from
this dissertation.

While these forms may be included
in the document page count,
their removal does not represent
any loss of content from the dissertation.

UNIVERSITY OF ALBERTA

**Electrophysiological Characterization of Concentrative Nucleoside Transport
Proteins**

by

Kyla Michelle Smith



A thesis submitted to the Faculty of Graduate Studies and Research in partial fulfillment
of the requirements for the degree of Doctor of Philosophy

Department of Physiology

Edmonton, Alberta
Fall 2003



National Library
of Canada

Bibliothèque nationale
du Canada

Acquisitions and
Bibliographic Services

Acquisitons et
services bibliographiques

395 Wellington Street
Ottawa ON K1A 0N4
Canada

395, rue Wellington
Ottawa ON K1A 0N4
Canada

Your file *Votre référence*

ISBN: 0-612-88049-4

Our file *Notre référence*

ISBN: 0-612-88049-4

The author has granted a non-exclusive licence allowing the National Library of Canada to reproduce, loan, distribute or sell copies of this thesis in microform, paper or electronic formats.

L'auteur a accordé une licence non exclusive permettant à la Bibliothèque nationale du Canada de reproduire, prêter, distribuer ou vendre des copies de cette thèse sous la forme de microfiche/film, de reproduction sur papier ou sur format électronique.

The author retains ownership of the copyright in this thesis. Neither the thesis nor substantial extracts from it may be printed or otherwise reproduced without the author's permission.

L'auteur conserve la propriété du droit d'auteur qui protège cette thèse. Ni la thèse ni des extraits substantiels de celle-ci ne doivent être imprimés ou autrement reproduits sans son autorisation.

Canada

UNIVERSITY OF ALBERTA

LIBRARY RELEASE FORM

Name of Author: Kyla M. Smith

Title of Thesis: Electrophysiological Characterization of Concentrative Nucleoside Transport Proteins

Degree: Doctor of Philosophy

Year this Degree Granted: 2003

Permission is hereby granted to the University of Alberta Library to reproduce single copies of this thesis and to lend or sell such copies for private, scholarly or scientific research purposes only.

The author reserves all other publication and other rights in association with the copyright in the thesis, and except as herein before provided, neither the thesis nor any substantial portion thereof may be printed or otherwise reproduced in any material form whatever without the author's prior written permission.

August 19, 2003

UNIVERSITY OF ALBERTA

FACULTY OF GRADUATE STUDIES AND RESEARCH

The undersigned certify that they have read, and recommend to the Faculty of Graduate Studies and Research for acceptance, a thesis entitled Electrophysiological Characterization of Concentrative Nucleoside Transport Proteins submitted by Kyla M. Smith in partial fulfillment of the requirements for the degree of Doctor of Philosophy.

Dr. James B. Young (supervisor)

Dr. Edward Karpinski (supervisor)

Dr. Xing-Zhen Chen

Dr. Marek Duszyk

Dr. Carol E. Cass

Dr. Wendy Gati

Dr. Wayne Giles (external examiner)

June 2, 2003

ABSTRACT

CNT proteins mediate active transport of nucleosides across cell membranes by coupling the uptake of nucleosides to the movement of Na^+ down its electrochemical gradient. Human CNT1 (hCNT1) and human CNT2 (hCNT2) are selective for pyrimidine nucleosides (system *cit*) and purine nucleosides (system *cif*), respectively. The CNT3 proteins from human (hCNT3) and mouse (mCNT3) are broadly selective for both pyrimidine and purine nucleosides (system *cib*). In addition to mammals and other vertebrates, the CNT family has members in insects, nematodes, yeast, and bacteria. Recombinant hCNT1, hCNT3, and mCNT3 were produced in *Xenopus laevis* oocytes and functionally characterized using the two-microelectrode voltage clamp. This thesis describes: (i) electrogenic substrate transport by hCNT1, hCNT3, and mCNT3; (ii) steady-state kinetic properties of hCNT1, hCNT3, and mCNT3; and (iii) presteady-state currents of hCNT3.

Transport of nucleosides and nucleoside drugs by hCNT1, hCNT3, and mCNT3 was electrogenic, the magnitude of the inward current being dependent on the concentrations of extracellular nucleosides and Na^+ , and on the membrane potential. The steady-state kinetic data for hCNT1 were consistent with a sequential ordered binding mechanism in which Na^+ binds to the transporter first followed by the nucleoside. The Na^+ /nucleoside coupling ratio of hCNT1 was 1:1 and independent of membrane potential. hCNT3 and mCNT3 mediated Na^+ -dependent (and H^+ - and Li^+ -dependent) transport of both pyrimidine and purine nucleosides. In contrast to hCNT1, the Na^+ /nucleoside coupling

ratio of hCNT3 and mCNT3 was 2:1 at hyperpolarized potentials. The H⁺/nucleoside coupling ratio was 2:1 determined from H⁺ activation experiments and 1:1 from charge/flux measurements. In the absence of uridine, step changes in membrane potential induced presteady-state or transient currents in oocytes producing hCNT3. hCNT3 charge movements were described by the Boltzmann equation and were due both to movement of the empty carrier within the membrane as well as Na⁺ binding/dissociation. An hCNT3 turnover rate of $\sim 9.7 \text{ sec}^{-1}$ was determined. Transporter numbers of $\sim 10^{10}$ per oocyte were estimated from the maximal charge movements. The steady-state and presteady-state electrophysiological studies represent important steps in the development of in depth kinetic models for CNT-mediated Na⁺/nucleoside cotransport and provide the basis for future structure/function experiments.

ACKNOWLEDGEMENTS

There are a number of people whose assistance made this thesis possible. I am indebted to my supervisors Dr. James Young and Dr. Edward Karpinski for their encouragement and direction throughout this project. Dr. Young gave me guidance, and both the opportunity and freedom to perform my research in the field of electrophysiology; for these things, I am extremely grateful. I express my deepest gratitude to Dr. Karpinski for his expertise in teaching me oocyte electrophysiology, for spending countless hours analyzing data, and for his friendship. I wish to thank Dr. Sylvia Yao, Amy Ng, and Mabel Ritzel for their support and valued advice in response to my questions. More specifically, I thank Dr. Yao for teaching me about *Xenopus* oocytes, and Amy Ng and Mabel Ritzel for training me in, and sharing their extensive knowledge of, molecular biology. I am grateful to Dr. Shaun Loewen for his collaboration over the years, and for all of our discussions with regard to CNT3. I express my great appreciation to our summer student, Kathy Labeledz, for all her electrophysiology work, and for her assistance in analyzing data.

I am most grateful to Dr. Carol Cass, Dr. Marek Duszyk and Dr. Xing-Zhen Chen and the members of their laboratories for their support and advice during my research. I especially thank Dr. Chen for his input in interpreting my results, and for providing ideas for further experimentation. I am grateful to Dr. Wendi Gati for agreeing to become a late addition to my examination committee. I also thank the National Cancer Institute of Canada (NCIC) and the Alberta Cancer Board (ACB), whose funding supported my research. Last, but not least, I would like to thank my family and friends for their love and continuing support.

TABLE OF CONTENTS

	<i>Page</i>
Chapter I: General Introduction	1
Preamble.....	2
Nucleoside Transport-an Overview.....	3
Mammalian Equilibrative Nucleoside Transporters (ENTs).....	4
Characteristics of Mammalian Equilibrative Nucleoside Transport Processes.....	4
Functional and Molecular Properties of Cloned Mammalian ENTs.....	6
ENT1.....	6
ENT2.....	8
ENT3.....	9
ENT4.....	10
ENT Family Members in Other Eukaryotes.....	11
Parasitic Protozoa.....	11
<i>Toxoplasma gondii</i> TgAT.....	11
<i>Plasmodium falciparum</i> PfENT1.....	12
<i>Leishmania donovani</i> LdNT1.1 and LdNT1.2.....	13
<i>Leishmania donovani</i> LdNT2.....	13
<i>Trypanosoma brucei brucei</i> TbNT2-9.....	14
<i>Trypanosoma brucei brucei</i> TbAT1.....	15
Yeast.....	16
<i>Saccharomyces cerevisiae</i> FUN26.....	16
Nematodes.....	17
<i>Caenorhabditis elegans</i> CeENT1.....	17
Plants.....	17
<i>Arabidopsis thaliana</i> AtENT1.....	17
Mammalian Concentrative Nucleoside Transporters (CNTs).....	18
Characteristics of Mammalian Concentrative Nucleoside Transport Processes.....	18

Functional and Molecular Properties of Cloned Mammalian CNTs.....	19
CNT1.....	19
CNT2.....	21
CNT3.....	22
CNT Family Members in Prokaryotes and Other Eukaryotes.....	23
<i>Eptatretus stouti</i> CNT (hfCNT).....	23
<i>Caenorhabditis elegans</i> CNT3 (CeCNT3).....	24
<i>Candida albicans</i> CNT (CaCNT).....	25
<i>Escherichia coli</i> NupC.....	25
Other Nucleoside Transport Processes.....	26
Bacteria.....	26
Nucleoside/H ⁺ Symporter (NHS) Family.....	26
Tsx Channel-Forming Protein Family.....	27
Yeast.....	28
FUI1 of the Uracil/Allantoin Permease Family.....	28
Nucleoside Permease (NUP) Family.....	29
Mammals.....	29
Organic Cation Transporter (OCT) Family.....	29
Organic Anion Transporter (OAT) Family.....	30
Electrophysiological Studies of Transport Proteins.....	31
Electrophysiological Techniques.....	32
Two-microelectrode voltage clamp technique.....	32
Cut-open oocyte technique.....	33
Macropatch.....	33
Patch-clamp.....	34
Electrophysiology of defined transporters	35
Na ⁺ /glucose cotransporter (SGLT1).....	35
A. Steady-state currents.....	36
B. Presteady-state currents.....	37
C. Stoichiometric ratio of the Na ⁺ /glucose cotransporter.....	40

Research Objectives.....	42
Bibliography.....	59
Chapter II: Electrophysiological Characterization of a Human Na⁺-coupled Nucleoside Transporter (hCNT1) Produced in <i>Xenopus laevis</i> Oocytes.....	81
Introduction.....	82
Materials and Methods.....	85
<i>In vitro</i> Transcription and Transporter Expression in <i>Xenopus</i> Oocytes.....	85
Electrophysiological Studies.....	85
Radioisotope Flux Studies.....	87
Cation/Nucleoside Coupling Ratios.....	87
Chemicals.....	88
Results.....	89
Na ⁺ -dependence.....	89
Voltage-Dependence of Transporter Currents.....	89
Cation Specificity.....	89
Substrate Specificity.....	90
Na ⁺ - and Uridine-Steady-State Kinetics and the Order of Substrate Binding.....	92
Phloridzin Inhibition of hCNT1 Currents.....	93
Cation/Nucleoside Coupling Ratios.....	95
Discussion.....	96
Bibliography.....	120
Chapter III: Electrophysiological Characterization of Novel Human and Mouse Concentrative Na⁺-Nucleoside Cotransporter Proteins (hCNT3 and mCNT3) Broadly Selective for Purine and Pyrimidine Nucleosides (System <i>cib</i>).....	126
Introduction.....	127
Materials and Methods.....	130
Expression of Recombinant hCNT3 and mCNT3 in <i>Xenopus</i> Oocytes.....	130
Electrophysiological Studies.....	130

Hill Analysis.....	131
hCNT3 Radioisotope Flux Studies.....	131
Cation/Nucleoside Coupling Ratios.....	132
Chemicals.....	132
Results.....	133
Substrate Selectivity and Na ⁺ -dependence of Recombinant hCNT3 and mCNT3.....	133
Voltage-dependence of hCNT3 and mCNT3 Transport Currents.....	133
pH- and Lithium-dependence of Recombinant hCNT3 and mCNT3.....	134
hCNT3- and mCNT3-mediated Transport of Anticancer and Antiviral Drugs.....	135
Na ⁺ Activation Kinetics and Na ⁺ /nucleoside Coupling Ratio.....	136
H ⁺ Activation Kinetics and H ⁺ /nucleoside Coupling Ratio.....	137
Coupling Ratio of hCNT3 Determined in the Presence of both Na ⁺ and H ⁺	137
Discussion.....	138
Bibliography.....	167

Chapter IV: Presteady-state Currents of the Human Concentrative Na⁺-Nucleoside Cotransporter hCNT3..... 171

Introduction.....	172
Materials and Methods.....	174
Production of Recombinant hCNT3 in <i>Xenopus</i> Oocytes.....	174
Electrophysiological Studies.....	174
Data Analysis.....	175
Results.....	177
Presteady-state Currents of hCNT3.....	177
ON/OFF Current Responses.....	177
Effect of Na ⁺ on Presteady-state Currents.....	177
ON/OFF Charge Movement.....	179
Uridine Reversal of Presteady-state Currents.....	179
Effect of V _h on Presteady-state Currents.....	179

Presteady-state Currents in the Absence of Na ⁺	179
Turnover Rate and Number of Transporters.....	180
Kinetics of Presteady-state Currents.....	181
Effect of Na ⁺ on the Kinetics of the Presteady-state Currents.....	182
Discussion.....	183
Bibliography.....	206
Chapter V: General Discussion.....	211
Order of Substrate Binding	213
System- <i>cib</i> is a Member of the CNT Family.....	214
Novel Proton- and Lithium-coupled Nucleoside Transport Characteristics...	214
Cation/nucleoside Coupling Ratio.....	215
Nucleoside Drug Transport.....	216
Presteady-state Currents of hCNT3.....	216
Kinetic Interpretation of τ_{slow} and τ_{fast}	217
Turnover Rate (Turnover Number).....	218
Limitations of Electrophysiological Studies of hCNT1/3 in <i>Xenopus</i> Oocytes.....	219
Bibliography.....	222
Appendix A: Gemcitabine transport in <i>Xenopus</i> oocytes expressing recombinant plasma membrane mammalian nucleoside transporters. <i>J Natl Cancer Inst</i> 91(21): 1876-1881, 1999.	226
Appendix B: Molecular identification and characterization of novel human and mouse concentrative Na⁺-nucleoside cotransporter proteins (hCNT3 and mCNT3) broadly selective for purine and pyrimidine nucleosides (System <i>cib</i>). <i>J Biol Chem</i> 276(4): 2914-2927, 2001.	233

LIST OF TABLES

	<i>Page</i>
Table 1-1 Members of the Equilibrative Nucleoside Transporter (ENT) Family.	43
Table 1-2 Concentrative Nucleoside Transport Processes of Mammalian Cells.	45
Table 1-3 Members of the Concentrative Nucleoside Transporter (CNT) Family.	46
Table 1-4 Members of the Nucleoside/H ⁺ Symporter (NHS) Family.	48
Table 1-5 Members of the Tsx Channel-Forming Protein Family.	49
Table 1-6 Members of the Uracil/Allantoin Permease Family.	50
Table 1-7 Members of the Nucleoside Permease (NUP) Family.	51
Table 1-8 Members of the Organic Cation Transporter (OCT) Family.	52
Table 1-9 Members of the Organic Anion Transporter (OAT) Family.	53
Table 2-1 hCNT1 Uridine Kinetic Parameters.	104
Table 2-2 hCNT1 Na ⁺ Kinetic Parameters.	105
Table 4-1 Numbers of Recombinant hCNT3 Transporters Present in the Oocyte Plasma Membrane.	189

LIST OF FIGURES

	<i>Page</i>
Figure 1-1 Inhibitors of some ENT-mediated transport processes.	54
Figure 1-2 Chemical structures of physiological nucleosides.	55
Figure 1-3 Topographical model of hENT1.	56
Figure 1-4 Topographical model of rCNT1.	57
Figure 1-5 Na ⁺ /glucose cotransport by SGLT1.	58
Figure 2-1 Na ⁺ -dependence of hCNT1-mediated uridine transport.	106
Figure 2-2 hCNT1 steady-state current/voltage relationship.	107
Figure 2-3 Cation specificity of hCNT1.	108
Figure 2-4 Nucleoside specificity of hCNT1.	109
Figure 2-5 hCNT1 competition studies.	110
Figure 2-6 Transport of AZT.	111
Figure 2-7 Transport of gemcitabine.	113
Figure 2-8 Transport of nucleoside mimics.	114
Figure 2-9 Steady-state hCNT1 kinetics and the order of solute binding.	115
Figure 2-10 Inhibition of hCNT1-mediated Na ⁺ currents by phloridzin.	117
Figure 2-11 Effect of phloridzin on hCNT1 steady-state kinetic parameters.	118
Figure 2-12 Stoichiometry of hCNT1.	119
Figure 3-1 Substrate selectivity and Na ⁺ -dependence of hCNT3 produced in <i>Xenopus</i> oocytes.	147
Figure 3-2 Substrate selectivity and Na ⁺ -dependence of mCNT3 produced in <i>Xenopus</i> oocytes.	148
Figure 3-3 Voltage-dependence of hCNT3- and mCNT3-mediated currents.	149

Figure 3-4	pH-dependence of uridine transport by recombinant mCNT3.	150
Figure 3-5	pH-dependence of uridine transport by recombinant hCNT3.	151
Figure 3-6	pH-dependence of thymidine and inosine transport by recombinant mCNT3.	152
Figure 3-7	Effect of pH on uridine-evoked currents in Na ⁺ -containing medium.	154
Figure 3-8	Cation/nucleoside currents.	155
Figure 3-9	AZT-induced currents in an mCNT3-producing <i>Xenopus</i> oocyte.	156
Figure 3-10	ddC-induced currents in an mCNT3-producing <i>Xenopus</i> oocyte.	157
Figure 3-11	Nucleoside drug-induced currents in an hCNT3-producing <i>Xenopus</i> oocyte.	158
Figure 3-12	Na ⁺ - and H ⁺ -dependence of radiolabeled ddC and uridine uptake in <i>Xenopus</i> oocytes producing recombinant hCNT3.	159
Figure 3-13	Na ⁺ activation of mCNT3-mediated currents.	160
Figure 3-14	Stoichiometry of Na ⁺ /uridine cotransport by recombinant hCNT3.	161
Figure 3-15	H ⁺ activation of hCNT3-mediated nucleoside transport.	162
Figure 3-16	Stoichiometry of H ⁺ /uridine cotransport by recombinant hCNT3.	163
Figure 3-17	Stoichiometry of Na ⁺ /uridine cotransport by recombinant hCNT3 at pH 5.5.	164
Figure 3-18	Proposed transport model for hCNT3 Na ⁺ /nucleoside cotransport.	165
Figure 3-19	hCNT3 total currents in the presence of external Na ⁺ .	166
Figure 4-1	Time course of current and voltage records.	190
Figure 4-2	Time constants of <i>Xenopus</i> oocyte capacitive transients.	191

Figure 4-3	hCNT3 presteady-state curve fits.	192
Figure 4-4	hCNT3 presteady-state currents elicited by voltage pulses.	193
Figure 4-5	hCNT3 ON and OFF current relaxations.	194
Figure 4-6	Dependence of hCNT3 presteady-state currents on external Na ⁺ .	195
Figure 4-7	Relationship between hCNT3 ON and OFF charge movements.	196
Figure 4-8	Effect of uridine on hCNT3 presteady-state currents.	197
Figure 4-9	Effect of holding potential on hCNT3 charge movements.	198
Figure 4-10	Charge movement of the hCNT3 empty carrier.	199
Figure 4-11	Analysis of hCNT3 charge movements due to the empty carrier.	200
Figure 4-12	Turnover rate of recombinant hCNT3.	201
Figure 4-13	Kinetics of hCNT3 current relaxations.	202
Figure 4-14	hCNT3 time constants for the OFF response.	203
Figure 4-15	Na ⁺ -dependence of hCNT3 current relaxation kinetics.	204
Figure 4-16	Proposed transport model for hCNT3 Na ⁺ /nucleoside cotransport.	205
Figure 5-1	Three-state kinetic model for hCNT3 in the absence of substrates.	221

LIST OF ABBREVIATIONS, SYMBOLS, AND NOMENCLATURE

A	Ampere; unit of electrical current
ACV	acyclovir
AtENT1	<i>Arabidopsis thaliana</i> equilibrative nucleoside transporter 1
AZT	3'-azido-3'-deoxythymidine, zidovudine
BLAST	<u>B</u> asic <u>L</u> ocal <u>A</u> lignment <u>S</u> earch <u>T</u> ool; method for searching nucleotide and protein databases
C	Coulomb; the meter-kilogram-second unit of electrical charge equal to the quantity of charge transferred in one second by a steady current of one ampere
<i>C.albicans</i>	<i>Candida albicans</i>
cDNA	complementary DNA
<i>C. elegans</i>	<i>Caenorhabditis elegans</i>
CeENT	<i>Caenorhabditis elegans</i> equilibrative nucleoside transporter (ENT)
ChCl	choline chloride
<i>cib</i>	<u>c</u> oncentrative, <u>i</u> nsensitive to NBMPR inhibition, <u>b</u> roadly selective
<i>cif</i>	<u>c</u> oncentrative, <u>i</u> nsensitive to NBMPR inhibition, <u>f</u> ormycin B is a permeant
<i>cit</i>	<u>c</u> oncentrative, <u>i</u> nsensitive to NBMPR inhibition, <u>t</u> hymidine is a permeant
cladribine	2'-chloro-2'-deoxyadenosine, CdA
CNT	concentrative nucleoside transporter
CNT1	CNT selective for pyrimidine nucleosides
CNT2	CNT selective for purine nucleosides
CNT3	CNT broadly selective for purine and pyrimidine nucleosides
cordycepin	3'-deoxyadenosine
<i>cs</i>	<u>c</u> oncentrative, <u>s</u> ensitive to NBMPR inhibition, transports adenosine analogs
<i>csg</i>	<u>c</u> oncentrative, <u>s</u> ensitive to NBMPR inhibition, transports guanosine
cytarabine	1- β -D-arabinofuranosyl cytosine, AraC
DAL4	member of the uracil/allantoin permease family; allantoin permease
ddC	2', 3'-dideoxycytidine, zalcitabine
ddI	2', 3'-dideoxyinosine, didanosine

DNA	deoxyribonucleic acid
<i>E. coli</i>	<i>Escherichia coli</i>
<i>ei</i>	<u>equilibrative insensitive</u> ; insensitive to inhibition by NBMPR
ENT	equilibrative nucleoside transporter
ENT1	refers to an <i>es</i> -type transporter, with broad permeant selectivity for purine and pyrimidine nucleosides, sensitive to NBMPR inhibition
ENT2	refers to an <i>ei</i> -type transporter, with broad permeant selectivity for purine and pyrimidine nucleosides, insensitive to NBMPR inhibition
ENT3	refers to a novel mammalian member of the ENT family with undetermined function
ENT4	refers to a novel mammalian member of the ENT family with undetermined function
<i>es</i>	<u>equilibrative sensitive</u> ; sensitive to inhibition by NBMPR
F	Faraday's constant, equivalent to 9.6494×10^4 coulombs/mol
fludarabine	9- β -D-arabinosyl-2-fluoroadenine, F-ara-A
FUI1	member of the uracil/allantoin permease family; transports uridine
FUN26	<i>Saccharomyces cerevisiae</i> ENT isoform
FUR4	member of the uracil/allantoin permease family; uracil permease
g	gram
G	giga; 10^9
GABA	γ -amino-butyric acid
GAT1	GABA transporter
GCV	ganciclovir
gemcitabine	2', 2'-difluorodeoxycytidine, dFdC
h	human
H ⁺	hydrogen
HE	designates the expression vector pGEM-HE
Hepes	N-[2-hydroxyethyl]piperazine-N'-[2-ethanesulfonic acid]; buffer with pH range 6.8 - 8.6
hf	hagfish
HIV	human immunodeficiency virus
Hz	unit of frequency equal to one cycle per second (sec^{-1})

I_{\max}	maximum current, in Amperes
I-V	current-voltage relationship
K_m	permeant concentration at half-maximal unidirectional flux; apparent affinity
l	litres
Li^+	lithium
<i>L. donovani</i>	<i>Leishmania donovani</i>
LdNT1.1/ LdNT1.2	nearly identical nucleoside transporters from <i>Leishmania donovani</i> whose substrate specificity has not been fully characterized
LdNT2	<i>Leishmania donovani</i> nucleoside transporter 2 (NT2) which prefers inosine and guanosine
m	milli; 10^{-3}
m	mouse
min	minute(s)
mm	millimeters
M	mega; 10^6
M	molar; mol/l
MES	(2-[N-morpholino]ethanesulfonic acid); buffer with pH range of 5.5 - 6.7
MBM	Modified Barth's Medium
n	nano; 10^{-9}
N	nucleoside
N	number of transporters
Na^+	sodium
NaCl	sodium chloride
NBMPR	nitrobenzylthioinosine
ND	not determined
NHS	nucleoside/ H^+ symporter family from bacteria
NT	nucleoside transporter
NUP	nucleoside permease family
NupC	H^+ /nucleoside transporter from <i>E. coli</i> ; transports purine and pyrimidine nucleosides, except guanosine; member of the CNT protein family

NupG	H ⁺ /nucleoside transporter from <i>E. coli</i> ; transports purine and pyrimidine nucleosides; member of the NHS protein family
OAT	organic anion transporter
OCT	organic cation transporter
OmpK	outer membrane protein of <i>Vibrio cholerae</i> , with unknown function
P1	high affinity equilibrative nucleoside transport system in <i>Trypanosoma brucei brucei</i> ; transports purine nucleosides
P2	high affinity equilibrative nucleoside transport system in <i>Trypanosoma brucei brucei</i> ; transports adenosine, adenine, melamino-phenylarsenicals
p	pico; 10 ⁻¹²
p	pig
PEPT1	H ⁺ -dependent oligopeptide cotransporter
PfENT1	<i>Plasmodium falciparum</i> equilibrative nucleoside transporter 1 (ENT1)
PfNT1	<i>Plasmodium falciparum</i> nucleoside transporter 1 (NT1); also known as PfENT1
<i>P. falciparum</i>	<i>Plasmodium falciparum</i>
pk	pig
Q	charge, in Coulombs
Q _{dep}	charge (Q) at the depolarizing limit, in coulombs
Q _{hyp}	charge (Q) at the hyperpolarizing limit, in coulombs
Q _{max}	maximal charge transferred, in coulombs
Q-V	charge-voltage relation
r	rat
R	ideal gas constant equivalent to 8.3143m ² kg/s ² Kmol
rb	rabbit
<i>S. cerevisiae</i>	<i>Saccharomyces cerevisiae</i>
SE	standard error of the fitted estimate
sec	second(s)
SGLT1	Na ⁺ -dependent glucose transporter 1

SEM	standard error of the mean
SNST1	Na ⁺ /nucleoside transporter 1; originally believed to be <i>cib</i> -type transporter, but is no longer considered a member of the CNT family
SPNT	Na ⁺ -dependent nucleoside transporter isolated from rat liver; also known as rCNT2
TbAT1	adenosine transporter from <i>Trypanosoma brucei brucei</i> displaying P2-type transporter characteristics
<i>T. b. brucei</i>	<i>Trypanosoma brucei brucei</i>
TbNT	<i>Trypanosoma brucei brucei</i> nucleoside/nucleobase transporter
TbNT2-9	<i>Trypanosoma brucei brucei</i> ENT isoforms
TgAT	<i>Toxoplasma gondii</i> adenosine-preferring transporter
<i>T. gondii</i>	<i>Toxoplasma gondii</i>
TM	transmembrane domain
TMs	transmembrane domains
Tsx	substrate-specific channel of <i>Escherichia coli</i> which transports nucleosides and deoxynucleosides across the outer membrane
T	absolute temperature
ν	number of fundamental charges translocated per molecule of uridine at the corresponding potential
V	Volts; unit of electric potential
V _h	holding potential, in millivolts (mV)
V _m	membrane potential
V _{max}	maximum transport rate
V _r	reversal potential, in millivolts (mV)
V _t	membrane voltage during pulse, in millivolts (mV)
V _{0.5}	membrane voltage at which half of the total charge has moved
XapB	H ⁺ /nucleoside transporter of bacteria; member of the NHS family of transporters
Z	apparent valence of moving charge
z _d	product of the valence of the charge and the apparent fraction of the field sensed by that charge
β-DFP-5I	1-(2-deoxy-β-D-ribofuranosyl)-2,4-difluoro-5-iodobenzene

β -DFP-5M	1-(2-deoxy- β -D-ribofuranosyl)-2,4-difluoro-5-methylbenzene
$^{\circ}\text{C}$	degrees Celsius
δ	effective fraction of membrane field sensed by the movable charge
e_0	elementary charge, 1.60228×10^{-19} coulombs
μ	micro; 10^{-6}
Ω	Ohm; unit of electrical resistance
τ	tau; time constant, in milliseconds (msec)
Φ	charge transfer rate; equal to the slope of the I_{\max} versus Q_{\max} graph $\times z_d$

PUBLICATIONS

Mackey JR, Yao SYM, Smith KM, Karpinski E, Baldwin SA, Cass CE, and Young JD. Gemcitabine transport in *Xenopus* oocytes expressing recombinant plasma membrane mammalian nucleoside transporters. *J Natl Cancer Inst* 91(21): 1876-1881, 1999.

Ritzel MW, Ng AM, Yao SY, Graham K, Loewen SK, Smith KM, Ritzel RG, Mowles DA, Carpenter P, Chen XZ, Karpinski E, Hyde RJ, Baldwin SA, Cass CE, and Young JD. Molecular identification and characterization of novel human and mouse concentrative Na⁺-nucleoside cotransporter proteins (hCNT3 and mCNT3) broadly selective for purine and pyrimidine nucleosides (system *cib*). *J Biol Chem* 276(4): 2914-2927, 2001.

Chapter I:

General Introduction

Preamble

The translocation of nucleosides and synthetic nucleoside analogs across the lipid bilayer of cell membranes is mediated by equilibrative and concentrative (Na^+ - and H^+ -dependent) transport mechanisms. In 1994, a cDNA encoding the first mammalian concentrative Na^+ /nucleoside cotransporter, designated rCNT1, was cloned from rat jejunum (Huang *et al.*, 1994), along with a cDNA encoding a related H^+ /nucleoside cotransporter (NupC) from *Escherichia coli* (Craig *et al.*, 1997). A second mammalian CNT homolog, rCNT2, was identified independently from rat liver and jejunum (Che *et al.*, 1995; Yao *et al.*, 1996b). Human orthologs of these Na^+ /nucleoside cotransporters, hCNT1 and hCNT2, were also identified (Ritzel *et al.*, 1997; Wang *et al.*, 1997; Ritzel *et al.*, 1998), along with the first equilibrative nucleoside transporters from rat (rENT1 and rENT2) and human (hENT1 and hENT2) tissues (Griffiths *et al.*, 1997a, b; Yao *et al.*, 1997; Crawford *et al.*, 1998).

The studies described in *Chapters II-IV* of this thesis were carried out between 1996 and 2003. The objective of this research was to functionally characterize mammalian members of the concentrative nucleoside transporter (CNT) family using electrophysiological techniques. Initial studies focused on the steady-state kinetic properties of hCNT1 and the results of these experiments are presented in *Chapter II*. As described in *Chapter III*, subsequent investigation of the steady-state kinetic properties of human (hCNT3) and mouse (mCNT3) representatives of a third recently discovered mammalian CNT isoform revealed unique cation-coupling and nucleoside-selectivity properties that functionally distinguish the CNT3 proteins from other members of the CNT family. The presteady-state currents of hCNT3, which provide information about transporter membrane abundance and partial reactions in the Na^+ /nucleoside cotransport cycle, were also investigated and are presented in *Chapter IV*.

The remainder of *Chapter I* describes current knowledge of the transporters mediating nucleoside transport in both prokaryotic and eukaryotic cells and their respective protein families. The final chapter of this thesis (*Chapter V*) is a general discussion of the results obtained using electrophysiological techniques and the direction of future research.

Nucleoside Transport - an Overview

Nucleosides have a multitude of physiological effects. In mammalian cells, adenosine binds to cell-surface receptors and exerts potent effects on various physiological processes, such as regulation of cardiovascular activity, modulation of immune responses, platelet aggregation, renal function, neurotransmission, and neuromodulation in the central nervous system (Young and Jarvis, 1983; Cass, 1995; Griffiths and Jarvis, 1996; Jennings *et al.*, 1998; Baldwin *et al.*, 1999). Inosine is an *in vivo* energy source in adult pig erythrocytes which are unable to metabolize glucose through lack of a functional glucose transporter (Young, 1983; Young and Jarvis, 1983; Young *et al.*, 1985). Inosine and guanosine serve as energy sources for embryonic and adult chicken erythrocytes (Griffiths and Jarvis, 1996). In bacteria, nucleosides are essential for replication (Kubitscek, 1968). Protozoan parasites and some mammalian cell types, such as bone marrow cells, enterocytes, and certain brain cells, lack *de novo* purine biosynthetic pathways and must therefore rely on salvage pathways for the synthesis of nucleic acid precursors (Griffiths and Jarvis, 1996; de Koning *et al.*, 1998; Baldwin *et al.*, 1999; Sanchez *et al.*, 1999). Since nucleosides are relatively hydrophilic molecules, their translocation across the lipid bilayer of biological membranes depends on specialized nucleoside transporter proteins. These transporters regulate physiological processes through their effects on the levels of free nucleosides. For example, nucleoside transporters determine the duration of interaction of adenosine with purinoceptors by affecting the concentration of adenosine in the immediate vicinity of the receptor (Cass, 1995; Jennings *et al.*, 1998; Baldwin *et al.*, 1999). In addition, the ability of nucleoside transporters to transport nucleoside analogue drugs used in the treatment of cancer and viral diseases is an important determinant of the therapeutic effectiveness of these drugs (Mackey *et al.*, 1998a; Baldwin *et al.*, 1999).

A diverse array of kinetically distinct nucleoside transport processes have been identified in prokaryotic and eukaryotic cells. Mammalian cells, for example, possess both concentrative, Na⁺-dependent and equilibrative, Na⁺-independent nucleoside transport systems (Cass, 1995; Griffiths and Jarvis, 1996; Baldwin *et al.*, 1999). The

former are inwardly directed Na^+ /nucleoside symporters capable of transporting nucleosides against their concentration gradient through coupled movement of Na^+ down its electrochemical gradient, while the latter mediate the bi-directional transport of nucleosides depending only on the concentration gradient of the transported nucleoside. Molecular cloning and functional expression of cDNAs has led to the identification of the nucleoside transporter proteins responsible for these and other nucleoside transport processes in humans and lower organisms. The proteins responsible for these processes belong to one of eight integral membrane protein families: the equilibrative nucleoside transporter (ENT) family, the concentrative nucleoside transporter (CNT) family, the nucleoside/ H^+ symporter (NHS) family, the Tsx channel-forming protein family, the uracil/allantoin permease family, the nucleoside permease (NUP) family, the organic cation transporter (OCT) family, and the organic anion transporter (OAT) family. Four of these (ENT, CNT, OCT and OAT) have representatives that transport nucleosides in mammalian cells, while the others (NHS, Tsx, uracil/allantoin permease family and NUP) appear to be limited to prokaryotes and/or lower eukaryotes. In some instances, not all members of the protein family transport nucleosides or function primarily as nucleoside transport proteins. For example, only OCT1 from the OCT family, which primarily mediates the uptake of various cations in epithelial tissues, is able to transport nucleosides and nucleoside analogs (Chen and Nelson, 2000; Hayer-Zilligen *et al.*, 2002; Takeda *et al.*, 2002). Similarly, OAT proteins function primarily as organic anion transporters (Sekine *et al.*, 2000; Wada *et al.*, 2000). Some ENTs also transport nucleobases (Parker *et al.*, 2000; Sanchez *et al.*, 2002; Yao *et al.*, 2002b). The following sections present an extensive review of the current nucleoside transport literature.

Mammalian Equilibrative Nucleoside Transporters (ENTs)

Characteristics of Mammalian Equilibrative Nucleoside Transport Processes -

Equilibrative nucleoside transport systems were the first mammalian nucleoside transport mechanisms to be studied. Characterized initially in erythrocytes, these equilibrative nucleoside transport systems exhibit the classic features of facilitated

diffusion; they are driven by the concentration gradient of the transported nucleoside and mediate bi-directional permeant fluxes across the cell membrane (Young and Jarvis, 1983; Plagemann *et al.*, 1990; Cass *et al.*, 1995; Griffiths and Jarvis, 1996; Cass *et al.*, 1998; Mackey *et al.*, 1998a; Baldwin *et al.*, 1999; Vickers *et al.*, 2000b; Young *et al.*, 2001, 2003). Two functional subtypes of equilibrative transporters have been identified based on their differential sensitivities to inhibition by the S⁶-substituted 6-thio-purine nucleoside derivative nitrobenzylthioinosine (NBMPR) (Fig. 1-1) (Young and Jarvis, 1983; Plagemann *et al.*, 1990; Cass *et al.*, 1995; Griffiths and Jarvis, 1996). Transport processes of the 'equilibrative sensitive' (*es*) subtype are inhibited by nanomolar concentrations of NBMPR, due to the high affinity binding of NBMPR at or near the permeant-binding site, whereas the 'equilibrative insensitive' (*ei*) subtype is unaffected by NBMPR, or is inhibited only by high (μM) concentrations. Equilibrative nucleoside transporters are widely distributed in different mammalian cells and tissues and exhibit broad permeant selectivities for both purine and pyrimidine physiological nucleosides (Fig. 1-2) and synthetic nucleoside analogs (Young and Jarvis, 1983; Plagemann *et al.*, 1990; Cass *et al.*, 1995; Griffiths and Jarvis, 1996; Cass *et al.*, 1998; Mackey *et al.*, 1998a; Baldwin *et al.*, 1999; Vickers *et al.*, 2000b; Young *et al.*, 2001, 2003).

In most mammals, *es* and *ei* transport processes are inhibited by the coronary vasodilators dipyridamole, dilazep, and draflazine (Fig. 1-1), with *es* transporters generally exhibiting greater susceptibility to inhibition than *ei* transporters from the same species (Young and Jarvis, 1983; Plagemann *et al.*, 1990; Cass *et al.*, 1995; Griffiths and Jarvis, 1996; Cass *et al.*, 1998; Mackey *et al.*, 1998a; Baldwin *et al.*, 1999; Vickers *et al.*, 2000b; Young *et al.*, 2001, 2003). There are, however, significant species differences in sensitivity of transporters to these compounds. For example, the human *es* transporter is inhibited by dipyridamole and draflazine with apparent K_i values in the nanomolar range, while rat *es* transporters require concentrations in excess of 1 μM to inhibit transport activity (Yao *et al.*, 1997; Hammond, 1991, 2000). Sensitivity of the mouse *es* transporter to inhibition by dipyridamole is intermediate between that of the human and rat *es* (Hammond, 1991, 2000).

Photoaffinity labeling experiments with NBMPR have identified the prototypic *es* transporter from human erythrocytes as a band 4.5 polypeptide (Wu *et al.*, 1983). The protein was subsequently separated from the more abundant band 4.5 erythrocyte glucose transporter by immunoaffinity chromatography on a column of immobilized glucose transporter antibodies, and its identity as an equilibrative NBMPR-sensitive nucleoside transporter confirmed by functional reconstitution of the purified protein into phospholipid vesicles (Kwong *et al.*, 1988).

Functional and Molecular Properties of Cloned Mammalian ENTs -

Members of the equilibrative nucleoside transporter (ENT) protein family are widely distributed in eukaryotes, including mammals, protozoa, yeast, nematodes, insects, and plants. A current list of identified ENTs from mammalian cells and other eukaryotes is provided in Table 1-1. These include cloned nucleoside/nucleobase transporters that have been characterized functionally as recombinant proteins in *Xenopus* oocytes or other heterologous expression systems, as well as putative transporters identified only by homology searches of complete and unfinished eukaryote sequence databases. Interestingly, searches of bacterial genome databases have failed to identify ENT homologs in prokaryotes. To date, four mammalian ENT isoforms have been identified.

ENT1 - A cDNA encoding the human equilibrative (*es*) nucleoside transporter (hENT1) was isolated from a placental cDNA library based on information derived from analysis of the N-terminal sequence of the purified human erythrocyte nucleoside transport protein (Griffiths *et al.*, 1997a). hENT1 was the first mammalian member of the ENT protein family to be identified (Griffiths *et al.*, 1997a; Cass *et al.*, 1998; Baldwin *et al.*, 1999; Hyde *et al.*, 2001). The isolated cDNA encoded a 456 amino acid protein with 11 potential transmembrane domains (TMs), containing a cytoplasmic N-terminus and extracellular C-terminus (Fig. 1-3) (Griffiths *et al.*, 1997a; Sundaram *et al.*, 2001b). Transmembrane domains are linked by short hydrophilic regions, except for a large glycosylated extracellular loop between transmembrane helices 1 and 2 and a large central cytoplasmic loop between transmembrane helices 6 and 7 (Griffiths *et al.*, 1997a). The predicted topology of hENT1 and the location of a single site of glycosylation

between TMs 1 and 2 have been confirmed by glycosylation scanning mutagenesis (Sundaram *et al.*, 2001b). When produced in *Xenopus* oocytes, hENT1 demonstrated broad substrate selectivity for purine and pyrimidine nucleosides, but was unable to transport nucleobases, and was sensitive to inhibition by NBMPR and the cardioprotective agents dipyridamole, dilazep, and draflazine (Griffiths *et al.*, 1997a, b; Yao *et al.*, 2002b). Transport of uridine was Na⁺-independent, saturable, and conformed to Michaelis-Menten kinetics with an apparent affinity, or K_m value, of 0.24 mM (Griffiths *et al.*, 1997a). In addition to physiological nucleosides, hENT1 also mediates the cellular uptake of nucleoside analogues used in cancer chemotherapy, including cladribine (2-chloro-2'-deoxyadenosine, CdA), cytarabine (1- β -D-arabinofuranosyl cytosine, AraC), fludarabine (9- β -D-arabinosyl-2-fluoroadenine, F-ara-A), and gemcitabine (2', 2'-difluorodeoxycytidine, dFdC) (Griffiths *et al.*, 1997a; Mackey *et al.*, 1998b, 1999). hENT1 does not transport the antiviral nucleoside drug AZT (3'-azido-3'-deoxythymidine, zidovudine), and only weakly transports the antiviral drugs ddC (2', 3'-dideoxycytidine, zalcitabine) and ddI (2', 3'-dideoxyinosine, didanosine), suggesting that the absence of the ribose 3'-hydroxyl group greatly reduces the ability of these compounds to be transported by hENT1 (Mackey *et al.*, 1998b, 1999; Hyde *et al.*, 2001; Yao *et al.*, 2001a). At the time it was cloned, hENT1 showed no significant sequence similarity to other known transport proteins, including members of the CNT/NupC gene family (Griffiths *et al.*, 1997a). Orthologs of hENT1 from rat (r) and mouse (m), designated rENT1 and mENT1, respectively, have been subsequently cloned and functionally characterized (Yao *et al.*, 1997; Kiss *et al.*, 2000). The rat homolog, rENT1 (457 residues), was isolated from a rat jejunal cDNA library and is 78 % identical to hENT1 in amino acid sequence (Yao *et al.*, 1997). mENT1 (458 residues) was isolated from mouse brain and is 78 % identical in amino acid sequence to hENT1 (Kiss *et al.*, 2000). Although hENT1, rENT1, and mENT1 have similar kinetic properties with respect to nucleoside transport, they exhibit distinctive species differences with respect to inhibition by dipyridamole, dilazep, and draflazine. Transport mediated by hENT1 is potently inhibited by these vasodilator drugs, while rENT1 is relatively insensitive to inhibition, and inhibition of mENT2 transport activity is intermediate between hENT1

and rENT1 (Griffiths *et al.*, 1997a, b; Hammond, 2000; Kiss *et al.*, 2000). These results agree with earlier studies with rat erythrocytes which demonstrated high sensitivity to NBMPR inhibition but resistance to inhibition by vasodilator drugs (Jarvis and Young, 1986). Chimeras constructed between the vasoactive drug-sensitive transporter hENT1 and its drug-resistant rat counterpart rENT1 revealed that the binding domain for vasodilator drugs, which compete with permeant for the substrate-binding site at the extracellular surface, lie in the TM 3 - 6 region of the transporter (Sundaram *et al.*, 1998). Random mutagenesis studies of recombinant hENT1 produced in yeast have also implicated TM1 (residue 33) in dipyridamole/dilazep binding (Visser *et al.*, 2002). ENT1 transporters are broadly distributed among cells and tissues, with mRNA transcript having been identified in a variety of normal tissues, including fetal brain, liver, and spleen, and adult adipose tissue, aortic endothelial cells, brain, breast, colon, heart, lung, ovary, placenta, prostate, and uterus, as well as in malignant cells (Cass *et al.*, 1998).

ENT2 - Following the identification of hENT1, cDNAs encoding the human *ei*-type transporter were cloned. hENT2 was identified from a human placental cDNA library based on sequence information derived from human HNP36, a putative protein with sequence similarity to the N-terminal region of hENT1 and unknown function (Griffiths *et al.*, 1997b). The same cDNA was independently cloned from a HeLa cell cDNA library by functional complementation of nucleoside transport deficiency in a subline of CEM human leukemic cells (Crawford *et al.*, 1998). hENT2 (456 amino acid residues) is 46 % identical in amino acid sequence to hENT1 and has a similar predicted membrane topology of 11 TMs, with two potential N-linked glycosylation sites in the exofacial loop between TMs 1 and 2 (Griffiths *et al.*, 1997b). hENT2 displayed functional properties consistent with *ei*-type transport, being much less sensitive than hENT1 to inhibition by NBMPR, dipyridamole, dilazep, and draflazine (Griffiths *et al.*, 1997b; Crawford *et al.*, 1998). hENT2 mediates the Na⁺-independent transport of a broad range of purine and pyrimidine nucleosides; however, the apparent affinities for these substrates, with the exception of inosine, are significantly lower than for hENT1 (K_m values ~ 0.3 - 5 mM) (Griffiths *et al.*, 1997b; Crawford *et al.*, 1998; Ward *et al.*, 2000). hENT2 shows a greater ability to transport the antiviral nucleoside drugs AZT, ddC, and ddi than hENT1,

and is also able to mediate the uptake of nucleobases such as hypoxanthine, adenine, guanine, uracil, thymine, and cytosine (Yao *et al.*, 2001a, 2002b). Rat and mouse orthologs of hENT2, designated rENT2 and mENT2, respectively, have also been cloned and functionally characterized (Yao *et al.*, 1997; Kiss *et al.*, 2000). rENT2 (456 amino acid residues) was cloned from a rat jejunal cDNA library while mENT2 (456 amino acid residues) was cloned from mouse brain (Yao *et al.*, 1997; Kiss *et al.*, 2000). rENT2 and mENT2 are 89 and 88 % identical in amino acid sequence to hENT2, respectively, and ~ 50 % identical to rENT1/hENT1 (Yao *et al.*, 1997; Kiss *et al.*, 2000). Both rENT2 and mENT2 have functional properties similar to hENT2, including broad substrate selectivity and relative insensitivity to inhibition by NBMPR, dipyrindamole, dilazep, and draflazine (Yao *et al.*, 1997; Kiss *et al.*, 2000). Chimeric constructs between NBMPR-sensitive, nucleobase transport-negative rENT1 and NBMPR-insensitive, nucleobase transport-positive rENT2 identified TMs 3 - 6 and TMs 5 - 6 of rENT2 as the sites of ENT interaction with NBMPR and nucleobases, respectively (Sundaram *et al.*, 2001a; Yao *et al.*, 2002b). Studies with the thiol reagent *p*-chloromercuriphenyl sulphonate (PCMBs) have identified a substrate-protectable cysteine residue in the outer half of TM 4 of rENT2 (Cys¹⁴⁰) that lies within the translocation pore of the transporter (Yao *et al.*, 2001b). Investigations of ENT2 mRNA in rat and human tissues indicate that, like ENT1, ENT2 has a wide tissue distribution. Transcript was detected in brain, heart, placenta, thymus, pancreas, prostate, and kidney, and is particularly abundant in skeletal muscle (Griffiths *et al.*, 1997b; Crawford *et al.*, 1998). ENT1, with *es*-type transport function, and ENT2, with *ei*-type transport function, account for the two main equilibrative nucleoside transport activities of mammalian cells.

ENT3 - Subsequent to the molecular cloning of ENT1 and ENT2, database searching using the BLAST algorithm identified a third, novel mammalian member of the ENT family, ENT3. Two cDNA sequences that were homologous to, but differed from published ENT1 and ENT2 sequences, were identified from mouse and human (Hyde *et al.*, 2001). Full-length cDNA clones were obtained from mouse kidney and human placenta (Hyde *et al.*, 2001). The encoded proteins, termed mENT3 (mouse) and hENT3 (human), exhibited 30 - 33 % sequence identity to the mouse, rat, and human ENT1 and

ENT2 proteins (Hyde *et al.*, 2001). mENT3 (474 amino acid residues) and hENT3 (475 amino acid residues) share 73 % amino acid sequence identity (Hyde *et al.*, 2001). In addition to kidney and placenta, ENT3 is expressed in a wide variety of human and mouse tissues, including adult breast, colon, and testis, and fetal liver and spleen (Hyde *et al.*, 2001). The substrate selectivity and other transport properties of mammalian ENT3 proteins remains to be fully established, but initial studies of the recombinant proteins produced in *Xenopus* oocytes have demonstrated functional nucleoside and nucleobase transport activity (Baldwin SA, Beal P, Yao SYM, King AE, Cass CE, and Young JD, personal communication). The hydrophilic N-terminal region preceding TM 1 of mENT3 and hENT3 is longer than that of ENT1/ENT2 (Hyde *et al.*, 2001). This region possesses two pairs of adjacent leucine residues, of which the first leucine in each pair is preceded by acidic residues (Hyde *et al.*, 2001). Sequence motifs such as this resemble intracellular retention signals that mediate the sorting of other membrane proteins at the trans-Golgi network, endosomes and plasma membrane (Sandoval and Bakke, 1994). It is possible, therefore, that ENT3 is localized to an intracellular compartment rather than to the cell surface (Hyde *et al.*, 2001).

ENT4 - Very recently, a fourth mammalian ENT isoform has also been found. Human ENT4 (hENT4) is a 530 residue protein 86 % identical in sequence to its mouse homolog (mENT4). Originally identified by genome database analysis (Acimovic and Coe, 2002), hENT4 is more closely related to insect ENTs (28 - 30 % identity) than to hENT1 (18 % identity), indicating ancient divergence from other mammalian ENTs. Recombinant h/mENT4 proteins have been shown to possess adenosine transport activity when produced in *Xenopus* oocytes (Baldwin SA, Beal P, Yao SYM, King AE, Cass CE, and Young JD, personal communication). Similar to hENT1-3, hENT4 is likely to be ubiquitously expressed in human tissues (Baldwin SA, Beal P, Yao SYM, King AE, Cass CE, and Young JD, personal communication).

ENT Family Members in Other Eukaryotes

The availability of on-line genomic databases, combined with BLAST searching techniques, has led to the identification of ENT family members in other eukaryotes, including parasitic protozoa, yeast, nematodes, and plants.

Parasitic Protozoa -

Parasitic protozoa of the genera *Toxoplasma*, *Plasmodium*, *Leishmania*, and *Trypanosoma* lack the ability to synthesize purines *de novo*, and their growth and survival is therefore dependent upon the salvage of purine nucleosides and nucleobases from their hosts (Baldwin *et al.*, 1999). The first step in the salvage of purines involves permeation of the substrate across the parasite plasma membrane, through the actions of nucleoside and nucleobase transport processes (de Koning *et al.*, 1998; Baldwin *et al.*, 1999; Sanchez *et al.*, 1999). Studies in various parasitic protozoa have led recently to the molecular cloning and functional characterization of a number of parasite nucleoside/nucleobase transport proteins. Since parasitic protozoa are responsible for diseases such as sleeping sickness and leishmaniasis and are completely dependent upon purine salvage mechanisms for nucleotide biosynthesis, these transporters represent a potentially important new drug target in antiparasite pharmacology (Baldwin *et al.*, 1999).

***Toxoplasma gondii* TgAT** - A cDNA encoding a nucleoside transporter was identified in the parasitic protozoan *Toxoplasma gondii* using insertional mutagenesis of *T. gondii* genomic DNA and selection of mutants resistant to the cytotoxic adenosine analog adenosine arabinoside (Chiang *et al.*, 1999). This transporter, referred to as TgAT, is a 462 amino acid protein which exhibits 22 % amino acid identity to hENT1, 26 % identity to hENT2, and 25 % identity to the adenosine-pyrimidine nucleoside transporter LdNT1 from the protozoan parasite *Leishmania donovani* (Chiang *et al.*, 1999). Functional expression of TgAT cDNA in *Xenopus* oocytes established that TgAT mediates the Na⁺-independent transport of adenosine with a K_m of 114 μ M (Chiang *et al.*, 1999). Adenosine transport was inhibited by purine nucleosides, adenosine analogs, and the

purine bases hypoxanthine and guanine (Chiang *et al.*, 1999). Pyrimidine nucleosides did not affect TgAT-mediated adenosine transport (Chiang *et al.*, 1999). Transport was significantly inhibited by dipyridamole, but only marginally inhibited by NBMPR (Chiang *et al.*, 1999). TgAT is the sole transporter of adenosine in *T. gondii*, and disruption of the TgAT gene locus resulted in resistance to adenosine arabinoside and complete elimination of adenosine uptake (Chiang *et al.*, 1999).

***Plasmodium falciparum* PfENT1** - An equilibrative nucleoside transporter was independently identified and cloned from the protozoan parasite *Plasmodium falciparum* by two different groups using sequence information obtained from the Malaria Genome Sequencing Project (Carter *et al.*, 2000b; Parker *et al.*, 2000; Enserink and Pennisi, 2002). The cDNAs encode almost identical 422 amino acid residue proteins termed PfENT1 (Parker *et al.*, 2000) and PfNT1 (Carter *et al.*, 2000b) which mediate the Na⁺-independent transport of a broad range of purine and pyrimidine nucleosides (Carter *et al.*, 2000b; Parker *et al.*, 2000). The *Plasmodium* transporters are 36 and 31 % identical in amino acid sequence to the human equilibrative transporters hENT1 and hENT2, respectively (Vickers *et al.*, 2000b). Functional expression studies in *Xenopus* oocytes by Carter *et al.* (2000b) and Parker *et al.* (2000) found apparent differences between PfENT1 and PfNT1 in their relative affinities for adenosine (apparent K_m values of 320 and 13 μ M, respectively), the ability to transport nucleobases (only Parker *et al.* (2000) detected transport of the nucleobases adenine and hypoxanthine), and sensitivity to inhibition by NBMPR and dipyridamole (Parker *et al.* (2000) reported no inhibition of transport by NBMPR and dipyridamole even at concentrations of 10 μ M, while Carter *et al.* (2000b) described significant inhibition of transport (85 %) by 10 μ M dipyridamole). PfENT1 resembled the mammalian ENT transporters in its ability to transport the anticancer drugs fludarabine, cladribine, and gemcitabine (Parker *et al.*, 2000). In contrast to the mammalian transporters, however, PfENT1 efficiently transported the antiviral nucleoside analogs AZT, ddC, and ddI (Parker *et al.*, 2000). Western blot analysis of parasite lysates using polyclonal antibodies specific for PfENT1 demonstrated that the transporter is localized to the parasite plasma membrane (Rager *et al.*, 2001). Searches of the unfinished sequence data available from the Malaria Genome Sequencing Project

suggest that PfENT1 is the only route by which nucleosides and nucleobases cross the *P. falciparum* plasma membrane (Parker *et al.*, 2000; Enserink and Pennisi, 2002).

***Leishmania donovani* LdNT1.1 and LdNT1.2** - Two nearly identical nucleoside transporters, LdNT1.1 and LdNT1.2, were cloned by functional rescue of a mutant *Leishmania donovani* cell line (Vasudevan *et al.*, 1998). This adenosine/pyrimidine nucleoside transport-deficient cell line was transfected with a cosmid library containing inserts of *L. donovani* genomic DNA and screened for restoration of tubercidin sensitivity, a cytotoxic analog of adenosine (Vasudevan *et al.*, 1998). Both LdNT1.1 and LdNT1.2 contain 491 amino acids and are nearly identical in amino acid sequence (99.5 %), differing only at six amino acid positions (Vasudevan *et al.*, 1998). They are encoded by two tandemly linked genes (Vasudevan *et al.*, 1998). LdNT1.1 and LdNT1.2 are approximately 33 % identical in sequence to hENT1 (Vasudevan *et al.*, 1998). Apparent K_m values of 0.17 μM (adenosine) and 5.6 μM (uridine) for LdNT1.1 and 0.66 μM (adenosine) and 40 μM (uridine) for LdNT1.2 were reported when the recombinant proteins were expressed in *Xenopus* oocytes, suggesting that the six amino acid positions which differ between the two transporters confer differences in kinetic properties (Vasudevan *et al.*, 1998). The substrate specificities of the two transporters have not been fully characterized, and transport of other nucleosides and nucleobases was not tested.

***Leishmania donovani* LdNT2** - Functional rescue was used to isolate LdNT2, a novel nucleoside transport protein related to LdNT1.1 and LdNT1.2, but with distinct transport characteristics (Carter *et al.*, 2000a). The molecular cloning of LdNT2 was based on the functional restoration of wild-type transport characteristics (sensitive to formycin B, nucleoside transport competent) in a formycin B-resistant, nucleoside transport-deficient background following transfection with a cosmid library containing inserts of *L. donovani* genomic DNA (Carter *et al.*, 2000a). The encoded protein LdNT2 (499 amino acid residues) is 25 - 44 % identical in amino acid sequence to hENT1/2 and LdNT1.1 (Carter *et al.*, 2000a). LdNT2 transported inosine and guanosine with apparent K_m values of 0.3 and 1.7 μM , respectively, as well as cytotoxic inosine and guanosine analogs

(Carter *et al.*, 2000a). Inhibition studies with other physiological nucleosides and nucleobases did not reveal any other potential substrates of LdNT2 (Carter *et al.*, 2000a). The equilibrative nucleoside transport inhibitor NBMPR did not inhibit LdNT2-mediated transport of inosine or guanosine (Carter *et al.*, 2000a).

***Trypanosoma brucei brucei* TbNT2-9** - Uptake studies in intact *Trypanosoma brucei brucei* parasites have identified two high affinity nucleoside transport systems, P1 and P2 (Carter and Fairlamb, 1993; Carter *et al.*, 1995; de Koning *et al.*, 1998; Sanchez *et al.*, 1999). The P1 system mediates uptake of purine nucleosides (adenosine, inosine, and guanosine), whereas the P2 system transports adenosine and adenine as well as melaminophenyl arsenicals, anti-trypanosomal drugs used in the treatment of sleeping sickness (Carter and Fairlamb, 1993; Carter *et al.*, 1995; de Koning *et al.*, 1998; de Koning and Jarvis, 1999; Sanchez *et al.*, 1999, 2002). The P1 system exhibits higher relative affinity for adenosine influx than P2 (apparent K_m values of 0.15 and 0.59 μM , respectively, were obtained in intact parasites) (Carter and Fairlamb, 1993). The P1 system is found in both bloodstream and procyclic lifecycle stages of *T. b. brucei*, while the P2 system is found only in bloodstream parasites (Sanchez *et al.*, 2002).

A nucleoside transporter demonstrating P1-type nucleoside transport activity was cloned by PCR amplification from a *T. b. brucei* cDNA library based on sequence information derived from the *Leishmania donovani* LdNT1.1 nucleoside transporter (Vasudevan *et al.*, 1998; Sanchez *et al.*, 1999). TbNT2 (463 amino acids) exhibits 30, 22, and 25 % sequence identity to LdNT1.1, hENT1, and hENT2, respectively (Sanchez *et al.*, 1999). When produced in *Xenopus* oocytes, TbNT2 mediated uptake of purine nucleosides (adenosine, inosine, and guanosine), with apparent K_m values of 0.99 μM for adenosine and 1.18 μM for inosine, confirming that TbNT2 is a high affinity purine nucleoside transporter (Sanchez *et al.*, 1999). In competition experiments, unlabeled adenosine, inosine, and guanosine, but not adenine or other nucleosides or nucleobases, inhibited ^3H -adenosine uptake by recombinant TbNT2 in oocytes (Sanchez *et al.*, 1999). Proton gradient uncouplers partially inhibited the uptake of adenosine by TbNT2, suggesting that this permease may be a proton symporter (Sanchez *et al.*, 1999). These

results are consistent with those seen in intact parasites where nucleoside uptake is dependent upon the proton motive force, and is therefore an energy-dependent process (de Koning *et al.*, 1998). TbNT2 mRNA was found only in procyclic form parasites. Since P1-type transporters are expressed both in procyclic and bloodstream form trypanosomes, it is possible that other P1-type transporters may be expressed in the procyclic parasites or in both the procyclic and the bloodstream forms of *T. b. brucei* (Sanchez *et al.*, 1999).

Recently, BLAST searches of the *T. b. brucei* genome database, based on sequence information derived from TbNT2, have led to the identification of eight cDNAs encoding additional members of the TbNT family of nucleoside/nucleobase transporters (Sanchez *et al.*, 2002). The gene with the highest sequence identity (96 %) to the original TbNT2 gene was given the designation TbNT2/927, since it was cloned from a different strain of *T. b. brucei* (TREU 927) (Sanchez *et al.*, 2002). The other P1-type genes were labeled TbNT3 through TbNT9 (Sanchez *et al.*, 2002). Collectively, these proteins share ~ 20 - 25 % amino acid sequence identity with human ENT family members and ~ 81 - 96 % identity to the original TbNT2 transporter (Sanchez *et al.*, 2002). When expressed in *Xenopus* oocytes, TbNT2/927, TbNT5, TbNT6, and TbNT7 transported adenosine, inosine, and guanosine with high affinity (apparent K_m values of 5 μ M were obtained for both adenosine and inosine), consistent with P1-type transport characteristics (Sanchez *et al.*, 2002). In addition, TbNT5, TbNT6, and TbNT7, but not TbNT2/927, were able to mediate uptake of hypoxanthine (Sanchez *et al.*, 2002). Functional expression studies in oocytes failed to identify substrates of TbNT3 and TbNT4; TbNT3 and TbNT4 did not demonstrate any clear transport activity for any of the nucleosides and nucleobases tested (Sanchez *et al.*, 2002). TbNT8 and TbNT9 remain to be characterized (Sanchez *et al.*, 2002). TbNT2/927 and TbNT3-7 are expressed in the bloodstream stage of the *T. b. brucei* life cycle, but only TbNT2/927 and TbNT5 are expressed in the procyclic parasites (Sanchez *et al.*, 2002).

***Trypanosoma brucei brucei* TbAT1** - *Trypanosoma brucei brucei* TbAT1 was cloned by transforming yeast cells defective in purine biosynthesis with a cDNA library from a

bloodstream form of *T. b. brucei*, followed by selection for growth in media containing adenosine as the sole purine source (Mäser *et al.*, 1999). The TbAT1 protein contains 463 amino acid residues and shares 25 % sequence identity with hENT1 and 27 - 32 % identity with TbNT2-9 (Mäser *et al.*, 1999). The functional activity of TbAT1, when produced in yeast, closely matched that of the reported P2-type transport activity in *T. b. brucei* (transports adenosine, adenine, melaminophenyl arsenicals, and diamidines) (Mäser *et al.*, 1999). High affinity transport of adenosine (apparent K_m of 2.2 μ M) by TbAT1 was inhibited by adenine, whereas inosine, guanosine, uridine, uracil, hypoxanthine and guanine had no effect (Mäser *et al.*, 1999). TbAT1-mediated transport of adenosine was also inhibited by melaminophenyl arsenicals but, unlike the native P2 transport activity, was unaffected by diamidines, which may be the result of a missing trypanosomal cofactor required for diamidine recognition (Mäser *et al.*, 1999). To investigate whether TbAT1 was involved in drug resistance seen in patients with sleeping sickness, a drug-resistant mutant of TbAT1 (TbAT1^r) was cloned (Mäser *et al.*, 1999). Yeast producing TbAT1^r were unable to transport adenosine and were insensitive to melaminophenyl arsenicals (Mäser *et al.*, 1999). In addition, yeast carrying TbAT1^r were unable to grow on other nucleosides as the purine source and did not transport radiolabeled adenine, hypoxanthine or inosine, suggesting that TbAT1^r may be nonfunctional rather than an altered substrate-specificity variant (Mäser *et al.*, 1999).

Yeast -

***Saccharomyces cerevisiae* FUN26** - Using sequence information derived from the GenBankTM database, a cDNA encoding FUN26 was isolated by PCR cloning from yeast chromosomal DNA (Vickers *et al.*, 2000a, 2001). FUN26 (517 amino acid residues) has limited (~ 18 %) amino acid sequence identity to members of the ENT family of transporters (Vickers *et al.*, 2000a). Expression of FUN26 cDNA failed to confer cell-surface FUN26-mediated uridine transport capability in nucleoside transport-deficient yeast and was therefore tested in *Xenopus* oocytes (Vickers *et al.*, 2000a). Functional characterization of FUN26 produced in oocytes demonstrated that FUN26 mediates the proton-independent transport of both purine and pyrimidine nucleosides, but not

nucleobases (Vickers *et al.*, 2000a). Transport of uridine was unaffected by the ENT transport inhibitors NBMPR, dilazep, and dipyridamole (Vickers *et al.*, 2000a). The lack of detectable FUN26-mediated uridine transport activity in transfected yeast suggested that FUN26 may be localized to intracellular membranes (Vickers *et al.*, 2000a). To investigate this possibility, the recombinant transporter was tagged with the c-Myc immunopeptide, to produce FUN26myc, and yeast membranes containing FUN26myc were subjected to sucrose gradient centrifugation (Vickers *et al.*, 2000a). Fractions from the gradient were then immunoblotted to detect FUN26myc. These experiments found that recombinant FUN26 displayed a distribution similar to that of an intracellular, prevacuolar membrane marker, suggesting that FUN26myc is predominantly present in intracellular membranes (Vickers *et al.*, 2000a).

Nematodes -

Caenorhabditis elegans CeENT1 - The genomic database of *Caenorhabditis elegans* contains 6 putative ENT homologs designated CeENT1-6. The cDNA encoding CeENT1 has been cloned and characterized for transport activity (Young *et al.*, 2001). When expressed in *Xenopus* oocytes, CeENT1 mediates the uptake of purine and pyrimidine nucleosides (Young *et al.*, 2001). CeENT1 also transports dideoxynucleosides (AZT, ddC, and ddI) (Young *et al.*, 2001). Transport of nucleosides by CeENT1 was unaffected by NBMPR, dilazep, and draflazine, but was inhibited by dipyridamole (IC_{50} = 300 nM) (Young *et al.*, 2001).

Plants -

Arabidopsis thaliana AtENT1 - cDNAs encoding the *Arabidopsis thaliana* nucleoside transporter AtENT1 were cloned independently by two groups using i) RT-PCR and ii) adenosine growth selection in *Saccharomyces cerevisiae* mutants unable to synthesize adenine (Li and Wang, 2000; Möhlmann *et al.*, 2001). The cDNAs encode a protein of 428 amino acid residues that is 24 % identical in sequence to hENT1 (Möhlmann *et al.*, 2001). When produced in mutant *S. cerevisiae*, AtENT1 demonstrated high affinity transport of adenosine (apparent K_m value 3.6 μ M) and insensitivity to the

inhibitors NBMPR, dilazep, and dipyridamole (Möhlmann *et al.*, 2001). Adenosine influx was inhibited by various purine (adenosine, inosine, guanosine) and pyrimidine (cytidine) nucleosides, but was unaffected by uridine or various nucleobases (Möhlmann *et al.*, 2001). AtENT1 therefore has a relatively broad permeant selectivity for purine and pyrimidine nucleosides. AtENT1 transport was inhibited by proton-ionophores, suggesting that AtENT1-mediated nucleoside transport is proton dependent (Möhlmann *et al.*, 2001).

Mammalian Concentrative Nucleoside Transporters (CNTs)

Characteristics of Mammalian Concentrative Nucleoside Transport Processes -

The presence of concentrative as well as equilibrative nucleoside transport systems in mammals first became apparent with studies reporting that uptake of adenosine and various other purine and pyrimidine nucleosides in rat, rabbit, and bovine renal brush-border membrane vesicles did not proceed by facilitated diffusion, but by high-affinity NBMPR-insensitive processes requiring the presence of a Na⁺ electrochemical gradient as the driving force (Le Hir and Dubach, 1984, 1985a, b; Lee *et al.*, 1988; Jarvis, 1989; Williams *et al.*, 1989; Le Hir, 1990; Williams and Jarvis, 1991). Subsequent investigations found that Na⁺-dependent nucleoside transport was mediated by multiple systems in a variety of specialized epithelia and other cells and tissues, including intestine, kidney, liver, choroid plexus, other regions of the brain, splenocytes, macrophages, and leukemic cells. Three major (*cit*, *cif*, and *cib*) and two minor (*csg* and *cs*) functional subclasses are currently recognized on the basis of their permeant selectivity and inhibitor sensitivity (Table 1-2) (Griffiths and Jarvis, 1996; Thorn and Jarvis, 1996; Cass *et al.*, 1998; Baldwin *et al.*, 1999; Young *et al.*, 2001). System *cit* (concentrative, insensitive to inhibition by NBMPR, and accepts thymidine as a permeant) transports pyrimidine nucleosides and adenosine, although the latter is a relatively poor substrate. The *cif* system (concentrative, insensitive to inhibition by NBMPR, and accepts formycin B as permeant) transports purine nucleosides and uridine. System *cib* (concentrative, insensitive to inhibition by NBMPR, and accepts a broad

range of permeants) transports both purine and pyrimidine nucleosides. Apparent Na^+ /nucleoside coupling ratios of 2:1 have been reported for system *cib* in rabbit choroid plexus and rat microglia (Wu *et al.*, 1992; Hong *et al.*, 2000), while stoichiometries of 1:1 have been described for systems *cit* and *cif* (Lee *et al.*, 1988; Williams and Jarvis, 1991). The minor concentrative processes, *csg* and *cs*, have been described in leukemic cells (Paterson *et al.*, 1993; Flanagan and Meckling-Gill, 1997). System *cs* was found in freshly isolated leukemic cells and transports adenosine analogs in an NBMPR-sensitive manner (Paterson *et al.*, 1993). System *csg* was observed in cultured human NB4 acute promyelocytic leukemia cells and murine L1210 leukemia cells and mediates NBMPR-sensitive guanosine transport (Flanagan and Meckling-Gill, 1997). The *csg* and *cs* systems have not been well characterized functionally, and the proteins responsible for their transport are unknown.

Functional and Molecular Properties of Cloned Mammalian CNTs -

Members of the concentrative nucleoside transporter (CNT) protein family are widely distributed in eukaryotes and prokaryotes. A current list of identified CNTs is provided in Table 1-3. These include cloned nucleoside transporters that have been characterized functionally as recombinant proteins in *Xenopus* oocytes or other heterologous expression systems, as well as putative transporters identified only by homology searches of complete and unfinished eukaryote and prokaryote sequence databases. To date, three mammalian CNT isoforms have been identified.

CNT1 - The first mammalian member of the CNT family of proteins was identified by expression screening of a size-selected cDNA library from rat jejunum in *Xenopus* oocytes (Huang *et al.*, 1994). Rat (r) concentrative nucleoside transporter 1 (termed rCNT1) contains 648 amino acid residues and has a predicted membrane topology of 13 TMs, with the hydrophilic N-terminal and glycosylated C-terminal domains located on the cytoplasmic and extracellular sides of the membrane, respectively (Fig. 1-4) (Huang *et al.*, 1994; Hamilton *et al.*, 1997, 2001). Within the extracellular C-terminal region, two sites of glycosylation have been identified (Hamilton *et al.*, 1997, 2001). Functional characterization in *Xenopus laevis* oocytes and in transiently transfected mammalian cells

demonstrated that rCNT1 exhibited the transport characteristics of the nucleoside transport system *cit* (Huang *et al.*, 1994; Fang *et al.*, 1996; Yao *et al.*, 1996b). rCNT1 was Na⁺-dependent, NBMPR-insensitive and transported pyrimidine nucleosides and adenosine with high affinity (uridine and adenosine apparent K_m values of 37 and 26 μM , respectively) (Huang *et al.*, 1994; Yao *et al.*, 1996b). Adenosine, however, was transported with a much lower V_{max} (0.07 pmol/oocyte min⁻¹ for adenosine *versus* 21 pmol/oocyte min⁻¹ for uridine) (Yao *et al.*, 1996b). K_{50} values for Na⁺-activation were 12.4 mM for adenosine and 9.5 mM for uridine (Yao *et al.*, 1996b). The relationship between nucleoside flux and Na⁺ concentration yielded hyperbolic curves, with Hill coefficients consistent with a 1:1 Na⁺/nucleoside stoichiometry for both nucleosides (Yao *et al.*, 1996b). Studies with recombinant rCNT1 produced in *Xenopus* oocytes also demonstrated Na⁺-dependent transport of the antiviral nucleoside drugs AZT and ddC, but with a lower apparent affinity compared to physiological nucleosides ($K_m \sim 0.5$ mM for both AZT and ddC) (Yao *et al.*, 1996a). Related cDNAs encoding human (hCNT1) and pig (pkCNT1) transporter proteins with *cit*-type activity have also been cloned and functionally characterized in *Xenopus* oocytes (Ritzel *et al.*, 1997; Pajor 1998). hCNT1 (650 amino acid residues) was isolated from human kidney by hybridization screening and RT-PCR amplification strategies and is 83 % identical to rCNT1 (Ritzel *et al.*, 1997). hCNT1 has functional properties similar to rCNT1, including high-affinity transport of physiological nucleosides (uridine apparent K_m 35 - 45 μM) and high-affinity, low-capacity transport of adenosine (Ritzel *et al.*, 1997). hCNT1 transports AZT and ddC and has also been demonstrated to mediate cellular uptake of gemcitabine (apparent K_m 24 μM), a clinically important anticancer deoxycytidine analog with activity against solid tumors (Ritzel *et al.*, 1997; Mackey *et al.*, 1998b, 1999). The paper describing gemcitabine transport by recombinant hCNT1 produced in *Xenopus* oocytes (Mackey *et al.*, 1999), to which I contributed, is included as an APPENDIX to this thesis. pkCNT1 (647 amino acid residues) was isolated from pig kidney by RT-PCR and is 84 % identical in amino acid sequence to rCNT1 (Pajor, 1998). Consistent with *cit*-type transport activity, pkCNT1-mediated uptake of uridine (apparent K_m 9 μM) was inhibited by cytidine, uridine, thymidine, and adenosine, but not by guanosine (Pajor, 1998). AZT

inhibited uridine transport, and may therefore also be a pkCNT1 substrate (Pajor, 1998). Chimeric constructs between pyrimidine nucleoside-selective hCNT1 and purine nucleoside-selective hCNT2 (next section) and site-directed mutagenesis of hCNT1 were used to identify two sets of adjacent residues in TMs 7 and 8 (Ser³¹⁹/Gln³²⁰ and Ser³⁵³/Leu³⁵⁴) that, when converted to the corresponding residues in hCNT2 (Gly³¹³/Met³¹⁴ and Thr³⁴⁷/Val³⁴⁸), altered the substrate selectivity of hCNT1 (*cit*) to that of hCNT2 (*cif*) (Loewen *et al.*, 1999). Mutation of the two adjacent residues in TM 7 alone changed the substrate specificity from *cit* to *cib* (Loewen *et al.*, 1999), an effect also seen by mutation of the corresponding serine residue in TM 7 of rCNT1 (Wang and Giacomini, 1997, 1999). Mutations of the two hCNT1 residues in TM 8 alone produced a protein with uridine-preferring transport characteristics (Loewen *et al.*, 1999). Transcripts encoding CNT1 transporters have been identified in brain, liver, kidney, uterus, lung, and small intestine (Baldwin *et al.*, 1999; Vickers *et al.*, 2000b). Results of in depth electrophysiological studies of recombinant hCNT1 produced in *Xenopus* oocytes are presented in *Chapter II* of this thesis.

CNT2 - A transporter related to rCNT1, but with *cif*-type nucleoside transport activity, was identified by expression cloning from rat liver (Che *et al.*, 1995). This protein was designated SPNT (sodium-dependent purine nucleoside transporter). A cDNA encoding an almost identical protein, termed rCNT2, was independently isolated from rat jejunum (Yao *et al.*, 1996b). The SPNT and rCNT2 proteins contained 659 amino acid residues with 13 predicted TMs and 5 potential sites of glycosylation (Yao *et al.*, 1996b). SPNT and rCNT2 are 64 % identical to rCNT1, with the N- and C- terminal domains showing greatest sequence divergence (Che *et al.*, 1995; Yao *et al.*, 1996b). When expressed in *Xenopus* oocytes, SPNT and rCNT2 exhibited high-affinity Na⁺-dependent transport of purine nucleosides and uridine (apparent K_m values of 6 and 21 μ M for adenosine and uridine, respectively) (Che *et al.*, 1995; Yao *et al.*, 1996b). RT-PCR cloning of cDNAs from kidney (Wang *et al.*, 1997) and intestine (Ritzel *et al.*, 1998) and expression in *Xenopus* oocytes identified the corresponding human *cif*-type transporter. The encoded proteins, designated hSPNT1 (Wang *et al.*, 1997) and hCNT2 (Ritzel *et al.*, 1998), were identical in sequence except for a polymorphic site at residue 75 (arginine to serine

substitution in hCNT2) and contained 658 amino acids. hCNT2/hSPNT1 have six potential glycosylation sites and are 83 and 72 % identical in amino acid sequence to rCNT2/SPNT and hCNT1, respectively (Ritzel *et al.*, 1998). Apparent K_m values for adenosine and uridine transport by hCNT2 are 8 and 40 μM , respectively (Ritzel *et al.*, 1998). Unlike h/rCNT1, both nucleosides have broadly similar V_{max} values (Ritzel *et al.*, 1998). Stable transfection of hCNT2 into nucleoside transport-deficient CEM-ARAC leukemia cells has been used to demonstrate hCNT2-mediated transport and cytotoxicity of anticancer fluoropyrimidine nucleoside drugs (Lang *et al.*, 2001), and studies in *Xenopus* have shown that hCNT2 also transports the antiviral nucleoside drug ddI (Ritzel *et al.*, 1998; Yao *et al.*, 2001a). There is, however, evidence that rCNT2 may have a broader substrate tolerance for nucleoside analog drugs than hCNT2 (Lang *et al.*, 2001; Gerstin *et al.*, 2002). cDNAs encoding murine (mCNT2) and rabbit (rbCNT2) *cif*-type transporters have also been cloned and functionally characterized in *Xenopus* oocytes (Gerstin *et al.*, 2000; Patel *et al.*, 2000). mCNT2 (660 amino acid residues) exhibits 93 and 80 % sequence identity to its rat (rCNT2) and human (hCNT2) homolog, respectively, and 65 % identity to rCNT1 and hCNT1 (Patel *et al.*, 2000). rbCNT2 (658 amino acid residues) is 84 % identical to hSPNT1, 82 % identical to rSPNT, and 65 % identical to rCNT1 and hCNT1 (Gerstin *et al.*, 2000). Investigations of the tissue distribution of CNT2/SPNT mRNA indicate that CNT2/SPNT may have a wider tissue distribution than CNT1, with multiple mRNA species identified in kidney, liver, small intestine, stomach, colon, rectum, pancreas, spleen, skeletal muscle, brain, lung, heart, placenta, cervix, prostate, and epididymis (Wang *et al.*, 1997; Ritzel *et al.*, 1998; Gerstin *et al.*, 2000; Patel *et al.*, 2000; Leung *et al.*, 2001).

CNT3 - A broadly selective nucleoside transport process (*cib*) mediating the Na^+ -dependent uptake of both purine and pyrimidine nucleosides has been described in a number of tissues, including freshly isolated human leukemic blasts (Belt *et al.*, 1993), human colon cancer Caco-2 cells (Belt *et al.*, 1993), rabbit choroid plexus (Wu *et al.*, 1992; Washington *et al.*, 1995), and rat intestine (Huang *et al.*, 1993; Redlak *et al.*, 1996). Prior to the molecular cloning of rCNT1 (Huang *et al.*, 1994), an earlier study identified a protein related to the rabbit intestinal Na^+ -dependent glucose transporter

(SGLT1) as the first putative nucleoside transport protein (Pajor and Wright, 1992). This protein, designated SNST1, demonstrated *cib*-type transport activity when expressed in *Xenopus* oocytes (Pajor and Wright, 1992). The rate of Na⁺-dependent uridine transport was, however, very low (only twofold above endogenous levels), and *cib*-type transport activity has not been demonstrated in tissues in which SNST1 was expressed (heart and kidney). Nucleosides do not appear to be physiological substrates of SNST1, and the protein is now recognized as the rabbit ortholog of the human glucose transporter hSGLT2 (Wright, 2001). Instead, it is now known that the human and mouse proteins responsible for *cib*-type transport activity are members of the CNT transporter family (hCNT3 and mCNT3, respectively) (Ritzel *et al.*, 2001). The paper describing the initial molecular cloning and identification of hCNT3 and mCNT3 (Ritzel *et al.*, 2001), to which I contributed, is included as an APPENDIX to this thesis. Results of in depth electrophysiological studies of this novel CNT isoform are presented in *Chapters III and IV*.

CNT Family Members in Prokaryotes and Other Eukaryotes

***Eptatretus stouti* CNT (hfcCNT)** - Hagfish CNT (hfcCNT) was cloned from the ancient marine prevertebrate *Eptatretus stouti* based on regions of amino acid similarity between CNT family members (Loewen *et al.*, 1999; Yao *et al.*, 2002a). A partial-length hagfish CNT cDNA was isolated by PCR using a cDNA library prepared from hagfish intestinal mucosa as template. The resulting fragment was then used as a hybridization probe to screen the hagfish intestinal cDNA library. The resultant cloned hagfish CNT cDNA encoded a 683 amino acid residue protein that was 52 % identical in sequence to hCNT1, 50 % identical to hCNT2, and 57 % identical to hCNT3 (Yao *et al.*, 2002a). When produced in *Xenopus* oocytes, hfcCNT displayed transport activities resembling system *cib* (Yao *et al.*, 2002a). hfcCNT transported all physiological pyrimidine and purine nucleosides tested and also accepted both pyrimidine (AZT, ddC) and purine (ddI) dideoxynucleoside drugs as permeants (Yao *et al.*, 2002a). Apparent K_m values for uridine, inosine, and thymidine transport were 10, 35, and 45 μ M, respectively (Yao *et al.*, 2002a). Electrophysiological studies demonstrated that nucleoside transport by

hfCNT was Na⁺-dependent and H⁺-independent. The relationship between nucleoside influx and Na⁺ uptake was nearly linear, consistent with the high Na⁺ concentrations (~ 500 mM) experienced by hagfish tissues, yielding a K₅₀ value of > 100 mM (Yao *et al.*, 2002a). A Na⁺/nucleoside coupling ratio of 2:1 was determined by the simultaneous measurement of Na⁺ current and ¹⁴C-uridine influx under voltage clamp conditions (Yao *et al.*, 2002a). To localize the domains involved in cation stoichiometry and binding affinity, a chimera was constructed in which the carboxyl-terminal half of hfCNT (TMs 7 - 13) was replaced with that of hCNT1 (Yao *et al.*, 2002a). The chimera exhibited hCNT1-like substrate specificity and the relationship between nucleoside influx and Na⁺ concentration was saturable, high-affinity and hyperbolic with a Hill coefficient of ~ 1, indicating a Na⁺/nucleoside coupling ratio of 1:1 (Yao *et al.*, 2002a). These results establish that the amino acid residues responsible for determining the Na⁺/nucleoside coupling ratio and Na⁺-binding affinity are located within the carboxyl-terminal half of the protein. The amino acid sequence and functional properties of hfCNT contributed to the identification of TM 7 and TM 8 amino acid residues responsible for hCNT1 substrate selectivity (Loewen *et al.*, 1999), and was instrumental in the molecular cloning of its human and mouse orthologs, hCNT3 and mCNT3 (Ritzel *et al.*, 2001). Although hagfish diverged from the main line of vertebrate evolution ~ 550 million years ago, there is remarkable amino acid sequence similarity between hfCNT and mammalian CNT3 proteins, particularly in the TM 4 - 13 region (Yao *et al.*, 2002a). This may indicate functional constraints on the primary structure of this region and provides structural evidence that *cib*-type nucleoside transporters fulfill important physiological functions.

***Caenorhabditis elegans* CNT3 (CeCNT3)** - *Caenorhabditis elegans* CeCNT3 was cloned by RT-PCR from *C. elegans* total RNA using primers designed to amplify the potential nucleoside transporter encoded within the F27E11.2 genetic locus (GenBank accession number AF016413) (Xiao *et al.*, 2001). At the amino acid sequence level, CeCNT3 is 30 % identical to mammalian CNTs and 14 - 24 % identical to bacterial CNTs. The most divergent regions between mammalian CNTs and CeCNT3 are the N- and C- terminal domains. When produced in *Xenopus* oocytes, CeCNT3 transported

inosine, thymidine, uridine, guanosine and adenosine, but not cytidine (Xiao *et al.*, 2001). Inosine and thymidine apparent K_m values were 15 and 11 μM , respectively (Xiao *et al.*, 2001). Transport of nucleosides by CeCNT3 was Na^+ -independent. Instead, CeCNT3 exhibited pH-dependence consistent with possible proton-coupling (Xiao *et al.*, 2001). CeCNT3 was termed "CNT3" under the presumption that it would be an ortholog of the mammalian *cib* system. However, CeCNT3 is not truly broadly selective, and its amino acid sequence is not closely related to either hCNT or human and mouse CNT3. At least one other CNT (F27E11.1) is present in the *C. elegans* genome database.

***Candida albicans* CNT (CaCNT)** - BLAST searches of the pathogenic yeast *Candida albicans* genome sequence databank led to the identification of a cDNA encoding a further member of the CNT family of nucleoside transporters (Loewen *et al.*, 2003a). CaCNT (608 amino acid residues) was 33 % identical in amino acid sequence to hCNT1, 34 % identical to hCNT2 and 38 % identical to hCNT3 (Loewen *et al.*, 2003a). Like other eukaryote members of the CNT family, CaCNT has 13 predicted TMs. When produced in *Xenopus* oocytes, recombinant CaCNT was electrogenic, H^+ -dependent, and Na^+ - and Li^+ -independent (Loewen *et al.*, 2003a). CaCNT mediated the high affinity transport of purine nucleosides and uridine, with apparent K_m values in the range 16 - 64 μM (adenosine < uridine < inosine < guanosine). In addition to physiological nucleosides, CaCNT also transported purine- and uridine-analog antineoplastic and antiviral drugs, including ddI, fludarabine, cladribine, 5-fluorouridine, and 5-fluoro-2'-deoxyuridine. The antifungal nucleoside drug cordycepin was also transported by CaCNT. The CaCNT H^+ /nucleoside coupling ratio was 1:1 (Loewen *et al.*, 2003a).

***Escherichia coli* NupC** - A cDNA encoding the NupC transport protein was isolated by functional rescue of transport-defective *Escherichia coli* grown on media containing cytidine as the sole carbon source (Craig *et al.*, 1997). Confirmation of the functional presence of NupC was also demonstrated in the ability of NupC to restore the sensitivity of transport deficient *E. coli* to the toxic nucleoside analog 5'-azacytidine (Craig *et al.*, 1997). NupC contains 400 amino acid residues and is 26 % identical to hCNT1, 22 % identical to hCNT2, and 25 % identical to hCNT3 (Craig *et al.*, 1997; Loewen *et al.*,

2003b). NupC lacks the first 3 transmembrane helices of eukaryote CNT and contains only 10 predicted TMs (*ie.* the 10 TMs of NupC correspond to TMs 4 - 13 of eukaryote CNT proteins) (Loewen *et al.*, 2003b). NupC produced in *Xenopus* oocytes transported pyrimidine nucleosides, adenosine, and, to a lesser extent, inosine, but not guanosine (Loewen *et al.*, 2003b). AZT, ddC, ddI and gemcitabine were also permeants, suggesting that NupC may provide a route for cellular uptake of antiviral and anticancer nucleoside drugs, some of which have secondary antibacterial activity. Apparent K_m values for both physiological nucleosides and nucleoside drugs were lower than for hCNT1 or rCNT1. Transport did not require Na^+ and was H^+ -dependent (Loewen *et al.*, 2003b). The finding that NupC lacks TMs 1 - 3 of eukaryote CNTs provides further evidence of the functional/structural importance of the TM 4 - 13 region. An engineered form of recombinant rCNT1 with TMs 1 - 3 removed retains low, but significant transport activity when produced in *Xenopus* oocytes (Hamilton *et al.*, 2001).

Other Nucleoside Transport Processes

Besides ENTs and CNTs, six other protein families with members in bacteria, yeast, and mammals have representatives which mediate the uptake of nucleosides and nucleoside analog drugs. These families are the nucleoside/ H^+ symporter (NHS) family, the Tsx channel-forming protein family, the uracil/allantoin permease family, the nucleoside permease (NUP) family, the organic cation transporter (OCT) family, and the organic anion transporter (OAT) family.

Bacteria-

Nucleoside/ H^+ Symporter (NHS) Family - The predominant high-affinity inner membrane nucleoside transport systems identified in *Escherichia coli*, termed NupC and NupG, differ in their substrate selectivities and sensitivity to inhibition by the uridine analog showdomycin (Munch-Petersen *et al.*, 1979; Craig *et al.*, 1997). Both proteins mediate the uptake of a broad selection of nucleosides and deoxynucleosides, but are distinguished by the poor ability of NupC to transport guanosine and deoxyguanosine (Craig *et al.*, 1997; Loewen *et al.*, 2003b). Transport studies on intact cells and

membrane vesicles using metabolic inhibitors have demonstrated that nucleoside transport by NupC and NupG is dependent on the inwardly directed proton gradient (Munch-Petersen *et al.*, 1979; Craig *et al.*, 1997), a finding consistent with results obtained with NupC produced in *Xenopus* oocytes (Loewen *et al.*, 2003b). NupC is a member of the CNT family of proteins, whereas NupG belongs to the NHS family and is unrelated either to CNTs or ENTs. NupG has 418 amino acid residues and 12 predicted TMs (Westh Hansen *et al.*, 1987).

The *xapB* gene product was initially identified in studies of *E. coli* investigating the metabolism of the purine nucleoside xanthosine (Seeger *et al.*, 1995). XapB, another member of the NHS family of proteins, has 418 amino acids and is 56 % identical in sequence to NupG (Seeger *et al.*, 1995; Nørholm and Dandanell, 2001). When XapB was expressed in a transport deficient *E. coli* strain, growth was seen with all nucleosides tested, except guanosine (Nørholm and Dandanell, 2001). Uptake of radiolabeled nucleosides confirmed the results of the growth studies. Transport of the purine nucleoside xanthosine is a distinguishing feature of XapB compared to NupG and NupC. Transport of xanthosine by XapB was H⁺-dependent (Nørholm and Dandanell, 2001). A current list of the members of the nucleoside/H⁺ symporter (NHS) family is given in Table 1-4.

Tsx Channel-Forming Protein Family - The outer membrane of *Escherichia coli* acts as a permeability barrier for hydrophilic substances and toxic compounds (Maier *et al.*, 1988; Nieweg and Bremer, 1997). Substrate permeation across this membrane occurs by several mechanisms, including nonspecific porins and substrate-specific channels (Maier *et al.*, 1988; Nieweg and Bremer, 1997). Nonspecific porins are water-filled channels which allow the passive diffusion of a large variety of molecules across the membrane based only on their concentration gradient, hydrophobicity, and size, while substrate-specific channels contain saturable substrate-specific binding sites which allow the transport of substrates across the membrane at low external concentrations (Hantke, 1976; Benz *et al.*, 1988; Maier *et al.*, 1988; Bremer *et al.*, 1990; Fsihi *et al.*, 1993; Nieweg and Bremer, 1997). The Tsx protein of *E. coli*, named after its structural gene

tsx, is a substrate-specific channel which mediates the transport of nucleosides and deoxynucleosides across the outer membrane when these substrates are present in the submicromolar extracellular concentration range (Hantke, 1976; Benz *et al.*, 1988; Maier *et al.*, 1988; Bremer *et al.*, 1990; Fsihi *et al.*, 1993; Nieweg and Bremer, 1997). Transport of nucleosides by Tsx was first demonstrated by Hantke (1976), who found that the uptake of adenosine and thymidine (but not cytidine) was impaired in *tsx* mutants. The Tsx protein is initially synthesized with an amino-terminal 22 amino acid signal sequence that is required for translocation across the cytoplasmic membrane (Nieweg and Bremer, 1997). The mature protein containing 272 amino acid residues is localized to the *E. coli* outer membrane with 14 predicted transmembrane regions and is depicted as a β -barrel (Nieweg and Bremer, 1997). Reconstitution of purified Tsx into artificial membranes has demonstrated broad substrate selectivity for nucleosides and deoxynucleosides, as well as the antibiotic albicidin which specifically blocks DNA replication in intact *E. coli* (Fsihi *et al.*, 1993; Nieweg and Bremer, 1997). The substrate specificity of Tsx is due to a ligand-binding site inside the channel (Hantke, 1976; Benz *et al.*, 1988; Maier *et al.*, 1988; Bremer *et al.*, 1990; Fsihi *et al.*, 1993; Nieweg and Bremer, 1997). Database searches reveal that Tsx proteins are distantly related to OmpK (~ 29 % identity), an outer membrane protein of *Vibrio parahaemolyticus* and *Vibrio cholerae* with unknown function (Inoue *et al.*, 1995a, b). Tsx is structurally unrelated to ENTs or CNTs, although a recent report, based on apparently conserved sequence motifs, has proposed that Tsx may represent an evolutionary precursor of the ENT family of proteins (Sankar *et al.*, 2002). This possibility is unlikely, given the totally different membrane architectures of the two groups of proteins. A list of known and putative members of the Tsx family of channel-forming proteins is provided in Table 1-5.

Yeast -

FUI1 of the Uracil/Allantoin Permease Family - The FUI1 (YBL042c) gene product was originally identified from a mutant with increased resistance to the cytotoxic nucleoside analog 5-fluorouridine and unable to grow on media containing uridine as the sole pyrimidine source, leading to the suggestion that FUI1 is a uridine transporter (Jund

and Lacroute, 1970; Wagner *et al.*, 1998). FUI1 is predicted to have 10 TMs (692 amino acids) and is a member of the uracil/allantoin permease family (Wagner *et al.*, 1998; Vickers *et al.*, 2000a). It is unrelated to ENTs or CNTs (Vickers *et al.*, 2000a). Disruption of FUI1 inhibited uridine transport in *S. cerevisiae*, while production of recombinant FUI1 in *fui1*-disruption mutants restored high affinity transport of uridine (apparent K_m 20 μ M) (Vickers *et al.*, 2000a). Similarly, the production of recombinant FUI1 in *fui1*-disruption mutants resulted in an increased cytotoxicity to 5-fluorouridine (Vickers *et al.*, 2000a). FUI1 is unaffected by the ENT nucleoside transport inhibitors (NBMPR, dilazep, and dipyridamole) and is highly selective for uridine, uridine analogs and, possibly, uracil (Vickers *et al.*, 2000a). Table 1-6 contains known and putative members of the uracil/allantoin permease family.

Nucleoside Permease (NUP) Family - The ability of *C. albicans*, but not *S. cerevisiae*, to transport purine nucleosides (Rao *et al.*, 1983; Fasoli *et al.*, 1990; Horák, 1997; Detke, 1998) allowed Detke (1998) to clone, by complementation, a *C. albicans* purine nucleoside permease gene (*NUP*). *S. cerevisiae* expressing the gene product NUP (407 amino acid residues) acquired purine, but not pyrimidine nucleoside transport capability and were able to grow on medium supplemented with adenosine and guanosine (Detke, 1998). NUP is unrelated to ENTs or CNTs (Detke, 1998). A list of known and putative members of the nucleoside uptake (NUP) protein family is given in Table 1-7.

Mammals -

Organic Cation Transporter (OCT) Family - Organic cation transport systems mediate transmembrane fluxes of endogenous bioactive amines, xenobiotics and various therapeutic drugs, including antihistamines, skeletal muscle relaxants, antiarrhythmics, and β -adrenoceptor blocking agents (Zhang *et al.*, 1998). Pharmacokinetic and membrane transport studies have also implicated these processes in the transport of nucleoside analog drugs (Kuttesch *et al.*, 1982; Nelson *et al.*, 1983, 1988; Griffiths *et al.*, 1992; Aiba *et al.*, 1995; Martel *et al.*, 1996; Bendayan, 1997). Recently, members of a family of proteins responsible for the transport of organic cations have been cloned from

various epithelial tissues, including kidney, liver, small intestine, and colon (Zhang *et al.*, 1998). Transport proteins in the Organic Cation Transporter (OCT) family fall into two categories- electrogenic, potential-sensitive basolateral transporters or apical organic cation/proton antiporters (Zhang *et al.*, 1997a, b, 1998). Of these, basolateral transporter OCT1 is the only mammalian family member that has been shown so far to transport nucleoside drugs. Demonstrated substrates for the recombinant transporter include the acyclic guanosine analogs acyclovir (ACV) and ganciclovir (GCV) and 2'-deoxytubercidin (Nelson *et al.*, 1995; Zhang *et al.*, 1997b; Chen and Nelson, 2000; Hayer-Zilligen *et al.*, 2002; Takeda *et al.*, 2002). Human, rat and mouse OCT1 (hOCT1, rOCT1 and mOCT1) are 551 - 553 amino acid residue proteins with 12 putative TMs and are structurally unrelated to ENTs and CNTs (Tamai *et al.*, 1997, 2000; Wu *et al.*, 2000). The currently known members of the organic cation (OCT) transporter family in mammals are listed in Table 1-8.

Organic Anion Transporter (OAT) Family - Organic anion transport systems are responsible for the renal secretion of organic anions and their distribution in the body (Hosoyamada *et al.*, 1999; Kusuhara *et al.*, 1999; Sekine *et al.*, 2000; Wada *et al.*, 2000). Pharmacokinetic and membrane transport studies have also implicated these processes in the transport of nucleoside analog drugs (de Miranda *et al.*, 1989; Hedaya and Sawchuk, 1989; Chatton *et al.*, 1990; Griffiths *et al.*, 1991; Masereeuw *et al.*, 1994; Takasawa *et al.*, 1997). Recently, cDNAs encoding mammalian OATs have been successively cloned, including OAT1 (Sekine *et al.*, 1997; Sweet *et al.*, 1997; Hosoyamada *et al.*, 1999), OAT2 (Sekine *et al.*, 1998), OAT3 (Kusuhara *et al.*, 1999), and OAT4 (Cha *et al.*, 2000). All members of the Organic Anion Transporter (OAT) family are expressed in kidney, while some are also found in liver, brain, and placenta (Sekine *et al.*, 2000). OATs contain 12 putative TMs and function as Na⁺-independent exchangers or facilitators (Sekine *et al.*, 2000). OATs show low degrees of sequence identity to members of the organic cation transporter (OCT) family (30 - 40 % amino acid identity) (Sekine *et al.*, 2000) and are structurally unrelated to ENTs or CNTs. Recombinant rat OAT1 (rOAT1) produced in *Xenopus* oocytes has been shown to transport the antiviral agents AZT, ACV, zalcitabine, didanosine, lamivudine, stavudine, and trifluridine (Wada *et al.*, 2000),

while stable transfection studies in mouse kidney cells have demonstrated transport of ACV and GCV by human OAT1 (hOAT1) and transport of AZT by hOAT1, hOAT2, hOAT3, and hOAT4 (apparent K_m values for AZT uptake ranged from 26 to 152 μM) (Takeda *et al.*, 2002). Members of the organic anion transporter (OAT) family are listed in Table 1-9.

Electrophysiological Studies of Transport Proteins

To understand transport processes at the molecular level, one must study individual transport steps in the transport event, such as binding and dissociation of ions and substrates and conformational changes in the protein that allow translocation of substrate from one side of the membrane to the other. Traditionally, transport properties of recombinant transporters have been studied using radioisotope flux measurements in *Xenopus* oocytes, as exemplified by the initial functional characterization of cloned CNTs (Huang *et al.*, 1993, 1994; Che *et al.*, 1995; Pajor, 1998). Although isotope studies have been important in the expression cloning and functional characterization of nucleoside and other transport proteins, certain disadvantages exist when using this method. Many transport proteins transport their substrates in a voltage-dependent manner. Since isotope studies do not allow control of the oocyte membrane potential, individual oocytes will have different membrane potentials. Therefore, a voltage-dependence of transport results in variable flux rates in different oocytes and electrogenic transport will itself alter its own rate as the distribution of ions affects the membrane potential (Busch *et al.*, 1996). In addition, flux experiments cannot resolve time-dependent changes in the transport system of less than 1 sec and, as a result, most flux measurements are performed in equilibrium or steady-state conditions (Mager *et al.*, 1998). These disadvantages can be overcome by examining electrogenic transport under voltage-clamp conditions. Electrophysiological techniques allow accurate control of the membrane potential while studying all events involving the movement of charge during the transport process, including electrogenic substrate transport (referred to as steady-state currents) as well as charge movements involved in cotransport (referred to as presteady-state or transient currents) (Stühmer, 1992; Mager *et al.*, 1998). There are several recording techniques

that are used to measure these bioelectric signals of recombinant transporters, including the two-microelectrode voltage clamp, the patch clamp, the cut-open oocyte technique, and the macropatch, or 'giant' patch, technique.

Electrophysiological Techniques -

Two-microelectrode voltage clamp technique - The two-microelectrode voltage clamp technique is the most widely used electrophysiological technique for the measurement of whole cell currents through ion channels, electrogenic transporters, or ion pumps expressed in *Xenopus* oocytes. The two-microelectrode voltage clamp allows control of the membrane potential (clamping) while measuring currents flowing through proteins expressed in the oocyte plasma membrane. To achieve this, one intracellular electrode (voltage electrode) is used to record the actual intracellular potential of the oocyte, while an amplifier compares the resting potential recorded by the voltage electrode to the desired clamping potential (Stühmer, 1992; Quick and Lester, 1994). Current is then injected into the oocyte from the second intracellular electrode (current electrode) to minimize this difference (Quick *et al.*, 1994; Stühmer, 1998). The two-microelectrode voltage clamp is simpler to use than other electrophysiological techniques. Its advantages include the ability to record large current responses ($> 10 \mu\text{A}$), allowing stable recordings over long periods of time, recording at lower protein densities, and ease of changing the extracellular solution (Stühmer, 1998). High-gain amplifiers speed up the time-response of the voltage-clamp and reduce the error between the command potential and the membrane potential (Wagner *et al.*, 2000). There are limits, however, to using the two-microelectrode voltage clamp. Small currents ($< 2 \text{ nA}$) with very fast kinetics are difficult to resolve and, in addition, the oocyte capacitive transient lasting $\sim 2 \text{ msec}$ can obscure the resolution of fast events, such as activation or deactivation of Na^+ channels, since the membrane potential is not the desired clamped potential until the capacitive transient is over (Taglialatela *et al.*, 1992). Very fast solution changes are not possible because of the large size of oocytes, affecting, for example, studies investigating the time-course of agonist-activated currents (Costa *et al.*, 1994). Another limitation of the two-microelectrode voltage clamp technique is the

inability to control the internal medium of the oocyte, which can contaminate recorded currents with endogenous currents, such as the Ca^{2+} -activated chloride conductance (Miledi, 1982).

Cut-open oocyte technique - The cut-open oocyte technique is a novel technique for the measurement of macroscopic currents generated in oocytes producing ligand-gated channels, transporters, and voltage-gated channels. This technique involves electrically isolating a small area of the membrane, comprising approximately 8 % of the total oocyte surface area, from which membrane currents are recorded while internally perfusing the oocyte (Tagliatela *et al.*, 1992; Chen *et al.*, 1995). The cut-open oocyte voltage clamp is based on partitioning the oocyte into three separate compartments: the top compartment for recording membrane currents, the middle as a guard partition, and the bottom for intracellular potential recording, current injection, and solution exchange (Tagliatela *et al.*, 1992; Stühmer, 1998). The cut-open oocyte technique overcomes some of the limitations of the two-microelectrode voltage clamp technique (Miledi, 1982; Tagliatela *et al.*, 1992; Costa *et al.*, 1994). Since the cut-open oocyte technique allows access to the interior of the oocyte, the intracellular milieu may be controlled by internal perfusion of the oocyte, therefore eliminating contaminating endogenous conductances, such as Ca^{2+} -activated chloride currents. Internal perfusion also permits greater experimental versatility, allowing oocytes to be used in studies examining the effects of intracellular modulatory agents and the measurement of internal kinetic constants (Costa *et al.*, 1994). Because only a fraction of the oocyte membrane is voltage-clamped, the oocyte membrane capacitance can be charged within 20 - 100 μsec (Tagliatela *et al.*, 1992; Costa *et al.*, 1994; Chen *et al.*, 1996). The voltage response will therefore follow the command response much more closely, allowing accurate resolution of the time course of fast ionic or gating events. Solution changes can be made in 30 - 50 msec, permitting accurate measurement of the time course of ligand-gated channels or transporters (Costa *et al.*, 1994).

Macropatch - While the enormous capacitance of the *Xenopus* oocyte can limit the time resolution of rapidly activating events studied with the two-microelectrode voltage

clamp technique, kinetics of fast events can be studied using a patch-clamp configuration to record currents from a relatively large area of membrane. The 'giant' membrane patch, or the macropatch, was developed to study the function and regulation of electrogenic membrane proteins, allowing access to the cytoplasmic surface and therefore control of substrate and ion concentrations on both sides of the membrane. The cell-attached or excised-patch mode can be used to record currents from patches of membrane having a diameter of 10 - 40 μm (Hilgemann and Lu, 1998). The principle of patch-clamping is to isolate a patch of membrane electrically from the external solution and to record current flowing through the patch. By electrically isolating an area of the membrane, the capacitance of the oocyte is relatively small, and the membrane can be charged much faster than that of a whole oocyte by a two-microelectrode voltage clamp (Hilgemann and Lu, 1998). The macropatch technique does have disadvantages, including patch instability over long periods of recording and the requirement that channels and transporters be expressed at densities higher than those needed for the two-microelectrode voltage clamp technique, since current is being recorded from a smaller area of membrane (Stühmer, 1998).

Patch-clamp - The extracellular patch clamp technique (cell-attached) allows currents in single ionic channels to be recorded, providing detailed information about individual channel ion transport and gating properties (Hamill *et al.*, 1981; Methfessel *et al.*, 1986). In this technique, a small blunt heat-polished glass pipette with a diameter of 1 μm is pressed against the cell membrane, forming an electrical seal with a resistance of the order of gigaohms ($\text{G}\Omega$). The current recorded is the current that flows through ion channels located in the patched membrane at the tip of the patch pipette. A high resistance seal is necessary to ensure that most of the currents originating in a small patch of membrane flow into the pipette and then into the current-measuring circuitry, and to reduce the background noise of the recording (Hamill *et al.*, 1981; Methfessel *et al.*, 1986). With the *Xenopus* oocyte, single channel currents are recorded from 'cell-free' membrane patches (Hamill *et al.*, 1981; Methfessel *et al.*, 1986). Due to the mechanical stability of the high resistance seal, the pipette can be drawn away from the oocyte cell surface without a decrease in the seal resistance (Hamill *et al.*, 1981). 'Inside-out'

membrane patches and 'outside-out' membrane patches can be formed by disrupting the oocyte cell membrane (Hamill *et al.*, 1981; Methfessel *et al.*, 1986). The low background noise makes patch-clamping advantageous for studying ion channels, providing information about unitary conductance and the kinetic behaviour of ionic channels, such as the time course of channel opening and closing (Hamill *et al.*, 1981; Methfessel *et al.*, 1986). Obtaining successful recordings from small membrane patches can be difficult because of the combination of the large oocyte surface area, the small tip diameter of the patch pipette (1 μm), and the non-uniform surface distribution of the expressed channel (Stühmer, 1998). This method is not suitable for recording currents from transporters, as the resolution of the patch-clamp (~ 0.25 pA) is well below the current measured through a single transporter. These disadvantages can be overcome by recording oocyte currents with the macropatch technique, which records currents from a larger 'patch' of membrane as a result of the larger tip diameter (10 - 40 μM).

Electrophysiology of defined transporters -

A number of transporters have been extensively characterized using electrophysiological techniques, including, but not limited to, members of the Na^+ -coupled glucose transporter family (SGLT1-3) (Parent *et al.*, 1992a, b; Wright *et al.*, 1994b), a Na^+ -dependent GABA transporter (Kavanaugh *et al.*, 1992), a Na^+ -dependent glutamate transporter (Wadiche *et al.*, 1995), a H^+ -dependent *myo*-inositol transporter (Klamo *et al.*, 1996), and members of the H^+ -coupled oligopeptide transporter family (PepT1 and PepT2) (Mackenzie *et al.*, 1996a; Chen *et al.*, 1999). This research has led to new and exciting knowledge regarding membrane transport proteins. The following section looks at information obtained using electrophysiological techniques for the most extensively characterized member of the Na^+ -dependent glucose transporter family, SGLT1.

Na^+ /glucose cotransporter (SGLT1) - Na^+ /glucose cotransporters are present in the brush-border membranes of renal tubules and small intestinal villous cells. The high affinity Na^+ /glucose cotransporter SGLT1 was among the first membrane cotransporters

to be cloned and is a member of a large family of 12-helix membrane transport proteins responsible for the 'active' transport of sugars, amino acids, vitamins, and osmolytes in bacteria and animals. cDNA clones encoding the Na⁺/glucose cotransporter have been isolated and characterized using electrophysiological techniques from rat, rabbit, and human intestine and from rabbit, pig, rat, and human kidney (Hediger *et al.*, 1987; Wells *et al.*, 1992; Lee *et al.*, 1994; Wright *et al.*, 1994b; Chen *et al.*, 1996; Mackenzie *et al.*, 1996b; Diez-Sampedro *et al.*, 2001; Quick *et al.*, 2001).

A. Steady-state currents

The transmembrane currents of the cloned Na⁺/glucose cotransporter have been studied using the two-microelectrode voltage clamp and the cut-open oocyte technique (Umbach *et al.*, 1990; Parent *et al.*, 1992a, b; Chen *et al.*, 1996). The two-microelectrode voltage clamp was used to show that SGLT1-mediated transport was electrogenic, as a current was associated with transporter operation (Umbach *et al.*, 1990). In oocytes producing SGLT1, the addition of glucose to a Na⁺ solution induced inward-directed currents which were reversibly blocked by the addition of phloridzin, a competitive inhibitor of Na⁺/glucose cotransport (Umbach *et al.*, 1990). The magnitude of the current was dependent upon the concentrations of extracellular glucose, Na⁺, and phloridzin tested (Umbach *et al.*, 1990; Parent *et al.*, 1992a). At all voltages, the magnitude of the inward current increased as the concentration of glucose or Na⁺ was increased (Umbach *et al.*, 1990). Operation of the transporter was also shown to be voltage-dependent, with the amplitude of the inward current increasing at hyperpolarizing membrane potentials (Umbach *et al.*, 1990; Parent *et al.*, 1992a). Electrophysiological measurements were also used to show that in the absence of extracellular Na⁺, SGLT1 is able use the electrochemical gradient of protons to drive the uptake of glucose into cells, with kinetics similar to those seen with Na⁺ as the driving cation (Hirayama *et al.*, 1994). Kinetically, the apparent affinities for Na⁺ ($K_m^{Na^+}$) and glucose ($K_m^{glucose}$) cotransport are dependent on membrane voltage. The apparent affinity of the cotransporter for Na⁺ increased as the membrane potential was made more negative, at any concentration of glucose tested (Parent *et al.*, 1992a). The apparent affinity of the cotransporter for glucose increased as

the membrane potential was made more negative, but only at low Na^+ concentrations, suggesting that the voltage-dependence of the transporter affinity for glucose is due to voltage-dependence of Na^+ binding (Parent *et al.*, 1992a). Information on the binding order of Na^+ and glucose was also obtained from analysis of steady-state kinetic parameters (Parent *et al.*, 1992a; Klamo *et al.*, 1996). The K_m^{glucose} increased as the concentration of Na^+ was reduced, suggesting that external Na^+ alters the apparent affinity of the transporter for glucose (Parent *et al.*, 1992a). These results are consistent with an ordered binding mechanism rather than a random one.

B. Presteady-state currents

Transport studies of cotransport mechanisms have generally been limited to steady-state analysis. Under these conditions it has been necessary to make assumptions about the number of transporters in the membrane, the rate-limiting steps, and the voltage-dependence of transport (translocation and/or Na^+ binding). Presteady-state currents are a general characteristic of cotransporters and have been observed for several gene families, including, but not limited to, transporters for sugars (glucose (SGLT1-3) and *myo*-inositol (H^+ /*myo*-inositol cotransporter)) (Parent *et al.*, 1992a, b; Loo *et al.*, 1993; Klamo *et al.*, 1996; Mackenzie *et al.*, 1996b; Hazama *et al.*, 1997), neurotransmitters (norepinephrine (hNET), glutamate, and GABA (GAT1)) (Mager *et al.*, 1993; Galli *et al.*, 1995; Wadiche *et al.*, 1995), peptides (hPEPT1 and hPEPT2) (Mackenzie *et al.*, 1996a; Chen *et al.*, 1999), and anions (Na^+ /iodide cotransporter) (Eskandari *et al.*, 1997). Presteady-state currents reflect charge movements of voltage-dependent processes involved in transporter-mediated transport, such as ion binding to the transporter and conformational changes involved in the reorientation of the ligand binding sites between external and internal membrane surfaces, and provide insights into partial reactions of the transport cycle (Parent *et al.*, 1992a, b; Wright *et al.*, 1994a, b; Hazama *et al.*, 1997). Presteady-state currents exhibit common properties in many of the cotransporters studied: (i) presteady-state currents are abolished by transported substrate(s) and/or inhibitors; (ii) charge movements (Q), obtained from the integral of the presteady-state currents, are dependent upon the membrane voltage and fit the Boltzmann relation to yield the

maximal charge movement (Q_{\max}); (iii) the voltage required to obtain 50 % Q_{\max} ($V_{0.5}$) is shifted towards more hyperpolarizing potentials as the concentration of the driving ion is reduced (Na^+ or H^+); (iv) the ON-charge movement is equal in magnitude but opposite in direction to the OFF-charge movement; (v) Q_{\max} is proportional to the level of transporter expression, such that Q_{\max} increases as I_{\max} is increased and the ratio of I_{\max}/Q_{\max} yields the turnover rate for the transporter (Hazama *et al.*, 1997). The observation of both steady-state and presteady-state currents has been essential for the development of kinetic models for ion/substrate cotransport for a number of transporters, including SGLT1 and the *Leishmania donovani* H^+ /myo-inositol transporter (Parent *et al.*, 1992a; Wright *et al.*, 1994b; Klamo *et al.*, 1996).

Electrophysiological experiments designed to measure the steady-state kinetic properties of the cloned intestinal Na^+ /glucose cotransporter SGLT1 expressed in *Xenopus* oocytes revealed the presence of presteady-state currents (Parent *et al.*, 1992a, b). These transient currents were observed following a step change in the membrane potential from negative to positive potentials in sugar-free Na^+ medium (Parent *et al.*, 1992a, b; Wright *et al.*, 1994b). Presteady-state currents were not observed following the addition of sugar to the extracellular solution and were modified by the external Na^+ concentration and by the membrane potential (Parent *et al.*, 1992a, b; Wright *et al.*, 1994b). The presteady-state currents were interpreted according to a six-state kinetic model for the cotransporter proposed by Parent *et al.* (1992a, b) (Fig. 1-5a). This model assumes that the transporter is negatively charged (valence -2) and that two Na^+ ions bind to the transporter before the sugar binds (Parent *et al.*, 1992a, b; Wright *et al.*, 1994b). In the absence of sugar, the main carrier states present are C' , CNa_2' , C'' , and CNa_2'' (C' is the empty carrier facing the external face of the membrane; C'' is the empty carrier facing the internal face of the membrane; CNa_2' is the carrier bound to Na^+ facing the external face of the membrane; CNa_2'' is the carrier bound to Na^+ facing the internal face of the membrane) (Parent *et al.*, 1992a, b). Since the intracellular fluid is sugar-free and contains a low concentration of Na^+ (oocyte intracellular concentration of Na^+ is 4 - 22 mM), the majority of SGLT1 (75 %) is in the form CNa_2' (Dascal, 1987; Parent *et al.*, 1992a, b). C' and C'' represent 15 and 7 %, respectively, of the carriers present at a

holding potential of -50 mV (Parent *et al.*, 1992a, b). Rapid depolarization of the membrane potential from -50 mV to a positive potential (*ie.* +50 mV) results in the dissociation of CNa_2' into external Na^+ and C' , and then the negatively charged empty carriers (C') reorientate in the membrane electric field to the internal face of the membrane (C'') (Parent *et al.*, 1992a, b; Wright *et al.*, 1994b). Presteady-state currents are therefore the net result of the rearrangement of three carrier states: $CNa_2' \rightarrow C' \rightarrow C''$ (Fig. 1-5b). Approximately 30 % of this charge movement is due to Na^+ dissociation from the carrier and 70 % to the reorientation of the transporter in the membrane (Parent *et al.*, 1992b; Loo *et al.*, 1993; Wright *et al.*, 1994b).

The magnitude of the presteady-state currents in SGLT1-producing oocytes may be modified by varying the holding potential, the concentration of external Na^+ , or the concentration of external sugar. As the holding potential was made more negative, the size of the presteady-state currents increased (Parent *et al.*, 1992a, b). The proposed kinetic model of Na^+ /glucose cotransport predicts that the number of transporters in the CNa_2' state will increase at more negative holding potentials, and therefore a greater proportion of carriers will be available for dissociation into external Na^+ and C' following a rapid depolarization of the membrane potential, resulting in a transient increase in C' (Parent *et al.*, 1992a, b). These events will lead to an increase in the number of negatively charged empty carriers reorienting within the membrane ($C' \rightarrow C''$) and to a corresponding increase in the magnitude of the presteady-state currents (Parent *et al.*, 1992a, b). As the concentration of external Na^+ was reduced, the maximum charge translocated was decreased. At a holding potential of -50 mV and saturating concentrations of Na^+ , the majority of carriers (75 %) are in the form CNa_2' . When the external concentration of Na^+ is significantly reduced (from 100 to 10 mM), at the same membrane potential, only 3 % of all carriers are in the CNa_2' state (Parent *et al.*, 1992a, b). As a result of this reduced concentration of CNa_2' , the progression $CNa_2' \rightarrow C' \rightarrow C''$, in response to a rapid depolarization of the membrane, is significantly reduced, virtually eliminating the presteady-state currents (Parent *et al.*, 1992a, b). The maximum charge translocated was also reduced following the addition of sugar to the external Na^+ solution. In the presence of both external Na^+ and sugar (S), the

major carrier states are CNa_2'' , CNa_2S' and C'' , with CNa_2' representing only 8 % of the carriers present (Parent *et al.*, 1992a, b). The addition of sugar decreases the magnitude of the presteady-state currents by reducing the number of carriers in the CNa_2' state (Parent *et al.*, 1992a, b).

Presteady-state currents provide estimates of the number of functional carriers expressed in the oocyte plasma membrane. Integration of current transients yields the charge transfer (Q). The maximum charge transfer (Q_{max}), obtained from a plot of membrane potential (V_m) *versus* charge (Q), is proportional to the number of transporters expressed in the oocyte plasma membrane, and is predicted by the function $N = Q_{max}/Z\delta e_o$, where N is equal to the number of transporters in the membrane, Z is the apparent valence of the moving charge, δ is the effective fraction of the membrane field sensed by the movable charge, and e_o is the elementary charge (Loo *et al.*, 1993; Wright *et al.*, 1994b; Klamo *et al.*, 1996). Integration of the SGLT1 presteady-state currents yielded Q_{max} values of 120 nC, which correspond to 10^{12} transporters per oocyte (Wright *et al.*, 1994b).

C. Stoichiometric ratio of the Na^+ /glucose cotransporter

One aspect of the SGLT1 kinetic model that has been extensively investigated is the coupling ratio of the transported substrates. The Na^+ /glucose coupling ratio is of physiological importance because it determines the concentrating capacity for coupled sugar transport and the energetic expenditure required to maintain such a transport (Mackenzie *et al.*, 1998). The higher the ion-substrate coupling ratio (one or more Na^+ ions transported per substrate molecule), the greater the ability to transport sugars against their concentration gradient and achieve higher intracellular concentrations within the cell. Early studies of the SGLT1 coupling ratio employed radiolabeled flux measurements in intestinal membrane vesicles (Kimmich and Randles, 1980, 1984). A Na^+ /glucose coupling ratio of 1:1 was reported under conditions when the membrane potential was not controlled (Kimmich and Randles, 1984). When the membrane potential was voltage-clamped, the coupling ratio approached a value of 2:1 (Kimmich

and Randles, 1980, 1984). Using the *Xenopus* oocyte expression system, it was concluded that two Na⁺ ions were transported per sugar molecule (Ikeda *et al.*, 1989; Parent *et al.*, 1992a). This proposed stoichiometry was determined indirectly from the Hill coefficient of the sigmoidal activation curve by extracellular Na⁺, with values ranging from 1.6 to 1.9 (Ikeda *et al.*, 1989; Parent *et al.*, 1992a). Hill analysis of Na⁺ activation curves provides an index of the number of Na⁺ ions necessary to activate the transport process, but does not necessarily determine the number of Na⁺ ions that actually enter the cell as a result of transport activity (Weiss, 1997). More direct investigations of the Na⁺/glucose coupling ratio have included (i) the simultaneous determination of transporter-specific Na⁺ currents and radioactive sugar uptake from the same oocyte under voltage-clamp conditions (Lee *et al.*, 1994; Mackenzie *et al.*, 1998), and (ii) the measurement of reversal potentials (Chen *et al.*, 1995). Comparison of radiolabeled sugar uptake and Na⁺ currents yielded a coupling ratio of 1.6 at a holding potential of -70 mV and 1.9 at -110 mV (Mackenzie *et al.*, 1998). The lower coupling ratio obtained at -70 mV may be due to incomplete dissociation of Na⁺ from the inward facing conformation of the transporter (Mackenzie *et al.*, 1998). Incomplete dissociation of Na⁺ from the internal surface of the membrane would result in the recycling of Na⁺ back to the extracellular face of the membrane through the internal 'leak' pathway (CNa₂' ← CNa₂'') and would therefore reduce the magnitude of the inward current, hence underestimating the Na⁺/glucose coupling ratio (Mackenzie *et al.*, 1998). At more negative potentials, dissociation of Na⁺ from the internal face of the cotransporter would be more complete and the magnitude of the inward current would not be underestimated, therefore yielding a more accurate coupling ratio. The second direct method to determine the SGLT1 Na⁺/sugar coupling ratio involved measurement the zero current potential for cotransport (Chen *et al.*, 1995). Using the two-microelectrode voltage clamp technique, current-voltage (I-V) curves were performed at various sugar concentrations. From these curves, the reversal potential (V_r) was calculated and plotted against sugar concentration. The slope of the linear relationship between the two parameters indicated a coupling ratio of ~ 2.3 Na⁺ ions transported per sugar molecule (Chen *et al.*, 1995). A more accurate measure of the coupling ratio by this approach using the cut-open oocyte technique to

control internal concentrations of sugar and Na^+ yielded a stoichiometry of ~ 1.96 (Chen *et al.*, 1995). Thus, a variety of techniques indicate a 2:1 coupling stoichiometry (Lee *et al.*, 1994; Chen *et al.*, 1995; Mackenzie *et al.*, 1998).

Research Objectives

Transport of nucleosides has been extensively studied over the last 35 years in a variety of prokaryotic and eukaryotic cells and tissues. A number of distinct nucleoside transport processes have been demonstrated on the basis of transport mechanism (Na^+ -dependent or Na^+ -independent), permeant selectivity, kinetic properties, and inhibitor sensitivity. The human and other mammalian membrane proteins responsible for most of these activities have now been identified. The overall goal of my research was to use the two-microelectrode voltage clamp in conjunction with heterologous expression in *Xenopus laevis* oocytes to study the electrophysiological properties of recombinant human members of the concentrative nucleoside transporter (CNT) family. Specific objectives were: (i) to demonstrate that transport of substrate by members of the CNT family is electrogenic (*Chapters II-IV*); (ii) to investigate the steady-state kinetic properties of hCNT1 (*Chapter II*); (iii) to investigate the steady-state kinetic properties of h/mCNT3 and reveal the unique transport characteristics of this protein; (iv) to demonstrate the presence of presteady-state currents for hCNT3 and characterize these currents to gain information about transporter turnover number and partial reactions in the Na^+ /nucleoside cotransport cycle (*Chapter IV*). At the time my project was initiated, no electrophysiological studies of CNTs had been undertaken.

Table 1-1. Members of the Equilibrative Nucleoside Transporter (ENT) Family.

NT	Species	Amino acids	GenBank™ accession	Permeant selectivity ^a	References
hENT1	<i>Homo sapiens</i>	456	AAC51103	nucleosides	Griffiths <i>et al.</i> , 1997a
rENT1	<i>Rattus norvegicus</i>	457	AAb88049	nucleosides	Yao <i>et al.</i> , 1997
mENT1.1	<i>Mus musculus</i>	460	AAF76429	nucleosides	Choi <i>et al.</i> , 2000
hENT2	<i>Homo sapiens</i>	456	AAC39526	nucleosides, nucleobases	Griffiths <i>et al.</i> , 1997b
rENT2	<i>Rattus norvegicus</i>	456	AAB88050	nucleosides, nucleobases	Yao <i>et al.</i> , 1997
mENT2	<i>Mus musculus</i>	456	AAF76431	ND	Kiss <i>et al.</i> , 2000
rbENT2	<i>Oryctolagus cuniculus</i>	456	AAK11605	ND	
rbENT2A	<i>Oryctolagus cuniculus</i>	415	AAK11606	ND	
hENT3	<i>Homo sapiens</i>	475	AAK00958	ND	
mENT3	<i>Mus musculus</i>	474	AAK00957	ND	Struasberg <i>et al.</i> , 2002
hENT4	<i>Homo sapiens</i>	430	AAH25599	ND	Acimovic and Coe, 2002
mENT4	<i>Mus musculus</i>	428	DAA00308	ND	
DmENT1	<i>Drosophila melanogaster</i>	476	AAF52405	ND	
DmENT2	<i>Drosophila melanogaster</i>	458	AAF51506	ND	
DmENT3	<i>Drosophila melanogaster</i>	586	AAF49871	ND	
AtENT1	<i>Arabidopsis thaliana</i>	428	AAC18807 AAF26446	nucleosides except uridine	
AtENT2	<i>Arabidopsis thaliana</i>	417	AAF04424	ND	
AtENT3	<i>Arabidopsis thaliana</i>	418	CAB81054	ND	
AtENT4	<i>Arabidopsis thaliana</i>	418	CAB81055	ND	
AtENT5	<i>Arabidopsis thaliana</i>	419	CAB81056	ND	
AtENT6	<i>Arabidopsis thaliana</i>	418	CAB81053	ND	
AtENT7	<i>Arabidopsis thaliana</i>	417	AAD25545	ND	
AtENT8	<i>Arabidopsis thaliana</i>	389	AAG10625	ND	
CeENT1	<i>Caenorhabditis elegans</i>	445	CAA92642	nucleosides	Young <i>et al.</i> , 2001
CeENT2	<i>Caenorhabditis elegans</i>	450	CAB01882	ND	
CeENT3	<i>Caenorhabditis elegans</i>	729	CAB01223	ND	
CeENT4	<i>Caenorhabditis elegans</i>	451	CAB62793	ND	
CeENT5	<i>Caenorhabditis elegans</i>	434	AAA98003	ND	
CeENT6	<i>Caenorhabditis elegans</i>	384	CAB03075	ND	
TeAT1	<i>Trypanosoma equiperdum</i>	463	CAC41330	ND	
TbAT1	<i>Trypanosoma brucei</i>	463	AAD45278	adenosine, adenine	Mäser <i>et al.</i> , 1999
TbNT2	<i>Trypanosoma brucei</i>	463	AAF04490	adenosine, inosine, guanosine	Sanchez <i>et al.</i> , 1999
TbNT2/927	<i>Trypanosoma brucei</i>	462	pending	adenosine, inosine	Sanchez <i>et al.</i> , 2002

(continued on following page)

NT, nucleoside transporter; ^a, purine and pyrimidine nucleosides/nucleobases unless otherwise indicated; ND, not determined

Table 1-1 (continued). Members of the Equilibrative Nucleoside Transporter (ENT) Family.

NT	Species	Amino acids	GenBank™ accession	Permeant selectivity ^a	References
TbNT3	<i>Trypanosoma brucei</i>	464	pending	ND	
TbNT4	<i>Trypanosoma brucei</i>	462	pending	ND	
TbNT5	<i>Trypanosoma brucei</i>	463	pending	adenosine, inosine	Sanchez <i>et al.</i> , 2002
TbNT6	<i>Trypanosoma brucei</i>	462	pending	adenosine, inosine, hypoxanthine	Sanchez <i>et al.</i> , 2002
TbNT7	<i>Trypanosoma brucei</i>	467	pending	adenosine, inosine, hypoxanthine	Sanchez <i>et al.</i> , 2002
TbNT8	<i>Trypanosoma brucei</i>	ND	pending	ND	
TbNT9	<i>Trypanosoma brucei</i>	ND	pending	ND	
LdNT1.1/ LdNT1.2	<i>Leishmania donovani</i>	491	AAC32597 AAC32315	adenosine, pyrimidine nucleosides	Vasudevan <i>et al.</i> , 1998
LdNT2	<i>Leishmania donovani</i>	499	AAF74264	guanosine, inosine	Carter <i>et al.</i> , 2000a
LmaNT1	<i>L. mexicana amazonensis</i>	491	AAL87658	ND	
LmaNT2	<i>L. mexicana amazonensis</i>	499	AAL87659	ND	
L2464.04	<i>Leishmania major</i>	501	CAB96736	ND	
CfNT1	<i>Crithidia fasciculata</i>	497	AAG22610	ND	
CfNT2	<i>Crithidia fasciculata</i>	502	AAG22611	ND	
TgAT	<i>Toxoplasma gondii</i>	462	AAF03247	adenosine	Chiang <i>et al.</i> , 1999
PfENT1/ PfNT1	<i>Plasmodium falciparum</i>	422	AAF67613 AAG09713	nucleosides, nucleobases	Carter <i>et al.</i> , 2000b Parker <i>et al.</i> , 2000
EhENT1	<i>Entamoeba histolytica</i>	396	S49592	ND	
FUN26	<i>Saccharomyces cerevisiae</i>	517	AAC04935	nucleosides	Vickers <i>et al.</i> , 2000a

NT, nucleoside transporter; ^a, purine and pyrimidine nucleosides/nucleobases unless otherwise indicated; ND, not determined

Table 1-2. Concentrative Nucleoside Transport Processes of Mammalian Cells.

NT Process	Permeant selectivity	NT protein	Inhibitor Sensitivity ^a	References
System <i>cit</i>	Pyrimidine nucleosides, adenosine	CNT1	No	Huang <i>et al.</i> , 1994 Ritzel <i>et al.</i> , 1997
System <i>cif</i>	Purine nucleosides, uridine	CNT2 ^b	No	Che <i>et al.</i> , 1995 Yao <i>et al.</i> , 1996b
System <i>cib</i>	Purine and pyrimidine nucleosides	CNT3	No	Ritzel <i>et al.</i> , 2001
System <i>cs</i>	Adenosine analogs	ND	Yes	Belt <i>et al.</i> , 1993 Paterson <i>et al.</i> , 1993
System <i>csg</i>	Guanosine	ND	Yes	Flanagan and Meckling-Gill, 1997

NT, nucleoside transport; ^a,sensitivity to inhibition by NBMPR; ^b,also known as SPNT; ND, not determined

Table 1-3. Members of the Concentrative Nucleoside Transporter (CNT) Family.

NT	Species	Amino Acids	GenBank™ Accession	Permeant Selectivity ^a	References
hCNT1a	<i>Homo sapiens</i>	650	AAB53837	pyrimidine nucleosides, adenosine	Ritzel <i>et al.</i> , 1997
hCNT1b	<i>Homo sapiens</i>	649	AAB53838	pyrimidine nucleosides, adenosine	Ritzel <i>et al.</i> , 1997
hCNT1c	<i>Homo sapiens</i>	649	AAB53839	pyrimidine nucleosides, adenosine	Ritzel <i>et al.</i> , 1997
rCNT1	<i>Rattus norvegicus</i>	648	AAB03626	pyrimidine nucleosides, adenosine	Huang <i>et al.</i> , 1994
pkCNT1	<i>Sus scrofa</i>	647	AAC17947	pyrimidine nucleosides, adenosine	Pajor, 1998
hCNT2	<i>Homo sapiens</i>	658	AAB88539	purine nucleosides, uridine	Ritzel <i>et al.</i> , 1998
SPNT	<i>Rattus norvegicus</i>	659	Q62773	purine nucleosides, uridine	Che <i>et al.</i> , 1995
rCNT2	<i>Rattus norvegicus</i>	659	AAD00159	purine nucleosides, uridine	Yao <i>et al.</i> , 1996b
mCNT2	<i>Mus musculus</i>	660	AAC28858	purine nucleosides, uridine	Patel <i>et al.</i> , 2000
rbCNT2	<i>Oryctolagus cuniculus</i>	658	AAF80451	purine nucleosides, uridine	Gerstin <i>et al.</i> , 2000
hCNT3	<i>Homo sapiens</i>	691	AAG22551	nucleosides	Ritzel <i>et al.</i> , 2001
rCNT3	<i>Rattus norvegicus</i>	705	AAL27097	nucleosides	
mCNT3	<i>Mus musculus</i>	703	AAG22552	nucleosides	Ritzel <i>et al.</i> , 2001
hfCNT	<i>Eptatretus stouti</i>	683	AAD52151	nucleosides	Yao <i>et al.</i> , 2002a
CaCNT	<i>Candida albicans</i>	608	pending	purine nucleosides, uridine	Loewen <i>et al.</i> , 2003b
AfCNT	<i>Aspergillus fumigatus</i>	598	pending	ND	
F27E11.1	<i>Caenorhabditis elegans</i>	568	AAB65255	ND	Waterston, 1998
CeCNT3	<i>Caenorhabditis elegans</i>	575	AAB65256	nucleosides except cytidine	Waterston, 1998 Xiao <i>et al.</i> , 2001
CG11778	<i>Drosophila melanogaster</i>	528	AAF58996	ND	Adams <i>et al.</i> , 2000
CG8083	<i>Drosophila melanogaster</i>	603	AAF58997	ND	Adams <i>et al.</i> , 2000
NupC	<i>Escherichia coli</i>	400	AAC75452	nucleosides except guanosine	Craig <i>et al.</i> , 1997
YeiJ	<i>Escherichia coli</i>	418	AAA60513	ND	Blattner <i>et al.</i> , 1997
YeiM	<i>Escherichia coli</i>	416	AAA60518	ND	Blattner <i>et al.</i> , 1997
SAV0313	<i>Staphylococcus aureus</i>	406	BAB56475	ND	Kuroda <i>et al.</i> , 2001
SAV0521	<i>Staphylococcus aureus</i>	404	BAB56683	ND	Kuroda <i>et al.</i> , 2001
SAV0645	<i>Staphylococcus aureus</i>	409	BAB56807	ND	Kuroda <i>et al.</i> , 2001
CPE1284	<i>Clostridium perfringens</i>	393	BAB80990	ND	Shimizu <i>et al.</i> , 2002
CPE2496	<i>Clostridium perfringens</i>	408	BAB82202	ND	Shimizu <i>et al.</i> , 2002
NupC	<i>Bacillus subtilis</i>	393	P39141	ND	Saxild <i>et al.</i> , 1996
YxjA	<i>Bacillus subtilis</i>	397	BAA11702	ND	Kunst <i>et al.</i> , 1997
YutK	<i>Bacillus subtilis</i>	404	CAB15208	ND	Kunst <i>et al.</i> , 1997
NupC	<i>Yersinia pestis</i>	394	CAC92227	ND	Parkhill <i>et al.</i> , 2001b
YPO0435	<i>Yersinia pestis</i>	423	CAC89293	ND	Parkhill <i>et al.</i> , 2001b

(continued on following page)

NT, nucleoside transporter; ^a, purine and pyrimidine nucleosides/nucleobases unless otherwise indicated; ND, not determined; ^b, based on prediction of the coding sequence from unfinished genome sequence databases

Table 1-3 (continued). Members of the Concentrative Nucleoside Transporter (CNT) Family.

NT	Species	Amino Acids	GenBank™ Accession	Permeant Selectivity ^a	References
VCA0179	<i>Vibrio cholerae</i>	402	AAF96092	ND	Heidelberg <i>et al.</i> , 2000
VC1953	<i>Vibrio cholerae</i>	405	AAF95101	ND	Heidelberg <i>et al.</i> , 2000
VC2352	<i>Vibrio cholerae</i>	418	AAF95495	ND	Heidelberg <i>et al.</i> , 2000
NupC	<i>Salmonella typhimurium</i>	400 ^b	CAD07647	ND	Parkhill <i>et al.</i> , 2001a
spyM18_1932	<i>Streptococcus pyogenes</i>	400 ^b	AAK34582	ND	Ferretti <i>et al.</i> , 2001 Smoot <i>et al.</i> , 2002
CC2089	<i>Caulobacter crescentus</i>	426 ^b	AAK24060	ND	Nierman <i>et al.</i> , 2001
HP1180	<i>Helicobacter pylori</i>	418 ^b	AAD08224	ND	Tomb <i>et al.</i> , 1997
HI0519	<i>Haemophilus influenzae</i>	417 ^b	AAC22177	ND	Fleischmann <i>et al.</i> , 1995
BH1446	<i>Bacillus halodurans</i>	406 ^b	BAB05165	ND	Takami <i>et al.</i> , 1999
AlI0378	<i>Nostoc (Anabaena) sp.</i>	402 ^b	BAB72336	ND	Kaneko <i>et al.</i> , 2001
PM1292	<i>Pasteruella multocida</i>	420 ^b	AAK03376	ND	May <i>et al.</i> , 2001
CBORF01	<i>Clostridium botulinum</i>	407 ^b	pending	ND	
YeORF01	<i>Yersinia enterocolitica</i>	423 ^b	pending	ND	
YeORF02	<i>Yersinia enterocolitica</i>	394 ^b	pending	ND	
SpORF01	<i>Shewanella putrefusciens</i>	432 ^b	pending	ND	
SpORF02	<i>Shewanella putrefusciens</i>	422 ^b	pending	ND	
SpORF03	<i>Shewanella putrefusciens</i>	423 ^b	pending	ND	
SpORF04	<i>Shewanella putrefusciens</i>	401 ^b	pending	ND	
HdORF01	<i>Haemophilus ducreyi</i>	422 ^b	pending	ND	
BaORF01	<i>Bacillus anthracis</i>	392 ^b	pending	ND	
BaORF02	<i>Bacillus anthracis</i>	392 ^b	pending	ND	
BaORF03	<i>Bacillus anthracis</i>	393 ^b	pending	ND	
BaORF04	<i>Bacillus anthracis</i>	398 ^b	pending	ND	
BaORF05	<i>Bacillus anthracis</i>	391 ^b	pending	ND	
BaORF06	<i>Bacillus anthracis</i>	400 ^b	pending	ND	
BaORF07	<i>Bacillus anthracis</i>	396 ^b	pending	ND	
BcORF01	<i>Bacillus cereus</i>	392 ^b	pending	ND	
BcORF01	<i>Bacillus cereus</i>	393 ^b	pending	ND	
BcORF02	<i>Bacillus cereus</i>	393 ^b	pending	ND	
BcORF03	<i>Bacillus cereus</i>	393 ^b	pending	ND	
BcORF04	<i>Bacillus cereus</i>	398 ^b	pending	ND	
BcORF05	<i>Bacillus cereus</i>	397 ^b	pending	ND	
BcORF06	<i>Bacillus cereus</i>	403 ^b	pending	ND	

NT, nucleoside transporter; ^a,purine and pyrimidine nucleosides/nucleobases unless otherwise indicated; ND, not determined; ^b,based on prediction of coding sequence from unfinished genome sequence databases

Table 1-4. Members of the Nucleoside/H⁺ Symporter (NHS) Family.

Transporter	Species	Amino acids	GenBank™ accession	Permeant selectivity	References
NupG	<i>Escherichia coli</i>	418	P09452	purine and pyrimidine nucleosides	Westh Hansen <i>et al.</i> , 1987 Blattner <i>et al.</i> , 1997
XapB	<i>Escherichia coli</i>	418	P45562	purine and pyrimidine nucleosides	Seeger <i>et al.</i> , 1995 Blattner <i>et al.</i> , 1997
YegT	<i>Escherichia coli</i>	425	BAA15967	ND	Itoh <i>et al.</i> , 1996 Blattner <i>et al.</i> , 1997
STY2371	<i>Salmonella enterica</i>	423	CAD02521	ND	Parkhill <i>et al.</i> , 2001a
STY2657	<i>Salmonella enterica</i>	418	CAD07653	ND	Parkhill <i>et al.</i> , 2001a
STY3268	<i>Salmonella enterica</i>	418	CAD02938	ND	Parkhill <i>et al.</i> , 2001a
CC1628	<i>Caulobacter crescentus</i>	413	AAK23606	ND	Nierman <i>et al.</i> , 2001
ECU11_1880	<i>Encephalitozoon cuniculi</i>	495	CAD26098	ND	Katinka <i>et al.</i> , 2001
NupG	<i>Salmonella typhimurium</i>	418	AAL21988	ND	McClelland <i>et al.</i> , 2001

ND, not determined

Table 1-5. Members of the Tsx Channel-Forming Protein Family.

Porin	Species	Amino acids	GenBank™ accession	Function	References
Tsx	<i>Escherichia coli</i>	294	AAA24701	nucleoside ^a facilitator	Bremer <i>et al.</i> , 1990
Tsx	<i>Enterobacter aerogenes</i>	294	CAA81397	nucleoside ^a facilitator	Nieweg and Bremer, 1997
Tsx	<i>Klebsiella pneumoniae</i>	294	CAA81396	nucleoside ^a facilitator	Nieweg and Bremer, 1997
Tsx	<i>Salmonella typhimurium</i>	287	CAD08869	nucleoside ^a facilitator	Nieweg and Bremer, 1997
OmpK	<i>Vibrio parahaemolyticus</i>	263	BAA09613	ND	Inoue <i>et al.</i> , 1995a
OmpK	<i>Vibrio cholerae</i>	296	AAF95449	ND	Heidelberg <i>et al.</i> , 2000

^a,purine and pyrimidine nucleosides; ND, not determined

Table 1-6. Members of the Uracil/Allantoin Permease Family.

Transporter	Species	Amino acids	GenBank™ accession	Permeant selectivity	References
FUI1	<i>Saccharomyces cerevisiae</i>	639	CAA84862	uridine	Jund and Lacroute, 1970 Feldmann <i>et al.</i> , 1994 Wagner <i>et al.</i> , 1998
FUR4	<i>Saccharomyces cerevisiae</i>	633	P05316	uracil, 5-fluorouridine	Jund <i>et al.</i> , 1988 Smits <i>et al.</i> , 1994
DAL4	<i>Saccharomyces cerevisiae</i>	635	CAA78826	allantoin	Yoo <i>et al.</i> , 1992
THI10	<i>Saccharomyces cerevisiae</i>	598	BAA09504	thiamin, adenosine	Enjo <i>et al.</i> , 1997
YORO71c	<i>Saccharomyces cerevisiae</i>	598	Q08485	ND	Enjo <i>et al.</i> , 1997 Valens <i>et al.</i> , 1997
YOR192c	<i>Saccharomyces cerevisiae</i>	599	Q08579	ND	Enjo <i>et al.</i> , 1997
NCS1	<i>Schizosaccharomyces pombe</i>	581	CAB16258	uracil	Wood <i>et al.</i> , 2002
FUR4	<i>Schizosaccharomyces pombe</i>	589	CAA67256	uracil	de Montigny <i>et al.</i> , 1998
SPBC1683.05	<i>Schizosaccharomyces pombe</i>	559	CAB91167	ND	
SPAC29-B12.14c	<i>Schizosaccharomyces pombe</i>	581	AB16258	ND	
ywoE	<i>Bacillus subtilis</i>	409	CAB05378	ND	Presecan <i>et al.</i> , 1997
BMEI0155	<i>Brucella melitensis</i>	409	AAL51337	ND	DelVecchio <i>et al.</i> , 2002
ybbW	<i>Escherichia coli</i>	437	AAC73613	ND	Blattner <i>et al.</i> , 1997
YBBW	<i>Escherichia coli</i>	484	P75712	ND	Blattner <i>et al.</i> , 1997
OB2293	<i>Oceanobacillus iheyensis</i>	419	BAC14249	ND	Takami <i>et al.</i> , 2002
pyrP	<i>Streptococcus pyogenes</i>	404	AAM76116	ND	Beres <i>et al.</i> , 2002
SSO1905	<i>Sulfolobus solfataricus</i>	488	AAK42097	ND	She <i>et al.</i> , 2001
SSO2042	<i>Sulfolobus solfataricus</i>	492	AAK42228	ND	She <i>et al.</i> , 2001

ND, not determined

Table 1-7. Members of the Nucleoside Permease (NUP) Family.

Transporter	Species	Amino acids	GenBank™ accession	Permeant selectivity	References
NUP	<i>Candida albicans</i>	407	AAC64324	purine nucleosides	Detke, 1998
SPCC285.05	<i>Schizosaccharomyces pombe</i>	348	CAA20844	ND	Wood <i>et al.</i> , 2002
BMEI0649	<i>Brucella melitensis</i>	345	AAL 51650	ND	DelVecchio <i>et al.</i> , 2002
CC0187	<i>Caulobacter crescentus</i>	374	AAK22174	ND	Nierman <i>et al.</i> , 2001
RSc0798	<i>Ralstonia solanacearum</i>	381	CAD14500	ND	Salanoubat <i>et al.</i> , 2002
RSc0799	<i>Ralstonia solanacearum</i>	346	CAD14501	ND	Salanoubat <i>et al.</i> , 2002

ND, not determined

Table 1-8. Members of the Organic Cation Transporter (OCT) Family.

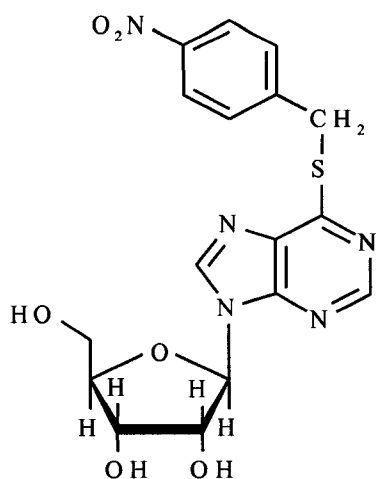
Transporter	Species	Amino acids	GenBank™ accession	Transport Mode	References
hOCTN1	<i>Homo sapiens</i>	551	BAA23356	Na ⁺ , H ⁺ -dependent	Tamai <i>et al.</i> , 1997
rOCTN1	<i>Rattus norvegicus</i>	553	AAD46922	Na ⁺ -independent H ⁺ -dependent	Wu <i>et al.</i> , 2000
mOCTN1	<i>Mus musculus</i>	553	BAA36626	Na ⁺ , H ⁺ -dependent	Tamai <i>et al.</i> , 2000
hOCTN2	<i>Homo sapiens</i>	557	AAC24828	Na ⁺ , H ⁺ -dependent	Wu <i>et al.</i> , 1998
rOCTN2	<i>Rattus norvegicus</i>	557	AAD54059	Na ⁺ , H ⁺ -dependent	Wu <i>et al.</i> , 1999
mOCTN2	<i>Mus musculus</i>	557	AAD54060	Na ⁺ , H ⁺ -dependent	Wu <i>et al.</i> , 1999
mOCTN3	<i>Mus musculus</i>	564	BAA78343	Na ⁺ , H ⁺ -independent	Tamai <i>et al.</i> , 2000
hOCT1	<i>Homo sapiens</i>	554	AAB67703	electrogenic/potential sensitive	Zhang <i>et al.</i> , 1997b
rOCT1/ rOCT1A	<i>Rattus norvegicus</i>	556 430	s50862 AAB67702	electrogenic/potential sensitive	Gründemann <i>et al.</i> , 1994 Zhang <i>et al.</i> , 1997a
mOCT1	<i>Mus musculus</i>	556	AAB19097	electrogenic/potential sensitive	Schweifer and Barlow, 1996
rbOCT1	<i>Oryctolagus cuniculus</i>	554	AAC23661	electrogenic/potential sensitive	Terashita <i>et al.</i> , 1998
hOCT2/ hOCT2-A	<i>Homo sapiens</i>	555 483	CAA66978 BAC02720	electrogenic/potential sensitive	Gorboulev <i>et al.</i> , 1997 Urakami <i>et al.</i> , 2002
rOCT2	<i>Rattus norvegicus</i>	593	BAA11754	electrogenic/potential sensitive	Okuda <i>et al.</i> , 1996
mOCT2	<i>Mus musculus</i>	553	CAA06827	electrogenic/potential sensitive	Mooslehner and Allen, 1999
rbOCT2	<i>Oryctolagus cuniculus</i>	554	AAM83256	electrogenic/potential sensitive	Xiaohong <i>et al.</i> , 2001
pOCT2	<i>Sus scrofa</i>	554	CAA70567	cation/H ⁺ antiporter	Gründemann <i>et al.</i> , 1997
hOCT3	<i>Homo sapiens</i>	551	BAA76350	electrogenic/potential sensitive	Nishiwaki <i>et al.</i> , 1998
rOCT3	<i>Rattus norvegicus</i>	551	AAC40150	electrogenic/potential sensitive	Kekuda <i>et al.</i> , 1998
mOCT3	<i>Mus musculus</i>	551	AAD20978	ND	Verhaagh <i>et al.</i> , 1999
hOCT4	<i>Homo sapiens</i>	594	BAA76351	electrogenic/potential sensitive	Nishiwaki <i>et al.</i> , 1998

ND, not determined

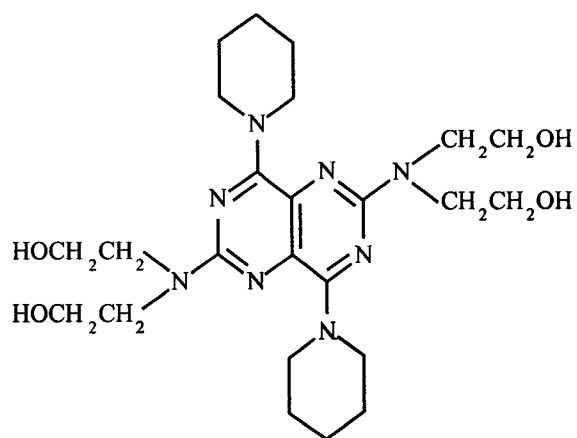
Table 1-9. Members of the Organic Anion Transporter (OAT) Family.

Transporter	Species	Amino acids	GenBank™ accession	Transport Mode	Substrate	References
hOAT1/ hOAT1-1	<i>Homo sapiens</i>	550	AAD19356 BAA75072	exchanger	PAH, dicarboxylates, cyclic nucleotides, neurotransmitter metabolites, anionic drugs, AZT, GCV	Race <i>et al.</i> , 1999 Hosoyamada <i>et al.</i> , 1999
rOAT1	<i>Rattus norvegicus</i>	551	AAC18772	exchanger	PAH, dicarboxylates, cyclic nucleotides, neurotransmitter metabolites, anionic drugs, AZT, ACV, zalcitabine, didanosine, lamivudine, stavudine, trifluridine	Sekine <i>et al.</i> , 1997 Sweet <i>et al.</i> , 1997
rbOAT1	<i>Oryctolagus cuniculus</i>	551	CAB62587	ND	ND	
mOAT1/ NKT	<i>Mus musculus</i>	545	AAC53112	ND	ND	Lopez-Nieto <i>et al.</i> , 1997
fROAT	<i>Pseudo-pleuronectes americanus</i>	562	CAB09724	exchanger	PAH	Wolff <i>et al.</i> , 1997
hOAT2	<i>Homo sapiens</i>	548	AAD37091	ND	most organic anions, salicylate, prostaglandin F, AZT	Takeda <i>et al.</i> , 2002
rOAT2/NLT	<i>Rattus norvegicus</i>	535	AAA57157	facilitator?	PAH, salicylate, dicarboxylate, PGE	Simonson <i>et al.</i> , 1994 Sekine <i>et al.</i> , 1998
mOAT2	<i>Mus musculus</i>	540	AAH13474	ND	ND	
hOAT3	<i>Homo sapiens</i>	568	AAD19357	ND	ND	Race <i>et al.</i> , 1999
hOAT3*	<i>Homo sapiens</i>	543	BAB47393	ND	PAH, estrone sulfate, PGE, methotrexate, cimetidine, cAMP, glutarate, NSAIDs, diuretics, antibiotics, AZT	Cha <i>et al.</i> , 2001
rOAT3	<i>Mus musculus</i>	536	BAA82552	facilitator?	PAH, estrone sulfate, PGE, methotrexate, cimetidine, cAMP, glutarate, NSAIDs, diuretics, antibiotics, AZT	Kusuhara <i>et al.</i> , 1999
hOAT4	<i>Homo sapiens</i>	550	BAA95316	facilitator?	estrone sulfate, DHEA-s, AZT	Cha <i>et al.</i> , 2000

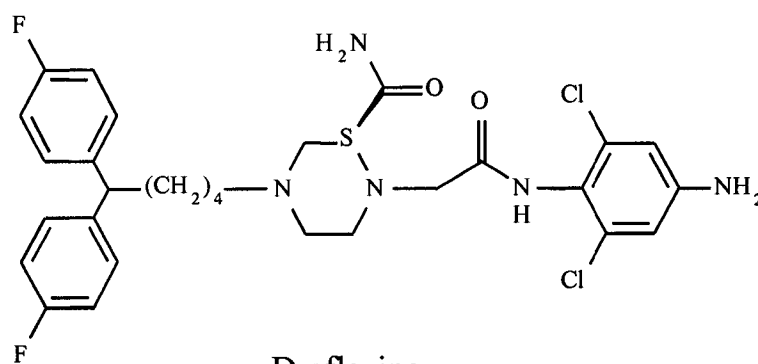
PAH, *p*-aminohippurate; AZT, 3'-azido-3'-deoxythymidine; GCV, ganciclovir; ACV, acyclovir; PGE, prostaglandin E; cAMP, adenosine 3', 5'-cyclic monophosphate; NSAIDs, nonsteroidal anti-inflammatory drugs; DHEA-s, dehydroepiandrosterone sulfate; ND, not determined



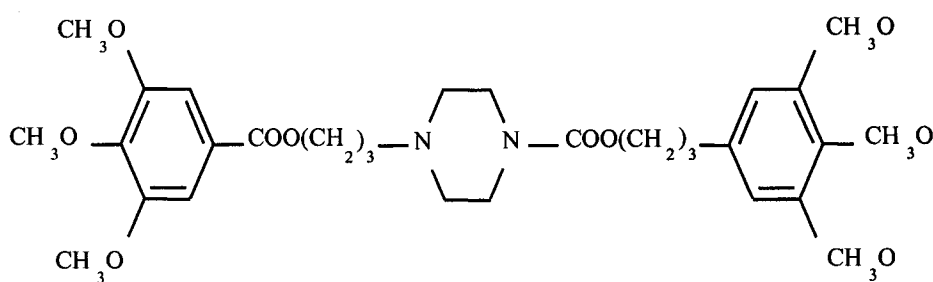
NBMPR



Dipyridamole



Draflazine



Dilazep

Figure 1-1. Inhibitors of some ENT-mediated transport processes. The structures of the nucleoside analog NBMPR and the coronary vasodilators dipyridamole, draflazine, and dilazep are presented.

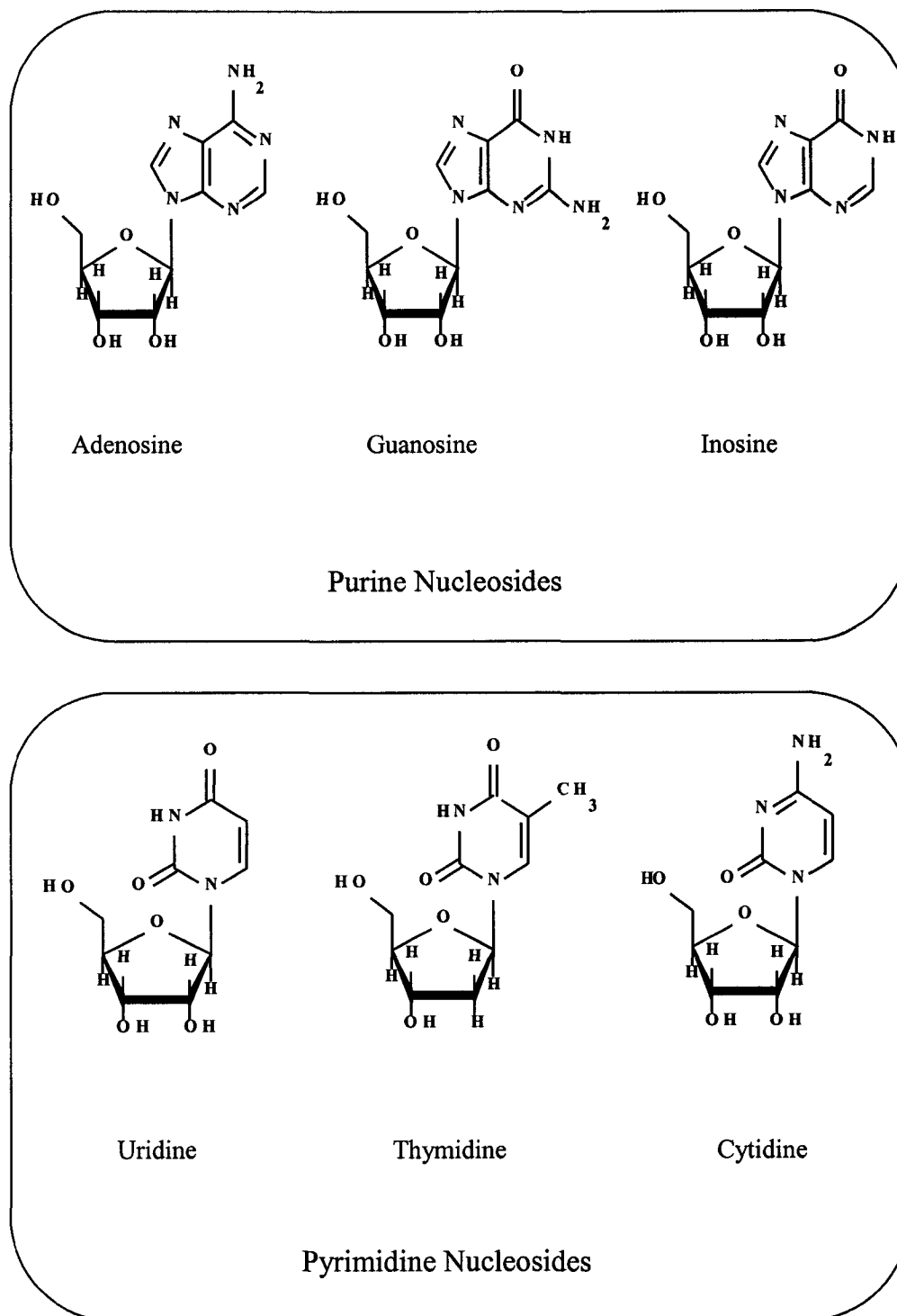


Figure 1-2. Chemical structures of physiological nucleosides. The physiologic purine and pyrimidine nucleosides transported by ENT and CNT proteins and by members of various other transporter families are shown.

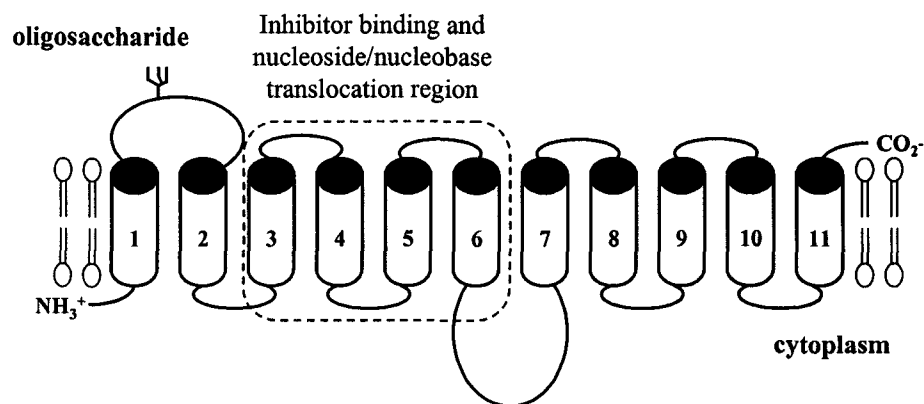


Figure 1-3. Topographical model of hENT1. Potential transmembrane helices are numbered (1 - 11) and the site of N-glycosylation is indicated. The transmembrane domains enclosed in the *dashed box* show the region (TMs 3 - 6) involved in recognition of transport inhibitors, nucleobases, and nucleosides.

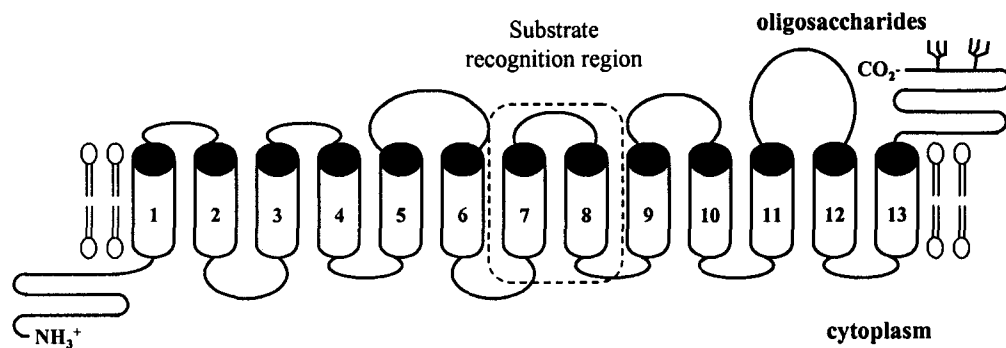
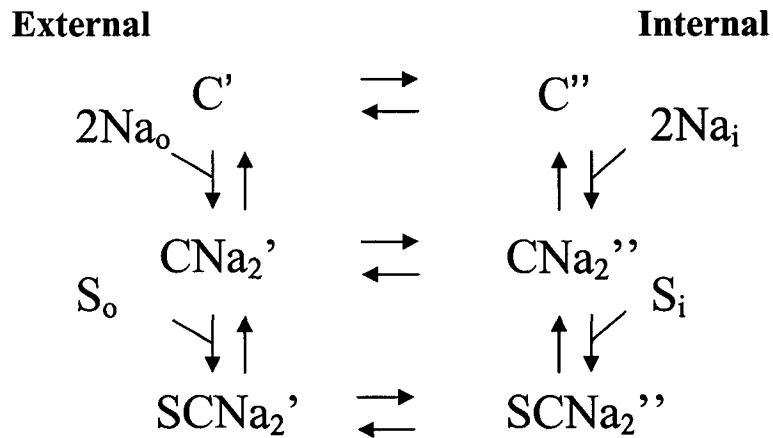


Figure 1-4. Topographical model of rCNT1. Potential transmembrane helices are numbered (1 - 13) and the sites of N-glycosylation are indicated. The transmembrane domains enclosed in the *dashed box* show the region (TMs 7 - 8) involved in substrate recognition.

A.



B.

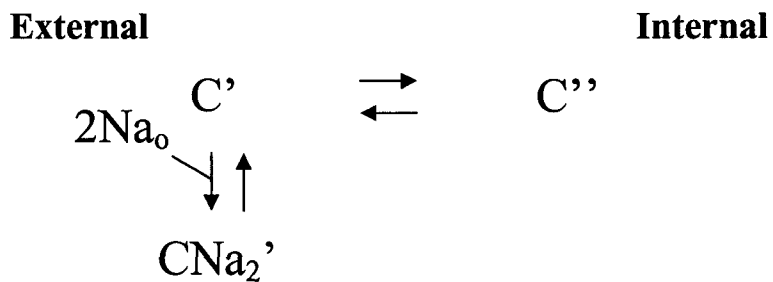


Figure 1-5. Na⁺/glucose cotransport by SGLT1. **A.** A model for Na⁺/glucose cotransport by SGLT1 is presented. C' is the empty carrier facing the external face of the membrane; C'' is the empty carrier facing the internal face of the membrane; CNa₂' is the carrier bound to Na⁺ facing the external face of the membrane; CNa₂'' is the carrier bound to Na⁺ facing the internal face of the membrane; SCNa₂' is the carrier bound to Na⁺ and sugar (S) facing the external face of the membrane; SCNa₂'' is the carrier bound to Na⁺ and sugar (S) facing the internal face of the membrane (Parent *et al.*, 1992a, b). **B.** Progression of the transporter through carrier stages following step-changes in the membrane potential, yielding presteady-state currents.

Bibliography

Acimovic Y and Coe IR. Molecular evolution of the equilibrative nucleoside transporter family: identification of novel family members in prokaryotes and eukaryotes. *Mol Biol Evol* 19(12): 2199-2210, 2002.

Adams MD, Celniker SE, Holt RA, Evans CA, Gocayne JD, et al. The genome sequence of *Drosophila melanogaster*. *Science* 287(5461): 2185-2195, 2000.

Aiba T, Sakurai Y, Tsukada S, and Korizumi T. Effects of probenecid and cimetidine on the renal excretion of 3'-azido-3'-deoxythymidine in rats. *J Pharmacol Exp Ther* 272: 94-99, 1995.

Baldwin SA, Mackey JR, Cass CE, and Young JD. Nucleoside transporters: molecular biology and implications for therapeutic development. *Mol Med Today* 5: 216-224, 1999.

Belt JA, Marina NM, Phelps DA, and Crawford CR. Nucleoside transport in normal and neoplastic cells. *Adv Enzyme Regul* 33: 235-252, 1993.

Bendayan R. Interaction of dipyridamole, a nucleoside transport inhibitor, with the renal transport of organic cations by LLCPK₁ cells. *Can J Physiol Pharmacol* 75: 52-56, 1997.

Benz R, Schmid A, Maier C, and Bremer E. Characterization of the nucleoside-binding site inside the Tsx channel of *Escherichia coli* outer membrane. Reconstitution experiments with lipid bilayer membranes. *Eur J Biochem* 176(3): 699-705, 1988.

Beres SB, Sylva GL, Barbian KD, Lei B, Hoff JS, Mammarella ND, Liu M-Y, Smoot JC, Porcella SF, Parkins LD, McCormick JK, Leung DYM, Schlievert PM, and Musser JM. Genome sequence of a serotype M3 strain of group A *Streptococcus*: phage-encoded toxins, the high-virulence phenotype, and clone emergence. *Proc Natl Acad Sci USA* 99(15): 10078-10083, 2002.

Blattner FR, Plunkett III G, Bloch CA, Perna NT, Burland V, Riley M, Collado-Vides J, Glasner JD, Rode CK, Mayhew GF, Gregor J, Davis NW, Kirkpatrick HA, Goeden MA, Rose DJ, Mau B, and Shao Y. The complete genome sequence of *Escherichia coli* K-12. *Science* 277: 1453-1462, 1997.

Bremer E, Middendorf A, Martinussen J, and Valentin-Hansen P. Analysis of the *tsx* gene, which encodes a nucleoside-specific channel-forming protein (Tsx) in the outer membrane of *Escherichia coli*. *Gene* 96: 59-65, 1990.

Busch AE, Waldegger S, Murer H, and Lang F. The molecules of proximal tubular transport: insights from electrophysiology. *Nephron* 72: 1-8, 1996.

Carter NS and Fairlamb AH. Arsenical-resistant trypanosomes lack an unusual adenosine transporter. *Nature* 361: 173175, 1993.

Carter NS, Berger BJ, and Fairlamb AH. Uptake of diamidine drugs by the P2 nucleoside transporter in melarsen-sensitive and -resistant *Trypanosoma brucei brucei*. *J Biol Chem* 270(47): 28153-27157, 1995.

Carter NS, Drew ME, Sanchez M, Vasudevan G, Landfear SM, and Ullman B. Cloning of a novel inosine-guanosine transporter gene from *Leishmania donovani* by functional rescue of a transport-deficient mutant. *J Biol Chem* 275(27): 20935-20941, 2000a.

Carter NS, Mamoun CB, Liu W, Silva EO, Landfear SM, Goldberg DE, and Ullman B. Isolation and functional characterization of the PfNT1 nucleoside transporter gene from *Plasmodium falciparum*. *J Biol Chem* 275(14): 10683-10691, 2000b.

Cass CE. In: Drug transport in antimicrobial and anticancer chemotherapy, edited by Georgopapadakou NH. New York: Marcel Dekker, 1995.

Cass CE, Young JD, and Baldwin SA. Recent advances in the molecular biology of nucleoside transporters of mammalian cells. *Biochem Cell Biol* 76: 761-770, 1998.

Cha SH, Sekine T, Kusuhara H, Yu E, Kim JY, Kim DK, Sugiyama Y, Kanai Y, and Endou H. Molecular cloning and characterization of multispecific organic anion transporter 4 expressed in the placenta. *J Biol Chem* 275: 4507-4512, 2000.

Cha SH, Sekine T, Fukushima J-I, Kanai Y, Kobayashi Y, Goya T, and Endou H. Identification and characterization of human organic anion transporter 3 expressing predominantly in the kidney. *Mol Pharmacol* 59: 1277-1286, 2001.

Chatton JY, Odone M, Besseghir K, and Roch-Ramel F. Renal secretion of 3'-azido-3'-deoxythymidine by the rat. *J Pharmacol Exp Ther* 225: 140-145, 1990.

Che M, Ortiz DF, and Arias IM. Primary structure and functional expression of a cDNA encoding the bile canalicular, purine-specific Na⁺-nucleoside cotransporter. *J Biol Chem* 270(23): 13596-13599, 1995.

Chen R and Nelson AJ. Role of organic cation transporters in renal secretion of nucleosides. *Biochem Pharmacol* 60: 215-219, 2000.

Chen X-Z, Coady MJ, Jackson F, Bertelott A, and Lapointe J-Y. Thermodynamic determination of the Na⁺:glucose coupling ratio for the human SGLT1 cotransporter. *Biophys J* 69: 2405-2414, 1995.

Chen X-Z, Coady MJ, and Lapointe J-Y. Fast voltage clamp discloses a new component of presteady-state currents from the Na⁺-glucose cotransporter. *Biophys J* 71: 2544-2552, 1996.

Chen X-Z, Zhu T, Smith DE, and Hediger MA. Stoichiometry and kinetics of the high-affinity H⁺-coupled peptide transporter PepT2. *J Biol Chem* 274(5): 2773-2779, 1999.

Chiang C-W, Carter N, Sullivan Jr. WJ, Donald RGK, Roos DS, Naguib FNM, el Kouni MH, Ullman B, and Wilson CM. The adenosine transporter of *Toxoplasma gondii*: identification by insertional mutagenesis, cloning, and recombinant expression. *J Biol Chem* 274(49): 35255-35261, 1999.

Choi DS, Handa M, Young H, Gordon AS, Diamond I, and Messing RO. Genomic organization and expression of the mouse equilibrative, nitrobenzylthioinosine-sensitive nucleoside transporter 1 (ENT1) gene. *Biochem Biophys Res Commun* 277(1): 200-8, 2000.

Costa ACS, Patrick JW, and Dani JA. Improved technique for studying ion channels expressed in *Xenopus* oocytes, including fast superfusion. *Biophys J* 67: 395-401, 1994.

Craig JE, Zhang Y, and Gallagher MP. Cloning of the NupC gene of *Escherichia coli* encoding a nucleoside transport system, and identification of an adjacent insertion element, IS 186. *Mol Microbiol* 11(6): 1159-1168, 1997.

Crawford CR, Patel DH, Naeve C, and Belt JA. Cloning of the human equilibrative, nitrobenzylmercaptapurine riboside (NBMPR)-insensitive nucleoside transporter *ei* by functional expression in a transport-deficient cell line. *J Biol Chem* 273(9): 5288-5293, 1998.

Dascal N. The use of *Xenopus* oocytes for the study of ion channels. *CRC Crit Rev Biochem* 22(4): 317-87, 1987.

de Koning HP, Watson CJ, and Jarvis SM. Characterization of a nucleoside/proton symporter in procyclic *Trypanosoma brucei brucei*. *J Biol Chem* 273(16): 9486-9494, 1998.

de Koning HP and Jarvis SM. Adenosine transporters in bloodstream forms of *Trypanosoma brucei brucei*: substrate recognition motifs and affinity for Trypanocidal drugs. *Mol Pharmacol* 56: 1162-1170, 1999.

de Miranda P, Good SS, Yarchoan R, Thomas RV, Blum MR, Myers CE, and Broder S. Alteration of zidovudine pharmacokinetics by probenecid in patients with AIDS or AIDS-related complex. *Clin Pharmacol Ther* 46:494-500, 1989.

de Montigny J, Straub ML, Wagner R, Bach ML, and Chevallier MR. The uracil permease of *Schizosaccharomyces pombe*: a representative of a family of 10 transmembrane helix transporter proteins of yeasts. *Yeast* 14(11): 1051-1059, 1998.

DelVecchio VG, Kapatral V, Redkar RJ, Patra G, Mujer C, Los T, Ivanova N, Anderson I, Bhattacharyya A, Lykidis A, Reznik G, Jablonski L, Larsen N, D'Souza M, Bernal A, Mazur M, Goltsman E, Selkov E, Elzer PH, Hagius S, O'Callaghan D, Lettesson J-J, Laselkorn R, Kyrpides N, and Overbeek R. The genome sequence of the facultative intracellular pathogen *Brucella melitensis*. *Proc Natl Acad Sci USA* 99(1): 443-448, 2002.

Detke S. Cloning of the *Candida albicans* nucleoside transporter by complementation of nucleoside transport-deficient *Saccharomyces*. *Yeast* 14: 1257-1265, 1998.

Diez-Sampedro A, Eskandari S, Wright EM, and Hirayama BA. Na⁺-to-sugar stoichiometry of SGLT3. *Am J Physiol Renal Physiol* 49: F278-F282, 2001.

Enjo F, Nosaka K, Ogata M, Iwashima A, and Nishimura H. Isolation and characterization of a thiamin transport gene, *THI10*, from *Saccharomyces cerevisiae*. *J Biol Chem* 272(13): 19165-19170, 1997.

Enserink M and Pennisi E. Researchers crack malaria genome. *Science* 295:1207, 2002.

Eskandari S, Loo DD, Dai G, Levy O, Wright EM, and Carrasco N. Thyroid Na⁺/I⁻ symporter. Mechanism, stoichiometry, and specificity. *J Biol Chem* 272(43): 27230-27238, 1997.

Fang X, Parkinson FE, Mowles DA, Young JD, and Cass CE. Functional characterization of a recombinant sodium-dependent nucleoside transporter with selectivity for pyrimidine nucleosides (cNT1_{rat}) by transient expression in cultured mammalian cells. *Biochem J* 317(2): 457-465, 1996.

Fasoli MO, Kerridge D, and Ryley JFAD. Pathogenicity of 5-fluorocytosine-resistant strains of *Candida albicans*. *J Med Vet Mycol* 28: 27-34, 1990.

Feldmann H, Aigle M, Aljnovic G, Andrea B, Baclet MC, et al. Complete DNA sequence of yeast chromosome II. *EMBO J* 13(24): 5795-5809, 1994.

Ferretti J, McShan W, Adjic D, Savic D, Savic G, et al. Complete genome sequence of an M1 strain of *Streptococcus pyogenes*. *Proc Natl Acad Sci USA* 98(8): 4658-4663, 2001.

Flanagan SA and Meckling-Gill KA. Characterization of a novel Na⁺-dependent, guanosine-specific, nitrobenzylthioinosine-sensitive transporter in acute promyelocytic leukemia cells. *J Biol Chem* 272(29): 18026-18032, 1997.

Fleischmann RD, Adams MD, White O, Clayton RA, Kirkness EF, et al. Whole-genome random sequencing and assembly of *Haemophilus influenzae* RD. *Science* 269(5223): 496-512, 1995.

Fsihi H, Kottwitz B, and Bremer E. Single amino acid substitutions affecting the substrate specificity of the *Escherichia coli* K-12 nucleoside-specific Tsx channel. *J Biol Chem* 268(23): 17495-17503, 1993.

Galli A, DeFelice LJ, Duke BJ, Moore KR, and Blakely RD. Sodium-dependent norepinephrine-induced currents in norepinephrine-transporter-transfected HEK-293 cells blocked by cocaine and antidepressants. *J Exp Biol* 198: 2197-2212, 1995.

Gerstin KM, Dresser MJ, Wang J, and Giacomini KM. Molecular cloning of a Na⁺-dependent nucleoside transporter from rabbit intestine. *Pharm Res* 17(8): 906-910, 2000.

Gerstin KM, Dresser MJ, and Giacomini KM. Specificity of human and rat orthologs of the concentrative nucleoside transporter, SPNT. *Am J Physiol Renal Physiol* 283: F344-F349, 2002.

Gorboulev V, Ulzheimer JC, Akhoundova A, Ulzheimer-Teuber L, Karbach U, Quester S, Baumann C, Lang F, Busch AE, and Koepsell H. Cloning and characterization of two human polyspecific organic cation transporters. *DNA Cell Biol* 16: 871-881, 1997.

Griffiths DA, Hall SD, and Sokol PP. Interaction of 3'-azido-3'-deoxythymidine with organic ion transport in rat renal basolateral membrane vesicles. *J Pharmacol Exp Ther* 257(1): 149-155, 1991.

Griffiths DA, Hall SD, and Sokol PP. Effect of 3'-azido-3'-deoxythymidine (AZT) on organic ion transport in rat renal brush border membrane vesicles. *J Pharmacol Exp Ther* 260: 128-133, 1992.

Griffiths DA and Jarvis SM. Nucleoside and nucleobase transport systems of mammalian cells. *Biochim Biophys Acta* 1286: 153-181, 1996.

Griffiths M, Beaumont N, Yao SYM, Sundaram M, Boumah CE, Davies A, Kwong FYP, Coe I, Cass CE, Young JD, and Baldwin SA. Cloning of a human nucleoside transporter implicated in the cellular uptake of adenosine and chemotherapeutic drugs. *Nat Med* 3(1): 89-93, 1997a.

Griffiths M, Yao SYM, Abidi F, Phillips SEV, Cass CE, Young JD, and Baldwin SA. Molecular cloning and characterization of a nitrobenzylthioinosine-insensitive (*ei*) equilibrative nucleoside transporter from human placenta. *Biochem J* 328: 739-743, 1997b.

Gründemann D, Gorboulev V, Gambaryan S, Veyhl M, and Koepsell H. Drug excretion mediated by a new prototype of polyspecific transporter. *Nature* 372(8): 549-552, 1994.

Gründemann D, Babin-Ebell J, Martel F, Örding N, Schmidt A, and Schömig E. Primary structure and functional expression of the apical organic cation transporter from kidney epithelial LLC-PK₁ cells. *J Biol Chem* 272(16): 10408-10413, 1997.

Hamill OP, Marty A, Neher E, Sakmann B, and Sigworth FJ. Improved patch-clamp techniques for high-resolution current recording from cells and cell-free membrane patches. *Pflügers Arch* 391: 85-100, 1981.

Hamilton SR, Yao SYM, Ingram J, Henderson PJF, Gallagher MP, Cass CE, Young JD, and Baldwin SA. Anti-peptide antibodies as probes of the structure and subcellular distribution of the sodium-dependent nucleoside transporter, rCNT1. *J Physiol (Lond)* 499: P50-P51, 1997.

Hamilton SR, Yao SYM, Ingram JC, Hadden DA, Ritzel MWL, Gallagher MP, Henderson PJF, Cass CE, Young JD, and Baldwin SA. Subcellular distribution and membrane topology of the mammalian concentrative Na⁺-nucleoside cotransporter rCNT1. *J Biol Chem* 276(30): 27981-27988, 2001.

Hammond JR. Comparative pharmacology of the nitrobenzylthioguanosine-sensitive and -resistant nucleoside transport mechanisms of Ehrlich ascites tumor cells. *J Pharmacol Exp Ther* 259: 799-807, 1991.

Hammond JR. Interaction of a series of draflazine analogues with equilibrative nucleoside transporters: species differences and transporter subtype selectivity. *Naunyn-Schmiedeberg's Arch Pharmacol* 361: 373-382, 2000.

Hantke K. Phage T6-colicin K receptor and nucleoside transport in *Escherichia coli*. *FEBS Lett* 70: 109-112, 1976.

Hayer-Zillgen M, Brüß M, and Bönisch H. Expression and pharmacological profile of the human organic cation transporters hOCT1, hOCT2, and hOCT3. *Brit J Pharmacol* 136: 829-836, 2002.

Hazama A, Loo DDF, and Wright EM. Presteady-state currents of the rabbit Na⁺/glucose cotransporter (SGLT1). *J Membr Biol* 155: 175-186, 1997.

Hedaya MA and Sawchuk RJ. Effect of probenecid on the renal and nonrenal clearances of zidovudine and its distribution into cerebrospinal fluid in the rabbit. *J Pharm Sci* 78: 717-722, 1989.

Hediger MA, Coady MJ, Ikeda TS, and Wright EM. Expression cloning and cDNA sequencing of the Na⁺/glucose cotransporter. *Nature* 330(6146): 379-381, 1987.

Heidelberg JF, Eisen JA, Nelson WC, Clayton RA, Gwinn ML, et al. DNA sequence of both chromosomes of the cholera pathogen *Vibrio cholerae*. *Nature* 406(6795): 477-483, 2000.

Hilgemann DW and Lu C-C. Giant membrane patches: improvements and applications. *Methods Enzymol* 293: 267-300, 1998.

Hirayama BA, Loo DF, and Wright EM. Protons drive sugar transport through the Na⁺/glucose cotransporter (SGLT1). *J Biol Chem* 269(34): 21407-21410, 1994.

Hong M, Schlichter L, and Bendayan R. A Na⁺-dependent nucleoside transporter in microglia. *J Pharmacol Exp Ther* 292: 366-374, 2000.

Horak J. Yeast nutrient transporters. *Biochim Biophys Acta* 1331: 41-79, 1997.

Hosoyamada M, Sekine T, Kanai Y, and Endou H. Molecular cloning and functional expression of a multispecific organic anion transporter from human kidney. *Am J Physiol* 276 (Renal Physiol 45): F122-F128, 1999.

Huang Q-Q, Harvey CM, Paterson ARP, Cass CE, and Young JD. Functional expression of Na⁺-dependent nucleoside transport systems of rat intestine in isolated oocytes of *Xenopus laevis*: Demonstration that rat jejunum expresses the purine-selective system N1 (*cif*) and a second, novel system N3 having broad specificity for purine and pyrimidine nucleosides. *J Biol Chem* 268(27): 20613-20619, 1993.

Huang Q-Q, Yao SYM, Ritzel MWL, Paterson ARP, Cass CE, and Young JD. Cloning and functional expression of a complementary DNA encoding a mammalian nucleoside transport protein. *J Biol Chem* 269(27): 17757-17760, 1994.

Hyde RJ, Cass CE, Young JD, and Baldwin SA. The ENT family of eukaryote nucleoside and nucleobase transporters: recent advances in the investigation of structure/function relationships and the identification of novel isoforms. *Mol Membr Biol* 18: 53-63, 2001.

Ikeda TS, Hwang E-S, Coady MJ, Hirayama BA, Hediger MA, and Wright EM. Characterization of a Na⁺/glucose cotransporter cloned from rabbit small intestine. *J Membr Biol* 110:87-95, 1989.

Inoue T, Matsuzaki S, and Tanaka S. Cloning and sequence analysis of *Vibrio parahaemolyticus* ompK gene encoding a 26-kDa outer membrane protein, OmpK, that serves as receptor for a broad-host-range vibriophage, KVP40. *FEMS Microbiol Lett* 134(2-3): 245-9, 1995a.

Inoue T, Matsuzaki S, and Tanaka S. A 26-kDa outer membrane protein, OmpK, common to *Vibrio* species is the receptor for a broad-host-range vibriophage, KVP40. *FEMS Microbiol Lett* 125(1): 101-5, 1995b.

Itoh T, Aiba H, Baba T, Fujita K, and Hayashi K. A 460-kb DNA sequence of the *Escherichia coli* K-12 genome corresponding to the 40.1-50.0 min region on the linkage map. *DNA Res* 3(6): 379-392, 1996.

Jarvis SM. Uniport carriers for metabolites. *Curr Opin Cell Biol* 1(4): 721-728, 1989.

Jarvis SM and Young JD. Nucleoside transport in rat erythrocytes. Two components with differences in sensitivity to inhibition by nitrobenzylthioinosine and p-chloromercuriphenyl sulfonate. *J Membr Biol* 93:1-10, 1986.

Jennings LL, Cass CE, Ritzel MWL, Yao SYM, Young JD, Griffiths M, and Baldwin SA. Adenosine transport: recent advances in the molecular biology of nucleoside transporter proteins. *Drug Dev Res* 45: 277-287, 1998.

Jund R and Lacroute F. Genetic and physiological aspects of resistance to 5-fluoropyrimidines in *S. cerevisiae*. *J Bacteriol* 102: 607-615, 1970.

Jund R, Weber E, and Chevallier MR. Primary structure of the uracil transport protein of *Saccharomyces cerevisiae*. *Eur J Biochem* 171(1-2): 417-424, 1988.

Kaneko T, Nakamura Y, Wolk CP, Kuritz T, Sasamoto S, et al. Complete genome sequence of the filamentous nitrogen-fixing cyanobacterium *Anabaena* sp. strain PCC 7120. *DNA Res* 8(5): 205-213, 2001.

Katinka MD, Duprat S, Cornillot E, Metenier G, Thomarat F, et al. Genome sequence and gene compaction of the eukaryote parasite *Encephalitozoon cuniculi*. *Nature* 414(6862): 450-453, 2001.

Kavanaugh MP, Arriza JL, North RA, and Amara SG. Electrogenic uptake of gamma-aminobutyric acid by a cloned transporter expressed in *Xenopus* oocytes. *J Biol Chem* 267: 22007-22009, 1992.

Kekuda R, Prasad PD, Wu X, Wang H, Fei Y-J, Leibach FH, and Ganapathy V. Cloning and functional characterization of a potential-sensitive, polyspecific organic cation transporter (OCT3) most abundantly expressed in placenta. *J Biol Chem* 273(26): 15971-15979, 1998.

Kimmich GA and Randles J. Evidence for an intestinal Na^+ :sugar transport coupling stoichiometry of 2.0. *J Membr Biol* 114: 1-27, 1980.

Kimmich GA and Randles J. Sodium-sugar coupling stoichiometry in chick intestinal cells. *Am J Physiol* 247: C74-C82, 1984.

Kiss A, Farah K, Kim J, Garriock R, Drysdale T, and Hammond JR. Molecular cloning and functional characterization of inhibitor-sensitive (mENT1) and inhibitor-resistant (mENT2) equilibrative nucleoside transporters from mouse brain. *Biochem J* 352: 363-372, 2000.

Klamo EM, Drew ME, Landfear SM, and Kavanaugh MP. Kinetics and stoichiometry of a proton/*myo*-inositol cotransporter. *J Biol Chem* 271(25): 14937-14943, 1996.

Kubitschek HE. Constancy of uptake during the cell cycle in *Escherichia coli*. *Biophys J* 8: 1401-1412, 1968.

Kunst F, Ogasawara N, Moszer I, Albertini AM, Alloni G, et al. The complete genome sequence of the gram-positive bacterium *Bacillus subtilis*. *Nature* 390(6657): 249-256, 1997.

Kuroda M, Ohta T, Uchiyama I, Baba T, Yutawa H, et al. Whole genome sequencing of methicillin-resistant *Staphylococcus aureus*. *Lancet* 357(9264): 1225-1240, 2001.

Kusuhara H, Sekine T, Utsunomiya-Tate N, Tsuda M, Kojima R, Cha SH, Sugiyama Y, Kanai Y, and Endou H. Molecular cloning and characterization of a new multispecific organic anion transporter from rat brain. *J Biol Chem* 274(19): 13675-13680, 1999.

Kuttesch JF, Robins MJ, and Nelson JA. Renal transport of 2'-deoxytubercidin in mice. *Biochem Pharmacol* 31: 3387-3394, 1982.

Kwong FY, Davies A, Tse CM, Young JD, Henderson PJ, and Baldwin SA. Purification of the human erythrocyte nucleoside transporter by immunoaffinity chromatography. *Biochem J* 255(1): 243-249, 1988.

Lang TT, Selner M, Young JD, and Cass CE. Acquisition of human concentrative nucleoside transporter 2 (hCNT2) activity by gene transfer confers sensitivity to fluoropyrimidine nucleosides in drug-resistant leukemic cells. *Mol Pharmacol* 60: 1143-1152, 2001.

Lee CW, Cheeseman CI, and Jarvis SM. Na^+ - and K^+ -dependent uridine transport in rat renal brush-border membrane vesicles. *Biochim Biophys Acta* 942: 139-149, 1988.

Lee W-S, Kanai Y, Well RG, and Hediger MA. The high affinity Na⁺/glucose cotransporter: re-evaluation of function and distribution of expression. *J Biol Chem* 269(16): 12032-12039, 1994.

Le Hir. Evidence for separate carriers for purine nucleosides and pyrimidine nucleosides in renal brush border membrane. *Renal Physiol Biochem* 13(3): 154-161, 1990.

Le Hir M and Dubach UC. Sodium gradient energized concentrative transport of adenosine in renal brush border vesicles. *Pflüger Archiv Eur J Physiol* 401: 58-63, 1984.

Le Hir M and Dubach UC. Concentrative transport of purine nucleosides in brush border vesicles of the rat kidney. *Eur J Clin Invest* 15(3): 121-7, 1985a.

Le Hir M and Dubach UC. Uphill transport of pyrimidine nucleosides in renal brush border vesicles. *Pflügers Arch* 404(3): 238-43, 1985b.

Leung GPH, Ward JL, Wong PYD, and Tse C-M. Characterization of nucleoside transport systems in cultured rat epididymal epithelium. *Am J Physiol Cell Physiol* 280: C1076-C1082, 2001.

Li J and Wang D. Cloning and *in vitro* expression of the cDNA encoding a putative nucleoside transporter from *Arabidopsis thaliana*. *Plant Sci* 157(1): 23-32, 2000.

Loewen SK, Ng AML, Yao SYM, Cass CE, Baldwin SA, and Young JD. Identification of amino acid residues responsible for the pyrimidine and purine nucleoside specificities of human concentrative Na⁺ nucleoside cotransporters hCNT1 and hCNT2. *J Biol Chem* 274(35): 24475-24484, 1999.

Loewen SK, Ng AML, Mohabir NN, Baldwin SA, Cass CE, and Young JD. Functional characterization of a H⁺/nucleoside cotransporter (CaCNT) from *Candida albicans*, the first fungal homolog of mammalian/bacterial concentrative nucleoside transporters. *Yeast* 2003a (*in press*).

Loewen SK, Yao SYM, Slugoski MD, Mohabir NN, Turner RJ, Weiner JH, Gallagher MP, Henderson PJF, Baldwin SA, Cass CE, and Young JD. Transport of antiviral and antineoplastic drugs by recombinant *Escherichia coli* nucleoside-H⁺ cotransporter (NupC) produced in *Xenopus laevis* oocytes. *Mol Membr Biol* 2003b (*in press*).

Loo DDF, Hazama A, Supplisson S, Turk E, and Wright EM. Relaxation kinetics of the Na⁺/glucose cotransporter. *Proc Natl Acad Sci* 90: 5767-5771, 1993.

Lopez-Nieto CE, You G, Bush KT, Barros EJJ, Beier DR, and Nigam SK. Molecular cloning and characterization of NKT, a gene product related to the organic cation transporter family that is almost exclusively expressed in the kidney. *J Biol Chem* 272: 6471-6478, 1997.

Mackenzie B, Loo DDF, Fei Y-J, Liu W, Ganapathy V, Leibach FH, and Wright EM. Mechanisms of the human intestinal H⁺-coupled oligopeptide transporter hPEPT1. *J Biol Chem* 271(10): 5430-5437, 1996a.

Mackenzie B, Loo DDF, Panayotova-Heiermann M, and Wright EM. Biophysical characteristics of the pig kidney Na⁺/glucose cotransporter SGLT2 reveal a common mechanism for SGLT1 and SGLT2. *J Biol Chem* 271(51): 32678-32683, 1996b.

Mackenzie B, Loo DDF, and Wright EM. Relationships between Na⁺/glucose cotransporter (SGLT1) currents and fluxes. *J Membr Biol* 162: 101-106, 1998.

Mackey JR, Baldwin SA, Young JD, and Cass CE. Nucleoside transport and its significance for anticancer drug resistance. *Drug Resist Updates* 1: 310-324, 1998a.

Mackey JR, Mani RS, Selner M, Mowles D, Young JD, Belt JA, Crawford CR, and Cass CE. Functional nucleoside transporters are required for gemcitabine influx and manifestation of toxicity in cancer cell lines. *Cancer Res* 58: 4349-4357, 1998b.

Mackey JR, Yao SYM, Smith KM, Karpinski E, Baldwin SA, Cass CE, and Young JD. Gemcitabine transport in *Xenopus* oocytes expressing recombinant plasma membrane mammalian nucleoside transporters. *J Natl Cancer Inst* 91(21): 1876-1881, 1999.

Maier C, Bremer E, Schmid A, and Benz R. Pore-forming activity of the Tsx protein from the outer membrane of *Escherichia coli*: demonstration of a nucleoside-specific binding site. *J Biol Chem* 263(15): 2493-2499, 1988.

Mager S, Naeve J, Quick M, Labarca C, Davidson N, and Lester HA. Steady states, charge movements, and rates for a cloned GABA transporter expressed in *Xenopus* oocytes. *Neuron* 10(2): 177-188, 1993.

Mager S, Cao Y, and Lester HA. Measurement of transient currents from neurotransmitter transporters expressed in *Xenopus* oocytes. *Methods Enzymol* 296: 551-566, 1998.

Martel F, Vetter T, Russ H, Gründemann D, Azevedo I, Koepsell H, and Schomig E. Transport of small organic cations in the rat liver. The role of the organic cation transporter OCT1. *Naunyn Schmiedebergs Arch Pharmacol* 354: 320-326, 1996.

Mäser P, Sütterlin C, Kralli A, and Kaminsky R. A nucleoside transporter from *Trypanosoma brucei* involved in drug resistance. *Science* 288: 242-244, 1999.

Masereeuw R, Jaehde U, Langemeijer MWE, de Boer AG, and Breimer DD. *In vitro* and *in vivo* transport of zidovudine (AZT) across the blood-brain barrier and the effects of transport inhibitors. *Pharm Res* 11(2): 324330, 1994.

May BJ, Zhang Q, Li LL, Paustian ML, Whittam TS, and Kapur V. Complete genome sequence of *Pasteurella multocida* Pm70. *Proc Natl Acad Sci USA* 98(6): 3460-3465, 2001.

McClelland M, Sanderson KE, Spieth J, Clifton SW, Latreille P, et al. Complete genome sequence of *Salmonella enterica* serovar *Typhimurium* LT2. *Nature* 413(6858): 852-856, 2001.

Methfessel C, Witzemann V, Takahashi T, Mishina M, Numan S, and Sakmann B. Patch clamp measurements on *Xenopus laevis* oocytes: currents through endogenous channels and implanted acetylcholine receptor and sodium channels. *Pflügers Arch* 407: 577-588, 1986.

Miledi R. A calcium-dependent transient outward current in *Xenopus laevis* oocytes. *Proc Royal Soc Lond B* 215: 491-497, 1982.

Möhlmann T, Mezher A, Schwerdtfeger G, and Ekkehard-Neuhaus H. Characterization of a concentrative type of adenosine transporter from *Arabidopsis thaliana* (ENT1, At). *FEBS Lett* 509: 370-374, 2001.

Mooslehner KA and Allen ND. Cloning of the mouse organic cation transporter 2 gene, Slc22a2, from an enhancer-trap transgene integration locus. *Mamm Genome* 10(3): 218-224, 1999.

Munch-Petersen A, Myind B, Nicolaisen A, and Pihl NJ. Nucleoside transport in cells and membrane vesicles from *Escherichia coli* K12. *J Biol Chem* 254(10): 3730-3737, 1979.

Nelson AJ, Kuttesch JF, and Herbert BH. Renal secretion of purine nucleosides and their analogs in mice. *Biochem Pharmacol* 32(15): 2323-2327, 1983.

Nelson AJ, Vidale E, and Enigbokan M. Renal transepithelial transport of nucleosides. *Drug Metab Dispos* 16(6): 789-792, 1988.

Nelson AJ, Anuradha D, Allen LH, and Wright DA. Functional expression of the renal organic cation transporter and P-glycoprotein in *Xenopus laevis* oocytes. *Cancer Chemother Pharmacol* 37: 187-189, 1995.

Nierman WC, Feldblyum TV, Paulsen IT, Nelson KE, Eisen J, et al. Complete genome sequence of *Caulobacter crescentus*. *Proc Natl Acad Sci USA* 98(7): 4136-4141, 2001.

Nieweg A and Bremer E. The nucleoside-specific Tsx channel from the outer membrane of *Salmonella typhimurium*, *Klebsiella pneumoniae* and *Enterobacter aerogenes*: functional characterization and DNA sequence analysis of the *tsx* genes. *Microbiology* 143: 603-615, 1997.

Nishiwaki T, Daigo Y, Tamari M, Fujii Y, and Nakamura Y. Molecular cloning, mapping, and characterization of two novel human genes, ORCTL3 and ORCTL4, bearing homology to organic-cation transporters. *Cytogenet Cell Genet* 83: 251-255, 1998.

Nørholm MHH and Dandanell G. Specificity and topology of the *Escherichia coli* xanthosine permease, a representative of the NHS subfamily of the major facilitator superfamily. *J Bacteriol* 183(16): 4900-4904, 2001.

Okuda M, Saito H, Urakami Y, Takano M, and Inui K. cDNA cloning and functional expression of a novel rat kidney organic cation transporter, OCT2. *Biochem Biophys Res Comm* 224(2): 500-507, 1996.

Pajor AM. Sequence of a pyrimidine-selective Na⁺/nucleoside cotransporter from pig kidney, pkCNT1. *Biochim Biophys Acta* 1415: 266-269, 1998.

Pajor AM and Wright EM. Cloning and functional expression of a mammalian Na⁺/nucleoside cotransporter: A member of the SGLT family. *J Biol Chem* 267(6): 35573560, 1992.

Parent L, Supplisson S, Loo DF, and Wright EM. Electrogenic properties of the cloned Na⁺/glucose cotransporter: Part I. Voltage-clamp studies. *J Membr Biol* 125: 49-62, 1992a.

Parent L, Supplisson S, Loo DF, and Wright EM. Electrogenic properties of the cloned Na⁺/glucose cotransporter: Part II. A transport model under non rapid equilibrium conditions. *J Membr Biol* 125: 63-79, 1992b.

Parker MD, Hyde RJ, Yao SYM, McRobert L, Cass CE, Young JD, McConkey GA, and Baldwin SA. Identification of a nucleoside/nucleobase transporter from *Plasmodium falciparum*, a novel target for anti-malarial chemotherapy. *Biochem J* 349: 67-75, 2000.

Parkhill J, Dougan G, James KD, Thomson NR, and Pickard D. Complete genome sequence of a multiple drug resistant *Salmonella enterica* serovar Typhi CT18. *Nature* 418(6858): 848-852, 2001a.

Parkhill J, Wren BW, Thomson NR, Titball RW, Holden MTG, et al. Genome sequence of *Yersinia pestis*, the causative agent of plague. *Nature* 413(6855): 523-527, 2001b.

Patel DH, Crawford CR, Naeve CW, and Belt JA. Cloning, genomic organization and chromosomal localization of the gene encoding the murine sodium-dependent, purine-selective, concentrative nucleoside transporter (CNT2). *Gene* 242: 51-58, 2000.

Paterson AR, Gati WR, Vijayalakshmi D, Cass CE, Mant MJ, Young JD, and Belch AR. Inhibitor-sensitive, Na⁺-linked transport of nucleoside analogs in leukemic cells from patients. *Proc Am Assoc Cancer Res* 34: A84, 1993.

Plagemann PGW, Aran JM, and Woffendin C. Na⁺-dependent, active and Na⁺-independent, facilitated transport of formycin B in mouse spleen lymphocytes. *Biochim Biophys Acta* 1022: 93-102, 1990.

Prescan E, Moszer I, Boursier L, Cruz H, de la Fuente V, Hullo MF, Lelong C, Schleich S, Sekowska A, Song BH, Villani G, Kunst F, Danchin A, and Glasser P. The *Bacillus subtilis* genome from gerBC (311 degrees) to licR (334 degrees). *Microbiol* 143(10): 3313-3328, 1997.

Quick MW and Lester HA. Methods for expression of excitability proteins in *Xenopus* oocytes. *Methods Neurosci* 19: 261-279, 1994.

Quick M, Loo DDF, and Wright EM. Neutralization of a conserved amino acid residue in the human Na⁺/glucose transporter (hSGLT1) generates a glucose-gated H⁺ channel. *J Biol Chem* 276(3): 178-1734, 2001.

Race JE, Grassel SM, Williams WJ, and Holtzman EJ. Molecular cloning and characterization of two novel renal organic anion transporters (hOAT1 and hOAT3). *Biochem Biophys Res Commun* 255(2): 508-514, 1999.

Rager N, Mamoun CB, Carter NS, Goldberg DE, and Ullman B. Localization of the *Plasmodium falciparum* PfNT1 nucleoside transporter to the parasite plasma membrane. *J Biol Chem* 276(44): 41095-41099, 2001.

Rao TV, Verma RS, and Prasad R. Transport of purine, pyrimidine bases and nucleosides in *Candida albicans*, a pathogenic yeast. *Biochem Int* 6: 409-417, 1983.

Redlak MJ, Zehner ZE, and Betcher SL. Expression of rabbit ileal N3 Na⁺/nucleoside cotransport activity in *Xenopus laevis* oocytes. *Biochem Biophys Res Comm* 225: 106-111, 1996.

Ritzel MWL, Yao SYM, Huang M-Y, Elliot JF, Cass CE, and Young JD. Molecular cloning and functional expression of cDNAs encoding a human Na⁺-nucleoside cotransporter (hCNT1). *Am J Physiol Cell Physiol* 272: C707-C714, 1997.

Ritzel MW, Yao SY, Ng AM, Mackey JR, Cass CE, and Young JD. Molecular cloning, functional expression and chromosomal localization of a cDNA encoding a human Na⁺/nucleoside cotransporter (hCNT2) selective for purine nucleosides and uridine. *Mol Membr Biol* 15(4): 203-211, 1998.

Ritzel MWL, Ng AML, Yao SYM, Graham K, Loewen SK, Smith KM, Ritzel GR, Mowles DA, Carpenter P, Chen X-Z, Karpinski E, Hyde RJ, Baldwin SA, Cass CE, and Young JD. Molecular identification and characterization of novel human and mouse concentrative Na⁺-nucleoside cotransporter proteins (hCNT3 and mCNT3) broadly selective for purine and pyrimidine nucleosides (System *cib*). *J Biol Chem* 276(4): 2914-2927, 2001.

Salanoubat M, Genin S, Artiguenave F, Gouzy J, Mangenot S, et al. Genome sequence of the plant pathogen *Ralstonia solanacearum*. *Nature* 415(6871): 497-502, 2002.

Sanchez MA, Ullman B, Landfear SM, and Carter NS. Cloning and functional expression of a gene encoding a P1 type nucleoside transporter from *Trypanosoma brucei*. *J Biol Chem* 274(42): 30244-30249, 1999.

Sanchez MA, Tryon R, Green J, Boor I, and Landfear SM. Six related nucleoside/nucleobase transporters from *Trypanosoma brucei* exhibit distinct biochemical functions. *J Biol Chem* 277(24): 21499-21504, 2002.

Sandoval IV and Bakke O. Targeting of membrane proteins to endosomes and lysosomes. *Trends Cell Biol* 4: 292-297, 1994.

Sankar M, Machado J, Abdulla P, Hilliker AJ, and Coe IR. Comparative genomic analysis of equilibrative nucleoside transporters suggests conserved protein structure despite limited sequence identity. *Nucleic Acids Res* 30(20): 4339-4350, 2002.

Saxild HH, Andersen LN, and Hammer K. Dra-nupC-pdp operon of *Bacillus subtilis* nucleotide sequence, induction by deoxyribonucleosides, and transcriptional regulation by the deoR-encoded DeoR repressor protein. *J Bacteriol* 178(2): 424-434, 1996.

Schweifer N and Barlow DP. The Lx1 gene maps to mouse chromosome 17 and codes for a protein that is homologous to glucose and polyspecific transmembrane transporters. *Mammalian Genome* 7: 735-740, 1996.

Seeger C, Poulsen C, and Dandanell G. Identification and characterization of genes (*xapA*, *xapB*, and *xapR*) involved in xanthosine catabolism in *Escherichia coli*. *J Bacteriol* 177(19): 5506-5516, 1995.

Sekine T, Watanabe N, Hosoyamada M, Kanai Y, and Endou H. Expression cloning and characterization of a novel multispecific organic anion transporter. *J Biol Chem* 272(30): 18526-18529, 1997.

Sekine T, Cha SH, Apiwattanakul TM, Hakajima N, Kanai Y, and Endou H. Identification of multispecific organic anion transporter 2 expressed predominantly in the liver. *FEBS Lett* 42: 179-182, 1998.

Sekine T, Cha SH, and Endou H. The multispecific organic anion transporter (OAT) family. *Pflügers Arch* 89: 337-344, 2000.

She Q, Siingh RK, Confalonieri F, Zivanovic Y, Allard G, et al. The complete genome of the crenarchaeon *Sulfolobus solfataricus* P2. *Proc Natl Acad Sci USA* 98(14): 7835-7840, 2001.

Shimizu T, Ohtani K, Hiradawa H, Ohshima K, Yamashita A, Shiha T, Ogasawara N, Hattori M, Kuhara S, and Hayashi H. Complete genome sequence of *Clostridium perfringens*, an anaerobic flesh-eater. *Proc Natl Acad Sci USA* 99(2): 966-1001, 2002.

Simonson GD, Vincent AC, Roberg KJ, Huang Y, and Iwanij V. Molecular cloning and characterization of a novel liver-specific transport protein. *J Cell Sci* 107: 1065-1072, 1994.

Smits PH, deHaan M, Maat C, and Grivell LA. The complete sequence of a 33kb fragment on the right arm of chromosome II of *Saccharomyces cerevisiae* reveals 16 open reading frames, including ten now open reading frames, five previously identified genes and a homologue of the SCO1 gene. *Yeast* 10(Suppl A): S75-S80, 1994.

Smoot JC, Barbian KD, Van Gompel JJ, Smoot LM, Chaussee MS, Sylva GL, Sturdevant DE, Ricklefs SM, Porcella SF, Parkins LD, Beres SB, Campell DS, Smith TM, Zhang Q, Kapur V, Daly JA, Veasy LG, and Musser JM. Genome sequence and comparative microarray analysis of serotype M18 group A *Streptococcus* strains associated with acute rheumatic fever outbreaks. *Proc Natl Acad Sci USA* 99(7): 4668-4673, 2002.

Strausberg RL, Feingold EA, Grouse LH, Derge JG, Klausner RD, et al. Generation and initial analysis of more than 15 000 full-length human and mouse cDNA sequences. *Proc Natl Acad Sci USA* 99(26): 16899-16903, 2002.

Stühmer W. Electrophysiological recording from *Xenopus* oocytes. *Methods Enzymol* 207: 319-339, 1998.

Sundaram M, Yao SYM, Ng AML, Griffiths M, Cass CE, Baldwin SA, and Young JA. Chimeric constructs between human and rat equilibrative nucleoside transporters (hENT1 and rENT1) reveal hENT1 structural domains interacting with coronary vasoactive drugs. *J Biol Chem* 273(34): 21519-21525, 1998.

Sundaram M, Yao SYM, Ng AML, Cass CE, Baldwin SA, and Young JD. Equilibrative nucleoside transporters: mapping regions of interaction for the substrate analogue nitrobenzylthioinosine (NBMPR) using rat chimeric proteins. *Biochemistry* 40(27): 8146-8151, 2001a.

Sundaram M, Yao SYM, Ingram JC, Berry ZA, Abidi F, Cass CE, Baldwin SA, and Young JD. Topology of a human equilibrative, nitrobenzylthioinosine (NBMPR)-sensitive nucleoside transporter (hENT1) implicated in the cellular uptake of adenosine and anti-cancer drugs. *J Biol Chem* 276(48): 45270-45275, 2001b.

Sweet DH, Wolff NA, and Pritchard JB. Expression cloning and characterization of ROAT1. The basolateral organic anion transporter in rat kidney. *J Biol Chem* 272: 30088-30095, 1997.

Taglialatela M, Toro L, and Stefani E. Novel voltage clamp to record small, fast currents from ion channels expressed in *Xenopus* oocytes. *Biophys J* 61(1): 78-82, 1992.

Takami H, Nakasone K, HIRAMA C, Takaki Y, Masui N, Fuji F, Nakamura Y, and Inoue A. An improved physical and genetic map of the genome of alkaliphilic *Bacillus* sp. C-125. *Extremophiles* 3(1): 21-28, 1999.

Takami H, Takaki Y, and Uchiyama I. Genome sequence of *Oceanobacillus iheyensis* isolated from the Iheya Ridge and its unexpected adaptive capabilities to extreme environments. *Nucleic Acids Res* 30(18): 3927-3935, 2002.

Takasawa K, Suzuki H, and Sugiyama Y. Transport properties of 3'-azido-3'-deoxythymidine in the rat choroid plexus. *Biopharm Drug Dispos* 18(7): 611-622, 1997.

Takeda M, Khamdang S, Narikawa S, Kimura H, Kobayashi Y, Yamamoto T, Ho Cha S, Sekine T, and Endou H. Human organic anion transporters and human organic cation transporters mediated renal antiviral transport. *J Pharmacol Exp Ther* 300(3): 918-924, 2002.

Tamai I, Yabuuchi H, Nezu J, Sai Y, Oku A, Shimane M, and Tsuji A. Cloning and characterization of a novel human pH-dependent organic cation transporter, OCNT1. *FEBS Lett* 419(1): 101-111, 1997.

Tamai I, Ohashi R, Nezu J, Sai Y, Kobayashi D, Oku A, Shimane M, and Tsuji A. Molecular and functional characterization of organic cation/carnitine transporter family in mice. *J Biol Chem* 275: 40064-40072, 2000.

Terashita S, Dresser MJ, Zhang L, Gray AT, Yost SC, and Giacomini KM. Molecular cloning and functional expression of a rabbit renal organic cation transporter. *Biochim Biophys Acta* 1369: 1-6, 1998.

Thorn JA and Jarvis SM. Adenosine transporters. *Gen Pharmac* 27(4): 613-620, 1996.

Tomb J-F, White O, Kerlavage AR, Clayton RA, Sutton GG, et al. The complete genome sequence of the gastric pathogen *Helicobacter pylori*. *Nature* 388(6642): 539-547, 1997.

Umbach JA, Coady MJ, and Wright EM. Intestinal Na⁺/glucose cotransporter expressed in *Xenopus* oocytes is electrogenic. *Biophys J* 57: 1217-1224, 1990.

Urakami Y, Akazawa M, Saito H, Okuda M, and Inui K. cDNA cloning, functional characterization, and tissue distribution of an alternatively spliced variant of organic cation transporter hOCT2 predominantly expressed in the human kidney. *J Am Soc Nephrol* 13(7): 1703-1710, 2002.

Valens M, Bohn C, Daignan-Fornier B, Dang VD, and Bolotin-Fukuhara M. The sequence of a 54.7kb fragment of yeast chromosome XV reveals the presence of two tRNAs and 24 new open reading frames. *Yeast* 13(4): 379-390, 1997.

Vasudevan G, Carter NS, Drew ME, Beverly SM, Sanchez MA, Seyfang A, Ullman B, and Landfear SM. Cloning of Leishmania nucleoside transporter genes by rescue of a transport-deficient mutant. *Proc Natl Acad Sci* 95(17): 9873-8, 1998.

Verhaagh S, Schweifer N, Barlow DP, and Zwart R. Cloning of the mouse and human solute carrier 22a3 (*Slc22a3/SLC22A3*) identifies a conserved cluster of three organic cation transporters on mouse chromosome 17 and human 6q26-q27. *Genomics* 55(2): 209-218, 1999.

Vickers MF, Yao SYM, Baldwin SA, Young JD, and Cass CE. Nucleoside transporter proteins of *Saccharomyces cerevisiae*: demonstration of a transporter (FUI1) with high uridine selectivity in plasma membranes and a transporter (FUN26) with broad nucleoside selectivity in intracellular membranes. *J Biol Chem* 275(34): 25931-25938, 2000a.

Vickers MF, Young JD, Baldwin SA, Mackey JR, and Cass CE. Nucleoside transporter proteins: emerging targets for drug discovery. *Emerg Ther Targets* 4(4): 515-539, 2000b.

Vickers MF, Young JD, Baldwin SA, Ellison MJ, and Cass CE. Functional production of mammalian concentrative nucleoside transporters in *Saccharomyces cerevisiae* 18: 73-79, 2001.

Visser F, Vickers MF, Ng AML, Baldwin SA, Young JD, and Cass CE. Mutation of residue 33 of human equilibrative nucleoside transporters 1 and 2 alters sensitivity to inhibition of transport by dilazep and dipyridamole. *J Biol Chem* 277(1): 395-401, 2002.

Wada S, Tsuda M, Sekine T, Cha SH, Kimura M, Kanai Y, and Endou H. Rat multispecific organic anion transporter 1 (rOAT1) transports zidovudine, acyclovir, and other antiviral nucleoside analogs. *J Pharmacol Exp Ther* 294(3): 844-849, 2000.

Wadiche JI, Arriza JL, Amara SG, and Kavanaugh MP. Kinetics of a human glutamate transporter. *Neuron* 14: 1019-1027, 1995.

Wagner R, deMontigny J, deWergifosse P, Souciet JL, and Potier S. The ORF YBLO42 of *Saccharomyces cerevisiae* encodes a uridine permease. *FEMS Microbiol Lett* 159: 69-75, 1998.

Wagner CA, Friedrich B, Setiawan I, Lang F, and Bröer S. The use of *Xenopus laevis* oocytes for the functional characterization of heterologously expressed membrane proteins. *Cellular Physiol Biochem* 10: 1-12, 2000.

Wang J and Giacomini KM. Molecular determinants of substrate selectivity in Na⁺-dependent nucleoside transporters. *J Biol Chem* 272(46): 28845-28848, 1997.

Wang J, Su S-F, Dresser MJ, Schaner ME, Washington CB, and Giacomini KM. Na⁺-dependent purine nucleoside transporter from human kidney: cloning and functional characterization. *Am J Physiol Renal Physiol* 273(42): F1058-F1065, 1997.

Wang J and Giacomini KM. Serine 318 is essential for the pyrimidine selectivity of the N2 Na⁺-nucleoside transporter. *J Biol Chem* 274(4): 2298-2302, 1999.

Ward JL, Sherali A, Mo Z-P, and Tse C-M. Kinetic and pharmacological properties of cloned human equilibrative nucleoside transporters, ENT1 and ENT2, stably expressed in nucleoside transporter-deficient PK15 cells. *J Biol Chem* 275(12): 8375-8381, 2000.

Washington CB, Brett CM, Wu X, and Giacomini KM. The effect of N-ethylmaleimide on the Na(+)-dependent nucleoside transporter (N3) in rabbit-choroid plexus. *J Pharmacol Exp Ther* 274 (1): 110-114, 1995.

Waterston R. Genome sequencing of the nematode *C. elegans*: a platform for investigating biology. The *C. elegans* Sequencing Consortium. *Science* 282(5396): 2012-2018, 1998.

Weiss JN. The Hill equation revisited: uses and misuses. *FASEB J* 11: 835-841, 1997.

Wells RG, Pajor AM, Kanai Y, Turk E, Wright EM, and Hediger MA. Cloning of a human kidney cDNA with similarity to the sodium-glucose cotransporter. *Am J Physiol Renal Fluid Electrolyte Physiol* 263: F459-F465, 1992.

Westh Hansen SE, Jensen N, and Munch-Petersen A. Studies on the sequence and structure of the *Escherichia coli* K-12 *nupG* gene encoding a nucleoside transport system. *Eur J Biochem* 168: 385-391, 1987.

Williams TC, Doherty AJ, Griffith DA, and Jarvis SM. Characterization of sodium-dependent and sodium-independent nucleoside transport systems in rabbit brush-border and basolateral plasma-membrane vesicles from the renal outer cortex. *Biochem J* 264(1): 223-231, 1989.

Williams TC and Jarvis SM. Multiple sodium-dependent nucleoside transport systems in bovine renal brush-border membrane vesicles. *Biochem J* 274(1): 27-33, 1991.

Wolff NA, Werner A, Burkhardt S, and Burkhardt G. Expression cloning and characterization of a renal organic anion transporter from winter flounder. *FEBS Lett* 417: 287-291, 1997.

Wood V, Gwilliam R, Rajandream M-A, Lyne M, et al. The genome sequence of *Schizosaccharomyces pombe*. *Nature* 415(6874): 871-880, 2002.

Wright EM. Renal Na⁽⁺⁾-glucose cotransporters. *Am J Physiol Renal Physiol* 280: F10-F18, 2001.

Wright EM, Loo M, Panayotova-Heiermann M, and Boorer KJ. Mechanisms of Na⁺-glucose cotransport. *Biochem Soc Trans* 22: 646-650, 1994a.

Wright EM, Loo M, Panayotova-Heiermann M, Pilar MP, Hirayama BH, Mackenzie B, Boorer K, and Zampighi G. 'Active' sugar transport in eukaryotes. *J Exp Biol* 196: 197-212, 1994b.

Wu J-SR, Kwong FYP, Jarvis SM, and Young JD. Identification of the erythrocyte nucleoside transporter as a band 4.5 polypeptide. Photoaffinity labeling studies using nitrobenzylthioinosine. *J Biol Chem* 258(22): 13745-13751, 1983.

Wu X, Yuan G, Brett CM, Hui AC, and Giacomini KM. Sodium-dependent nucleoside transport in choroid plexus from rabbit. Evidence for a single transporter for purine and pyrimidine nucleosides. *J Biol Chem* 267(13): 8813-8818, 1992.

Wu X, Prasad PD, Leibach FH, and Ganaphathy V. cDNA sequence, transport function, and genomic organization of human OCTN2, a new member of the organic cation transporter family. *Biochem Biophys Res Comm* 246(3): 589-595, 1998.

Wu X, Huang W, Prasad PD, Seth P, Rajan DP, Leibach FH, Chen J, Conway SJ, and Ganapathy V. Functional characteristics and tissue distribution pattern of organic cation transporter 2 (OCTN2), an organic cation/carnitine transporter. *J Pharmacol Exp Ther* 290(3): 1482-1492, 1999.

Wu X, George RL, Huang W, Wang H, Conway SJ, Leibach FH, and Ganapathy V. Structural and functional characteristics and tissue distribution pattern of rat OCTN1, an organic cation transporter, cloned from placenta. *Biochim Biophys Acta* 1466(1-2): 315-327, 2000.

Xiao G, Wang J, Tangen T, and Giacomini KM. A novel proton-dependent nucleoside transporter, CeCNT3, from *Caenorhabditis elegans*. *Mol Pharmacol* 50: 1529-1535, 2001.

Xiaohong Z, Evans KK, and Wright SH. Molecular cloning of rabbit organic cation transporter rbOCT2 and functional comparisons with rbOCT1. *Am J Physiol Renal Physiol* 283: F124-F133, 2001.

Yao SYM, Cass CE, and Young JD. Transport of antiviral nucleoside analogs 3'-azido-3'-deoxythymidine and 2', 3'-dideoxycytidine by a recombinant nucleoside transporter (rCNT) expressed in *Xenopus laevis* oocytes. *Mol Pharmacol* 50: 388-393, 1996a.

Yao SYM, Ng AML, Ritzel MWL, Gati WP, Cass CE, and Young JD. Transport of adenosine by recombinant purine- and pyrimidine-selective sodium/nucleoside cotransporters from rat jejunum expressed in *Xenopus laevis* oocytes. *Mol Pharmacol* 50: 1529-1535, 1996b.

Yao SYM, Ng AML, Muzyka WR, Griffiths M, Cass CE, Baldwin SA, and Young JD. Molecular cloning and functional characterization of nitrobenzylthioinosine (NBMPR)-sensitive (*es*) and NBMPR-insensitive (*ei*) equilibrative nucleoside transporter proteins (rENT1 and rENT2) from rat tissues. *J Biol Chem* 272(45): 28423-28430, 1997.

Yao SYM, Ng AML, Sundaram M, Cass CE, Baldwin SA, and Young JD. Transport of antiviral 3'-deoxy-nucleoside drugs by recombinant human and rat equilibrative, nitrobenzylthioinosine (NBMPR)-insensitive (ENT2) nucleoside transporter proteins produced in *Xenopus* oocytes. *Mol Membr Biol* 18: 161-167, 2001a.

Yao SYM, Sundaram M, Chomey EG, Cass CE, Baldwin SA, and Young JD. Identification of Cys¹⁴⁰ in helix 4 as an exofacial cysteine residue within the substrate-translocation channel of rat equilibrative nitrobenzylthioinosine (NBMPR)-insensitive nucleoside transporter rENT2. *Biochem J* 353: 387-393, 2001b.

Yao SYM, Ng AML, Loewen SK, Cass CE, Baldwin SA, and Young JD. An ancient prevertebrate Na⁺-nucleoside cotransporter (hfCNT) from the Pacific hagfish (*Eptatretus stouti*). *Am J Physiol Cell Physiol* 283: C155-C168, 2002a.

Yao SYM, Ng AML, Vickers MF, Sundaram M, Cass CE, Baldwin SA, and Young JD. Functional and molecular characterization of nucleobase transport by recombinant human and rat equilibrative nucleoside transporters 1 and 2. Chimeric constructs reveal a role for the ENT2 helix 5 - 6 region in nucleobase translocation. *J Biol Chem* 277(28): 24938-24948, 2002b.

Yoo HS, Cunningham TS, and Cooper TG. The allantoin and uracil permease gene sequences of *Saccharomyces cerevisiae* are nearly identical. *Yeast* 8(12): 997-1006, 1992.

Young JD. In: Erythrocyte amino acid and nucleoside transport, edited by Agar NS and Board PG. Elsevier Science Publishers BV, 1983.

Young JD and Jarvis SM. Nucleoside transport in animal cells. *Biosci Reports* 3: 309-322, 1983.

Young JD, Paterson ARP, and Henderson FJ. Nucleoside transport and metabolism in erythrocytes from the Yucatan miniature pig. Evidence that inosine functions as an *in vivo* energy source. *Biochimica Biophysica Acta* 842: 214-224, 1985.

Young JD, Cheeseman C, Mackey JR, Cass CE, and Baldwin SA. Molecular mechanisms of nucleoside and nucleoside drug transport. *Curr Top Membr* 50: 329-378, 2001.

Young JD, Yao SYM, Cass CE, and Baldwin SA. Equilibrative nucleoside transport proteins. In: Red Cell Membrane Transport in Health and Disease, edited by Bernhardt I and Ellory JC. Heidelberg, Germany: Springer Verlag, 2003.

Zhang L, Dresser MJ, Chun JK, Babbit PC, and Giacomini KM. Cloning and functional characterization of a rat renal organic cation transporter isoform (rOCT1A). *J Biol Chem* 272(26): 16548-16554, 1997a.

Zhang L, Dresser MJ, Gray AT, Yost AC, Terashita S, and Giacomini KM. Cloning and functional characterization of a human liver organic cation transporter. *Mol Pharmacol* 51: 913-921, 1997b.

Zhang L, Brett CM, and Giacomini KM. Role of organic cation transporters in drug absorption and elimination. *Annu Rev Pharmacol Toxicol* 38: 431-460, 1998.

Chapter II.*

Electrophysiological Characterization of a Human Na⁺-coupled Nucleoside Transporter (hCNT1) Produced in *Xenopus laevis* Oocytes

**The gemcitabine results presented in this chapter have been published and are presented in Appendix A. A version of the remainder of the chapter is in preparation for publication.*

Mackey JR, Yao SYM, Smith KM, Karpinski E, Baldwin SA, Cass CE, and Young JD. Gemcitabine transport in *Xenopus* oocytes expressing recombinant plasma membrane mammalian nucleoside transporters. *J Natl Cancer Inst* 91(21): 1876-1881, 1999.

Smith KM, Ng AML, Yao SYM, Labedz K, Knaus EE, Wiebe LI, Baldwin SA, Cass CE, Karpinski E, and Young JD. Electrophysiological characterization of a recombinant human Na⁺-coupled nucleoside transporter hCNT1. (in preparation).

Introduction

Physiologic nucleosides and synthetic nucleoside analogs have important biochemical, physiological, and pharmacological activities in humans. Adenosine, for example, has cell-surface receptor-mediated functions in processes such as modulation of immune responses, platelet aggregation, renal function, and coronary vasodilation (Fredholm, 1997; Shryock and Belardinelli, 1997). Synthetic analogs of nucleosides are commonly used in the therapy of leukemias and lymphomas, as well as solid tumors, and are the most effective agents for treatment of viral infections, including those that threaten cancer patients receiving immunosuppressive chemotherapy (Handschumacher and Cheng, 1993; Perigaud *et al.*, 1994). Representative antineoplastic and antiviral nucleoside drugs include gemcitabine, a pyrimidine analog of deoxycytidine used in the treatment of epithelial cancers, and AZT, a deoxythymidine analog used in the treatment of human immunodeficiency virus infection (HIV). Most nucleosides, including those with antineoplastic and/or antiviral activities are hydrophilic, and specialized plasma membrane nucleoside transporter (NT) proteins are required for uptake into or release from cells (Baldwin *et al.*, 1999; Mackey *et al.*, 1999; Young *et al.*, 2001). NT-mediated transport is therefore a critical determinant of metabolism and, for nucleoside drugs, their pharmacological actions.

Multiple nucleoside transport systems that differ in their cation dependence, permeant selectivities and inhibitor sensitivities have been observed in human and other mammalian cells and tissue systems (Cass, 1995; Griffiths and Jarvis, 1996; Young *et al.*, 2001). The major concentrative systems (*cit*, *cif* and *cib*) are inwardly-directed Na^+ -dependent processes that have been described primarily in specialized cells, such as intestinal and renal epithelia, hepatocytes, choroid plexus, macrophages, splenocytes, and leukemic cells (Cass, 1995; Griffiths and Jarvis, 1996; Young *et al.*, 2001). The equilibrative (bidirectional) transport processes (*es* and *ei*) mediate passive downhill transport of nucleosides, have generally lower substrate affinities and occur in most, possibly all, cell types (Cass, 1995; Griffiths and Jarvis, 1996; Young *et al.*, 2001). Systems *cit* and *cif* are generally pyrimidine and purine nucleoside selective, respectively,

whereas systems *cib*, *es* and *ei* transport both pyrimidine and purine nucleosides. The *es* process is sensitive to inhibition by nanomolar concentrations of the nucleoside analog nitrobenzylthioinosine (NBMPR), while system *ei* also transports nucleobases.

Recent molecular cloning studies have led to the isolation and functional expression of cDNAs encoding the human and rodent proteins responsible for each of these nucleoside transport systems (Huang *et al.*, 1994; Che *et al.*, 1995; Yao *et al.*, 1996b; Ritzel *et al.*, 1997; Wang *et al.*, 1997; Crawford *et al.*, 1998; Ritzel *et al.*, 1998, 2001). They belong to two unrelated and previously unrecognized families of integral membrane proteins (CNT and ENT), and their relationship to the processes defined by functional studies is as follows: CNT1 (*cit*), CNT2 (*cif*), CNT3 (*cib*), ENT1 (*es*), and ENT2 (*ei*). Two further ENT isoforms (ENT3 and ENT4) of undetermined function have also been identified (Hyde *et al.*, 2001; Acimovic and Coe, 2002). Mammalian members of the CNT family have 13 predicted transmembrane helices (TMs), with an intracellular amino-terminus and an extracellular glycosylated carboxyl-terminus (Hamilton *et al.*, 2001). NupC, a proton-coupled bacterial member of the CNT family from *Escherichia coli*, has a similar membrane topology, but lacks TMs 1 - 3 (Craig *et al.*, 1997; Hamilton *et al.*, 2001). Other identified CNTs include hfCNT from an ancient marine prevertebrate, the Pacific hagfish (*Eptatretus stouti*) (Loewen *et al.*, 1999; Yao *et al.*, 2002), CeCNT3 from *Caenorhabditis elegans* (Xiao *et al.*, 2001) and CaCNT from *Candida albicans* (Loewen *et al.*, 2003).

Human CNT1 (hCNT1, 650 amino acid residues) (Huang *et al.*, 1994) and rat CNT1 (rCNT1, 648 amino acid residues) (Ritzel *et al.*, 1997) are 83 % identical in amino acid sequence and have been studied functionally as recombinant proteins produced in *Xenopus* oocytes (hCNT1 and rCNT1) and COS-1 cells (rCNT1). Radioisotope flux studies have demonstrated pyrimidine nucleoside-selective (*cit*-type) Na⁺-dependent fluxes of both ³H/¹⁴C-labeled physiological nucleosides and antineoplastic and antiviral nucleoside drugs (Huang *et al.*, 1994; Fang *et al.*, 1996; Yao *et al.*, 1996a, b; Ritzel *et al.*, 1997; Mackey *et al.*, 1998; Yao *et al.*, 2001). The present *Chapter* describes experiments using the two-microelectrode voltage clamp to undertake a complementary steady-state

electrophysiological analysis of recombinant hCNT1 produced in *Xenopus* oocytes. Experiments are described that investigate hCNT1 Na⁺-dependence, cation specificity, voltage-dependence, substrate selectivity and inhibitor sensitivity. Electrophysiology was also used to investigate hCNT1 voltage-dependence, order of Na⁺/nucleoside binding and Na⁺/nucleoside coupling ratio.

Materials and Methods

***In vitro* Transcription and Transporter Expression in *Xenopus* Oocytes** - hCNT1 cDNA in the plasmid expression vector pGEM-T (Ritzel *et al.*, 1997; Loewen *et al.*, 1999) was linearized with *Not1* and transcribed with T3 polymerase using the mMMESSAGE mMACHINE™ (Ambion, Austin, TX) transcription system. Remaining template was removed by digestion with RNase-free DNase1. Stage V-VI oocytes were dissected from the ovaries of mature oocyte-positive *Xenopus laevis* and treated with collagenase (2 mg/ml for 2 h) (Huang *et al.*, 1994). As required, any remaining follicular layers were removed manually. Twenty-four hours after defolliculation, oocytes were injected with either 10 nl of water containing 10 ng of capped RNA transcript or 10 nl of water alone. Injected oocytes were then incubated for 4 days at 18 °C in modified Barth's solution (daily change) (88 mM NaCl, 1 mM KCl, 0.33 mM Ca(NO₃)₂, 0.41 mM CaCl₂, 0.82 mM MgSO₄, 2.4 mM NaHCO₃, 10 mM Hepes, 2.5 mM Na⁺ pyruvate, 0.05 mg/ml penicillin, and 0.1 mg/ml gentamycin sulfate, pH 7.5) prior to the measurement of membrane currents. In experiments to investigate phloridzin inhibition of hCNT1 and hCNT3 and the Na⁺/nucleoside coupling ratio of hCNT1, the enhanced *Xenopus* expression vector pGEM-HE was used (Liman *et al.*, 1992; Ritzel *et al.*, 2001). By providing additional 5'- and 3'-untranslated sequences from a *Xenopus* β-globin gene, the pGEM-HE construct produces greater CNT functional activity (Ritzel *et al.*, 2001). hCNT1 and hCNT3 pGEM-HE plasmid DNAs were linearized with *Nhe1* and transcribed with T7 polymerase mMMESSAGE mMACHINE™.

Electrophysiological Studies - Oocyte membrane currents were measured by use of a GeneClamp 500B oocyte clamp (Axon Instruments, Inc., Foster City, California) in the two-electrode, voltage clamp mode. The GeneClamp 500B was interfaced to an IBM compatible PC *via* a Digidata 1200A/D converter and controlled by pCLAMP software (Version 8.0, Axon Instruments, Inc., Foster City, California). Current signals were filtered at 20 Hz (four-pole Bessel filter) and sampled at a sampling interval of 20 msec. For data presentation, the signals were further filtered at 0.5 Hz by the pCLAMP program suite. All electrophysiological experiments were performed at room temperature (20 °C)

at least twice on different batches of oocytes. The microelectrodes were filled with 3 M KCl and had resistances that ranged from 0.5 - 2.5 MΩ (megaohms). Oocytes were penetrated with the microelectrodes and their membrane potential monitored for a period of 10 - 15 min. Oocytes were discarded if the membrane potential was unstable or more positive than -30 mV. For measurements of transporter-mediated currents, the oocyte membrane potential was clamped at a holding potential (V_h) of -50 mV. The Na⁺-containing transport medium contained (in mM): NaCl, 100; KCl, 2; CaCl₂, 1; MgCl₂, 1; and Hepes, 10 (pH 7.5). The substrate to be tested was added to this medium at the appropriate concentration (100 μM, unless otherwise indicated). In experiments testing the Na⁺-dependence of nucleoside transport, Na⁺ in the transport medium was replaced by equimolar choline. Current-voltage (I-V) curves were determined from the difference between steady-state currents generated in the presence and absence of substrate during 175 msec voltage pulses to potentials between -90 and +60 mV (10 mV increments). The ability of H⁺ to drive nucleoside transport by hCNT1 was tested by replacing Na⁺ in the transport medium with choline and varying the pH between 7.5 and 5.5 (10 mM MES was used in place of Hepes in solutions with pH values ≤6.5). Exposure of oocytes to acid pH was kept to intervals of < 2 min to minimize irreversible changes in the oocyte plasma membrane. The hCNT1 uridine kinetic parameters apparent affinity ($K_m^{uridine}$) and maximal current ($I_{max}^{uridine}$) were determined by current measurements at different uridine concentrations and analyzed by least squares fits to the Michaelis-Menten equation $I = I_{max}^{uridine} [U] / (K_m^{uridine} + [U])$, where I is the substrate-induced current and U represents uridine (SigmaPlot Version 4, Jandel Scientific Software, San Rafael, CA). The results from Na⁺ activation experiments were fitted to the Hill equation, $I = I_{max} [Na^+]^n / (K_m^{Na^+ n} + [Na^+]^n)$, where n is the Hill coefficient, $K_m^{Na^+}$ is the half-saturation constant for Na⁺ activation, I is the uridine-induced steady-state current, and I_{max} is the predicted current maximum (SigmaPlot Version 4, Jandel Scientific Software, San Rafael, CA). For studies of phloridzin inhibition of hCNT1 and hCNT3, uridine-induced currents were measured in the same oocyte before and after a 10 min pre-incubation with inhibitor. Repeat exposures to increasing concentrations of

phloridzin (0 - 5 mM) were preceded by wash-out in Na⁺-free medium, followed by re-equilibration in Na⁺-containing transport medium and exposure to the next concentration of inhibitor. Results for each phloridzin application were calculated as a percentage of the control uridine-induced current measured prior to addition of inhibitor. The IC₅₀ for phloridzin inhibition was determined based on a normalized curve.

Data are presented as means ±SEM of values for 4 or more oocytes. Each experiment was repeated at least twice on oocytes from different frogs. Kinetic parameters are presented as means ±SE, where SE is standard error of the fitted estimate.

Radioisotope Flux Studies - Phloridzin interactions with recombinant hCNT1 and hCNT3 were also studied by uptake of ¹⁴C-labeled uridine (1 μCi/ml, Amersham Pharmacia Biotech). Initial rates of transport (1 min flux) were measured at room temperature as described previously (Huang *et al.*, 1993; Ritzel *et al.*, 1997) in groups of 12 oocytes in 200 μl of the same Na⁺-containing transport medium used for electrophysiological studies. Oocytes were pre-incubated with and without inhibitor for 30 min prior to the assay of transport activity and, except where otherwise indicated, the uridine concentration was 10 μM. At the end of the incubation period, extracellular medium was removed by six rapid washes in ice-cold transport medium, and individual oocytes were dissolved in 5 % (w/v) SDS for quantitation of oocyte-associated radioactivity by liquid-scintillation counting (LS 6000 IC, Beckman, Mississauga, ON). Influx was corrected for basal non-mediated uridine uptake in control water-injected oocytes and expressed as a percentage of the uninhibited flux measured in the absence of phloridzin. Values are presented as means ±SEM of 10 - 12 oocytes, and each experiment was repeated at least twice on different batches of cells. The IC₅₀ for phloridzin inhibition was calculated based on a normalized curve.

Cation/Nucleoside Coupling Ratios - hCNT1 Na⁺/nucleoside stoichiometry was determined by the simultaneous measurement of Na⁺ current and ¹⁴C-uridine influx under voltage-clamp conditions. This technique permits a direct comparison of cotransporter current and unidirectional nucleoside uptake over the same time course in a single oocyte

(Chen *et al.*, 1998). Na⁺-containing transport medium (substrate-free, pH 7.5) was used as the control solution for external perfusion of the oocytes. The uptake solution consisted of the control solution plus nonradioactive and radioactive ¹⁴C-uridine (1 μCi/ml, Amersham Pharmacia Biotech) to give a final uridine concentration of 200 μM. Individual oocytes were placed in a perfusion chamber and voltage-clamped at V_h of -30, -50, or -90 mV. Baseline currents were monitored and recorded while the oocyte was perfused with substrate-free control solution. When the baseline was stable, the perfusion was stopped. Uptake solution (500 μl) was then added manually to the oocyte chamber with a pipettor, which washed the control solution out of the chamber. Uptake of uridine lasted for 3 minutes and was terminated by washing the oocyte with control solution until the current returned to baseline. Oocytes were then transferred to individual scintillation vials and counted. Nucleoside-induced current was obtained as the difference between baseline and the inward uridine current. The total charge transported into the oocyte during the uptake period was calculated from the current-time integral and correlated with the measured radiolabeled uptake for each oocyte. Basal ¹⁴C-uridine uptake was determined in control water-injected oocytes (from the same donor) under equivalent conditions and used to correct for endogenous non-mediated uridine uptake. Coupling ratios are presented as means ±SE of 7 or more oocytes.

Chemicals - Nucleosides, nucleoside analogs, including AZT (3'-azido-3'-deoxythymidine) and gemcitabine (2', 2'-difluorodeoxycytidine), and phloridzin were purchased from Sigma (Oakville, ON). β-DFP-5M (1-(2-deoxy-β-D-ribofuranosyl)-2, 4-difluoro-5-methylbenzene) and β-DFP-5I (1-(2-deoxy-β-D-ribofuranosyl)-2, 4-difluoro-5-iodobenzene) were a generous gift from Dr. EE Knaus and Dr. LI Wiebe (Department of Pharmacology, University of Alberta).

Results

Na⁺-dependence - Using the whole-cell two-microelectrode voltage-clamp technique, hCNT1-mediated transport of uridine was shown to be electrogenic and Na⁺-dependent. In the representative experiment presented in Figure 2-1A, addition of uridine (100 μM) to an hCNT1-producing oocyte in Na⁺-containing transport medium produced an inward current of 80 nA ($V_h = -50$ mV; 100 mM NaCl; pH 7.5). This current returned to baseline when uridine was removed by washout with substrate-free Na⁺ transport medium. To examine the Na⁺-dependence of this transport, Na⁺ in the transport medium was replaced by equimolar choline (Fig. 2-1B; 100 mM ChCl). No inward current was generated following perfusion of the same hCNT1-producing oocyte with uridine under Na⁺-free conditions. Inward currents were not produced when a control water-injected oocyte was perfused with uridine in either Na⁺ (Fig. 2-1C) or choline (Fig. 2-1D) transport medium.

Voltage-Dependence of Transporter Currents - The effect of membrane potential on the uridine-induced steady-state current was examined by comparing hCNT1 currents recorded at the end of a 175 msec command pulse to potentials between -90 and +60 mV (10 mV increments) in the presence (Fig. 2-2A, *left current record*) and in the absence (Fig. 2-2A, *right current record*) of uridine. Currents evoked by the addition of uridine (100 μM) were voltage-dependent; subtraction of the currents generated in the presence and absence of uridine revealed that the inward current induced by the addition of uridine increased at more negative potentials (Fig. 2-2B). This uridine-induced current approached zero, but did not reverse polarity at potentials up to +60 mV.

Cation Specificity - Several members of the CNT protein family in lower eukaryotes and prokaryotes are proton-dependent (Craig *et al.*, 1997; Xiao *et al.*, 2001; Loewen *et al.*, 2003), and studies presented in *Chapter III* of this thesis demonstrate that human and mouse CNT3 (hCNT3 and mCNT3) are both Na⁺- and H⁺-dependent. The ability of H⁺ to drive transport of uridine by hCNT1 was examined by comparing the magnitudes of currents produced in Na⁺-containing transport medium (pH 7.5) to currents produced when Na⁺ was replaced by choline and the pH was decreased from 7.5 to 5.5. In the

representative experiment presented in Figure 2-3A, uridine (100 μM) induced an inward current of 56 nA in Na^+ -containing transport medium at pH 7.5, while no currents were observed in choline transport medium at any of the pHs tested (7.5, 6.5 and 5.5). No currents were observed in a control water-injected oocyte under any of the conditions tested (Fig. 2-3B).

Substrate Specificity - The ability of hCNT1 to transport the pyrimidine nucleosides uridine, thymidine and cytidine has been previously demonstrated using conventional radioisotope flux measurements (Ritzel *et al.*, 1997). It has also been shown that hCNT1 and its rat ortholog rCNT1 mediate low, but significant fluxes of adenosine, but not the other purine nucleosides inosine or guanosine (Huang *et al.*, 1994; Yao *et al.*, 1996b). These results were confirmed for hCNT1 using electrophysiological techniques (Fig. 2-4). Currents elicited by application of substrate (100 μM) in Na^+ -containing transport medium to the same oocyte ranked in the following order: uridine > thymidine > cytidine >> adenosine (Fig. 2-4A). Guanosine and inosine and deoxyadenosine, each at a concentration of 100 μM , and the nucleobases uracil (100 μM) and hypoxanthine (100 μM) did not evoke inward currents. Increasing the concentrations of uracil and hypoxanthine to 1 mM also did not generate any detectable currents. No currents were observed in control water-injected oocytes (Fig. 2-4B).

In radioisotope flux studies, adenosine is transported by rCNT1 with a similar apparent K_m as uridine ($\sim 30 \mu\text{M}$), but with a much lower V_{max} (Yao *et al.*, 1996b). Competition experiments were undertaken to investigate if the same kinetic behavior could be detected electrophysiologically. To do this, the current produced by a saturating concentration of uridine alone (100 μM) was compared in the same oocyte to that produced by uridine and another nucleoside both present at the same concentration of 100 μM (Fig. 2-5). The simultaneous addition of uridine and thymidine (both good h/rCNT1 permeants) to an hCNT1-producing oocyte generated an inward current of 45 nA that was similar in magnitude to the 48 nA given by uridine alone (Fig. 2-5A). Similarly, uridine and guanosine, which is not an h/rCNT1 substrate, also produced an inward current (46 nA) similar to that given by uridine alone (44 nA) (Fig. 2-5C). In marked contrast, however,

simultaneous perfusion of uridine and adenosine decreased the inward uridine current from 53 nA to only 10 nA (Fig. 2-5B).

Transport of the antiviral nucleoside drug AZT by hCNT1 has previously been demonstrated using radioisotope flux studies (Ritzel *et al.*, 1997). Consistent with these results, the addition of AZT (1 mM) to an hCNT1-producing oocyte produced an inward current of 15 nA in Na⁺-containing transport medium (Fig. 2-6B, *top panel*), while no current was generated in the same oocyte perfused with AZT under Na⁺-free conditions (choline transport medium). No currents were produced by the addition of AZT to a control water-injected oocyte in either transport medium (Fig. 2-6B, *bottom panel*). As shown in Figure 2-6C, the average current seen following addition of 1 mM AZT was 17 nA, compared to 52 nA with 100 μM uridine.

Transport of the antineoplastic drug gemcitabine was also investigated (Fig. 2-7). External application of gemcitabine (100 μM) in Na⁺-containing medium induced an inward current of 15 nA that returned to baseline on removal of the drug (Fig. 2-7B). The gemcitabine-induced inward current was not seen in control, water-injected oocytes (Fig. 2-7D) and was abolished when extracellular Na⁺ was replaced with choline (Fig. 2-7C). For comparison, uridine (100 μM) induced an inward current of 65 nA in the same hCNT1-producing oocyte (Fig. 2-7F).

The novel nucleoside mimics β-DFP-5M (1-(2-deoxy-β-D-ribofuranosyl)-2, 4-difluoro-5-methylbenzene) and β-DFP-5I (1-(2-deoxy-β-D-ribofuranosyl)-2, 4-difluoro-5-iodobenzene) (Figs. 2-8A and 2-8B, respectively), in which the pyrimidine nucleobase is replaced by a substituted aromatic ring, were similarly tested as potential hCNT1 permeants. Addition of β-DFP-5M and β-DFP-5I (both at a concentration of 100 μM) induced inward currents of 10 nA each in hCNT1-producing oocytes (Fig. 2-8C, *top panel*). The currents were reversible and Na⁺-dependent, and no currents were observed in control water-injected oocytes either in the presence or absence of Na⁺ (Fig. 2-8C, *bottom panel*).

Na⁺- and Uridine-Steady-State Kinetics and the Order of Substrate Binding - The two-microelectrode voltage clamp was also used to investigate the effects of varying the concentrations of uridine and Na⁺ on recombinant hCNT1 steady-state transport kinetics.

The dependence of hCNT1-mediated Na⁺ currents on the external concentration of uridine (0 - 1000 μM) was examined at three different extracellular Na⁺ concentrations (5, 25, and 100 mM NaCl; pH 7.5). Application of varying concentrations of uridine resulted in saturable inward current responses that were consistent with simple Michaelis-Menten kinetics (Fig. 2-9A). The apparent affinity for uridine ($K_m^{uridine}$) increased as the [Na⁺]_{out} increased, with no significant change in the maximal current ($I_{max}^{uridine}$). At 5, 25 and 100 mM external Na⁺, apparent $K_m^{uridine}$ (±SE) values were 139 ± 10, 80 ± 7 and 32 ± 5 μM, respectively, with corresponding $I_{max}^{uridine}$ (±SE) of 54 ± 1, 55 ± 2 and 54 ± 2 nA, respectively (Table 2-1).

The corresponding dependence of hCNT1-mediated Na⁺ currents on the external concentration of Na⁺ (0 - 100 mM NaCl; pH 7.5) was examined at two different concentrations of extracellular uridine (25 and 100 μM) (Fig. 2-9B). The Na⁺ concentration dependence of the steady-state transport current also conformed to simple Michaelis-Menten kinetics. Similar to the effect of increasing [Na⁺]_{out} on the apparent affinity of the transporter for uridine, increasing [uridine]_{out} also increased the apparent affinity of the transporter for Na⁺. However, in contrast to the lack of effect seen by varying [Na⁺]_{out} on $I_{max}^{uridine}$, the value of $I_{max}^{Na^+}$ increased when the external concentration of uridine increased. At 25 and 100 μM external uridine, apparent $K_m^{Na^+}$ (±SE) values were 12 ± 2 and 3 ± 1 mM, respectively, with corresponding $I_{max}^{Na^+}$ (±SE) values of 38 ± 2 and 64 ± 3 nA, respectively (Table 2-2). The predicted Na⁺/nucleoside coupling ratio, determined by Hill-type analysis of the relationship between uridine-induced current and Na⁺ concentration was 1:1. Fitting the 25 and 100 μM uridine current data in Figure 2-9B to the Hill equation yielded Hill coefficients of 0.73 ± 0.21 and 0.70 ± 0.17, respectively. In another independent Na⁺ activation experiment, a Hill coefficient of 1.1

was obtained (Fig. 2-11B). In subsequent experiments, the hCNT1 Na⁺/uridine coupling ratio was determined directly by measuring the charge to tracer uptake ratio.

Phloridzin Inhibition of hCNT1 Currents - Phloridzin is a high-affinity competitive inhibitor of the Na⁺-dependent sugar transporter family (SGLT1-3). Phloridzin has also been shown to inhibit Na⁺-dependent transport of radiolabeled uridine in bovine kidney epithelial brush-border membrane vesicles (Lee *et al.*, 1988) and in oocytes injected with rat jejunal mRNA (Huang *et al.*, 1993). Here, experiments were undertaken to investigate phloridzin inhibition of hCNT1 by examining the current magnitude in hCNT1-producing oocytes before and after incubation with phloridzin in Na⁺-containing transport medium. In order to increase levels of expression, these experiments used the enhanced *Xenopus* expression vector pGEM-HE. In the representative oocyte shown in Figure 2-10A, addition of 100 μM uridine produced an inward current of 60 nA (*left trace*). Following a 10 minute pre-incubation with a high concentration of phloridzin (10 mM), the magnitude of the inward current was reduced to 18 nA, corresponding to an inhibition of 70 % (*right trace*). The addition of 10 mM phloridzin alone did not induce any inward currents (data not shown), indicating that it is not a substrate of hCNT1. To determine the concentration of phloridzin causing half-maximal current response (IC₅₀) for phloridzin inhibition, uridine-induced currents (100 μM uridine) were measured following exposure of hCNT1-producing oocytes to progressively increasing concentrations of inhibitor. As shown in Figure 2-10B (*left panel*), inhibition of hCNT1-mediated uridine transport by phloridzin was incomplete; even with the highest concentration of phloridzin tested, a residual Na⁺ current equal to ~ 20 % of the control current could still be measured (see also Fig. 2-10A). From the data presented in Figure 2-10B (*left panel*), the IC₅₀ for phloridzin inhibition of that component of the current blocked by inhibitor was 0.21 ± 0.05 mM. For comparison, the effects of phloridzin on another human member of the CNT family, the broadly selective Na⁺-dependent nucleoside transporter hCNT3, were also investigated (Fig. 2-10B, *right panel*). In hCNT3-producing oocytes, phloridzin inhibited the uridine-induced currents to a greater extent than for hCNT1, although a small residual current of ~ 5 - 10 % was still observed. The IC₅₀ for phloridzin inhibition of the inhibitor-sensitive component of hCNT3

transport activity was 0.32 ± 0.09 mM. For comparison, the phloridzin inhibition profiles for hCNT1 and hCNT3 were also determined from measurements of ^{14}C -labeled uridine uptake (Fig. 2-10C). Results were similar to those seen with current measurements, giving IC_{50} values for the inhibitor-sensitive component of transport of 0.35 ± 0.12 mM for hCNT1 (Fig. 2-10C, *left panel*) and 0.32 ± 0.07 mM for hCNT3 (Fig. 2-10C, *right panel*). The components of hCNT1 and hCNT3 transport insensitive to phloridzin inhibition were similar to those found by current analysis.

Subsequent studies determined the effects of phloridzin on hCNT1 uridine and Na^+ transport kinetics (Fig. 2-11). To facilitate characterization of the inhibited transporter, these experiments also used the enhanced *Xenopus* expression vector pGEM-HE. In the first experiment, the dependence of hCNT1-mediated Na^+ currents on the external concentration of uridine (0 - 1000 μM) was examined at 100 mM external Na^+ before and after pre-incubation with 5 mM phloridzin (Fig. 2-11A). External application of uridine in the absence of phloridzin yielded dose-dependent saturable inward currents with an apparent K_m^{uridine} ($\pm\text{SE}$) of 22 ± 3 μM , a value similar to that obtained previously (Fig. 2-9A). Consistent with the use of pGEM-HE, however, the $I_{\text{max}}^{\text{uridine}}$ ($\pm\text{SE}$) of 151 ± 5 nA was substantially higher than obtained with pGEM-T (compare with Fig. 2-9), and can be accounted for by increased levels of transporter expression. Following incubation with phloridzin, both the apparent affinity of the transporter for uridine and the maximal current were reduced, giving K_m^{uridine} and $I_{\text{max}}^{\text{uridine}}$ ($\pm\text{SE}$) values of 131 ± 27 μM and 73 ± 9 nA, respectively. The parallel analysis of the effects of 5 mM phloridzin on the Na^+ concentration dependence of steady-state hCNT1 transport currents is shown in Figure 2-11B. The external application of uridine (100 μM), in the absence of phloridzin, yielded dose-dependent saturable inward currents with an apparent $K_m^{\text{Na}^+}$ ($\pm\text{SE}$) of 3 ± 0.3 mM, a value identical to that determined previously (Fig. 2-9B), with an $I_{\text{max}}^{\text{Na}^+}$ ($\pm\text{SE}$) of 95 ± 2 nA. Following incubation of the transporter with phloridzin, the apparent affinity of the transporter for Na^+ was increased, while the maximal rate of transport was reduced, giving $K_m^{\text{Na}^+}$ and $I_{\text{max}}^{\text{Na}^+}$ values ($\pm\text{SE}$) of 0.8 ± 0.2 mM and 22 ± 0.7 nA, respectively.

Cation/Nucleoside Coupling Ratios - The stoichiometry of Na⁺/uridine cotransport was determined in individual hCNT1-producing oocytes by measuring simultaneously the uridine-evoked hCNT1 current and ¹⁴C-uridine uptake under voltage-clamp conditions (Fig. 2-12). Figure 2-12A shows a representative uridine-dependent current recording in an hCNT1-producing oocyte clamped at -30 mV. Initially, the oocyte was perfused with substrate-free 100 mM Na⁺ transport medium (pH 7.5). Following the addition of 200 μM ¹⁴C-uridine (also in Na⁺ transport medium), an inward current of ~ 50 nA was produced. When uridine was removed from the bath by washing with substrate-free solution, the current returned to baseline. The current was integrated with time to determine the charge moved during the uptake period. The charge was then converted to its molar equivalent and compared to the ¹⁴C-uridine uptake measured in the same oocyte. The process was repeated in 10 different oocytes. As shown in Figure 2-12, the slope of the linear plot of charge (pmol) *versus* uptake (pmol) is equal to the Na⁺/nucleoside coupling ratio. This ratio was independent of voltage. At V_h = -30 mV, the linear correlation between uridine-dependent charge and uridine accumulation gave a stoichiometry of 0.92 ± 0.15 (mean ± SE, n = 10, Fig. 2-12B). Similar ratios of 0.89 ± 0.02 (n = 7, Fig. 2-12C) and 0.90 ± 0.09 (n = 9, Fig. 2-12D) were obtained at holding potentials of -50 and -90 mV, respectively.

Discussion

Using electrophysiological techniques in combination with heterologous expression in *Xenopus* oocytes, we have revealed new kinetic features of the human Na⁺-dependent pyrimidine nucleoside transporter hCNT1, including the current/voltage relationship, the order of substrate binding, and the stoichiometry of Na⁺/uridine cotransport determined under voltage-clamp conditions. Aspects of substrate specificity, including transport of adenosine, representative antineoplastic and antiviral drugs, and novel pyrimidine nucleoside mimics have also been investigated. The study also demonstrated, for the first time, hCNT1 (and hCNT3) inhibition by phloridzin. At the time the experiments described in this *Chapter* were initiated, no other electrophysiological investigations of CNT nucleoside transporters had been undertaken.

The transport of nucleosides by hCNT1 was shown to be electrogenic and Na⁺-dependent (Fig. 2-1). Inward currents, which were reversible following substrate removal, were generated after the addition of nucleosides in Na⁺-containing medium (Fig. 2-1A). The addition of an hCNT1 substrate in the absence of Na⁺ did not generate any detectable inward currents (Fig. 2-1B), in contrast to what has been reported recently for h/rCNT1 by other investigators (Dresser *et al.*, 2000; Lostao *et al.*, 2000). The present results are, however, in agreement with previous radiotracer uptake studies which found only very small amounts of nucleoside uptake in the absence of Na⁺ (Huang *et al.*, 1994; Ritzel *et al.*, 1997). This residual component of radiotracer nucleoside transport in the absence of Na⁺ had the characteristics of “slippage” (*ie.* uncoupled nucleoside transport) and would not be expected to be electrogenic. Transport of uridine was voltage-dependent, since the magnitude of the inward current was increased at more negative potentials, suggesting that transport of nucleosides across the cell membrane *via* nucleoside transport proteins is influenced by membrane potential (Fig. 2-2B). These results are in agreement with those reported by Lostao *et al.* (2000) in which an increase in I_{\max} was observed at hyperpolarized potentials in oocytes producing hCNT1. Earlier experiments in isolated rat hepatocytes also found that Na⁺-linked nucleoside uptake was dependent upon membrane potential (Gomez-Angelats *et al.*, 1996). Radiotracer uptake

and competition studies have previously demonstrated that h/rCNT1 selectively transport pyrimidine nucleosides and, to a lesser extent, the purine nucleoside adenosine (Fang *et al.*, 1996; Yao *et al.*, 1996a, b; Ritzel *et al.*, 1997). Consistent with these findings, hCNT1-mediated Na⁺ currents were observed following the addition of the pyrimidine nucleosides uridine, thymidine, and cytidine and, to a lesser extent, adenosine (Fig. 2-4A). The reduced magnitude of the adenosine-induced current relative to, for example, uridine is the consequence of a much reduced I_{\max} , resulting from a low rate of conversion of the CNT1-adenosine complex from outward-facing to inward-facing conformations (Yao *et al.*, 1996b). The present demonstration of hCNT1-mediated currents generated following the addition of adenosine are in contrast to results seen with recombinant rCNT1 in oocytes in which no currents were observed with adenosine (Dresser *et al.*, 2000). The apparent species discrepancy between hCNT1 and rCNT1 in this regard is technical in nature, since I have been able to detect rCNT1-mediated currents in the presence of adenosine (data not shown). Unlike adenosine, however, hCNT1 did not exhibit Na⁺ currents in the presence of either guanosine or inosine.

Competition studies, which involved the simultaneous addition of two potential substrates to the transporter, further illustrated the unique interaction of adenosine with hCNT1 (Fig. 2-5). In such experiments, the magnitude of the resulting current is dependent upon whether both nucleosides are transported by hCNT1 and, if so, their respective kinetic parameters (apparent K_m and V_{\max}). For example, the simultaneous addition of uridine and thymidine produced an inward current of similar magnitude to that seen with uridine alone (Fig. 2-5A). Flux studies have shown that uridine and thymidine are transported to a similar extent by hCNT1, with similar K_m and V_{\max} values (Ritzel *et al.*, 1997; Loewen *et al.*, 1999). The electrophysiological results show, therefore, that if two substrates compete for the same binding site on the transporter and have similar kinetic parameters for transport, the magnitude of the inward current will be similar to that seen when only one of the substrates is present, even though one will inhibit transport of the other, and *vice versa*. In the case of uridine and guanosine a similar result was obtained (Fig. 2-5C), in this case because the purine nucleoside guanosine is not an hCNT1 permeant and does not compete with uridine for binding to

the transporter. In marked contrast, however, the simultaneous addition of uridine and adenosine, both permeants of hCNT1, markedly reduced the magnitude of the inward current compared to that seen with uridine alone (Fig. 2-5B). This reflects the similar K_m values of the two nucleosides, but adenosine's very much decreased V_{max} (Yao *et al.*, 1996b; Ritzel *et al.*, 1997; Loewen *et al.*, 1999). The resultant cross-inhibition exerted by adenosine on hCNT1-mediated transport of uridine illustrates the potential for adenosine to act, in appropriate circumstances, as an hCNT1 inhibitor. Physiologically, local adenosine concentrations in the vicinity of the transporter would need to exceed the adenosine apparent K_m value of $\sim 25 \mu\text{M}$ for this effect to be exerted.

Radioisotope flux studies have shown that hCNT1 and rCNT1 not only transport physiological nucleosides, but also transport various synthetic nucleoside analogs (Huang *et al.*, 1994; Fang *et al.*, 1996; Yao *et al.*, 1996a, b; Ritzel *et al.*, 1997; Mackey *et al.*, 1998; Yao *et al.*, 2001). These findings are important because they establish a possible role for members of the CNT family in the intestinal absorption and renal handling of synthetic nucleoside analogs, as well as CNT involvement in drug uptake into other cell types that express the transporters. The pyrimidine nucleoside drug AZT, which is widely used in the treatment of acquired immunodeficiency syndrome (AIDS), has been shown to be a substrate of both hCNT1 and rCNT1 (Huang *et al.*, 1994; Yao *et al.*, 1996a; Ritzel *et al.*, 1997; Yao *et al.*, 2001). In agreement with these results, the addition of AZT to hCNT1-producing oocytes generated an inward current which was reversible and Na^+ -dependent (Fig. 2-6B). AZT was, however, a poorer substrate for hCNT1 than uridine, as demonstrated by the high concentration of drug (1 mM) needed to induce a significant inward current (Fig. 2-6C). Gemcitabine, a pyrimidine nucleoside analog used in the treatment of epithelial cancers, was also transported by hCNT1 (Fig. 2-7). This deoxycytidine analog generated similar currents as AZT, but at a 10-fold lower substrate concentration of 100 μM (Fig. 2-7B). Using electrophysiology, we were also able to test the ability of two novel compounds, which are not available in radioisotope form, to induce Na^+ currents in hCNT1-producing oocytes. These compounds, named β -DFP-5M and β -DFP-5I, belong to a new family of nucleoside analogs synthesized for evaluation as anticancer and antiviral agents (Figs. 2-8A and 2-8B, respectively) (Wang *et al.*,

2001). β -DFP-5M and β -DFP-5I were designed as thymidine mimics, in which the pyrimidine ring has been replaced by a substituted aromatic ring structure that does not contain nitrogen. The substituent on the aromatic ring for β -DFP-5M is a methyl group, while that for β -DFP-5I is an iodine group. Inward currents, which were reversible and Na^+ -dependent, were generated following bath application of both β -DFP-5M or β -DFP-5I, demonstrating that both of these novel compounds are substrates for the hCNT1 transporter (Fig. 2-8C). These results demonstrated that the pyrimidine ring structure *per se* is not required for translocation by hCNT1, and suggested that nucleoside mimics may have applications in studies to elucidate the substrate structural features important for CNT/permeant interactions. The ability of an aromatic ring structure to substitute for the pyrimidine nucleobase moiety of nucleosides indicates that $\pi - \pi$ interactions similar to those documented for trypanosomal ENT nucleoside transport proteins (de Koning and Jarvis, 1999) may be important also in CNT substrate interactions. Further characterization of hCNT1-mediated transport of the nucleoside mimics was not pursued as these analogs exhibited only negligible cytotoxicity against a variety of cancer cell lines and were inactive as antiviral agents (Wang *et al.*, 2001).

Cotransporters are integral membrane proteins which couple the electrochemical gradient of a cation (Na^+ or H^+) to the transport of substrate into cells. Na^+ -dependent cotransporters are found mostly in animal cells, whereas H^+ -dependent cotransporters occur in plants, bacteria, as well as animal cells. Cotransporters are often considered as specific for one cation, but several studies indicate that certain transporters utilize more than one cation to drive transport of the cosubstrate. The Na^+ /glucose cotransporters SGLT1 and SGLT2, for example, are able to utilize the electrochemical gradients of Na^+ , Li^+ , and H^+ to drive sugar transport into cells (Hirayama *et al.*, 1994; Mackenzie *et al.*, 1996). Similar observations have been reported for the bacterial melibiose transporter in which both Na^+ and H^+ can stimulate melibiose transport (Tsuchiya and Wilson, 1978; Bassilana *et al.*, 1987). In comparison, hCNT1 did not demonstrate detectable nucleoside transport when Na^+ was replaced with H^+ (Fig. 2-3A). This behaviour is in marked contrast to the broad specificity human and mouse nucleoside transporters hCNT3 and

mCNT3 which are able to use the electrochemical gradient of H^+ to drive the uptake of nucleosides into cells when Na^+ is not present (*Chapter III*). The present results demonstrate, therefore, that mammalian CNT isoforms exhibit other forms of functional diversity in addition to their differences in permeant selectivity. In contrast to mammalian CNT1 and CNT3, CNTs from *C. albicans* (CaCNT), *C. elegans* (CeCNT3), and *E. coli* (NupC) function exclusively as H^+ -dependent nucleoside cotransporters.

Analysis of the steady-state kinetic parameters (I_{max} and K_m) provides information about the binding order of substrates to cotransport processes (Stein, 1990; Klamo *et al.*, 1996). The transport of uridine by recombinant hCNT1 was saturable and conformed to Michaelis-Menten kinetics. As shown in Figure 2-9A, reducing the $[Na^+]_{out}$ increased $K_m^{uridine}$, while the $I_{max}^{uridine}$ was unaffected (Table 2-1). This suggests that limiting $[Na^+]_{out}$ can be overcome by increasing the concentration of uridine to achieve the same maximal rate of transport. This was in contrast to the effect seen when uridine was limiting, where $K_m^{Na^+}$ increased while $I_{max}^{Na^+}$ was reduced (Fig. 2-9B; Table 2-2). These steady-state data indicate a sequential ordered binding mechanism in which Na^+ binds to the transporter first, increasing the affinity of the protein for the nucleoside which then binds second (Jauch and Lauger, 1986; Klamo *et al.*, 1996; Mackenzie *et al.*, 1998). Transport of nucleoside and ion is simultaneous because decreasing the concentration of either Na^+ or uridine results in a decrease in the apparent affinity of the other (Eskandari *et al.*, 1997). A sequential ordered binding mechanism is consistent with results of earlier studies of native *cit/cif* Na^+ /nucleoside transport in bovine renal brush-border membrane vesicles which demonstrated that the apparent affinity of the transporters for nucleoside increased as the external Na^+ concentration was raised (Williams and Jarvis, 1991).

Phloridzin is an inhibitor of the Na^+ -dependent glucose transporter family (SGLT1-3) (Mackenzie *et al.*, 1996; Hirayama *et al.*, 2001) that has also been shown to block intestinal and kidney Na^+ -dependent nucleoside transport activity (Lee *et al.*, 1988; Huang *et al.*, 1993). There are no other known or potential inhibitors of the CNT transporters, and we therefore investigated the ability of phloridzin to inhibit hCNT1-mediated Na^+ -dependent uridine transport using electrophysiological techniques (Fig. 2-

10). Phloridzin inhibited uridine-dependent hCNT1 currents in a concentration dependent manner (Fig. 2-10B, *left panel*), but was unable to completely block transport even at very high inhibitor concentrations. The IC_{50} for phloridzin blockade of that component of the hCNT1-mediated Na^+ current sensitive to phloridzin inhibition was 0.21 ± 0.05 mM. Phloridzin also inhibited hCNT3-mediated currents with a lower IC_{50} value of 0.32 ± 0.09 mM (Fig. 2-10B, *right panel*), and inhibition of both recombinant transporters was confirmed by ^{14}C -uridine flux studies (Fig. 2-10C). Phloridzin may therefore function as a general CNT transport inhibitor, but its potency against CNTs is substantially less than against SGLT transporters, where IC_{50} values in the low micromolar concentration range have been obtained (IC_{50} of $0.17 \mu M$ for rat SGLT1) (Lee *et al.*, 1994). Analysis of steady-state kinetic parameters in the presence and absence of phloridzin were undertaken to provide information about the method by which phloridzin inhibits hCNT1-mediated nucleoside transport activity. As shown in Figure 2-11A, phloridzin increased $K_m^{uridine}$ and reduced $I_{max}^{uridine}$. Both $K_m^{Na^+}$ and $I_{max}^{Na^+}$ were reduced by phloridzin inhibition (Fig. 2-11B).

Analysis of the interactions of substrates and inhibitors provides unique insights into transporter function. Classically, inhibitors are defined by the method of inhibition (Dixon and Webb, 1958). The effects seen with phloridzin on the kinetic parameters of hCNT1 Na^+ -activation are consistent with uncompetitive inhibition; both $K_m^{Na^+}$ and $I_{max}^{Na^+}$ decreased, but the ratio between $K_m^{Na^+}$ and $I_{max}^{Na^+}$ before and after phloridzin inhibition was unchanged (Wong, 1975). In contrast, the effects on uridine transport kinetics (increased $K_m^{uridine}$ and decreased $I_{max}^{uridine}$) are consistent with mixed-noncompetitive inhibition (Wong, 1975). The interpretation of these different patterns of inhibition is that phloridzin binds to the transporter after Na^+ (*ie.* phloridzin binding is Na^+ -dependent) at a site possibly overlapping with, but not identical to, that occupied by nucleoside. There are parallels, therefore, between phloridzin inhibition of hCNT3 and SGLT1. For the latter transporter, various studies have shown that inhibition of Na^+ /glucose cotransport is competitive (Vick *et al.*, 1973; Lin and Hahn, 1983) and binding of phloridzin to the

transporter is Na⁺-dependent (Parent *et al.*, 1992a, b). Structurally, the phloridzin molecule is composed of a pyranoside ring and two aromatic rings joined by an alkyl spacer (Weilert-Badt *et al.*, 2000). It has been postulated that multiple domains are involved in phloridzin inhibition of SGLT1, with both the sugar binding site of the transporter and a binding site for the phloridzin aglucone moiety participating in carrier/inhibitor interactions through hydrogen bonding and hydrophobic interactions, respectively (Hirayama *et al.*, 2001; Novakova *et al.*, 2001). Similarly, phloridzin binding to hCNT1 may partially overlap the translocation pore. In the search for new and more effective CNT transport inhibitors, it is noteworthy that h/rCNT1 has a greater apparent affinity for adenosine than hCNT1 has for phloridzin (Yao *et al.*, 1996b; Ritzel *et al.*, 1997; Loewen *et al.*, 1999). Future studies of adenosine-related compounds may therefore discover more effective hCNT1 transport inhibitors.

Na⁺-dependent transporters rely on the inwardly-directed Na⁺ gradient to accumulate substrate within the cell, where the concentrating capacity of the transporter is determined by its Na⁺/substrate coupling ratio. The higher the coupling ratio (one or more Na⁺ per substrate), the greater the ability of the transporter to accumulate substrate against its concentration gradient and achieve higher concentrations within the cell. Previous Na⁺/nucleoside coupling ratios for members of the CNT family have been determined indirectly from Hill-type analysis of the relationship between nucleoside flux and Na⁺ concentration. Na⁺/nucleoside coupling ratios of 1:1 have been proposed for recombinant rCNT1 for both adenosine and uridine based on Hill coefficients (Yao *et al.*, 1996b), and similar Hill coefficients have been found in studies of Na⁺-dependent nucleoside transport in kidney brush-border membrane vesicles (Lee *et al.*, 1988; Williams and Jarvis, 1991). Hill coefficients obtained for hCNT1 in this *Chapter* were also consistent with a 1:1 coupling stoichiometry. However, Hill analysis of Na⁺ activation curves provides an index of the number of Na⁺ ions necessary to activate the transport process, but does not determine the number of Na⁺ ions that actually enter the cell as a result of transport activity (Weiss, 1997). We therefore utilized simultaneous measurement of transporter-specific currents and radioactive nucleoside uptake from the same oocyte under voltage-clamp conditions to determine directly the Na⁺/nucleoside

coupling ratio of hCNT1. Currents, which were monitored continuously during the uptake period, reached an initial maximal value and then progressively decreased (Fig. 2-12A). This decline in current magnitude has also been observed for other cotransporters and is thought to be the result of decreased concentrations of ions at the immediate proximity of the extracellular membrane and *trans*-inhibition of transport activity resulting from the accumulation of intracellular substrates and/or ions (Chen *et al.*, 1998; Mackenzie *et al.*, 1998; Chen *et al.*, 1999). To examine the effect of membrane potential on the Na⁺/nucleoside coupling ratio, the hCNT1 coupling stoichiometry was examined at various holding potentials (-30, -50, and -90 mV). When charge was converted to picomoles, the ratio of charge to nucleoside uptake for hCNT1 yielded a stoichiometry of 0.92 ± 0.15 at a holding potential of -30 mV, 0.89 ± 0.02 at -50 mV, and 0.90 ± 0.09 at -90 mV (Fig. 2-12). Therefore, both direct and indirect methods agree on a Na⁺/nucleoside coupling ratio of 1:1 for the CNT1 transporters, independent of the membrane potential. This is in marked contrast to results obtained with hCNT3 (*Chapter III*) where the coupling ratio approaches a value of 2:1 as the membrane becomes more hyperpolarized. In this respect, CNTs demonstrate similarities to other transporter families, in which different family members exhibit different coupling ratios. For example, different members of the SGLT glucose transporter family have Na⁺/glucose coupling ratios of either 1:1 or 2:1 (1:1 for SGLT2 and 2:1 for SGLT1/3) (Chen *et al.*, 1995; Mackenzie *et al.*, 1996, 1998; Diez-Sampedro *et al.*, 2001). Similarly, the PepT1 and PepT2 proton-linked peptide transporters have 1:1 and 2:1 H⁺/peptide coupling ratios, respectively (Chen *et al.*, 1999).

Table 2-1. hCNT1 Uridine Kinetic Parameters.

[Na⁺] (mM)	Apparent $K_m^{uridine}$ (μM)^a	$I_{max}^{uridine}$ (nA)^a
5	139 ± 10	54 ± 1
25	80 ± 7	55 ± 2
100	32 ± 5	54 ± 2

^a, from Fig. 2-9A

Table 2-2. hCNT1 Na⁺ Kinetic Parameters.

[Uridine] (μM)	Apparent $K_m^{\text{Na}^+}$ (mM) ^a	$I_{\text{max}}^{\text{Na}^+}$ (nA) ^a
25	12 \pm 2	38 \pm 2
100	3 \pm 1	64 \pm 3

^a, from Fig. 2-9B

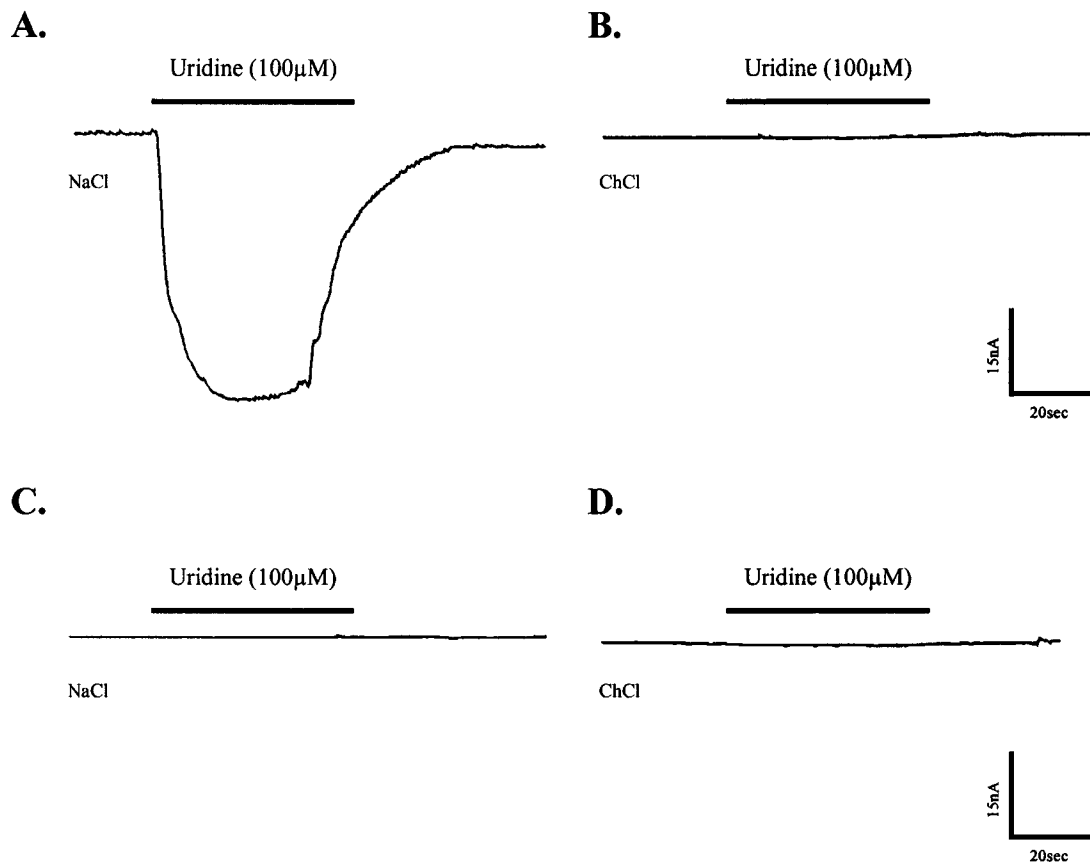


Figure 2-1. Na⁺-dependence of hCNT1-mediated uridine transport. Oocytes were injected with 10 nl of water containing 10 ng of RNA transcript encoding hCNT1 or 10 nl of water alone (control). **A.** Inward current generated by perfusing an RNA-injected oocyte with 100 μM uridine in Na⁺-containing transport medium (100 mM NaCl; pH 7.5). **B.** The same oocyte perfused with 100 μM uridine in transport medium in which Na⁺ was replaced by choline (100 mM ChCl; pH 7.5). No inward current was generated. **C** and **D** show the same experiment described in **A** and **B** above, but with a control water-injected oocyte. No inward currents were generated.

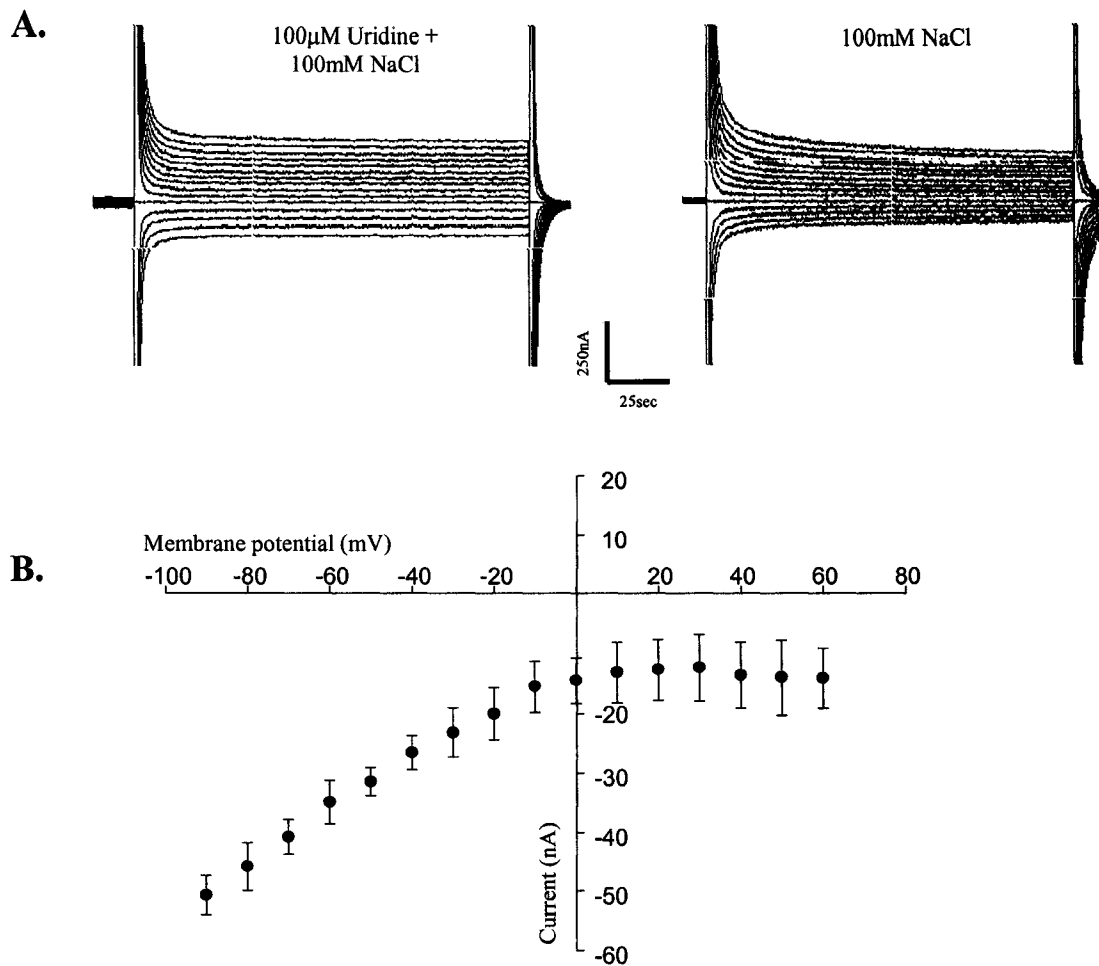
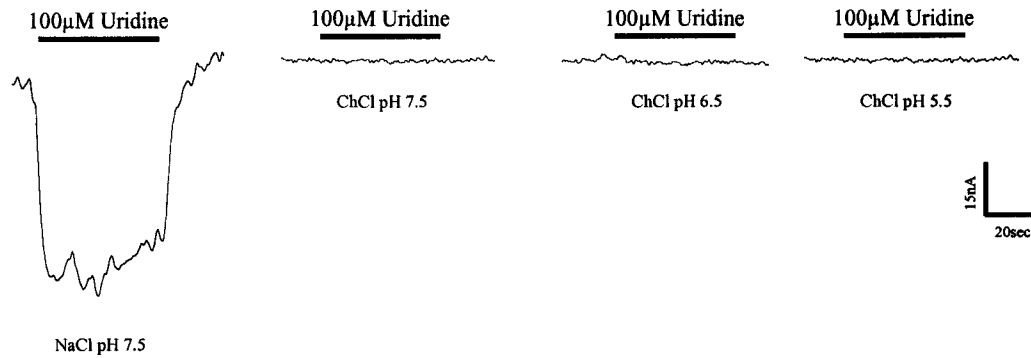


Figure 2-2. hCNT1 steady-state current/voltage relationship. **A.** Time course of transmembrane currents recorded in the presence of 100 μ M external uridine (100 mM NaCl; pH 7.5) upon voltage steps from a holding potential (V_h) of -50 mV to final potentials ranging between -90 and +60 mV, in 10 mV increments (*left trace*). The capacitive transients have been truncated in order to clearly demonstrate the steady-state currents. Currents from the same oocyte were recorded in the absence of uridine (100 mM NaCl; pH 7.5; *right trace*). **B.** The current/voltage (I/V) curve was generated by subtraction of the steady-state currents in the presence and absence of 100 μ M uridine. The current produced at each potential was averaged from 4 - 5 different oocytes.

A.

hCNT1



B.

Control

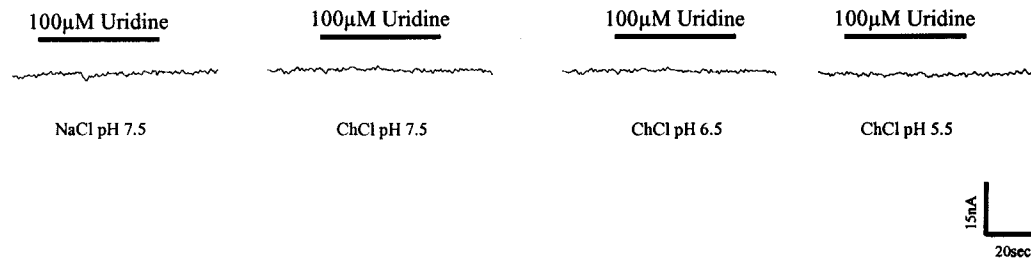
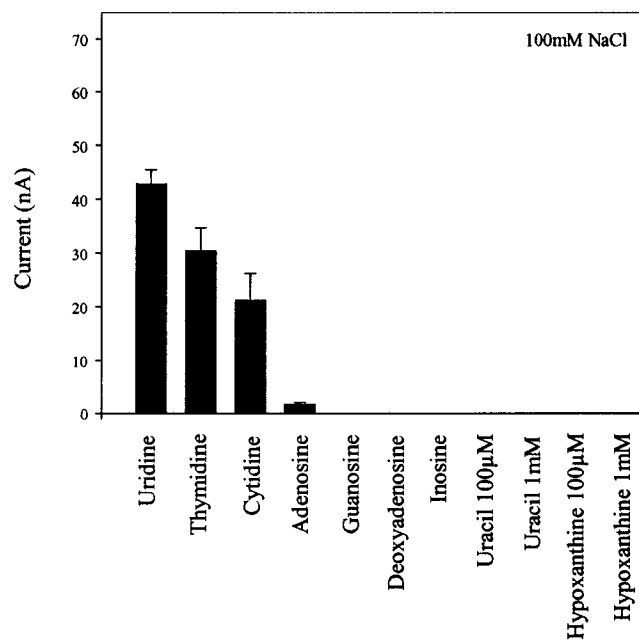


Figure 2-3. Cation specificity of hCNT1. **A.** The ability of H^+ to drive the transport of uridine by hCNT1 was investigated by comparing the magnitudes of current produced in Na^+ -containing transport medium (100 mM NaCl; pH 7.5) to current produced when Na^+ was replaced with choline and the pH was varied from 7.5 to 5.5 (100 mM ChCl). **B.** The same experiment was performed as in **A**, but with a control water-injected oocyte. No inward currents were generated.

A.



B.

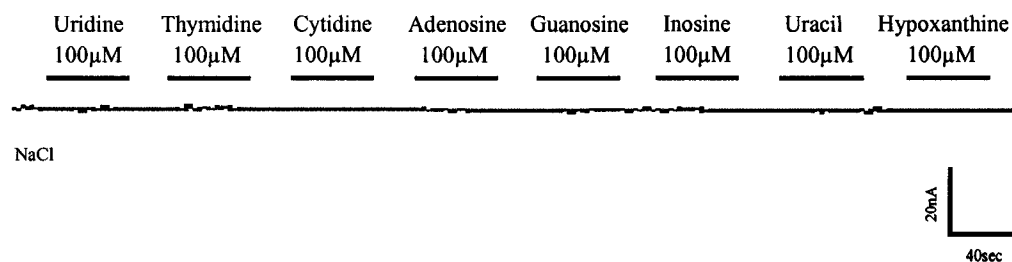


Figure 2-4. Nucleoside specificity of hCNT1. **A.** The substrate selectivity of hCNT1 was investigated in Na^+ -containing transport medium (100 mM NaCl; pH 7.5) by measuring the currents evoked by a variety of pyrimidine and purine nucleosides, each at a concentration of 100 μM . The nucleobases uracil and hypoxanthine (100 μM and 1 mM) were also tested. hCNT1-mediated currents are expressed as the mean current produced in 4 - 5 different oocytes. **B.** Current trace from a control water-injected oocyte perfused with various substrates in Na^+ -containing transport medium (100 mM NaCl; pH 7.5). No inward currents were observed with any of the substrates tested.

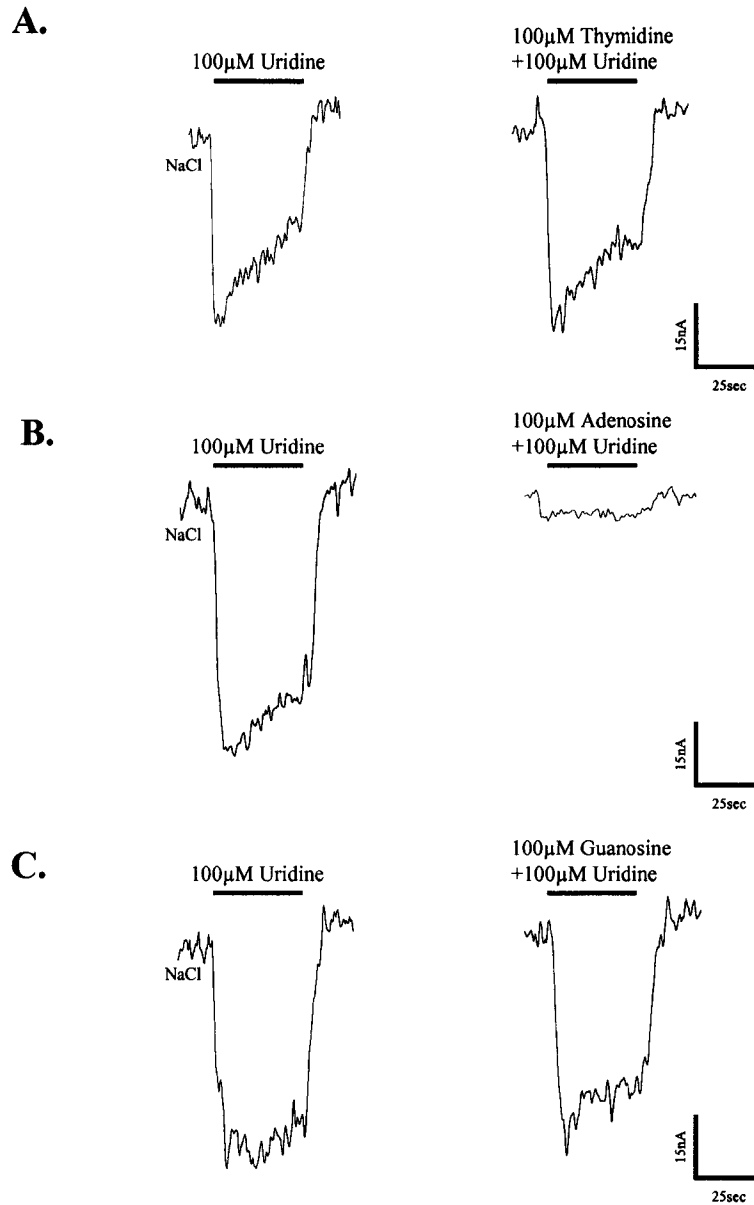


Figure 2-5. hCNT1 competition studies. **A.** The current produced by perfusing an hCNT1-producing oocyte with 100 μM uridine (*left trace*) in Na^+ -containing transport medium (100 mM NaCl; pH 7.5) was compared to the current generated when the same oocyte was simultaneously perfused with 100 μM uridine plus 100 μM thymidine (*right trace*). **B.** The same experiment was performed as in **A** but with 100 μM uridine plus 100 μM adenosine added to the transport medium. **C.** The nucleosides guanosine and uridine (each at a concentration of 100 μM) were added simultaneously to the oocyte.

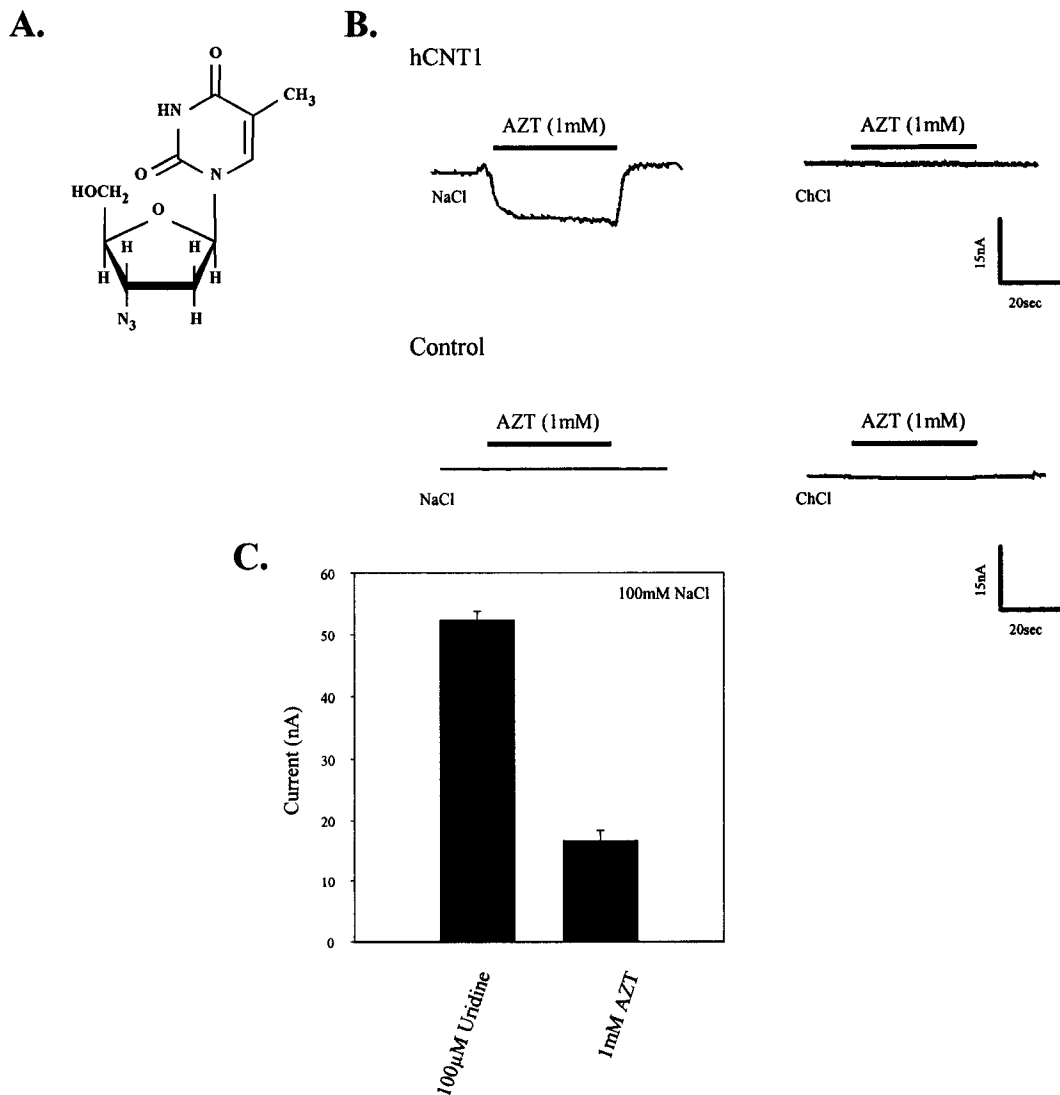
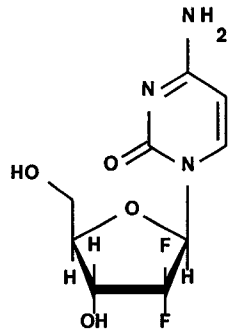
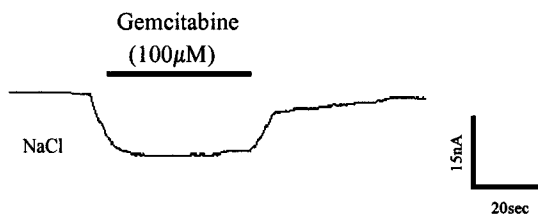


Figure 2-6. Transport of AZT. **A.** Structure of AZT (3'-azido-3'-deoxythymidine). **B.** Oocytes were injected with 10 nl of water containing 10 ng of RNA transcript encoding hCNT1 or 10 nl of water alone (control). Current responses generated by perfusing an hCNT1-producing oocyte with 1 mM AZT in Na^+ (100 mM NaCl; pH 7.5)- and choline (100 mM ChCl; pH 7.5)-containing transport media (*top panel*). The same experiment was also performed in a control water-injected oocyte (*bottom panel*). No inward currents were generated. **C.** A comparison of currents generated in hCNT1-producing oocytes following the addition of uridine (100 μ M) or AZT (1 mM) in Na^+ -containing transport medium. Values are for mean currents produced in 3 - 4 different oocytes from at least two different donors.

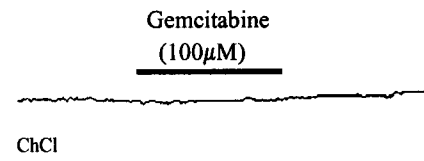
A.



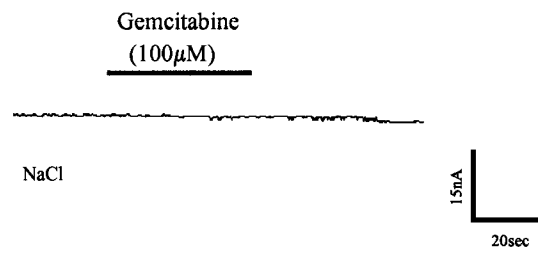
B.



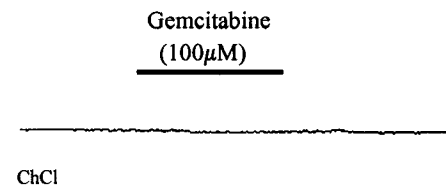
C.



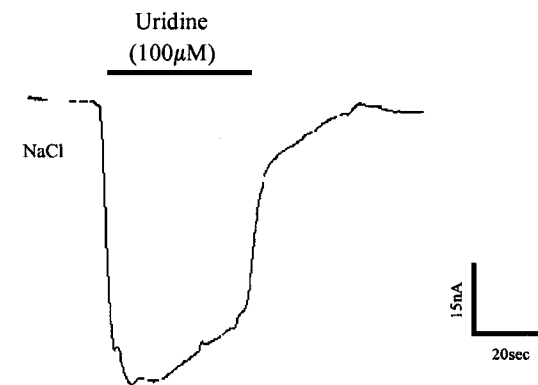
D.



E.



F.



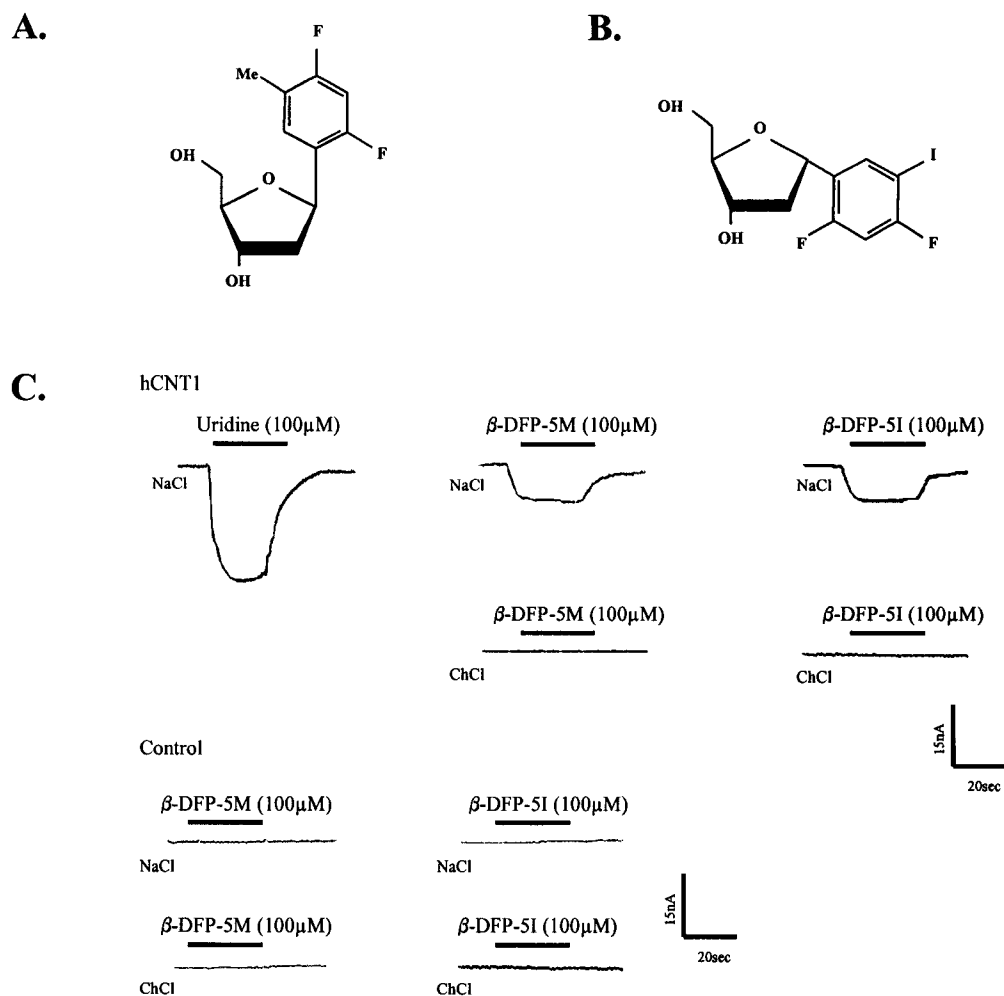


Figure 2-8. Transport of nucleoside mimics. **A.** Structure of β -DFP-5M (1-(2-deoxy- β -D-ribofuranosyl)-2, 4-difluoro-5-methylbenzene). **B.** Structure of β -DFP-5I (1-(2-deoxy- β -D-ribofuranosyl)-2, 4-difluoro-5-iodobenzene). **C.** Oocytes were injected with 10 nl of water containing 10 ng of RNA transcript encoding hCNT1 or 10 nl of water alone (control). Current responses generated by perfusing an hCNT1-producing oocyte with the nucleoside mimics β -DFP-5M and β -DFP-5I (each at a concentration of 100 μ M) in Na^+ - (100 mM NaCl)- and choline (100 mM ChCl)-containing transport mediums (*top panel*) (pH 7.5). The current produced with 100 μ M uridine in Na^+ -transport medium is shown for comparison. The same experiment was performed in a control water-injected oocyte (*bottom panel*). No currents were generated with either nucleoside mimic in the two transport media.

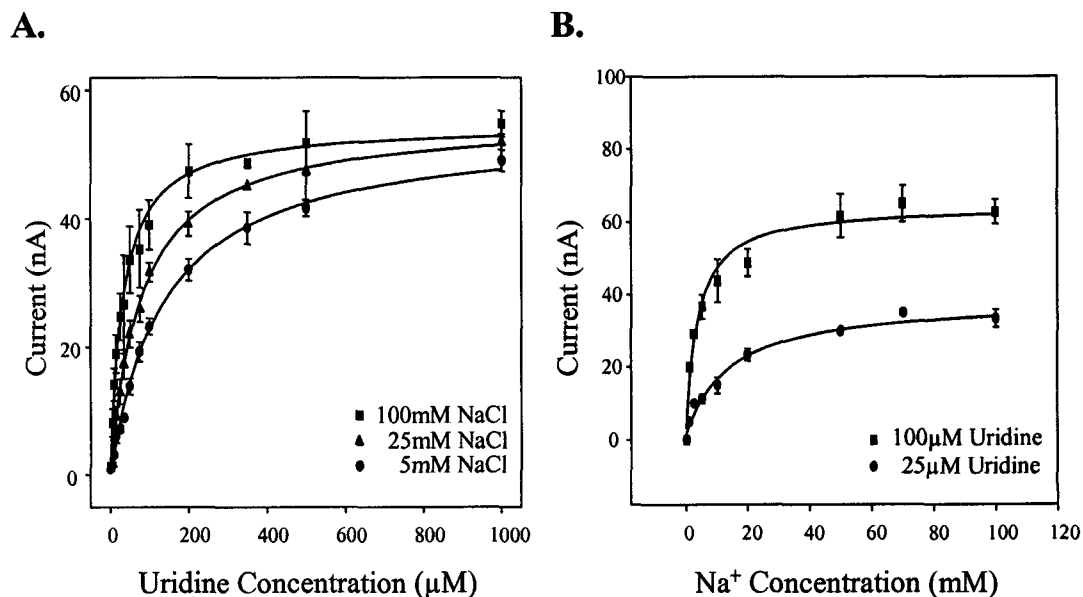
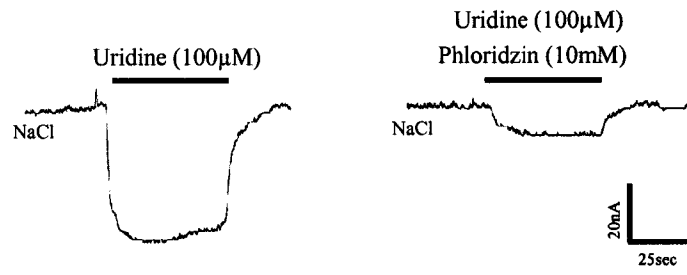
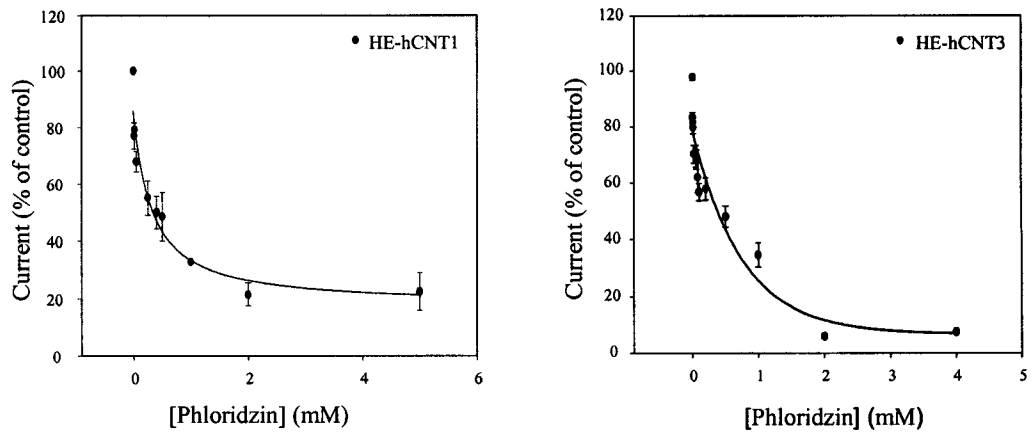


Figure 2-9. Steady-state hCNT1 kinetics and the order of solute binding. **A.** The dependence of hCNT1-mediated currents on the external concentration of uridine (0 - 1000 μM) was examined at three different concentrations of Na^+ (5, 25, and 100 mM NaCl; pH 7.5). hCNT1 mediated currents are expressed as the mean current produced in 5 - 6 different oocytes from at least 2 different donors. **B.** The dependence of hCNT1-mediated currents on the external concentration of Na^+ (0 - 100 mM NaCl; pH 7.5) was examined at two different concentrations of uridine (25 and 100 μM). hCNT1-mediated currents are expressed as the mean current produced in 4 - 5 different oocytes from at least 2 different donors.

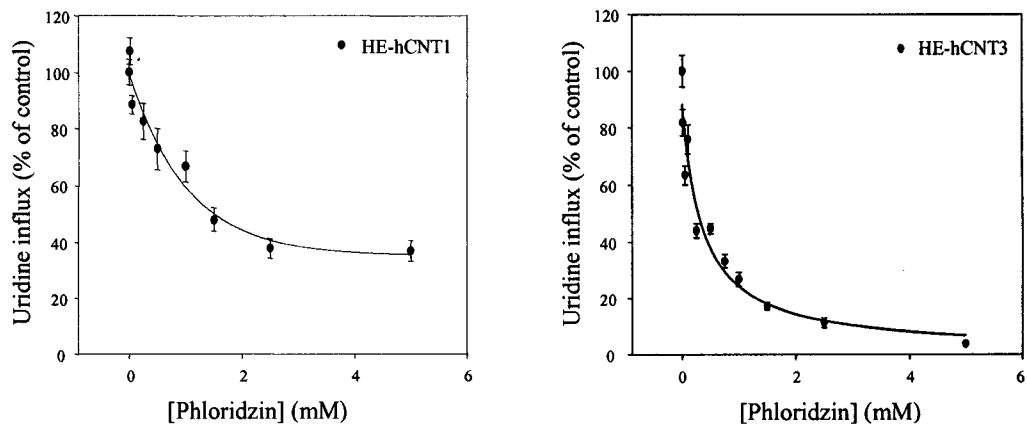
A.



B.



C.



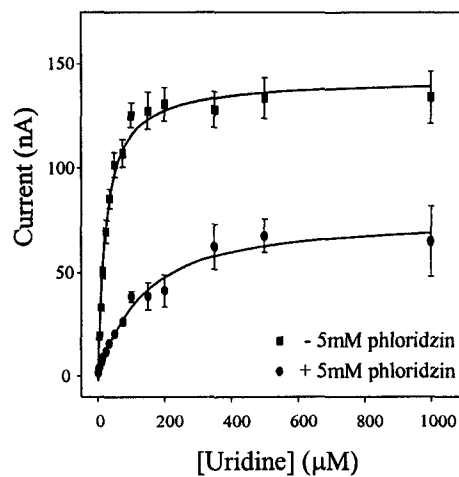
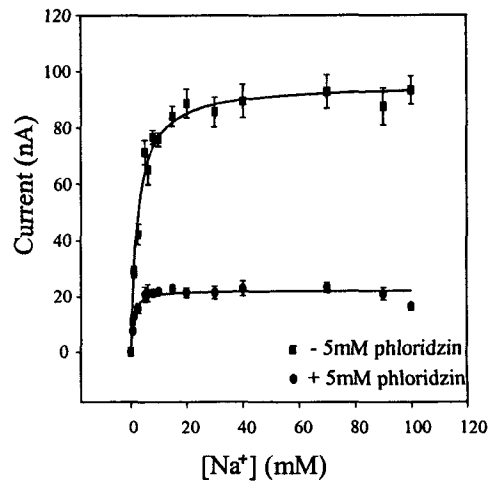
A.**B.**

Figure 2-11. Effect of phloridzin on hCNT1 steady-state kinetic parameters. A. The dependence of hCNT1-mediated currents on the external concentration of uridine was examined in the presence and absence of phloridzin. Uridine-induced currents (0 - 1000 μM) were measured in the presence of 100 mM external Na⁺ before and after a 10 min incubation with 5 mM phloridzin. Currents are expressed as the mean current produced in 5 - 6 different oocytes. **B.** The dependence of hCNT1-mediated currents on the external concentration of Na⁺ was examined in the presence and absence of phloridzin. Uridine-induced currents (100 μM) were measured in the presence of increasing concentrations of external Na⁺ (0 - 100 mM) before and after a 10 min incubation with 5 mM phloridzin. Currents are expressed as the mean current produced in 5 - 6 different oocytes.

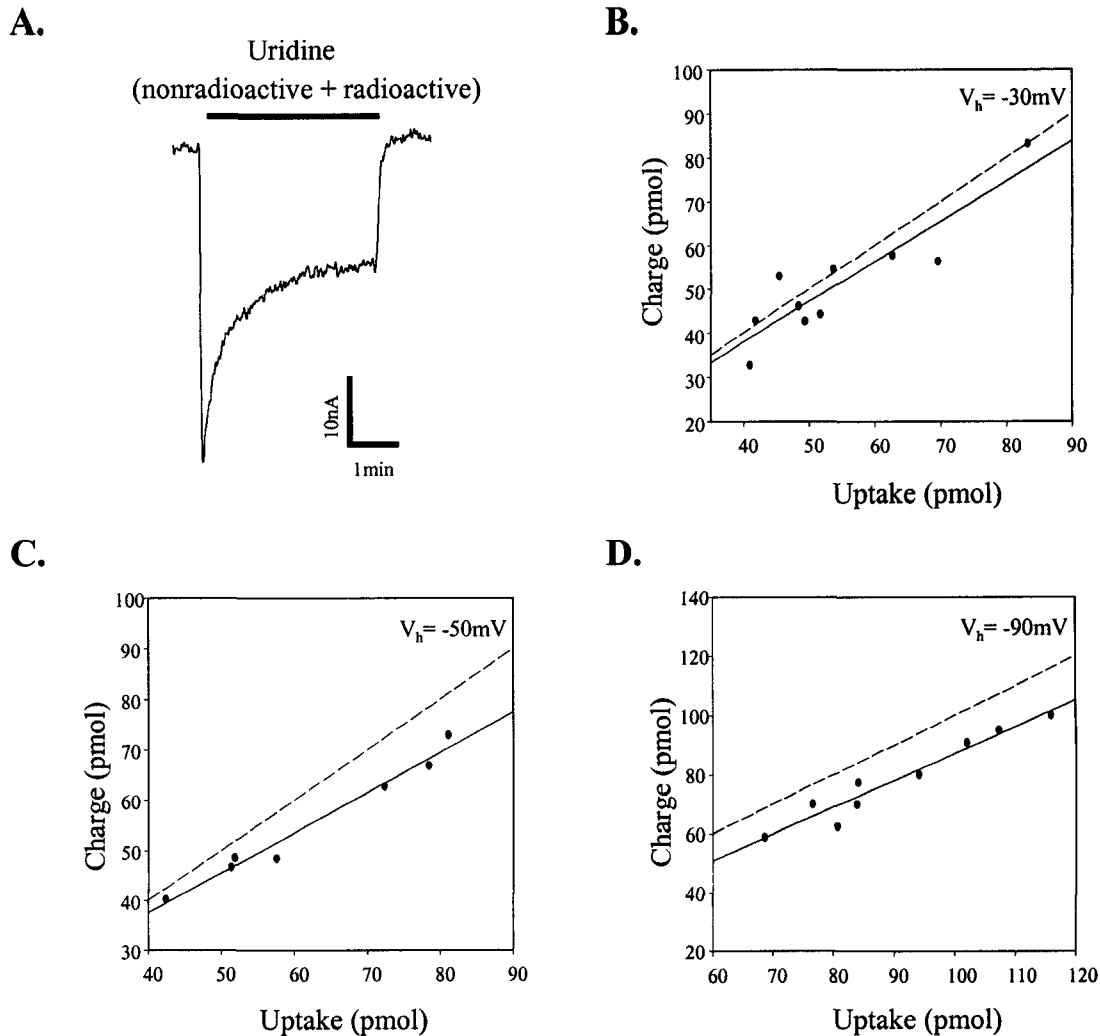


Figure 2-12. Stoichiometry of hCNT1. **A.** Representative example of the current generated during application of 200 μM uridine (nonradioactive + radioactive) to an hCNT1-producing oocyte ($V_h = -30\text{ mV}$). **B.** Oocytes were clamped at $V_h = -30\text{ mV}$ and perfused with 200 μM uridine (nonradioactive + radioactive). Integration of the uridine-evoked current over the uptake period (3 min) yielded the charge moved. The charge moved was converted to pmol and plotted against radiolabeled uridine uptake (pmol) in the same oocyte. The experiment was performed in 10 different oocytes. The slope of the linear fit ($\text{Na}^+/\text{nucleoside}$ ratio) was equal to 0.92 ± 0.15 (n = 10) (*solid line*). The dashed line indicates a slope of 1. **C.** At $V_h = -50\text{ mV}$, the $\text{Na}^+/\text{nucleoside}$ ratio was 0.89 ± 0.02 (n = 7). **D.** At $V_h = -90\text{ mV}$, the $\text{Na}^+/\text{nucleoside}$ ratio was 0.90 ± 0.09 (n = 9).

Bibliography

Acimovic Y and Coe IR. Molecular evolution of the equilibrative nucleoside transporter family: identification of novel family members in prokaryotes and eukaryotes. *Mol Biol Evol* 19(12): 2199-2210, 2002.

Baldwin SA, Mackey JR, Cass CE, and Young JD. Nucleoside transporters: molecular biology and implications for therapeutic development. *Mol Med Today* 5: 216-224, 1999.

Bassilana M, Pourcher T, and Leblance G. Facilitated diffusion properties of melibiose permease in *Escherichia coli* membrane vesicles. Release of co-substrates is rate limiting for permease cycling. *J Biol Chem* 262 (35): 16865-16870, 1987.

Cass CE. In: Drug transport in antimicrobial and anticancer chemotherapy, edited by Georgopapadakou NH. New York: Marcel Dekker, 1995.

Che M, Ortiz DF, and Arias IM. Primary structure and functional expression of a cDNA encoding the bile canalicular, purine-specific Na⁺ nucleoside cotransporter. *J Biol Chem* 270: 13596-13599, 1995.

Chen XZ, Coady MJ, Jackson F, Bertleoot A, and Lapointe J-Y. Thermodynamic determination of the Na⁺:glucose coupling ratio for the human SGLT1 cotransporter. *Biophys J* 69: 2405-2414, 1995.

Chen XZ, Shayakul C, Berger UV, Tian W, and Hediger MA. Characterization of a rat Na⁺-dicarboxylate cotransporter. *J Biol Chem* 273 (33): 20972-20981, 1998.

Chen X-Z, Zhu T, Smith DE, and Hediger MA. Stoichiometry and kinetics of the high-affinity H⁺-coupled peptide transporter PepT2. *J Biol Chem* 274: 2773-2779, 1999.

Craig JE, Zhang Y, and Gallagher MP. Cloning of the *nupC* gene of *Escherichia coli* encoding a nucleoside transport system, and identification of an adjacent insertion element, IS 186. *Mol Microbiol* 11: 1159-1168, 1997.

Crawford CR, Patel DH, Naeve C, and Belt JA. Cloning of the human equilibrative, nitrobenzylmercaptapurine riboside (NBMPR)-insensitive nucleoside transporter *ei* by functional expression in a transport-deficient cell line. *J Biol Chem* 273(9): 5288-5293, 1998.

de Koning HP and Jarvis SM. Adenosine transporters in bloodstream forms of *Trypanosoma brucei brucei*: Substrate recognition motifs and affinity for trypanocidal drugs. *Mol Pharmacol* 56: 1162-1170, 1999.

Diez-Sampedro A, Eskandari S, Wright EM, and Hirayama BA. Na⁺-to-sugar stoichiometry of SGLT3. *Am J Physiol Renal Physiol* 49: F278-F282, 2001.

Dixon M and Webb E. In: *Enzymes*. London, W.I.: Longmans, Green and Co., Ltd., 1958.

Dresser MJ, Gerstin KM, Gray AT, Loo DF, and Giacomini KM. Electrophysiological analysis of the substrate selectivity of a sodium-coupled nucleoside transporter (rCNT1) expressed in *Xenopus laevis* oocytes. *Drug Metab Dispos* 28: 1135-1140, 2000.

Eskandari S, Loo DDF, Dai G, Levy O, Wright EM, and Carrasco N. Thyroid Na⁺/I⁻ symporter. *J Biol Chem* 272 (43): 27230-27238, 1997.

Fang X, Parkinson FE, Mowles DA, Young JD, and Cass CE. Functional characterization of a recombinant sodium-dependent nucleoside transporter with selectivity for pyrimidine nucleosides (CNT1_{rat}) by transient expression in cultured mammalian cells. *Biochem J* 317: 457-465, 1996.

Fredholm BB. Adenosine and neuroprotection. *Int Rev Neurobiol* 40: 259-80, 1997.

Griffiths DA and Jarvis SM. Nucleoside and nucleobase transport systems of mammalian cells. *Biochim Biophys Acta* 1286: 153-181, 1996.

Gomez-Angelats M, Del Santo B, Mercader J, Ferrer-Martinex A, Gelipe A, Casado J, and Pastor-Anglada M. Hormonal regulation of concentrative nucleoside transport in liver parenchymal cells. *Biochem J* 313: 915-920, 1996.

Hamilton SR, Yao SYM, Ingram JC, Hadden DA, Ritzel MWL, Gallagher MP, Henderson PJF, Cass CE, Young JD, and Baldwin SA. Subcellular distribution and membrane topology of the mammalian concentrative Na⁺-nucleoside cotransporter rCNT1. *J Biol Chem* 276(30): 27981-27988, 2001.

Handschumacher RE and Cheng CY. In: *Cancer Metabolism* (Holland E, Frei E, Bast RC, Kufe DW, Morton DL, and Weichselbaum RR, eds.). pp. 712-732, Lea & Febiger, Philadelphia, 1993.

Hirayama BA, Loo DDF, and Wright EM. Protons drive sugar transport through the Na⁺/glucose cotransporter (SGLT1). *J Biol Chem* 269 (34): 21407-21410, 1994.

Hirayama BA, Diez-Sampedro A, and Wright EM. Common mechanisms of inhibition for the Na⁺/glucose (hSGLT1) and Na⁺/Cl⁻/GABA (hGAT1) cotransporter. *Br J Pharmacol* 134: 484-495, 2001.

Huang Q-Q, Harvey CM, Paterson ARP, Cass CE, and Young JD. Functional expression of Na⁺-dependent nucleoside transport systems of rat intestine in isolated oocytes of *Xenopus laevis*: Demonstration that rat jejunum expresses the purine-selective system N1 (*cif*) and a second, novel system N3 having broad specificity for purine and pyrimidine nucleosides. *J Biol Chem* 27: 20613-20619, 1993.

Huang Q-Q, Yao SYM, Ritzel MWL, Paterson ARP, Cass CE, and Young JD. Cloning and functional expression of a complementary DNA encoding a mammalian nucleoside transport protein. *J Biol Chem* 269: 17757-17760, 1994.

Hyde RJ, Cass CE, Young JD, and Baldwin SA. The ENT family of eukaryote and nucleobase transporters: recent advances in the investigation of structure/function relationships and the identification of novel isoforms. *Mol Membr Biol* 18: 53-63, 2001.

Jauch P and Lauger P. Electrogenic properties of the sodium-alanine cotransporter in pancreatic acinar cells: II. Comparison with transport models. *J Membr Biol* 94: 117-127, 1986.

Klamo EM, Drew ME, Landfear SM, and Kavanaugh MP. Kinetics and stoichiometry of a proton/*myo*-inositol cotransporter. *J Biol Chem* 271 (25): 14937-14943, 1996.

Kiss A, Farah K, Kim J, Garriock RJ, Drysdale TA, and Hammond JR. Molecular cloning and functional characterization of inhibitor-sensitive (mENT1) and inhibitor-resistant (mENT2) equilibrative nucleoside transporters from mouse brain. *Biochem J* 352: 363-372, 2000.

Lee CW, Cheeseman CI, and Jarvis SM. Na⁺- and K⁺-dependent uridine transport in rat renal brush-border membrane vesicles. *Biochim Biophys Acta* 942(1): 139-149, 1988.

Lee W-S, Kanai Y, Wells RG, and Hediger MA. The high affinity Na⁺/glucose cotransporter. Re-evaluation of function and distribution of expression. *J Biol Chem* 269 (16): 12032-12039, 1994.

Liman ER, Tytgat J, and Hess P. Subunit of stoichiometry of a mammalian K⁺ channel determined by construction of multimeric cDNAs. *Neuron* 9: 861-871, 1992.

Lin JT and Hahn K-D. Synthesis of ³H-phloridzin and its binding behaviour to renal brush border membranes. *Anal Biochem* 129: 337-344, 1983.

Loewen SK, Ng AML, Yao SYM, Cass CE, Baldwin SA, and Young JD. Identification of amino acid residues responsible for the pyrimidine and purine nucleoside specificities of human concentrative Na⁺ nucleoside cotransporters hCNT1 and hCNT2. *J Biol Chem* 274 (35): 24475-24484, 1999.

Loewen SK, Ng AML, Mohabir NN, Baldwin SA, Cass CE, and Young JD. Functional characterization of a H⁺/nucleoside cotransporter (CaCNT) from *Candida albicans*, the first fungal homolog of mammalian/bacterial concentrative nucleoside transporters. *Yeast* 2003 (*in press*).

Lostao MP, Mata JF, Larrayoz IM, Inzillo SM, Casado FJ, and Pastor-Anglada M. Electrogenic uptake of nucleosides and nucleoside-derived drugs by the human nucleoside transporter 1 (hCNT1) expressed in *Xenopus laevis* oocytes. *FEBS Lett* 481(2): 137-140, 2000.

Mackenzie B, Loo DDF, Panayotova-Heiermann M, and Wright EM. Biophysical characteristics of the pig kidney Na⁺/glucose cotransporter SGLT2 reveal a common mechanism for SGLT1 and SGLT2. *J Biol Chem* 271 (51): 32678-32683, 1996.

Mackenzie B, Loo DDF, and Wright EM. Relationships between Na⁺/glucose cotransporter (SGLT1) currents and fluxes. *J Membr Biol* 162: 101-106, 1998.

Mackey JR, Baldwin SA, Young JD, and Cass CE. Nucleoside transport and its significance for anticancer drug resistance. *Drug Resist Updat* 1: 310-324, 1998.

Mackey JR, Yao SYM, Smith KM, Karpinski E, Baldwin SA, Cass CE, and Young JD. Gemcitabine transport in *Xenopus* oocytes expressing recombinant plasma membrane mammalian nucleoside transporters. *J Natl Cancer Inst* 91(21): 1876-1881, 1999.

Novakova R, Homerova D, Kinne RKH, Kinne-Saffran E, and Lin JT. Identification of a region critically involved in the interaction of phloridzin with the rabbit sodium-D-glucose cotransporter SGLT1. *J Membr Biol* 184:55-60, 2001.

Parent L, Supplisson S, Loo DF, and Wright EM. Electrogenic properties of the cloned Na⁺/glucose cotransporter: Part I. Voltage-clamp studies. *J Membr Biol* 125: 49-62, 1992a.

Parent L, Supplisson S, Loo DF, and Wright EM. Electrogenic properties of the cloned Na⁺/glucose cotransporter: Part II. A transport model under non rapid equilibrium conditions. *J Membr Biol* 125: 63-79, 1992b.

Perigaud C, Aubertin AM, Benzaria S, Pelicano H, Girardet JL, Maury G, Gosselin G, Kirn A, and Imbach JL. Equal inhibition of the replication of human immunodeficiency virus in human T-cell culture by ddA bis(SATE)phosphotriester and 3'-azido-2',3'-dideoxythymidine. *Biochem Pharmacol* 48(1): 11-14, 1994.

Ritzel MWL, Yao SYM, Huang M-Y, Elliot JF, Cass CE, and Young JD. Molecular cloning and functional expression of cDNAs encoding a human Na⁺-nucleoside cotransporter (hCNT1). *Am J Physiol Cell Physiol* 272: C707-C714, 1997.

Ritzel MWL, Yao SYM, Ng AML, Mackey JR, Cass CE, and Young JD. Molecular cloning, functional expression and chromosomal localization of a cDNA encoding a human Na⁺ nucleoside cotransporter (hCNT2) selective for purine nucleosides and uridine. *Mol Membr Biol* 15: 203-211, 1998.

Ritzel MWL, Ng AML, Yao SYM, Graham K, Loewen SK, Smith KM, Ritzel GR, Mowles DA, Carpenter P, Chen XZ, Karpinski E, Hyde RJ, Baldwin SA, Cass CE, and Young JD. Molecular identification and characterization of novel human and mouse concentrative Na⁺-nucleoside cotransporter proteins (hCNT3 and mCNT3) broadly selective for purine and pyrimidine nucleosides (system *cib*). *J Biol Chem* 276 (4): 2914-2927, 2001.

Shryock JC and Belardinelli L. Adenosine and adenosine receptors in the cardiovascular system: biochemistry, physiology, and pharmacology. *Am J Cardiol* 79: 2-10, 1997.

Stein WD. In: Channels, Carriers, and Pumps. San Diego: Academic Press Inc., 1990, p173.

Tsuchiya T and Wilson TH. Cation-sugar cotransport in the melibiose transport system of *Escherichia coli*. *Membr Biochem* 2 (1): 63-79, 1978.

Vasudevan G, Carter NS, Drew ME, Beverley SM, Sanchez MA, Seyfang A, Ullman B, and Landfear SM. Cloning of *Leishmania* nucleoside transporter genes by rescue of a transport deficient mutant. *Proc Natl Acad Sci* 95(17): 9873-8, 1998.

Vick H, Diedrich DF, and Baumann K. Reevaluation of renal tubular glucose transport inhibition by phloridzin analogues. *Am J Physiol* 224: 552-557, 1973.

Wang J, Su S-F, Dresser MJ, Schaner ME, Washington CB, and Giacomini KM. Na⁺-dependent purine nucleoside transporter from human kidney: cloning and functional characterization. *Am J Physiol Renal Physiol* 273(42): F1058-F1065, 1997.

Wang ZX, Duan W, Wiebe LI, Balzarini J, De Clereq E, and Knauss EE. Synthesis of 1-(2-deoxy-beta-D-ribofuranosyl)-2, 4-difluoro-5-substituted-benzene thymidine mimics, some related alpha-anomers, and their evaluation as antiviral and anticancer agents. *Nucleosides Nucleotides Nucleic Acids* 20(1-2): 11-40, 2001.

Weiss JN. The Hill equation revisited: uses and misuses. *FASEB J* 11: 835-841, 1997.

Wielert-Badt S, Jiann-Trzuo L, Lorenz M, Rritz S, and Kinne RKH. Probing the conformation of the sugar transport inhibitor phloridzin by 2D-NMR, molecular dynamics studies, and pharmacophore analysis. *J Med Chem* 43: 1692-1698, 2000.

Williams TC and Jarvis SM. Multiple sodium-dependent nucleoside transport systems in bovine renal brush-border membrane vesicles. *Biochem J* 274: 27-33, 1991.

Wong J. In: Kinetics of enzyme mechanisms, edited by Harcourt, Brace, Jovanovich. New York: Academic Press, Inc., 1975.

Xiao G, Wang J, Tangen T, and Giacomini KM. A novel proton-dependent nucleoside transporter, CeCNT3 from *Caenorhabditis elegans*. *Mol Pharmacol* 59: 339-348, 2001.

Yao SYM, Cass CE, and Young JD. Transport of the antiviral nucleoside analogs 3'-azido-3'-deoxythymidine (AZT) and 2',3'-dideoxycytidine (ddC) by a recombinant nucleoside transporter (rCNT1) expressed in *Xenopus* oocytes. *Mol Pharmacol* 50: 388-393, 1996a.

Yao SYM, Ng AML, Ritzel MWL, Gati WP, Cass CE, and Young JD. Transport of adenosine by recombinant purine- and pyrimidine-selective sodium/nucleoside cotransporters from rat jejunum expressed in *Xenopus laevis* oocytes. *Mol Pharmacol* 50: 1529-1535, 1996b.

Yao SYM, Ng AML, Muzyka WR, Griffiths M, Cass CE, Baldwin SA, and Young JD. Molecular cloning and functional characterization of nitrobenzylthioinosine (NBMPR)-sensitive (*es*) and NBMPR-insensitive (*ei*) equilibrative nucleoside transporter proteins (rENT1 and rENT2) from rat tissues. *J Biol Chem* 272: 28423-28430, 1997.

Yao SY, Ng AM, Sundaram M, Cass CE, Baldwin SA, and Young JD. Transport of antiviral 3'-deoxy-nucleoside drugs by recombinant human and rat equilibrative, nitrobenzylthioinosine (NBMPR)-insensitive (ENT2) nucleoside transporter proteins produced in *Xenopus* oocytes. *Mol Membr Biol* 18(2): 161-7, 2001.

Yao SYM, Ng AML, Loewen SK, Cass CE, Baldwin SA, and Young JD. An ancient prevertebrate Na⁺-nucleoside cotransporter (hfCNT) from the Pacific hagfish (*Eptatretus stouti*). *Am J Physiol Cell Physiol* 283: C155-C168, 2002.

Young JD, Chessemann CI, Mackey JR, Cass CE, and Baldwin SA. Molecular mechanisms of nucleoside and nucleoside drug transport. *Current Top Membr* 50: 329-378, 2001.

Chapter III:*

Electrophysiological Characterization of Novel Human and Mouse Concentrative Na⁺-Nucleoside Cotransporter Proteins (hCNT3 and mCNT3) Broadly Selective for Purine and Pyrimidine Nucleosides (System *cib*)

**Some results presented in this chapter have been published and are presented in Appendix B. A version of the remainder of the chapter is in preparation for publication.*

Ritzel MWL, Ng AML, Yao SYM, Graham K, Loewen SK, Smith KM, Ritzel GR, Mowles DA, Carpenter P, Chen X-Z, Karpinski E, Hyde RJ, Baldwin SA, Cass CE, and Young JD. Molecular identification and characterization of novel human and mouse concentrative Na⁺-nucleoside cotransporter proteins (hCNT3 and mCNT3) broadly selective for purine and pyrimidine nucleosides (system *cib*). *J Biol Chem* 276(4): 2914-2927, 2001.

Smith KM, Labedz K, Cass CE, Baldwin SA, Karpinski E, and Young JD. Electrophysiological characterization of novel human and mouse concentrative Na⁺-nucleoside cotransporter proteins (hCNT3 and mCNT3) broadly selective for purine and pyrimidine nucleosides (system *cib*). (in preparation).

Introduction

Adenosine, other physiologic nucleosides, and most synthetic nucleosides are hydrophilic and require specialized membrane nucleoside transporter (NT) proteins for passage across cell membranes (Cass, 1995; Griffiths and Jarvis, 1996; Mackey *et al.*, 1998; Baldwin *et al.*, 1999; Young *et al.*, 2001). NTs regulate interactions of adenosine with its cell surface receptors, provide salvage precursors for nucleic acid biosynthesis, and are a critical determinant of the pharmacological actions of antineoplastic and antiviral nucleoside drugs. Five major nucleoside transport processes (systems *cit*, *cif*, *cib*, *es*, and *ei*) that differ in their permeant selectivities, cation dependence, and inhibitor sensitivities have been demonstrated in mammalian cells (Cass, 1995; Griffiths and Jarvis, 1996; Young *et al.*, 2001). Systems *cit*, *cif*, and *cib* are concentrative inwardly-directed Na⁺-dependent nucleoside symporters found mainly in epithelia and other specialized cells, while systems *es* and *ei* are equilibrative bidirectional Na⁺-independent nucleoside transport processes found in most, possibly all, cell types. System *cit* is selective for pyrimidine nucleosides and, to a lesser extent, adenosine, whereas system *cif* exhibits a permeant selectivity for purine nucleosides and uridine. Systems *cib*, *es*, and *ei* transport both pyrimidine and purine nucleosides. Equilibrative nucleoside transport processes of the *es* type are inhibited by nanomolar concentrations of nitrobenzylthioinosine (NBMPR), whereas the *ei*-type mechanisms are unaffected by NBMPR. Transporters of the *ei* type also transport nucleobases.

Molecular cloning studies have led to the identification of the human and rodent integral membrane proteins responsible for each of these nucleoside transport activities. Systems *cit*, *cif*, and *cib* correspond to transporters CNT1, CNT2, and CNT3, respectively, of the CNT protein family, while systems *es* and *ei* correspond to transporters ENT1 and ENT2, respectively, of the structurally unrelated ENT protein family (Huang *et al.*, 1994; Che *et al.*, 1995; Yao *et al.*, 1996; Ritzel *et al.*, 1997; Wang *et al.*, 1997; Yao *et al.*, 1997; Crawford *et al.*, 1998; Ritzel *et al.*, 1998; Hyde *et al.*, 2001; Ritzel *et al.*, 2001). The ENT protein family also contains two further human and mouse ENT isoforms (ENT3 and ENT4) of undetermined function (Hyde *et al.*, 2001; Acimovic

and Coe, 2002). Other members of the CNT family include the *Escherichia coli* NupC (Craig *et al.*, 1997; Hamilton *et al.*, 2001), CeCNT3 from *Caenorhabditis elegans* (Xiao *et al.*, 2001), CaCNT from *Candida albicans* (Loewen *et al.*, 2003a), and hfCNT from an ancient marine prevertebrate, the Pacific hagfish (*Eptatretus stouti*) (Loewen *et al.*, 1999; Yao *et al.*, 2002).

The hagfish transporter hfCNT mediates *cib*-type functional activity when produced in *Xenopus* oocytes, and forms a separate phylogenetic subfamily of CNTs together with human and mouse CNT3 (hCNT3 and mCNT3), the two most recently identified mammalian CNT transport proteins (Ritzel *et al.*, 2001). cDNA encoding hCNT3 (691 amino acid residues) was isolated from human mammary gland and differentiated myeloid HL-60 cells, while cDNA encoding mCNT3 (703 amino acid residues) was cloned from mouse liver (Ritzel *et al.*, 2001). Both proteins have 13 predicted transmembrane segments (TMs). hCNT3 and mCNT3 are 78 % identical in amino acid sequence, 57 % identical to hfCNT, and ~ 47 % identical to their mammalian CNT1 and CNT2 counterparts. Amino acid sequence identity between hfCNT and h/mCNT3 rises to a remarkable 67 % when the core structures of the transporters (TMs 4 - 13) are compared (Ritzel *et al.*, 2001). Typical of native *cib*-type functional activity in mammalian cells, radioisotope flux studies in *Xenopus* oocytes established that recombinant hCNT3 and mCNT3, unlike mammalian CNT1 and CNT2 proteins, exhibit a broad permeant selectivity for both pyrimidine and purine nucleosides and nucleoside analogs (Ritzel *et al.*, 2001). Hill type-analysis of the relationship between nucleoside influx and Na⁺ concentration indicated a Na⁺/nucleoside coupling ratio of at least 2:1, compared to 1:1 for hCNT1/2 (Ritzel *et al.*, 1997, 1998, 2001). This *Chapter* presents an extensive study using electrophysiological techniques to further characterize the functional properties of h/mCNT3. Experiments are described that investigate h/mCNT3-mediated nucleoside and nucleoside drug transport, Na⁺-dependence, current-voltage relationship, and cation specificity. In contrast to hCNT1 (*Chapter II*), it is demonstrated that human and mouse CNT3 mediate both Na⁺/nucleoside and H⁺/nucleoside cotransport. Coupling ratios for each cation were determined indirectly by

measuring the dependence of the inward current on the concentrations of Na^+ and H^+ , and directly through simultaneous measurement of voltage-clamp current and isotope flux.

Materials and Methods

Expression of Recombinant hCNT3 and mCNT3 in *Xenopus* Oocytes - hCNT3 and mCNT3 plasmid DNA in the enhanced *Xenopus* expression vector pGEM-HE was linearized with *NheI* and transcribed with T7 polymerase using the mMACHINE mMACHINE™ (Ambion, Austin, TX) transcription system. The remaining template was removed by digestion with RNase-free DNase1. Stage V-VI oocytes dissected from *Xenopus laevis* were treated with collagenase (2 mg/ml) for 2 h, and remaining follicular layers removed manually (Huang *et al.*, 1994). Twenty-four hours after defolliculation, oocytes were injected with either 10 nl of water containing 10 ng of RNA transcript encoding either hCNT3 or mCNT3 or 10 nl of water alone. Injected oocytes were then incubated for 4 days at 18 °C in modified Barth's solution (daily change) (88 mM NaCl, 1 mM KCl, 0.33 mM Ca(NO₃)₂, 0.41 mM CaCl₂, 0.82 mM MgSO₄, 2.4 mM NaHCO₃, 10 mM Hepes, 2.5 mM sodium pyruvate, 0.05 mg/ml penicillin, and 0.1 mg/ml gentamycin sulfate, pH 7.5) prior to the measurement of membrane currents.

Electrophysiological Studies - Oocyte membrane currents were measured by use of a GeneClamp 500B oocyte clamp (Axon Instruments, Inc., Foster City, California) in the two-electrode, voltage clamp mode. The GeneClamp 500B was interfaced to an IBM compatible PC *via* a Digidata 1200A/D converter and controlled by pCLAMP software (Version 8.0, Axon Instruments, Inc., Foster City, California). Current signals were filtered at 20 Hz (four-pole Bessel filter) and sampled at a sampling interval of 20 msec. For data presentation, the signals were further filtered at 0.5 Hz by the pCLAMP program suite. All electrophysiological experiments were performed at room temperature (20 °C) at least twice on different batches of oocytes. The microelectrodes were filled with 3 M KCl and had resistances that ranged from 0.5 - 2.5 MΩ (megaohms). Oocytes were penetrated with the microelectrodes and their membrane potential monitored for a period of 10 - 15 min. Oocytes were discarded if the membrane potential was unstable, or more positive than -30 mV. For measurements of hCNT3- or mCNT3-mediated currents, the oocyte membrane potential was clamped at a holding potential (V_h) of -50 mV. The sodium-containing transport medium contained (in mM): NaCl, 100; KCl, 2; CaCl₂, 1;

MgCl₂, 1; and Hepes, 10 (pH 7.5), and the substrate to be tested was added to this medium at the appropriate concentration (100 μM, unless otherwise indicated). Current-voltage (I-V) curves were determined from the difference in steady-state currents generated in the presence and absence of substrate during 175 msec voltage pulses to potentials between -90 and +60 mV (10 mV increments). In experiments examining the Na⁺-dependence of transport, Na⁺ in the transport medium was replaced by equimolar choline. Proton-dependence was tested in choline transport medium (100 mM ChCl) at pH values between 5.5 and 8.5 (10 mM MES was used in place of Hepes in solutions with pH values ≤6.5). Experiments testing Li⁺-coupling of transport function were performed in medium at pH 8.5 containing Li⁺ (100 mM LiCl) in place of Na⁺.

Hill Analysis - For Na⁺-activation experiments, oocytes were voltage-clamped at -50 mV in Na⁺-containing transport medium. The current produced in response to the addition of 100 μM uridine was measured as the Na⁺ concentration was varied from 0 to 100 mM (pH 7.5). For experiments measuring H⁺ activation, oocytes were voltage-clamped at -50 mV in choline transport medium (Na⁺-free; 100 mM ChCl) and the currents produced in response to the addition of 100 μM uridine were measured as the pH was varied from 5.5 to 8.5. Results from these experiments were fitted using SigmaPlot software (Version 4, Jandel Scientific Software, San Rafael, CA) to the Hill equation, $I = I_{\max} [X^+]^n / (K_{50}^n + [X^+]^n)$, where X is either Na⁺ or H⁺, *n* is the Hill coefficient, K₅₀ is the half-saturation constant for Na⁺ or H⁺ activation, *I* is the uridine-induced steady-state current, and *I*_{max} is the predicted current maximum. Kinetic parameters are presented as means ±SE, where SE is the standard error of the fitted estimate.

hCNT3 Radioisotope Flux Studies - In parallel with electrophysiological measurements, the pH dependence of ddC transport by hCNT3 was also investigated by measuring the uptake of ³H-labeled ddC (2 μCi/ml, Moravek Biochemicals, Brea, CA) in the same Na⁺-containing (100 mM NaCl; pH 7.5) and Na⁺-free (100 mM ChCl; pH 7.5 and 5.5) transport media used for current recordings. Flux measurements were performed at room temperature (20 °C) as described previously (Huang *et al.*, 1994) on groups of 12 oocytes in 200 μl of transport medium containing 20 μM ³H-ddC. At the end of the

incubation period (30 min), extracellular label was removed by six rapid washes in ice-cold transport solution, and individual oocytes were dissolved in 5 % (w/v) SDS for quantitation of oocyte-associated radioactivity by liquid scintillation counting (LS 60000 IC, Beckman Mississauga, ON). The flux values presented are means \pm SEM of 10 - 12 oocytes, and each experiment was performed at least twice on different batches of oocytes.

Cation/Nucleoside Coupling Ratios - Na^+ /nucleoside and H^+ /nucleoside coupling ratios for hCNT3 and mCNT3 were determined by simultaneously measuring Na^+ or H^+ currents and ^{14}C -uridine (200 μM , 1 $\mu\text{Ci/ml}$, Amersham Pharmacia Biotech) influx under voltage-clamp conditions. Individual oocytes were placed in a perfusion chamber and voltage-clamped at V_h of -30, -50, or -90 mV in the appropriate substrate-free medium for a 10 min period to monitor baseline currents. When the baseline was stable, the substrate-free medium was exchanged with medium of the same composition containing radiolabeled uridine. Current was measured for 3 min, and uptake of uridine was terminated by washing the oocyte with substrate-free transport medium until the current returned to baseline. Oocytes were then transferred to individual scintillation vials and solubilized with 5 % (w/v) SDS for quantitation of oocyte-associated radioactivity. Nucleoside-induced current was obtained as the difference between baseline current and the inward uridine current. The total charge translocated into the oocyte during the uptake period was calculated from the current-time integral and correlated with the measured radiolabeled uptake for each oocyte to determine the charge/uptake ratio. Basal ^{14}C -uridine uptake was determined in control water-injected oocytes (from the same donor frog) under equivalent conditions and used to correct for endogenous non-mediated uridine uptake over the same incubation period. Coupling ratios are presented as means \pm SE of 8 or more oocytes.

Chemicals - Nucleosides and nucleoside analogs, including AZT (3'-azido-3'-deoxythymidine), ddC (2', 3'-dideoxycytidine), and gemcitabine (2', 2'-difluorodeoxycytidine) were purchased from Sigma (Oakville, ON).

Results

Substrate Selectivity and Na⁺-dependence of Recombinant hCNT3 and mCNT3 - Figure 3-1 demonstrates the substrate specificity and Na⁺-dependence of hCNT3-mediated transport by measuring inward currents produced following the addition of three diagnostic nucleoside permeants (inosine, uridine, and thymidine) to an hCNT3-producing oocyte (Ritzel *et al.*, 2001). External application of inosine, uridine, and thymidine (each at a concentration of 100 μ M) in Na⁺-containing transport medium (100 mM NaCl; pH 7.5) induced inward currents of 183 - 220 nA that returned to baseline upon removal of the permeant (Fig. 3-1A, *left panel*). Inward currents were not observed in hCNT3-injected oocytes in sodium-free choline medium in this experiment (Fig. 3-1A, *right panel*; 100 mM ChCl; pH 7.5). No currents were seen in water-injected oocytes, either in the presence or absence of Na⁺ (Fig. 3-1B).

Figure 3-2 shows a similar representative mCNT3 transport experiment in *Xenopus* oocytes measuring the currents associated with external application of uridine and a more extensive panel of other pyrimidine and purine nucleosides (thymidine, cytidine, adenosine, inosine, and guanosine). In Na⁺-containing transport medium (100 mM NaCl; pH 7.5), all of the nucleosides tested (each at a concentration of 100 μ M) induced similar mCNT3-mediated inward currents in the range 42 - 58 nA (Fig. 3-2A, *upper panel*). No inward currents were detected when Na⁺ was replaced by equimolar choline (Fig. 3-2A, *lower panel*; 100 mM ChCl; pH 7.5), and no currents were seen in water-injected oocytes either in the presence or absence of Na⁺ (Fig. 3-2B). All of the nucleosides tested were therefore mCNT3 permeants, indicating that mCNT3, like hCNT3, is broadly selective for both purine and pyrimidine nucleosides.

Voltage-dependence of hCNT3 and mCNT3 Transport Currents - Figure 3-3A shows representative current traces in an hCNT3-expressing oocyte examining the effect of membrane potential on the uridine-induced steady-state current. Currents were compared at the end of a 175 msec command pulse to potentials between -90 and +60 mV (10 mV increments) in the presence and absence of uridine (100 μ M) (Fig. 3-3A).

Currents evoked by the addition of uridine in both hCNT3- and mCNT3-containing oocytes were voltage-dependent and increased at more negative potentials (Fig. 3-3B). The uridine-induced current approached zero but did not reverse polarity at potentials up to +60 mV.

pH- and Lithium-dependence of Recombinant hCNT3 and mCNT3 - The two-microelectrode voltage clamp was used to assess the ability of protons or Li^+ to substitute for Na^+ as a possible driving force for hCNT3- and mCNT3-mediated nucleoside uptake. The effect of a proton gradient on the nucleoside transport activities of hCNT3 and mCNT3 was examined at pH values ranging from 5.5 to 8.5 in Na^+ -free conditions. Figure 3-4A shows representative current traces for uridine uptake in an mCNT3-producing oocyte in the presence (100 mM NaCl; pH 7.5) and absence (100 mM ChCl; pH 5.5 - 8.5) of extracellular Na^+ , and Figure 3-4B summarizes mean results for 5 - 6 oocytes. In marked contrast to the situation seen with hCNT1 (*Chapter II*), the results revealed an inward pH-dependent (pH 5.5 > pH 8.5) uridine-evoked current in mCNT3-producing oocytes under Na^+ -free conditions. Proton currents measured at the lowest pH tested (5.5) were 20 - 30 % of Na^+ currents obtained at pH 7.5 in standard Na^+ transport medium, and declined markedly as the pH was raised. No inward proton currents were seen in control water-injected oocytes (data not shown). Similar results were obtained with recombinant hCNT3-producing oocytes (Fig. 3-5A, B). At pH 7.5, the average h/mCNT3 proton current in the absence of Na^+ was < 4 % of that observed with Na^+ present and was not, therefore, detected above the background noise level in some electrophysiological recordings (*ie.* Figs. 3-1A and 3-2A). Proton currents were not unique to uridine, and were also observed in mCNT3-producing oocytes exposed to thymidine and the purine nucleoside inosine (Fig. 3-6A, B). Inward Na^+ currents produced by thymidine and inosine at pH 7.5 in the same groups of oocytes were ~ 60 nA (data not shown). Although a proton gradient alone was sufficient to drive transport, studies conducted in the presence of Na^+ showed a stimulatory effect on transport activity as the pH of Na^+ -containing transport medium was lowered from 8.5 to 5.5 (mCNT3; Fig. 3-7A, B). Similar results were also seen with hCNT3 (data not shown). In addition, replacement of Na^+ with equimolar Li^+ (100 mM LiCl; pH 8.5) produced inward uridine-

evoked currents in hCNT3-producing oocytes of similar magnitude to currents generated in choline medium at pH 5.5. This is illustrated in Figure 3-8, where replacing Na^+ with an inward H^+ gradient (pH 5.5) produced an inward current of 47 nA in response to the addition of uridine, compared to 44 nA in Li^+ medium (pH 8.5).

hCNT3- and mCNT3-mediated Transport of Anticancer and Antiviral Drugs -

The ability of hCNT3 and mCNT3 to transport anticancer and antiviral nucleoside drugs has previously been demonstrated using radioisotope techniques (Ritzel *et al.*, 2001). hCNT3- and mCNT3-mediated transport of gemcitabine, AZT, and ddC were further investigated using electrophysiological techniques and representative traces are shown in Figures 3-9, 3-10, and 3-11. In Na^+ -containing transport medium (100 mM NaCl; pH 7.5), AZT and ddC elicited an electrogenic response in mCNT3-producing oocytes (Figs. 3-9A and 3-10A, *upper panels*). Inward currents ranged from 8 - 10 nA (100 μM AZT or ddC) to 30 - 38 nA (1 mM AZT or ddC). Corresponding uridine-induced Na^+ -currents were 60 - 80 nA (100 μM uridine). Since the currents observed with 100 μM AZT and ddC were relatively small, subsequent experiments were performed at the higher AZT and ddC concentration of 1 mM. Replacing Na^+ with an inwardly-directed proton gradient (100 mM ChCl; pH 5.5) did not produce any detectable AZT- or ddC-evoked inward currents (Figs. 3-9A and 3-10A, *lower panels*). In contrast, proton currents of 28 - 40 nA were seen with 100 μM uridine in Na^+ -free medium at pH 5.5 in the same mCNT3-producing oocytes. No inward currents were seen in water-injected control oocytes at 1 mM AZT or ddC either in Na^+ - (pH 7.5) or choline- (pH 5.5) containing transport media (Figs. 3-9B and 3-10B).

Figure 3-11 investigated corresponding Na^+ and H^+ currents associated with AZT and ddC transport by recombinant hCNT3, and compared the results obtained with currents elicited by the anticancer nucleoside drug gemcitabine. In Na^+ -containing transport medium (pH 7.5), gemcitabine (100 μM), AZT (1 mM), and ddC (1 mM) induced electrogenic responses, with currents of 144, 120, and 92 nA, respectively (Fig. 3-11A). When Na^+ was replaced with an inwardly-directed proton gradient (100mM ChCl; pH 5.5), gemcitabine (100 μM) induced an inward current of 40 nA. In marked contrast, no

inward currents were observed with either AZT or ddC at pH 5.5, in agreement with the results obtained with mCNT3 (Figs. 3-9 and 3-10). For comparison, uridine-induced currents (100 μ M) in the same oocyte were 210 nA in Na⁺-containing medium at pH 7.5 and 90 nA in sodium-free medium at pH 5.5. In control experiments, no inward currents were seen in water-injected oocytes exposed to gemcitabine, AZT, or ddC in either Na⁺ (pH 7.5) or choline (pH 5.5) transport media (Fig. 3-11B). These electrophysiological results, demonstrating an absence of hCNT3- and mCNT3-mediated proton currents in response to perfusion with AZT and ddC, were confirmed by ³H-ddC uptake assays, which found no hCNT3-mediated transport of ddC in choline transport medium at pH 5.5 (Fig. 3-12).

Na⁺ Activation Kinetics and Na⁺/nucleoside Coupling Ratio - Figure 3-13 demonstrates that the relationship at pH 7.5 (100 μ M uridine) between uridine-evoked current and Na⁺ concentration for mCNT3 was sigmoidal with a Hill coefficient of 2.2 ± 0.3 , suggesting a coupling ratio of 2 Na⁺ ions transported per molecule of uridine. Subsequent experiments demonstrated directly a 2:1 Na⁺/uridine stoichiometry for hCNT3 by simultaneously measuring uridine-evoked currents and ¹⁴C-uridine uptake under voltage-clamp conditions, as described for the Na⁺/glucose cotransporter SGLT1, the rat kidney dicarboxylate transporter SDCT1 (Lee *et al.*, 1994; Chen *et al.*, 1998) and, in *Chapter II* of this thesis, hCNT1. Figure 3-14A shows a representative current trace demonstrating the uridine-dependent Na⁺ current in an hCNT3-expressing oocyte clamped at -30 mV. Initially, the oocyte was perfused with Na⁺ medium (100 mM NaCl; pH 7.5) and, following the addition of 200 μ M ¹⁴C-uridine, an inward current of ~ 120 nA was produced. When uridine was removed from the bath by washing with substrate-free Na⁺ medium, the current returned to baseline. Current was integrated with time to determine the charge moved during the uptake period. The charge was converted to its molar equivalent and compared to the ¹⁴C-uridine uptake measured in the same oocyte. The process was repeated in 9 different hCNT3-producing oocytes, such that each data point presented in Figure 3-14B represents a single oocyte. The slope of the linear fit of a plot of charge (pmol) *versus* uptake (pmol) is equal to the Na⁺/nucleoside coupling ratio. At -30 mV, the slope was 1.25 ± 0.96 (mean \pm SE, n = 9, Fig. 3-14B). To

examine the voltage-dependence of the Na^+ /nucleoside coupling ratio, the same experiment was repeated with hCNT3-expressing oocytes voltage clamped at two other holding potentials, -50 and -90 mV. At $V_h = -50$ mV, the linear correlation between uridine-dependent charge and uridine accumulation gave a stoichiometry of 1.66 ± 0.21 ($n = 9$, Fig. 3-14C). A ratio of 2.10 ± 0.24 ($n = 9$, Fig. 3-14D) was obtained at a holding potential of -90 mV.

H^+ Activation Kinetics and H^+ /nucleoside Coupling Ratio - Figure 3-15 shows the relationship for hCNT3 between uridine-evoked current and external pH in the absence of Na^+ . Inward currents were measured in response to the addition of uridine (100 μM) at pH values ranging from 5.5 to 8.5. A plot of current *versus* H^+ concentration revealed a sigmoidal relationship with a Hill coefficient of 1.78 ± 0.26 . Subsequent experiments utilized charge/flux assays to determine directly the H^+ /nucleoside stoichiometry of hCNT3. Coupling ratio experiments were performed with 100 μM uridine in Na^+ -free transport medium (100 mM ChCl) at pH 5.5, and at holding potentials of -30, -50, and -90 mV to examine the voltage-dependence of the H^+ /nucleoside coupling ratio (Fig. 3-16). At $V_h = -30$ mV, the slope of the linear correlation between uridine-dependent charge and uridine accumulation was 0.84 ± 0.12 (mean \pm SE, $n = 9$, Fig. 3-16A). Ratios of 1.19 ± 0.20 ($n = 9$, Fig. 3-16B) and 0.96 ± 0.26 ($n = 8$, Fig. 3-16C) were obtained at holding potentials of -50 and -90 mV, respectively.

Coupling Ratio of hCNT3 Determined in the Presence of both Na^+ and H^+ - Figure 3-17 utilized charge/flux assays to examine the cation/nucleoside coupling ratio of hCNT3 in the presence of both Na^+ and H^+ (100 mM NaCl; pH 5.5). Experiments were performed at holding potentials of -30, -50, and -90 mV. At $V_h = -30$ mV, the slope of the linear correlation between uridine-dependent charge and uridine accumulation was 2.01 ± 0.08 ($n = 9$, Fig. 3-17A). Ratios of 2.09 ± 0.38 ($n = 8$, Fig. 3-17B) and 2.10 ± 0.18 ($n = 10$, Fig. 3-17C) were obtained at holding potentials of -50 and -90 mV, respectively.

Discussion

The present study utilized electrophysiological techniques to confirm and extend our knowledge of the functional properties of the broadly selective human and mouse nucleoside transporters hCNT3 and mCNT3 (Ritzel *et al.*, 2001). The substrate selectivity and Na⁺ dependence of h/mCNT3 was confirmed by measuring inward Na⁺ currents. Electrophysiology was also used to investigate h/mCNT3 current-voltage relationships, pH-dependence of nucleoside and nucleoside drug transport, Li⁺-dependence of transport function, and h/mCNT3 Na⁺/nucleoside and H⁺/nucleoside coupling ratios.

Electrophysiological recordings confirmed that hCNT3 and mCNT3 function as broadly selective electrogenic Na⁺/nucleoside symporters (Ritzel *et al.*, 2001). Inward Na⁺ currents, which were reversible following substrate removal, were generated upon addition of various pyrimidine and purine nucleosides in hCNT3- and mCNT3-producing oocytes (Figs. 3-1A and 3-2A, respectively). Currents were largely abolished when Na⁺ was removed from the transport medium (Figs. 3-1A and 3-2A). Transport of uridine was also voltage-dependent. The magnitude of the inward current increased at more negative potentials, suggesting that transport of nucleosides across the cell membrane *via* h/mCNT3 was influenced by membrane potential (Fig. 3-3).

Electrophysiological experiments investigated the cation specificity of h/mCNT3-mediated nucleoside transport, and demonstrated that the CNT3 proteins are capable of functioning as H⁺/nucleoside and Li⁺/nucleoside symporters. Thus, hCNT3- and mCNT3-mediated transport of nucleosides was shown to be pH-dependent, and uridine induced large inward currents in acidified (pH 5.5), Na⁺-free transport medium (Figs. 3-4 and 3-5). Raising the pH decreased the magnitude of this inward current in a manner consistent with H⁺/nucleoside cotransport. Currents were minimal at pH 7.5 or higher as the extracellular pH rose above the intracellular oocyte pH of 7.3 - 7.6 (Burckhardt *et al.*, 1992), eliminating any inwardly-directed H⁺ ion gradient. Proton currents were seen with each of the three pyrimidine and purine nucleoside permeants (uridine, thymidine, and inosine) that are diagnostic for CNT3 (Figs. 3-4, 3-5, and 3-6). In the presence of Na⁺, a

stimulatory effect on transport activity was observed as the pH of the transport medium was lowered, suggesting the possibility that Na⁺ and H⁺ ions might have additive or cooperative effects on transporter activity (Fig. 3-7). In contrast, hCNT1 and rCNT1 are strictly Na⁺-dependent (Loewen *et al.*, 2003b; *Chapter II*). In addition, other cation replacement experiments demonstrated the ability of hCNT3 to utilize Li⁺ as the coupling cation (Fig. 3-8). The present study therefore establishes human and mouse CNT3 as the first members of the concentrative nucleoside transport family capable of using H⁺, Li⁺, and Na⁺ electrochemical gradients as driving forces for concentrative cellular nucleoside uptake. In this regard, CNT3 proteins resemble SGLT1 and SGLT3, the bacterial MelB melibiose transporter, and the mammalian Na⁺/dicarboxylate cotransporter (SDCT1/NaDC-1) which can also utilize the energy of transmembrane electrochemical gradients for Na⁺, H⁺, and Li⁺ to drive cellular accumulation of substrate against its concentration gradient (Pourcher *et al.*, 1990; Hirayama *et al.*, 1994; Hirayama *et al.*, 1997; Chen *et al.*, 1998; Pajor *et al.*, 1998; Quick *et al.*, 2001). Cation binding induces a cation-specific conformational change in the substrate-binding pocket (Hirayama *et al.*, 1997; Pajor *et al.*, 1998). Once the substrate is bound, it is then transported at a rate that is characteristic of the cation (Hirayama *et al.*, 1997; Pajor *et al.*, 1998).

Since the pharmacological targets of antiviral and anticancer nucleoside analogs are intracellular, permeation across the plasma membrane is an important first step in the cytotoxicity of nucleoside drugs. The hydrophilic nature of nucleoside analogs makes diffusion through the plasma membrane slow, and the major routes by which nucleoside drugs gain access to the intracellular compartment are *via* CNT and ENT nucleoside transporter proteins (Cass, 1995; Mackey *et al.*, 1998; Young *et al.*, 2001). CNT and ENT proteins are important molecular determinants of drug selectivity, intestinal absorption, therapeutic efficacy, systemic cytotoxicity, and drug resistance (Mackey *et al.*, 1998; Young *et al.*, 2001). Differences in substrate selectivity exhibited between members of the CNT family for physiological nucleosides are reflected in their transport capacity for various pyrimidine and purine anticancer and antiviral nucleoside drugs. Radioisotope flux studies of recombinant transporters produced in *Xenopus* oocytes have been used to characterize the transport of nucleoside drugs by the mammalian CNT

proteins. The antiviral drugs AZT and ddC are transported by h/rCNT1, while ddI is transported by h/rCNT2 (Huang *et al.*, 1994; Yao *et al.*, 1996; Ritzel *et al.*, 1997, 1998). Gemcitabine, a pyrimidine analog of deoxycytidine, is transported by hCNT1 but not by hCNT2 (Mackey *et al.*, 1998, 1999). Anticancer pyrimidine (5-fluorouridine, 5-fluoro-2'-deoxyuridine, zebularine, and gemcitabine) and purine (cladribine and fludarabine) nucleoside drugs are transported by hCNT3 (Ritzel *et al.*, 2001). Transport of antiviral pyrimidine (AZT and ddC) and purine (ddI) nucleoside drugs has also been demonstrated for hCNT3 (Ritzel *et al.*, 2001) although, as with the CNT1 and CNT2 transporters, rates of transport were generally lower than for anticancer nucleoside analogs. Consistent with its ability to transport a broad range of physiological pyrimidine and purine nucleosides, hCNT3 is also capable of transporting both pyrimidine and purine nucleoside drugs. The studies of hCNT3- and mCNT3-mediated transport of nucleoside drugs described here utilized the two-microelectrode voltage clamp to investigate the Na⁺ and H⁺ currents associated with transport of the antiviral nucleoside drugs AZT and ddC and the anticancer nucleoside drug gemcitabine. In mCNT3- and hCNT3-producing oocytes, AZT and ddC elicited electrogenic responses in Na⁺-containing transport medium that were abolished following replacement of Na⁺ with an inwardly-directed H⁺ gradient (Figs. 3-9, 3-10, and 3-11). In hCNT3-expressing oocytes, inward currents were also produced with gemcitabine in Na⁺-containing transport medium and, to a lesser extent, with the presence of a proton gradient (Fig. 3-11). These results were confirmed with radioisotope studies which did not detect hCNT3-mediated transport of ddC in choline transport medium at pH 5.5 (Fig. 3-12). Therefore, with respect to nucleoside drugs, H⁺ gradients can drive transport of gemcitabine, but not that of antiviral nucleoside drugs. The H⁺/nucleoside cotransporters NupC from *E. coli* and CaCNT from *C. albicans* also use H⁺ ions to transport nucleosides and nucleoside drugs, including antiviral dideoxynucleoside drugs, demonstrating that H⁺ gradients can support antiviral nucleoside drug fluxes by other CNT family members (Loewen *et al.*, 2003a, b). A common feature of antiviral dideoxynucleoside antiviral nucleoside drugs is the absence of a hydroxyl group at position 3 of the sugar moiety. The absence of the 3' hydroxyl group may explain lower levels of hCNT3-mediated antiviral drug transport, compared to

transport of anticancer nucleoside analogs (Ritzel *et al.*, 2001), and may potentially be required for substrate/transporter binding interactions when H^+ is the driving ion.

The Na^+ /nucleoside coupling ratio has been investigated for various members of the CNT family. Based on Hill-type analysis of the relationship between nucleoside influx and Na^+ concentration, Na^+ /nucleoside stoichiometries of 1:1 have been described for *cit* and *cif* transport activities in different mammalian cells and tissues (Cass, 1995; Griffiths and Jarvis, 1996; Young *et al.*, 2001), and for recombinant rCNT1 produced in *Xenopus* oocytes (Yao *et al.*, 1996). Charge *versus* uridine flux experiments for hCNT1 directly confirmed a Na^+ /nucleoside coupling ratio of 1:1 (*Chapter II*). Similarly, charge *versus* uridine flux experiments for proton-dependent CaCNT found a H^+ /nucleoside coupling ratio of 1:1 (Loewen *et al.*, 2003a). In contrast, Na^+ /nucleoside stoichiometries of 2:1 have been published for system *cib* in rabbit choroid plexus and rat microglia based on Na^+ -activation studies (Wu *et al.*, 1992; Hong *et al.*, 2000). In charge *versus* uridine flux experiments, the hagfish Na^+ /nucleoside *cib*-type transporter hfCNT was shown to have a 2:1 coupling stoichiometry (Yao *et al.*, 2002). In initial studies of hCNT3 and mCNT3, radioisotope fluxes were used to demonstrate that the relationship between uridine influx and Na^+ concentration was sigmoidal, with Hill coefficients consistent with a Na^+ /nucleoside coupling ratio of 2:1 for both transporters (Ritzel *et al.*, 2001). In the experiments of Figure 3-13, electrophysiological techniques were used to demonstrate that the relationship between uridine-evoked current and Na^+ concentration in mCNT3-expressing oocytes is also sigmoidal. Fitting the data to the Hill equation gave a Hill coefficient consistent with the results from radioisotope studies (Ritzel *et al.*, 2001), thereby also indicating a coupling ratio of 2 Na^+ ions transported for every molecule of nucleoside translocated across the cell membrane. These data established that the cation/nucleoside coupling ratio is different for different members of the CNT family. In this respect, CNTs resemble other transporter families in which individual members have different coupling ratios. For example, members of the SGLT glucose transporter family have been described with 1:1 and 2:1 Na^+ /glucose coupling ratios (1:1 for SGLT2 and 2:1 for SGLT1/3) (Chen *et al.*, 1995; Mackenzie *et al.*, 1996, 1998; Diez-Sampedro *et al.*,

2001). Similarly, the PepT1 and PepT2 proton-linked peptide transporters have 1:1 and 2:1 H⁺/peptide coupling ratios, respectively (Chen *et al.*, 1999).

Subsequent experiments utilized simultaneous measurement of transporter-specific currents and radioactive nucleoside uptake from the same oocyte under voltage-clamp conditions to determine directly the Na⁺/nucleoside coupling ratio of hCNT3 and to examine the effects of membrane potential on the coupling stoichiometry. The experimentally determined Na⁺/nucleoside coupling ratios for hCNT3 were 1.25 at membrane potentials of -30 mV, 1.66 at -50 mV, and 2.10 at -90 mV (Fig. 3-14). The hCNT3 coupling ratio was therefore voltage-dependent and, under hyperpolarized conditions, was confirmed to be 2 Na⁺ ions transported for every molecule of nucleoside translocated across the cell membrane. These results are consistent with those seen for the Na⁺/glucose cotransporter SGLT1 in which the Na⁺/glucose coupling ratio more closely approached a value of 2:1 under hyperpolarized conditions (coupling ratios of 1.6 and 1.9 were obtained at -50 and -110 mV, respectively) (Mackenzie *et al.*, 1998).

Since CNT3 proteins are also able to use the electrochemical gradient of H⁺ to drive the influx of nucleosides into cells, experiments were also performed to determine the H⁺/nucleoside coupling ratio. Hill-type analysis of the relationship between hCNT3-mediated nucleoside influx and external pH indicated an H⁺/nucleoside stoichiometry of 2:1 (Hill coefficient ~ 1.8; Fig. 3-15). Charge/flux measurements were also performed to directly determine the H⁺/nucleoside coupling ratios at various membrane potentials (Fig. 3-16). The H⁺/nucleoside coupling ratios for hCNT3 were 0.84 at membrane potentials of -30 mV, 1.19 at -50 mV, and 0.96 at -90 mV. Results from the charge/flux assays therefore indicate an H⁺/nucleoside stoichiometry of 1:1 that was largely membrane potential-independent. Results from the H⁺ activation experiments and the charge/flux assays therefore indicate different coupling ratios for H⁺/nucleoside cotransport.

We have interpreted our data in the context of the prototypical six-state transport model first proposed for the SGLT transporter family (Parent *et al.*, 1992a, b), and presented in Figure 3-18A a possible model for hCNT3-mediated Na⁺/nucleoside cotransport in order to explain the results from the coupling ratio experiments. The

carrier (C) (*ie.* the transporter) can exist in several different conformations, depending upon the membrane potential and the concentration of ligands, Na^+ and nucleosides (N), on either side of the membrane. It is assumed that the empty carrier has a negative charge (valence -2) and, in the absence of ligands, the membrane potential determines whether the ligand binding sites face the outer (C') or inner (C'') face of the membrane. There are three transmembrane steps: the charge transport step (C' \rightarrow C''), a Na^+ leak (CNa₂' \rightarrow CNa₂''), and the fully-loaded carrier translocation (NCNa₂' \rightarrow NCNa₂''). Current is carried by the empty carrier, while the translocations CNa₂' \rightarrow CNa₂' and NCNa₂' \rightarrow NCNa₂' are electrically silent. At a membrane potential of -50 mV, the empty carrier has binding sites facing the extracellular surface. Binding of ligands to the carrier is an ordered process, with the cation binding first followed by the nucleoside (*Chapter II*). With saturating concentrations of external Na^+ present, the empty carrier binds Na^+ , inducing a conformational change which increases the affinity of the carrier for the nucleoside. Binding of the nucleoside to the Na^+ -loaded carrier induces another conformational change, resulting in exposure of the binding sites to the inner face of the membrane. Nucleoside and Na^+ then dissociate and the final step of the transport cycle is a conformational change reorientating the ligand-binding sites from the inner to the outer face of the membrane. The complete reaction cycle results in the cotransport of Na^+ and nucleoside from the outside to the inside of the cell and the generation of a net inward current.

Determining the Na^+ /uridine coupling ratio using electrophysiology involves comparing the net Na^+ flux through hCNT3 (estimated from the inward current) to the simultaneous unidirectional uptake of radiolabeled nucleoside in the same oocyte (Chen *et al.*, 1998). During the transport cycle, coupled transport of Na^+ and ^{14}C -uridine produces an inward current as the empty transporter reorientates within the membrane following the intracellular release of Na^+ and ^{14}C -uridine. ^{14}C -uridine accumulates within the cell during this transport cycle through the electroneutral fully-loaded translocation step NCNa₂' \rightarrow NCNa₂''. The assumption that unidirectional uridine uptake is equal to the net uridine flux is not, however, always accurate and is a function of the experimental conditions (Chen *et al.*, 1995). An electroneutral exchange of extracellular radiolabeled

uridine with endogenous intracellular unlabeled substrates, without dissociation of Na^+ , can occur through the fully-loaded translocation step (Fig. 3-18B) (Chen *et al.*, 1998). Electroneutral exchange results in intracellular ^{14}C -uridine levels that are higher than would be observed with coupled $\text{Na}^+ / ^{14}\text{C}$ -uridine transport alone and, since no currents are produced during this exchange, artifactually low stoichiometric ratios are produced. Evidence for the efflux of intracellular endogenous substrates through hCNT3 comes from experiments looking at the time course of membrane currents in response to voltage steps from a holding potential of -50 mV to various test potentials in the presence of extracellular Na^+ , but in the complete absence of added extracellular uridine (Fig. 3-19A). The outward currents observed following voltage steps were larger than the inward currents, suggesting efflux of an endogenous substrate through the transporter. These currents were not observed in water-injected oocytes (Fig. 3-19B). At depolarized membrane potentials, such as -30 mV, the contribution of electroneutral exchange to net ^{14}C -uridine flux is significant, resulting in low Na^+ /nucleoside coupling ratios (Na^+ /nucleoside coupling ratio of 1.25; Fig. 3-14B). As the membrane potential was made more negative (*ie.* -50 and -90 mV), the turnover rate of the transporter increased and Na^+ ions more fully dissociated from the transporter such that electroneutral exchange contributed less to the net ^{14}C -uridine flux. The coupling ratio therefore becomes more accurate and approaches the true value (Na^+ /nucleoside coupling ratios of 1.66 and 2.10 at -50 mV and -90 mV, respectively; Fig. 3-14C, D). The Na^+ /nucleoside coupling ratio of hCNT3 therefore exhibited voltage-dependence, and was 2:1 under hyperpolarized conditions. This was in contrast to results seen with hCNT1 in which a Na^+ /nucleoside coupling ratio of 1:1 was obtained at all membrane potentials tested (Fig. 2-12). An examination of the time course of membrane currents for an hCNT1-producing oocyte in response to voltage pulses in the presence of extracellular Na^+ (Fig. 2-2A; *right current record*) revealed a profile consistent with negligible efflux of endogenous substrates through the transporter; there was no apparent difference in the inward and outward currents produced during voltage steps. A lower affinity of hCNT1 for Na^+ , as compared to hCNT3 (Ritzel *et al.*, 1997, 2001), allows Na^+ to dissociate more fully from the transporter, thereby reducing the possibility of electroneutral exchange of

extracellular radiolabeled uridine with endogenous substrates. The low rate of electroneutral exchange coupled with more complete dissociation of Na^+ from the inward face of the transporter at the various membrane potentials tested would result in a coupling ratio for hCNT1 that is apparently voltage-independent.

A common mechanism of cation coupling for hCNT3 requires that H^+ and Na^+ bind to common sites on the transporter. However, while two H^+ ions interact with the transporter, as indicated by the Hill coefficient (Fig. 3-15), charge/flux assays suggest a H^+ /nucleoside coupling ratio of 1:1 (Fig. 3-16). This apparent discrepancy between the H^+ /nucleoside coupling ratios obtained for hCNT3 from H^+ -activation experiments (2:1) and charge/flux assays (1:1) may, potentially, be explained by differing affinities of the two cation binding sites for H^+ . In a sequential ordered binding mechanism, the empty carrier must bind two H^+ in order to induce the conformational change increasing the affinity of the transporter for the nucleoside (Stein, 1986). Binding of the nucleoside to the H^+ -loaded carrier then results in another conformational change, exposing the substrate-bound transporter to the inner face of the membrane and allowing dissociation of nucleoside and H^+ . An artifactually low coupling ratio would result if there are differences in the affinities of the two binding sites for H^+ , and only one H^+ ion dissociates fully from the transporter while the other is recycled back to the outer face of the membrane. Since only one H^+ is bound to the transporter under these conditions, endogenous substrates would not be translocated, and the measured H^+ /nucleoside coupling ratio of 1:1 would be voltage-independent (Fig. 3-16).

In the presence of both Na^+ and H^+ (Na^+ -containing transport medium at pH 5.5), calculated cation/nucleoside coupling ratios from charge/flux assays were 2.01 at a membrane potential of -30 mV, 2.09 at -50 mV, and 2.10 at -90 mV (Fig. 3-17). With Na^+ only as the driving cation, the coupling ratio was voltage-dependent and 2:1 at hyperpolarized potentials (Fig. 3-14); with H^+ only as the driving cation, the coupling ratio was 1:1 and potential-independent (Fig. 3-16). Therefore, with both cations present, the coupling ratio shows characteristics of both Na^+ and H^+ (2:1 and voltage-independent), and suggests that both cations contribute to the driving force under these

conditions. Although there was an increase in current magnitude at low pH in Na⁺ medium (Fig. 3-7), which might indicate separate Na⁺ and H⁺ binding sites on the transporter, the experimentally determined coupling ratio of 2:1 in the presence of both cations argues for a mechanism in which Na⁺ and H⁺ bind to the same sites on the transporter. Common binding sites for Na⁺ and H⁺ have also been postulated for SGLT1 (Hirayama *et al.*, 1994).

Although it is likely that H⁺ and Na⁺ share the same binding sites on the transporter, the possibility also exists that there is a unique interaction site for H⁺ distinct from those for Na⁺. Human and mouse CNT3 belong to a large family of concentrative nucleoside transporters isolated from both prokaryotes and eukaryotes. In addition to the proton-coupled nucleoside transporters *E. coli* NupC, CaCNT from *C. albicans*, and CeCNT3 from *C. elegans* (Xiao *et al.*, 2001; Loewen *et al.*, 2003a, b), these include the broadly selective hagfish *cib*-type Na⁺/nucleoside transporter hfCNT (Yao *et al.*, 2002) which, together with hCNT3 and mCNT3, form a distinct CNT subfamily separate from other family members. hfCNT does not appear to be pH-dependent, despite possessing the same 2:1 Na⁺/nucleoside coupling ratio as h/mCNT3. While the ability of human and mouse CNT3 to utilize Na⁺ and H⁺ (and Li⁺) gradients to drive nucleoside uptake suggests greater functional diversity amongst CNTs than previously anticipated, the different CNT transporters now identified and characterized provide a rich resource for future structure function analyses that will ultimately allow identification of CNT structural domains and specific amino acid residues responsible for cation recognition and coupling. The very close sequence similarity between hfCNT and h/mCNT3, for example, provides a unique opportunity to characterize the molecular mechanism of proton-coupling.

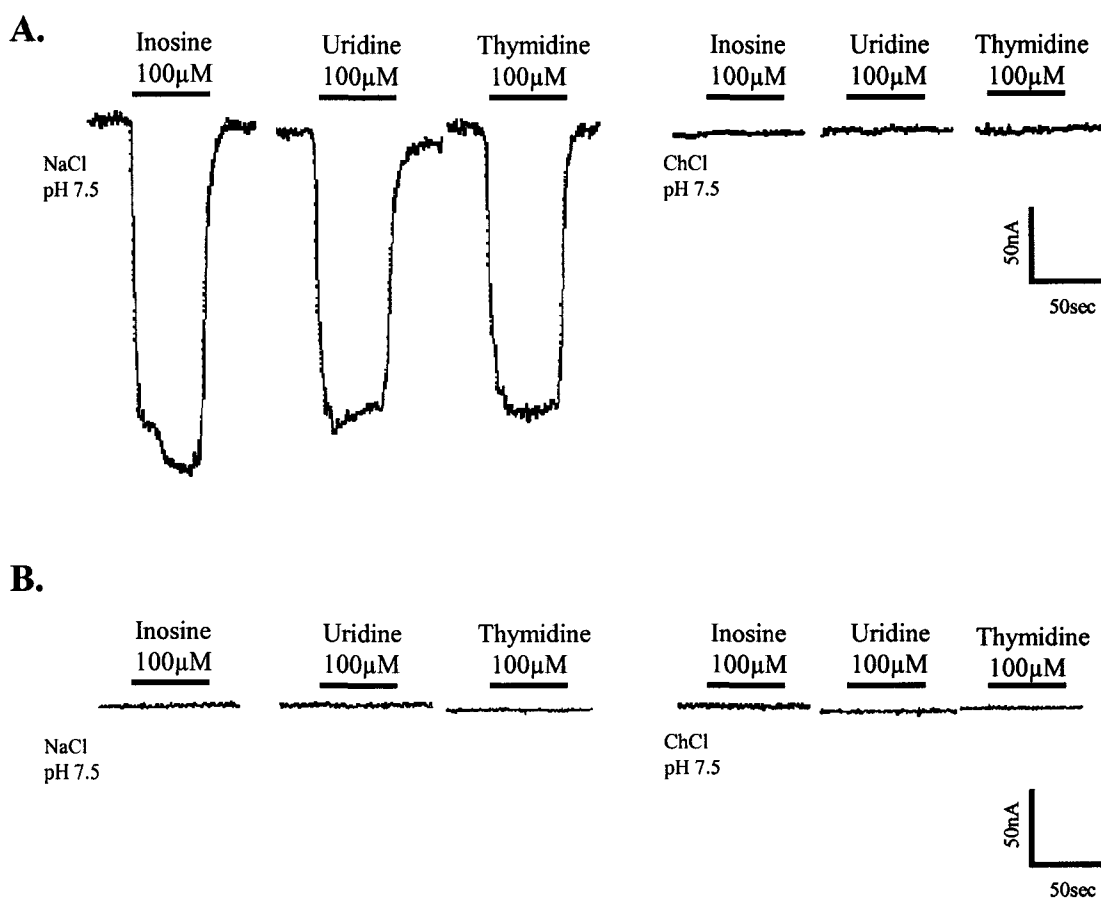


Figure 3-1. Substrate selectivity and Na⁺-dependence of hCNT3 produced in *Xenopus* oocytes. The uptake of the purine nucleoside inosine and the pyrimidine nucleosides uridine and thymidine, each at a concentration of 100 μM, in oocytes injected with hCNT3 RNA transcript (**A**) or water alone (**B**) was measured in the presence (100 mM NaCl; pH 7.5) or absence (100 mM ChCl; pH 7.5) of Na⁺.

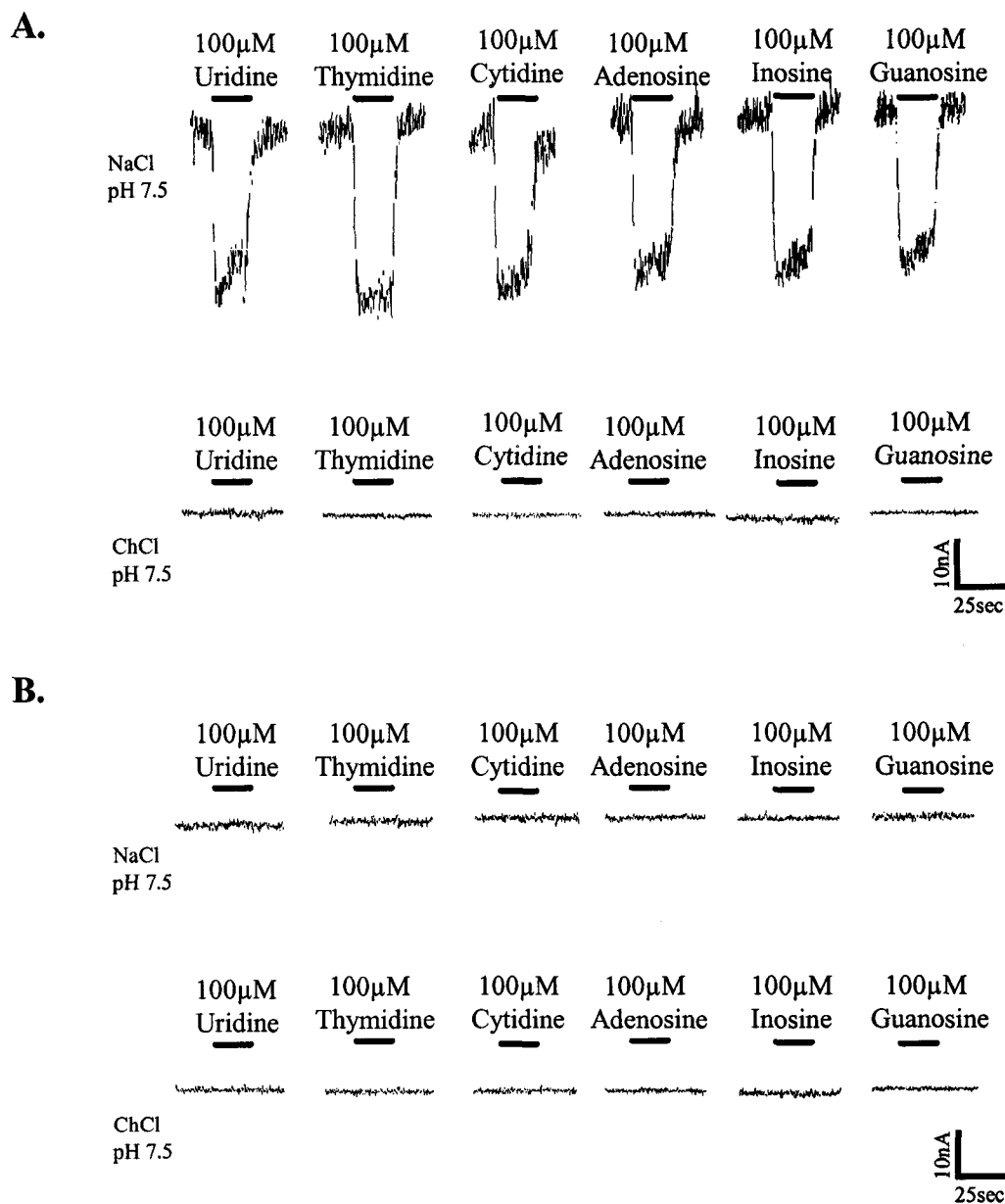


Figure 3-2. Substrate selectivity and Na^+ -dependence of mCNT3 produced in *Xenopus* oocytes. **A.** Inward currents evoked by various purine and pyrimidine nucleosides (each at a concentration of 100 μM) in oocytes producing mCNT3 in transport medium at pH 7.5 containing Na^+ (100 mM NaCl) (*upper panel*). The same oocyte was perfused with purine and pyrimidine nucleosides in transport medium in which Na^+ was replaced by equimolar choline (100 mM ChCl; pH 7.5) (*lower panel*). **B** shows the same experiment described in A above but with a control water-injected oocyte.

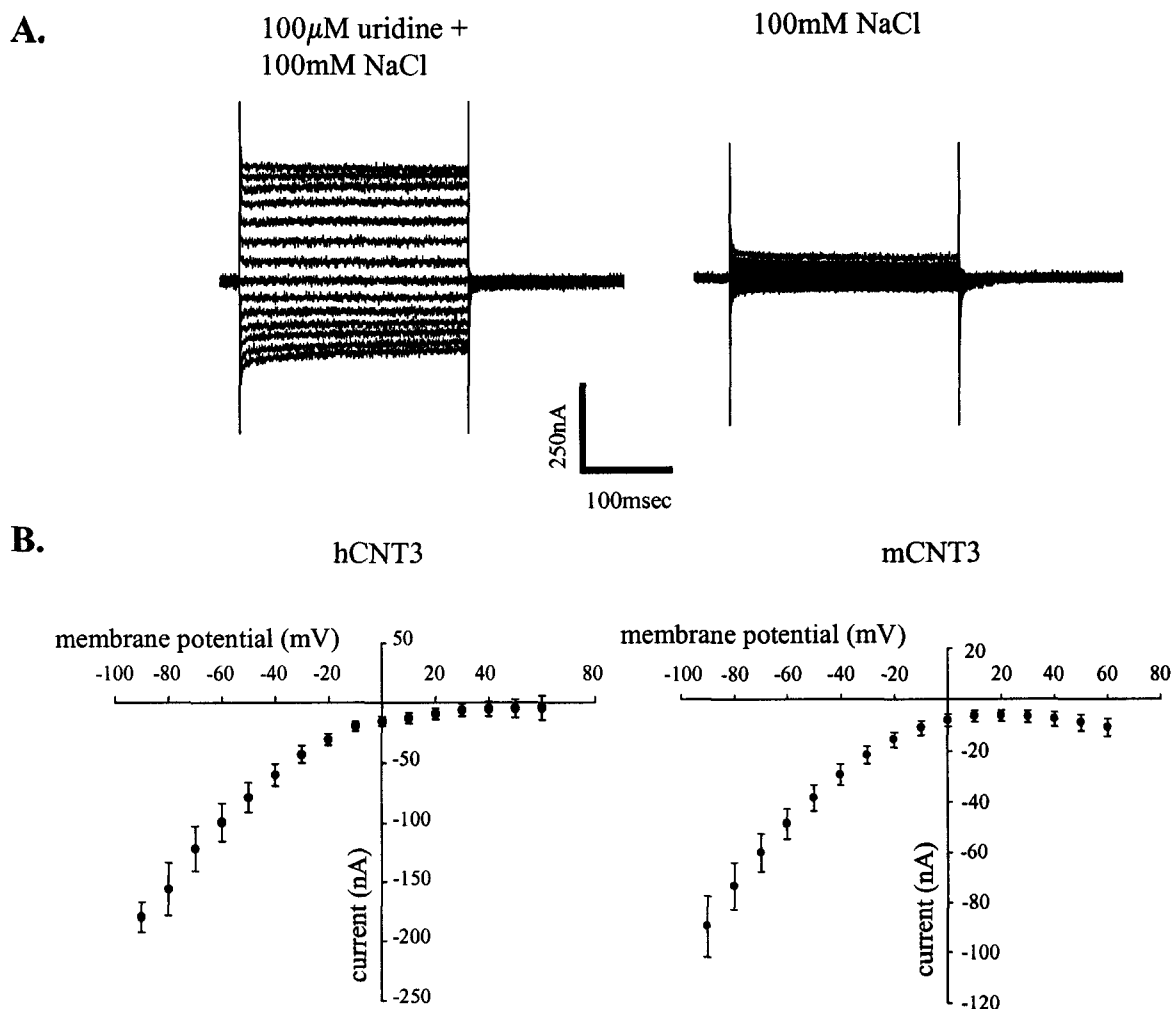


Figure 3-3. Voltage-dependence of hCNT3- and mCNT3-mediated currents. **A.** Time course of transmembrane currents recorded from an hCNT3-producing oocyte in the presence of 100 μ M external uridine (100 mM NaCl; pH 7.5) in response to voltage pulses from a holding potential of -50 mV (*left trace*). The capacitive transients have been truncated in order to clearly demonstrate the steady-state currents. Currents from the same oocyte were recorded in the absence of uridine (100 mM NaCl; pH 7.5; *right trace*). **B.** The current-voltage (I-V) curves for hCNT3 (*left panel*) and mCNT3 (*right panel*) were generated from the difference between steady-state currents recorded in the presence and absence of 100 μ M uridine in Na⁺-containing transport medium (100 mM NaCl; pH 7.5) upon voltage steps from V_h of -50 mV to final potentials ranging between -90 and +60 mV, in 10 mV increments. The current produced at each potential was averaged from 4 - 5 different oocytes.

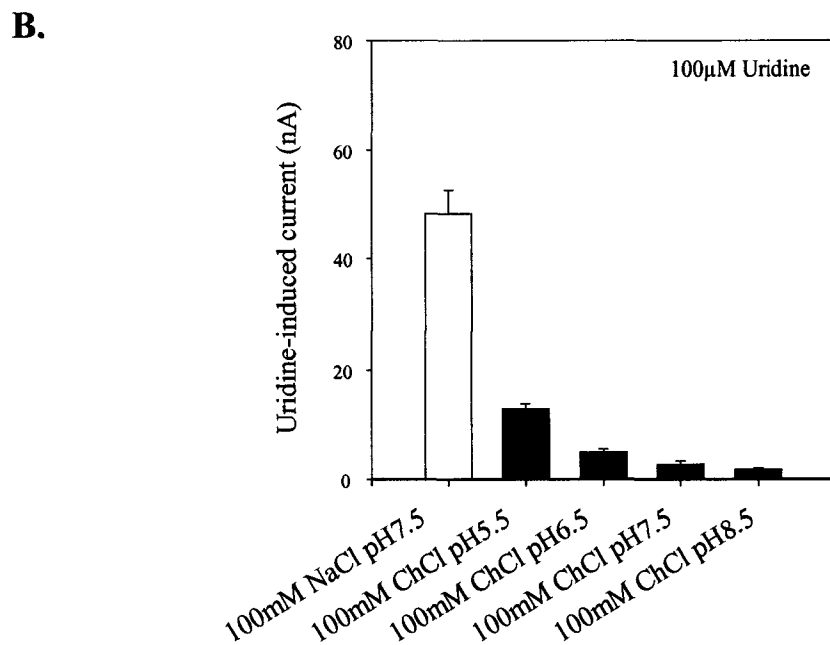
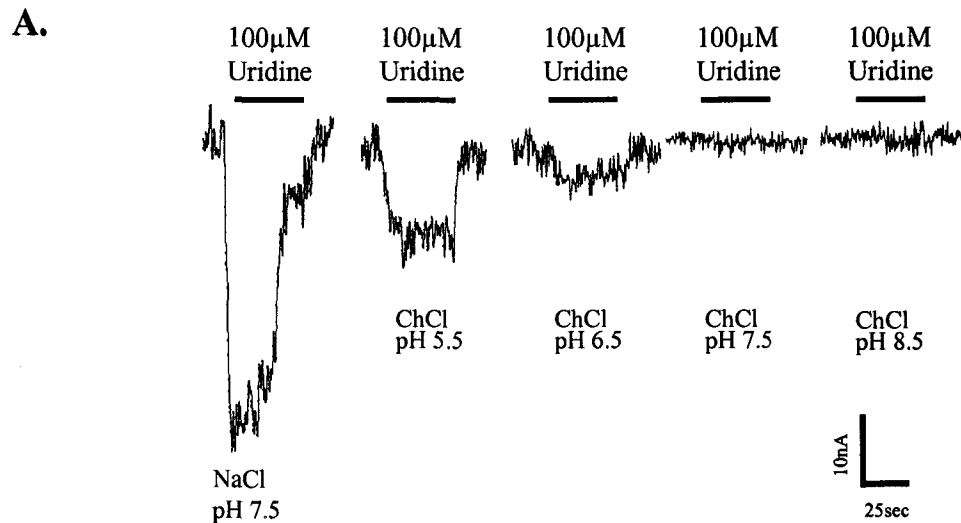


Figure 3-4. pH-dependence of uridine transport by recombinant mCNT3. **A.** Representative current traces demonstrating the pH-dependence of mCNT3-mediated uridine transport ($100 \mu\text{M}$) in Na^+ (100 mM NaCl ; pH 7.5) or choline (100 mM ChCl ; pH 5.5 - 8.5) transport media. **B.** Average inward currents measured by perfusing mCNT3-producing oocytes with $100 \mu\text{M}$ uridine in transport media containing Na^+ (100 mM NaCl ; *open bars*) or choline (100 mM ChCl ; *black bars*). pH values are indicated under each bar. No currents were seen in control water-injected oocytes (data not shown). Each value represents the mean \pm SEM of 5 - 6 oocytes.

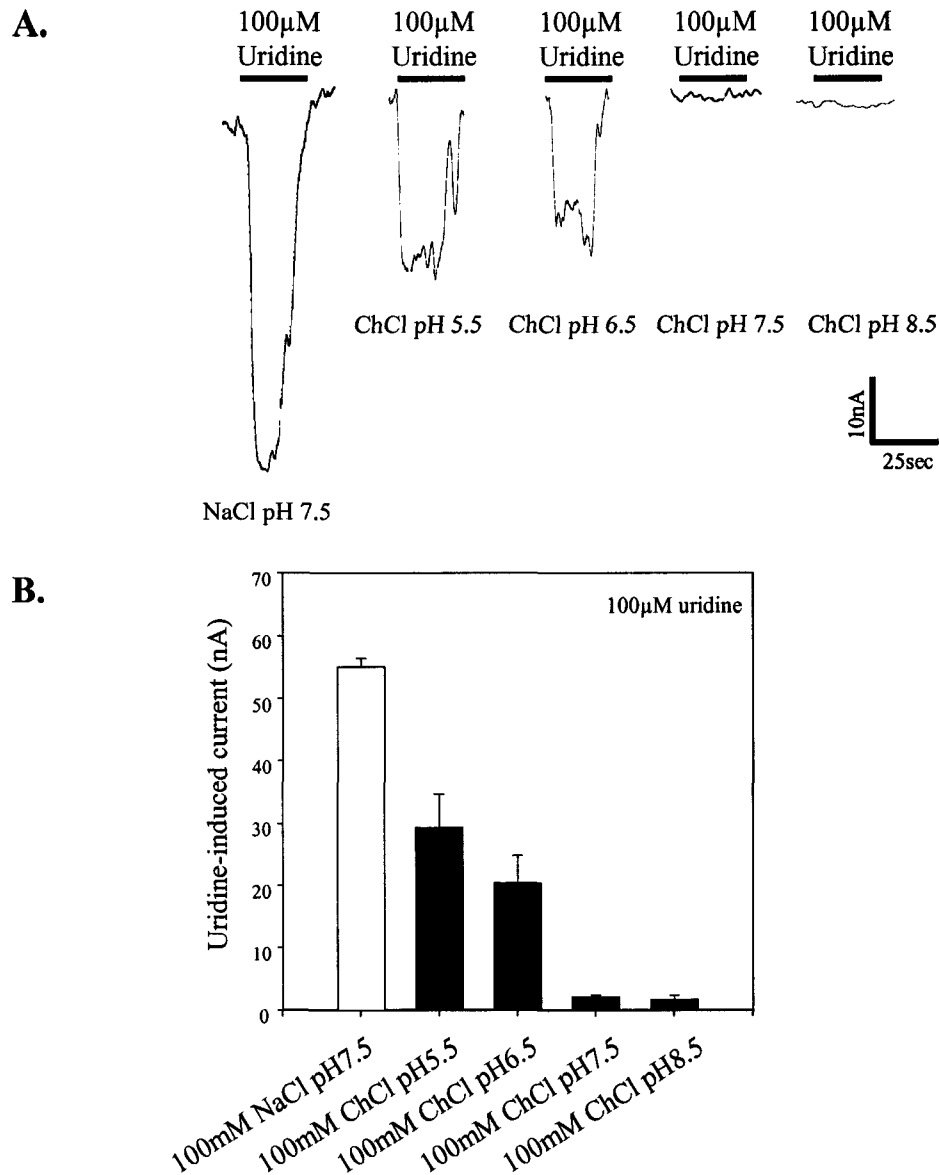
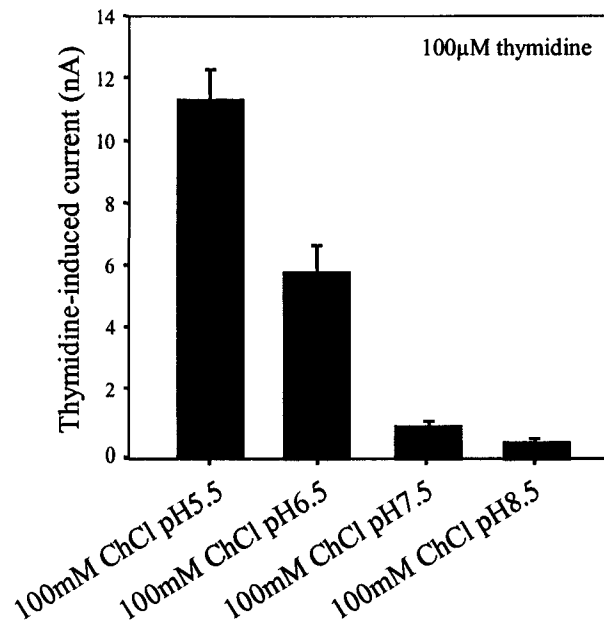


Figure 3-5. pH-dependence of uridine transport by recombinant hCNT3. **A.** Representative current traces demonstrating the pH-dependence of hCNT3-mediated uridine transport (100 μ M) in Na^+ (100 mM NaCl; pH 7.5) or choline (100 mM ChCl; pH 5.5 - 8.5) transport media. **B.** Average inward currents measured by perfusing hCNT3-producing oocytes with 100 μ M uridine in transport media containing Na^+ (100 mM NaCl; *open bars*) or choline (100 mM ChCl; *black bars*). pH values are indicated under each bar. No currents were seen in control water-injected oocytes (data not shown). Each value represents the mean \pm SEM of 6 - 7 oocytes.

A.



B.

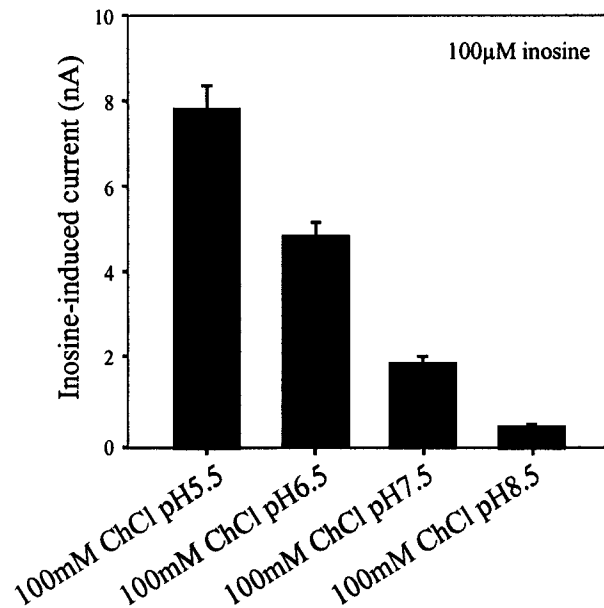
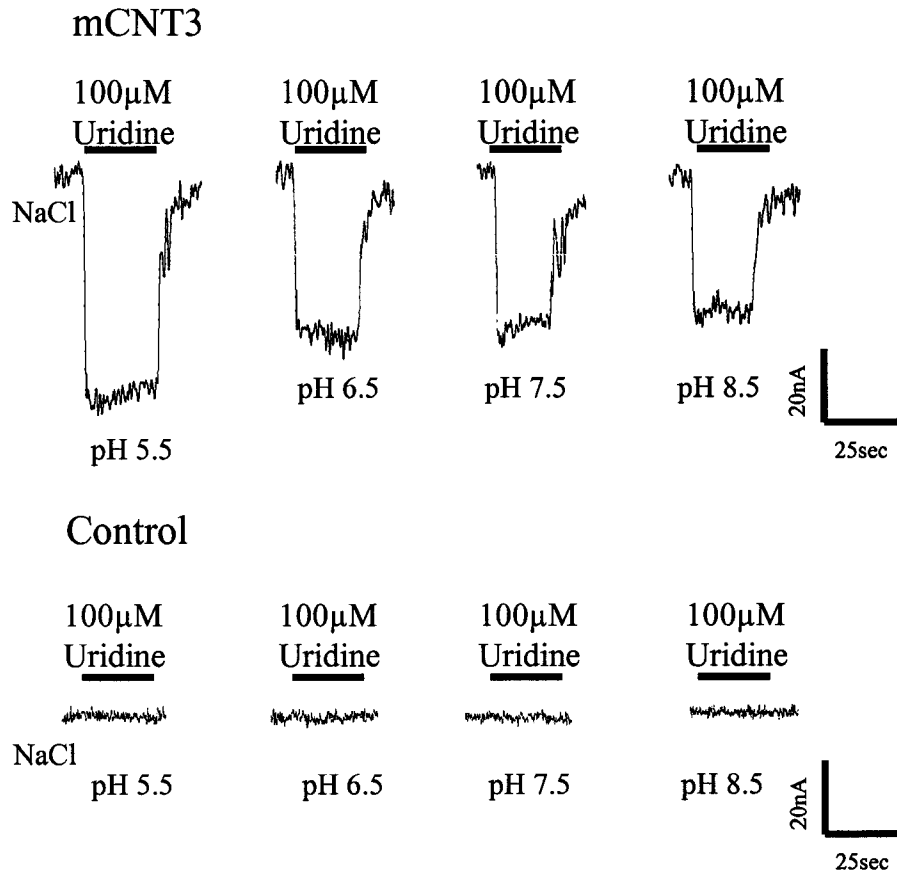
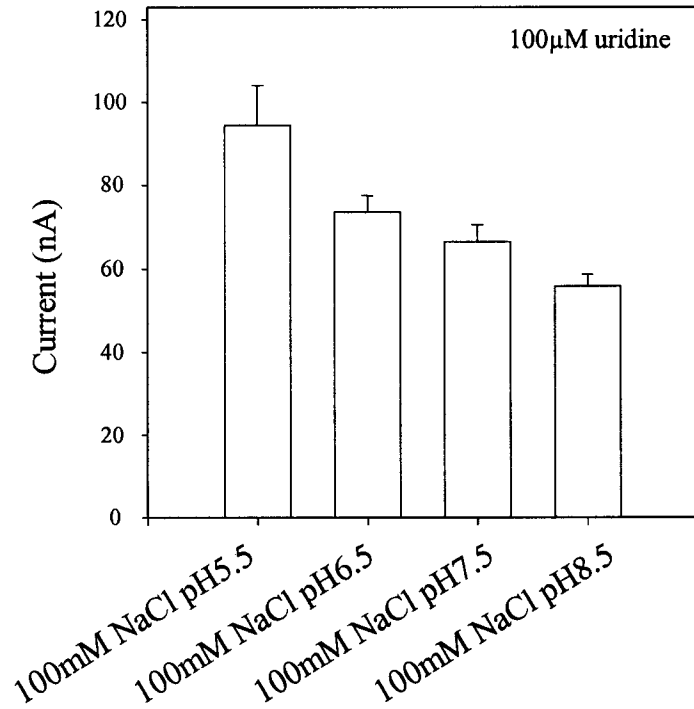


Figure 3-6. pH-dependence of thymidine and inosine transport by recombinant mCNT3. Average inward currents measured by perfusing mCNT3-producing oocytes with 100 μ M thymidine (A) or 100 μ M inosine (B) in the absence of Na^+ (100 mM ChCl; pH 5.5 - 8.5). pH values are indicated under each bar. No currents were seen in control water-injected oocytes (data not shown). Each value represents the mean \pm SEM of 5 - 6 oocytes.

A.



B.



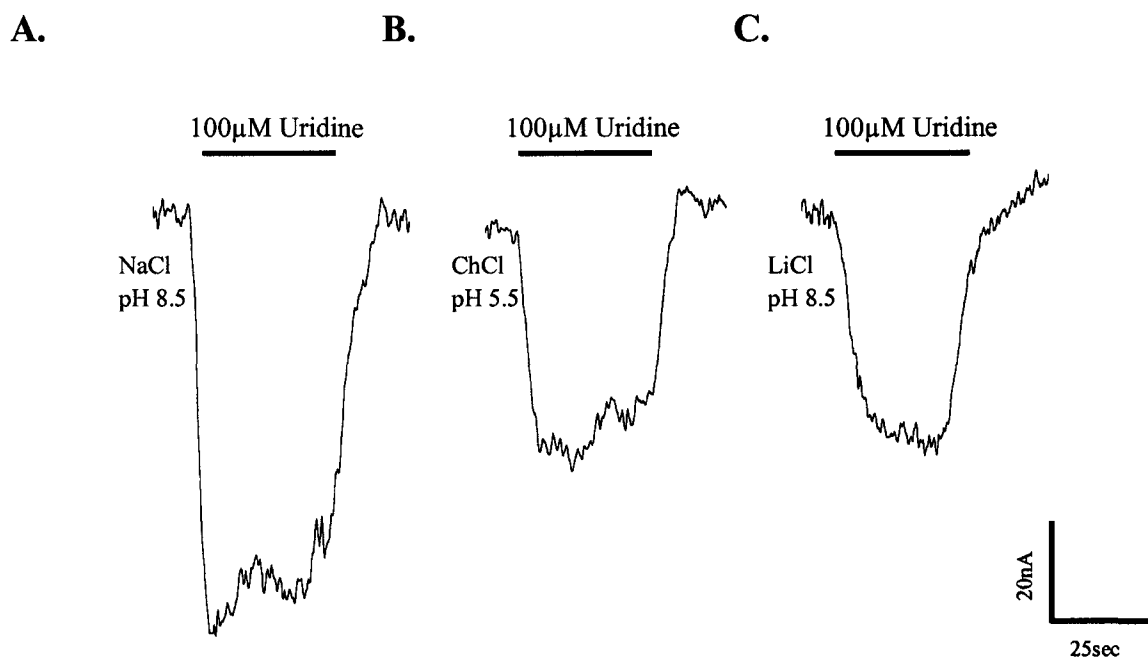
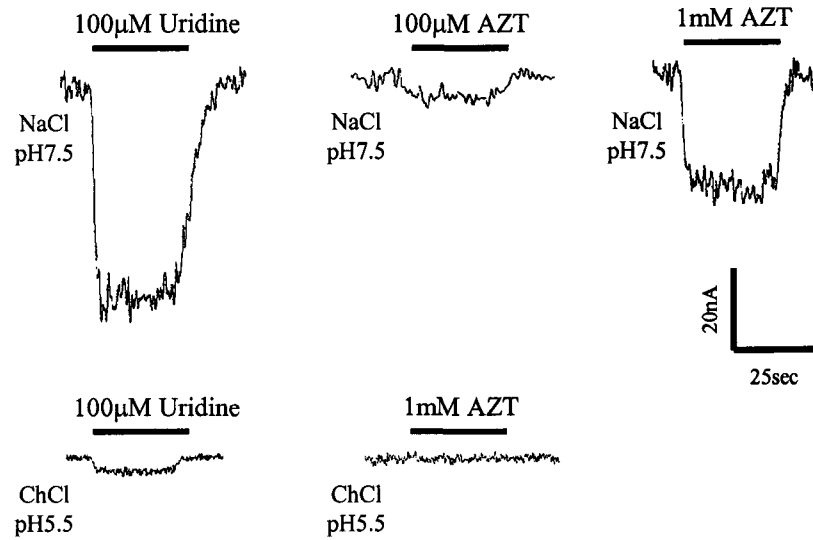


Figure 3-8. Cation/nucleoside currents. An hCNT3-producing oocyte was clamped at -50 mV, and the current recorded as uridine (100 μM) was added to the bath. **A.** The oocyte was clamped in Na⁺-containing transport medium (100 mM NaCl; pH 8.5). **B.** The same oocyte was clamped in Na⁺-free medium at pH 5.5 (100 mM ChCl). **C.** The oocyte was bathed in Li⁺-containing transport medium (100 mM LiCl; pH 8.5).

A.



B.

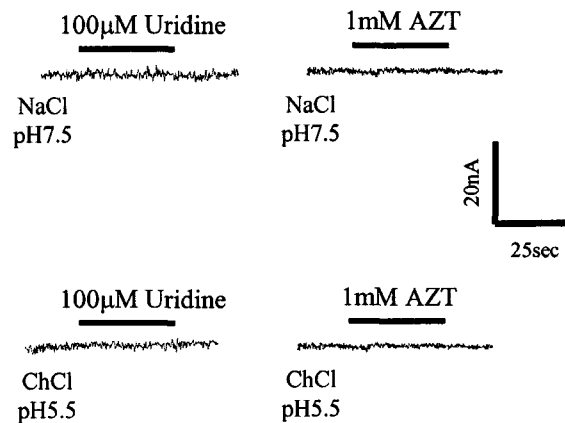


Figure 3-9. AZT-induced currents in an mCNT3-producing *Xenopus* oocyte. **A.** Inward currents induced by uridine (100 μM) and AZT (100 μM and 1 mM) in an mCNT3-producing oocyte in transport medium containing either Na⁺ (100 mM NaCl; pH 7.5; *upper panel*) or choline (100 mM ChCl; pH 5.5; *lower panel*). **B.** Inward currents induced by uridine (100 μM) and AZT (1 mM) in a control water-injected oocyte in transport medium containing either Na⁺ (100 mM NaCl; pH 7.5; *upper panel*) or choline (100 mM ChCl; pH 5.5; *lower panel*). No currents were seen in the water-injected cell.

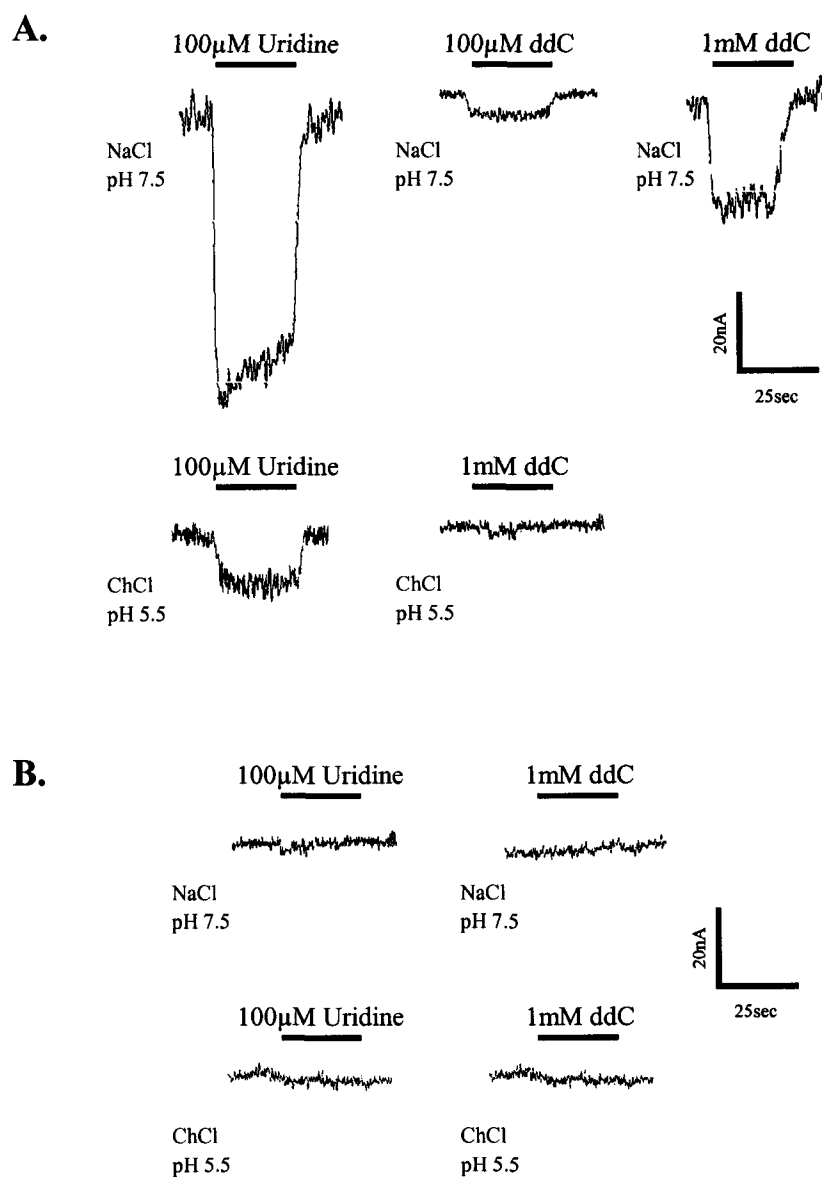


Figure 3-10. ddC-induced currents in an mCNT3-producing *Xenopus* oocyte. A. Inward currents induced by uridine (100 μ M) and ddC (100 μ M and 1 mM) in an mCNT3-producing oocyte in transport medium containing either Na⁺ (100 mM NaCl; pH 7.5; *upper panel*) or choline (100 mM ChCl; pH 5.5; *lower panel*). **B.** Inward currents induced by uridine (100 μ M) and ddC (1 mM) in a control water-injected oocyte in transport medium containing either Na⁺ (100 mM NaCl; pH 7.5; *upper panel*) or choline (100 mM ChCl; pH 5.5; *lower panel*). No currents were seen in the water-injected cell.

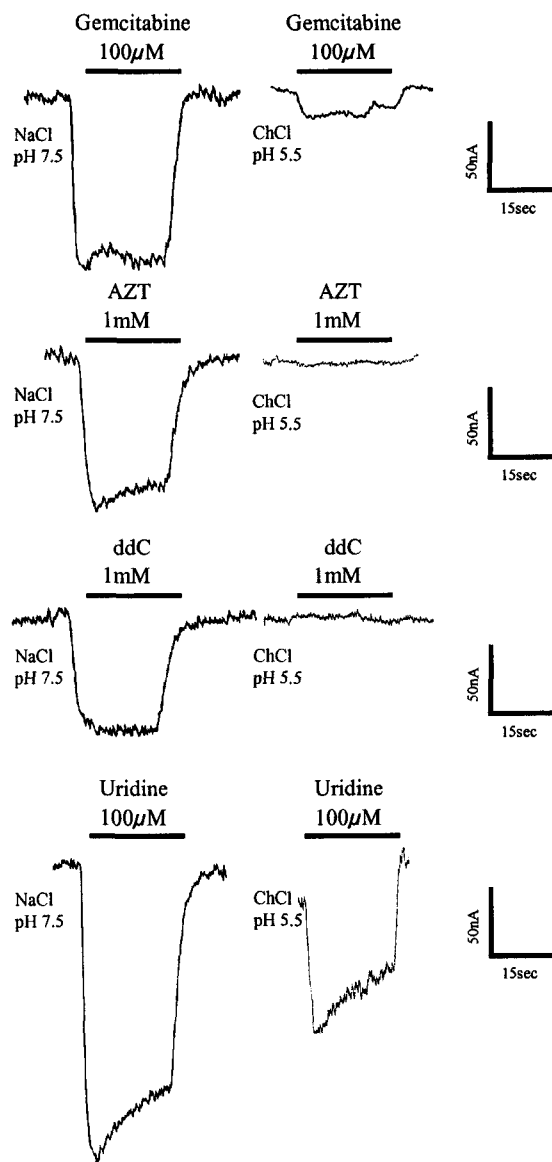
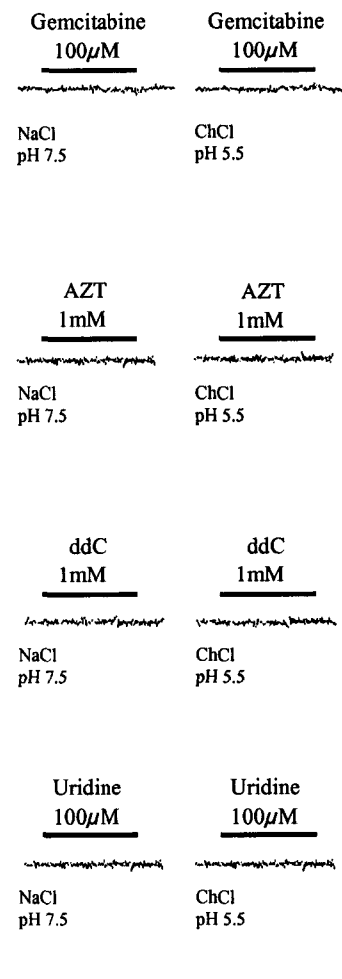
A. hCNT3**B. Control**

Figure 3-11. Nucleoside drug-induced currents in an hCNT3-producing *Xenopus* oocyte. **A.** Inward currents induced by gemcitabine (100 μM), AZT (1 mM), or ddC (1 mM) in an hCNT3-producing oocyte in transport medium containing either Na⁺ (100 mM NaCl; pH 7.5) or choline (100 mM ChCl; pH 5.5). Uridine-evoked currents in the same hCNT3-producing oocyte were 210 and 90 nA in Na⁺ (100 mM NaCl; pH 7.5) and choline (100 mM ChCl; pH 5.5) transport media, respectively. **B.** The same experiment was repeated in a control water-injected oocyte. No currents were seen in the water-injected cell.

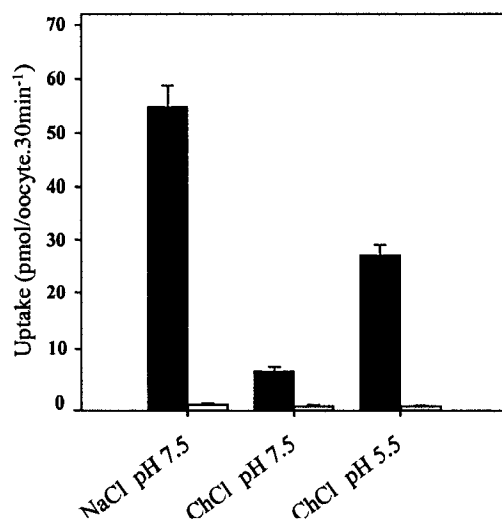
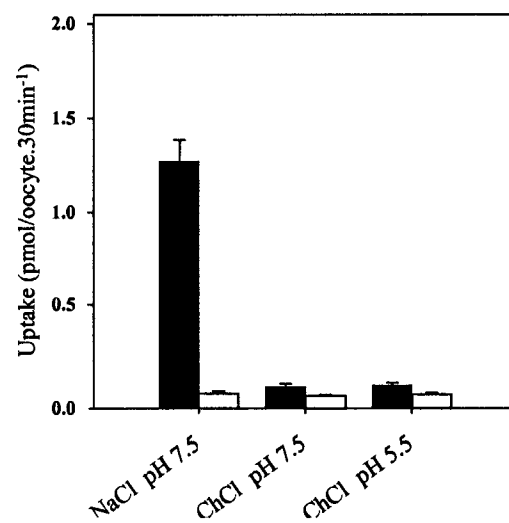
A.**B.**

Figure 3-12. Na⁺- and H⁺-dependence of radiolabeled ddC and uridine uptake in *Xenopus* oocytes producing recombinant hCNT3. Uptake of ¹⁴C-labeled uridine (A) and ³H-labeled ddC (B) (20 μM, 20 °C, and 30 min flux) in hCNT3-producing oocytes (black bars) and control water-injected oocytes (open bars) was measured in Na⁺ (100 mM NaCl; pH 7.5) or choline (100 mM ChCl; pH 7.5/5.5) transport media. Values are means ±SEM of 10 - 12 oocytes.

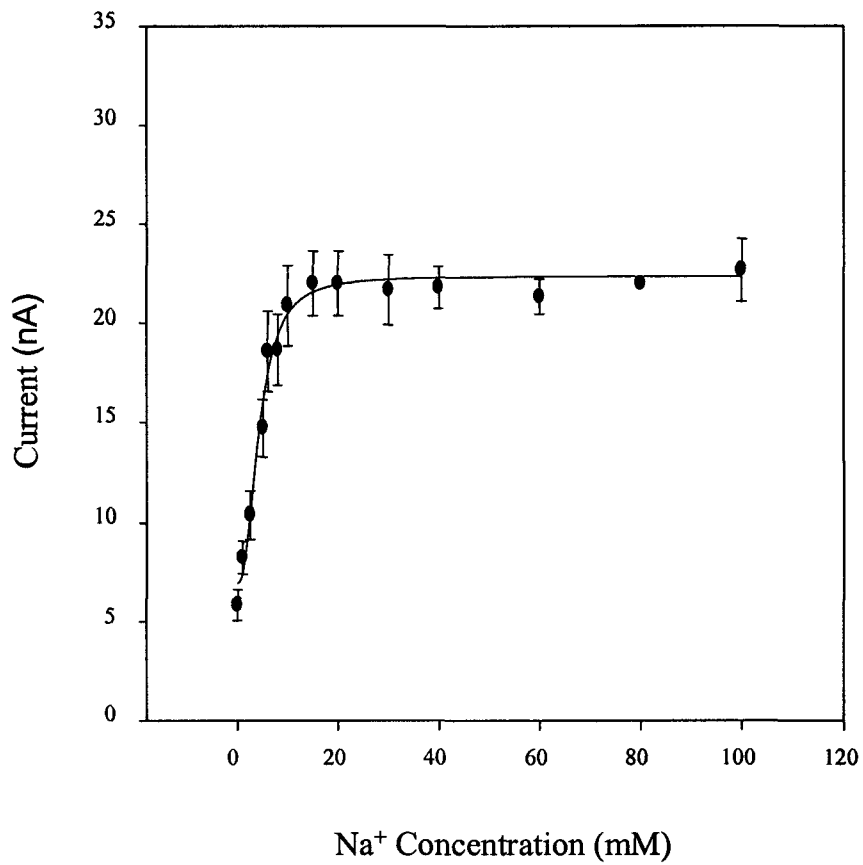


Figure 3-13. Na⁺ activation of mCNT3-mediated currents. Inward currents as a function of external Na⁺ concentration (0 - 100 mM NaCl; pH 7.5) were measured following the addition of 100 μ M uridine. mCNT3-mediated currents are expressed as the mean current (\pm SEM) produced in 5 - 6 different oocytes.

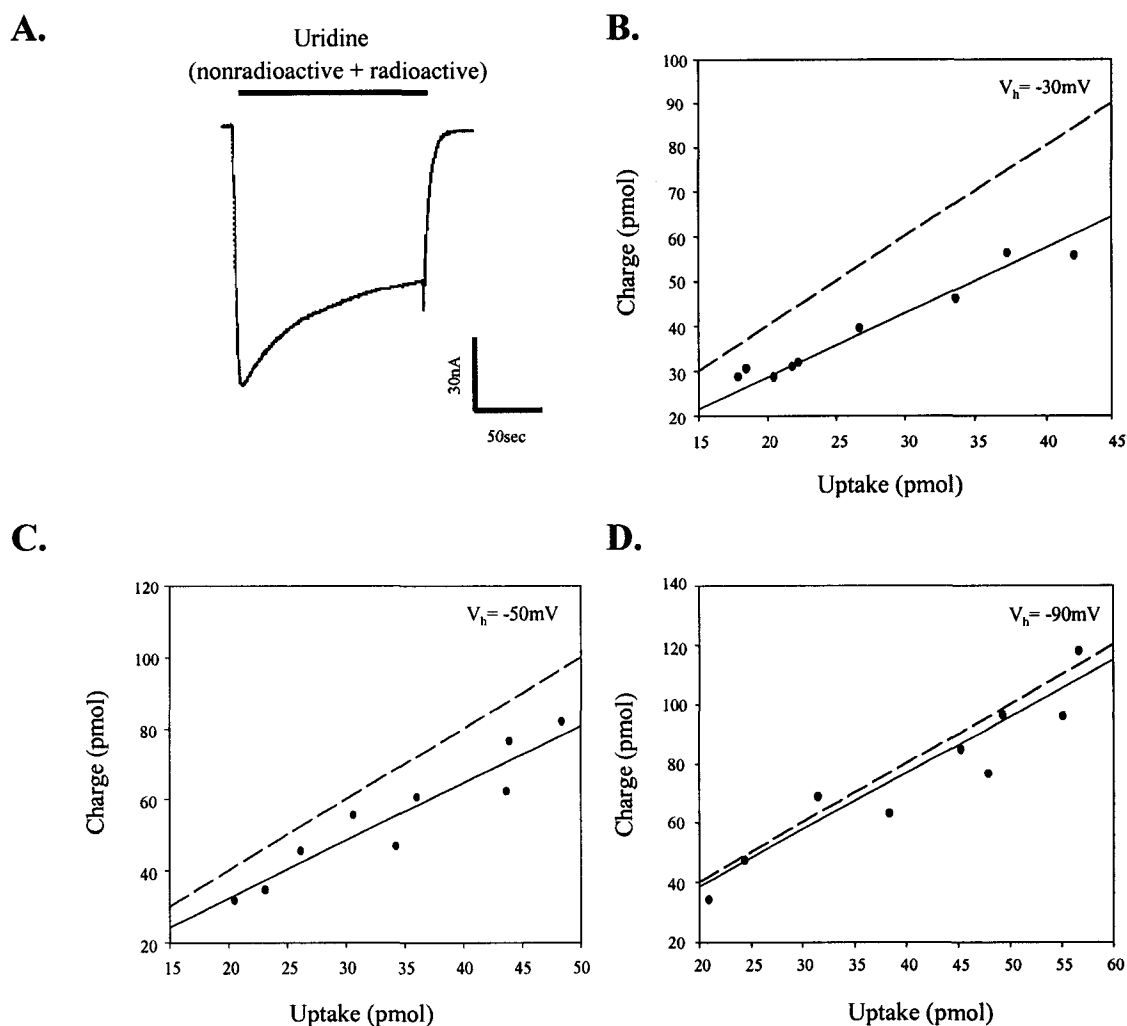


Figure 3-14. Stoichiometry of Na^+ /uridine cotransport by recombinant hCNT3. **A.** Representative example of the current generated during application of $200 \mu\text{M}$ uridine (nonradioactive + radioactive) to an hCNT3-producing oocyte in Na^+ transport media (100mM NaCl ; $\text{pH } 7.5$; $V_h = -30 \text{mV}$). **B.** Oocytes were clamped at $V_h = -30 \text{mV}$. Integration of the uridine-evoked current was used to calculate the net cation influx which was correlated to the net uridine influx. The experiment was repeated in 9 different oocytes. The slope of the linear fit (Na^+ /nucleoside ratio) was equal to 1.25 ± 0.96 (solid line). The dashed line indicates a slope of 2. **C.** At $V_h = -50 \text{mV}$, the Na^+ /nucleoside ratio was 1.66 ± 0.21 ($n = 9$). **D.** At $V_h = -90 \text{mV}$, the Na^+ /nucleoside ratio was 2.10 ± 0.24 ($n = 9$).

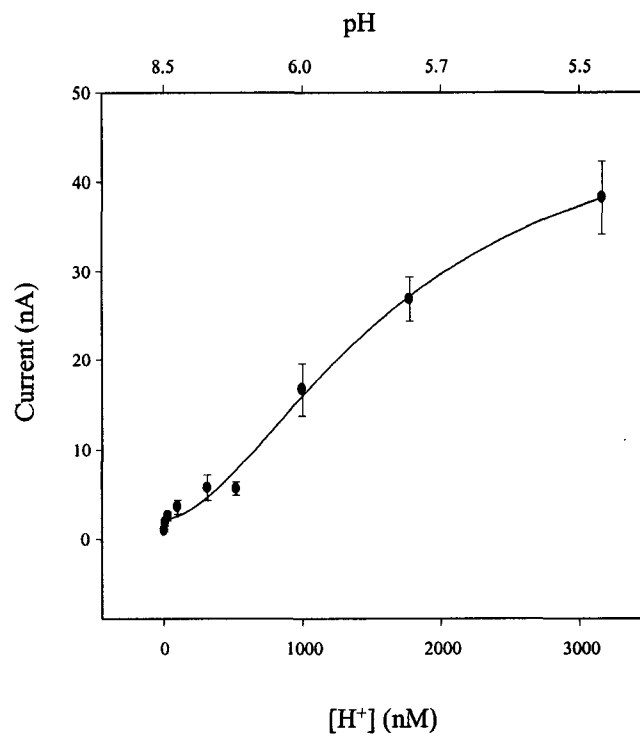


Figure 3-15. H⁺ activation of hCNT3-mediated nucleoside transport. The dependence of hCNT3 nucleoside transport upon the external H⁺ concentration was determined by measuring the inward current produced in choline (100 mM ChCl) transport medium as the pH was varied from 5.5 - 8.5.

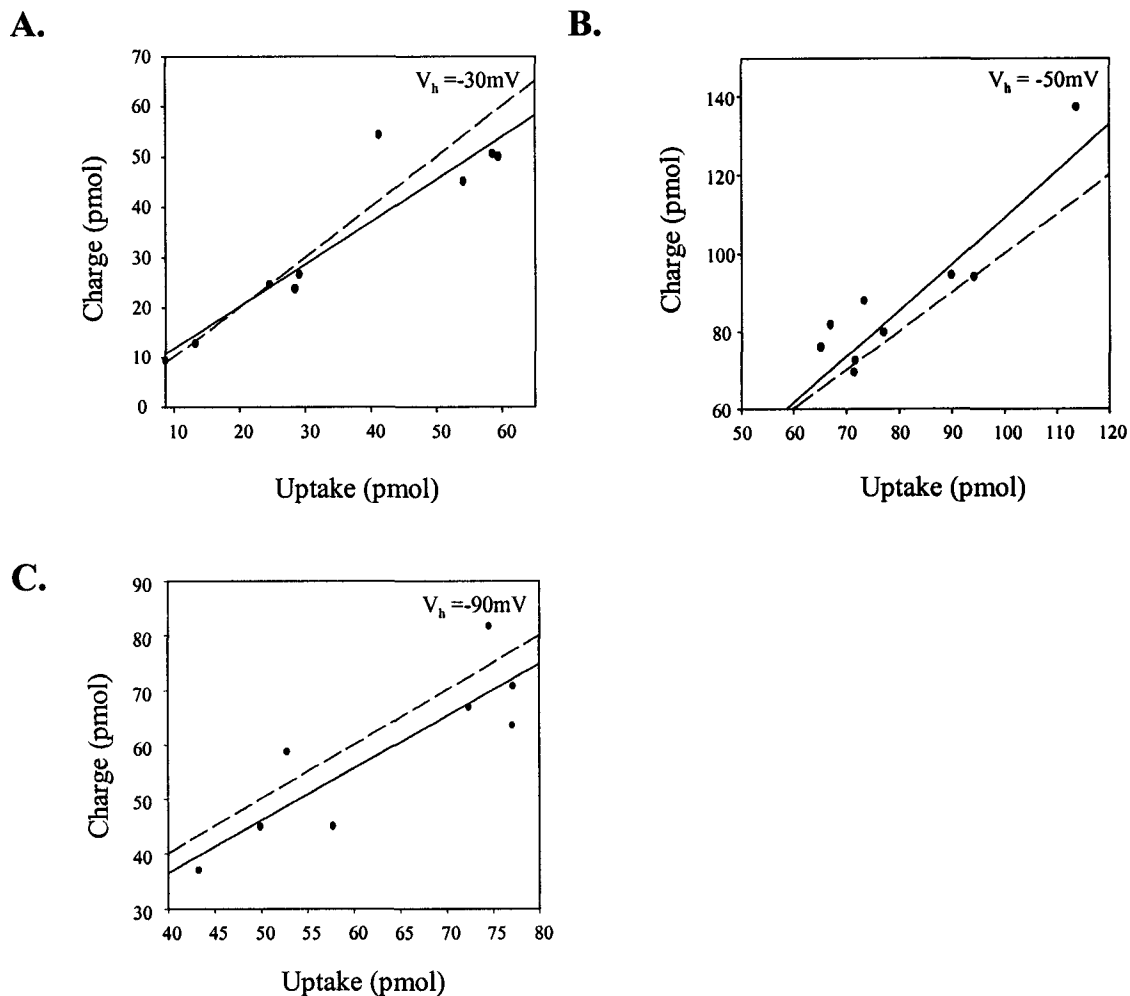


Figure 3-16. Stoichiometry of H^+ /uridine cotransport by recombinant hCNT3. **A.** Oocytes were clamped at $V_h = -30\text{ mV}$ in choline (100 mM ChCl; pH 5.5) transport medium and 200 μM uridine (nonradioactive + radioactive) was added. Integration of the uridine-evoked current was used to calculate the net cation influx which was correlated to the net uridine influx. The experiment was repeated in 9 different oocytes. The slope of the linear fit (H^+ /nucleoside ratio) was equal to 0.84 ± 0.12 (solid line). The dashed line indicates a slope of 1. **B.** At $V_h = -50\text{ mV}$, the H^+ /nucleoside ratio was 1.19 ± 0.20 ($n = 9$). **C.** At $V_h = -90\text{ mV}$, the H^+ /nucleoside ratio was 0.96 ± 0.26 ($n = 8$).

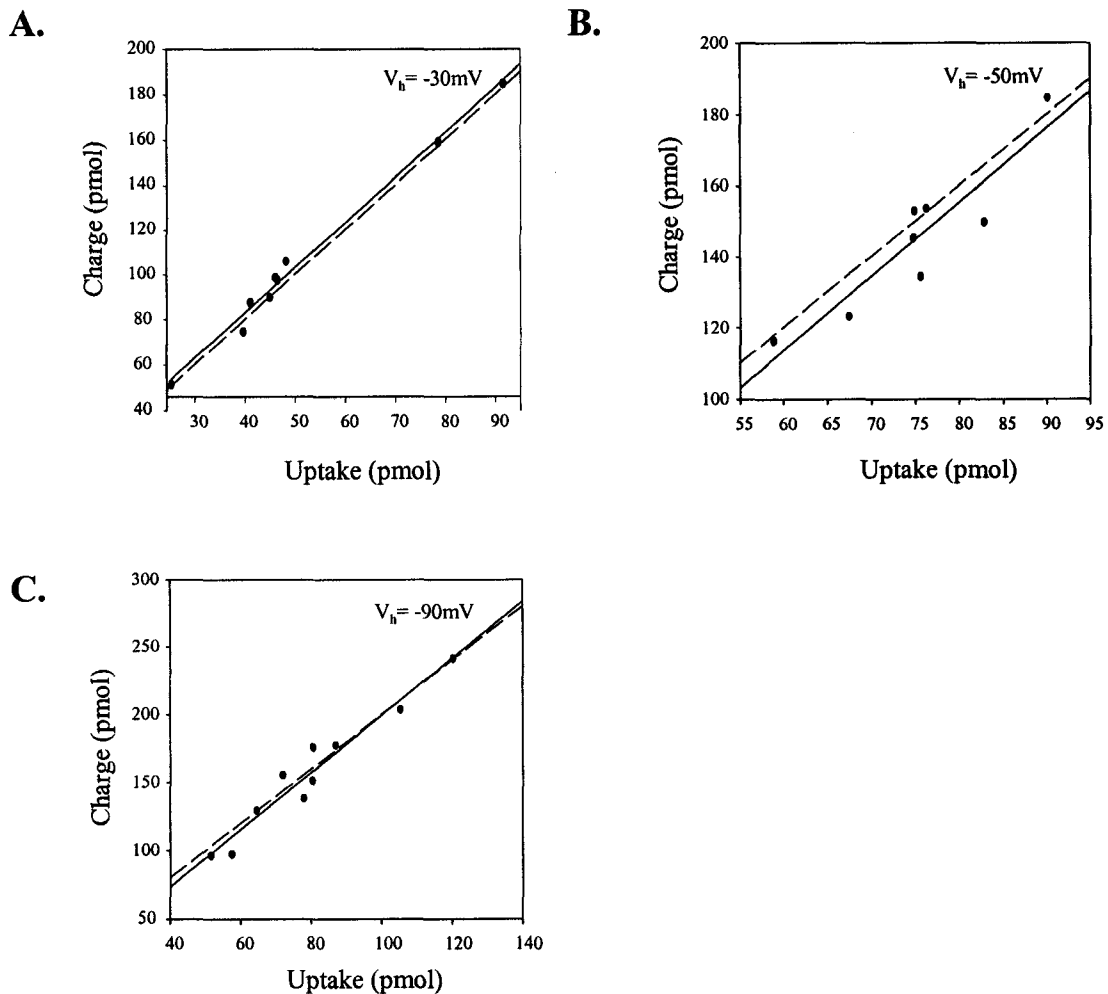


Figure 3-17. Stoichiometry of Na^+ /uridine cotransport by recombinant hCNT3 at pH 5.5. **A.** Oocytes were clamped at $V_h = -30\text{ mV}$. The current generated in response to the addition of $200\text{ }\mu\text{M}$ uridine (nonradioactive + radioactive) to an hCNT3-producing oocyte in Na^+ transport medium (100 mM NaCl ; pH 5.5) was measured. Integration of the uridine-evoked current was used to calculate the net cation influx which was correlated to the net uridine influx. The experiment was repeated in 9 different oocytes. The slope of the linear fit (Na^+ /nucleoside ratio) was equal to 2.01 ± 0.08 (*solid line*). The dashed line indicates a slope of 2. **B.** At $V_h = -50\text{ mV}$, the Na^+ /nucleoside ratio was 2.09 ± 0.38 ($n = 8$). **C.** At $V_h = -90\text{ mV}$, the Na^+ /nucleoside ratio was 2.10 ± 0.18 ($n = 10$).

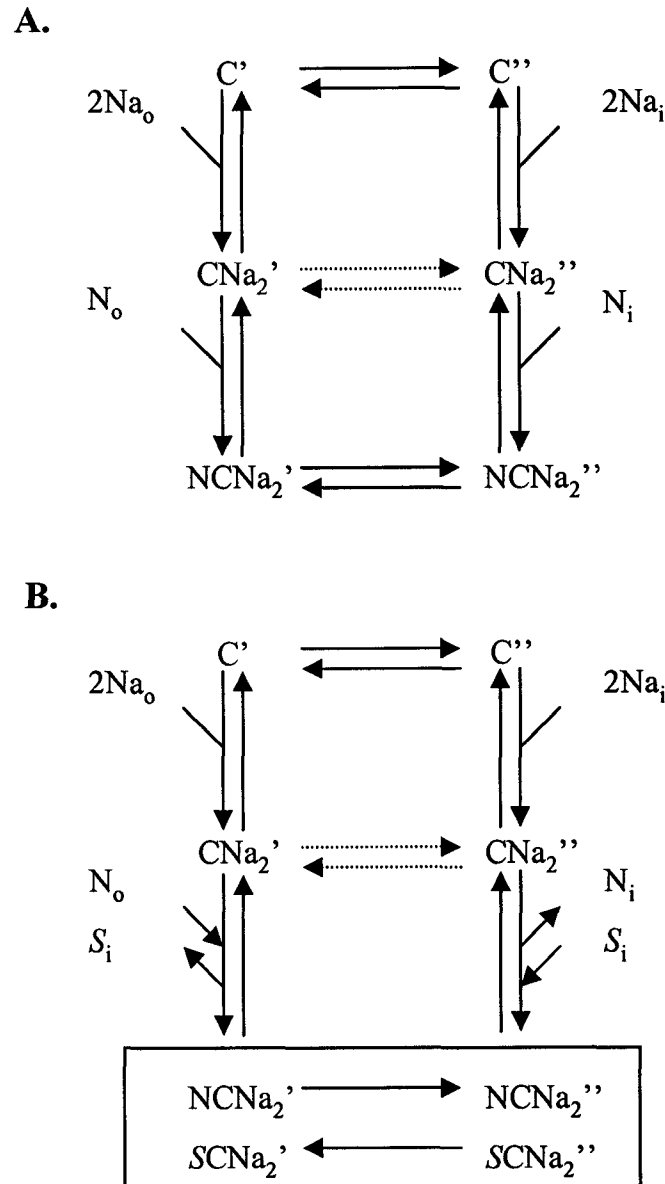


Figure 3-18. Proposed transport model for hCNT3 Na^+ /nucleoside cotransport. A. The carrier (C) possesses 2 binding sites for the driving ion Na^+ and one binding site for the nucleoside (N). The carrier can face the outer (C') or inner (C'') face of the membrane. **B.** The boxed region shows the transmembrane steps involved in the electroneutral exchange of extracellular radiolabeled nucleosides (N) for unlabeled intracellular endogenous substrates (S).

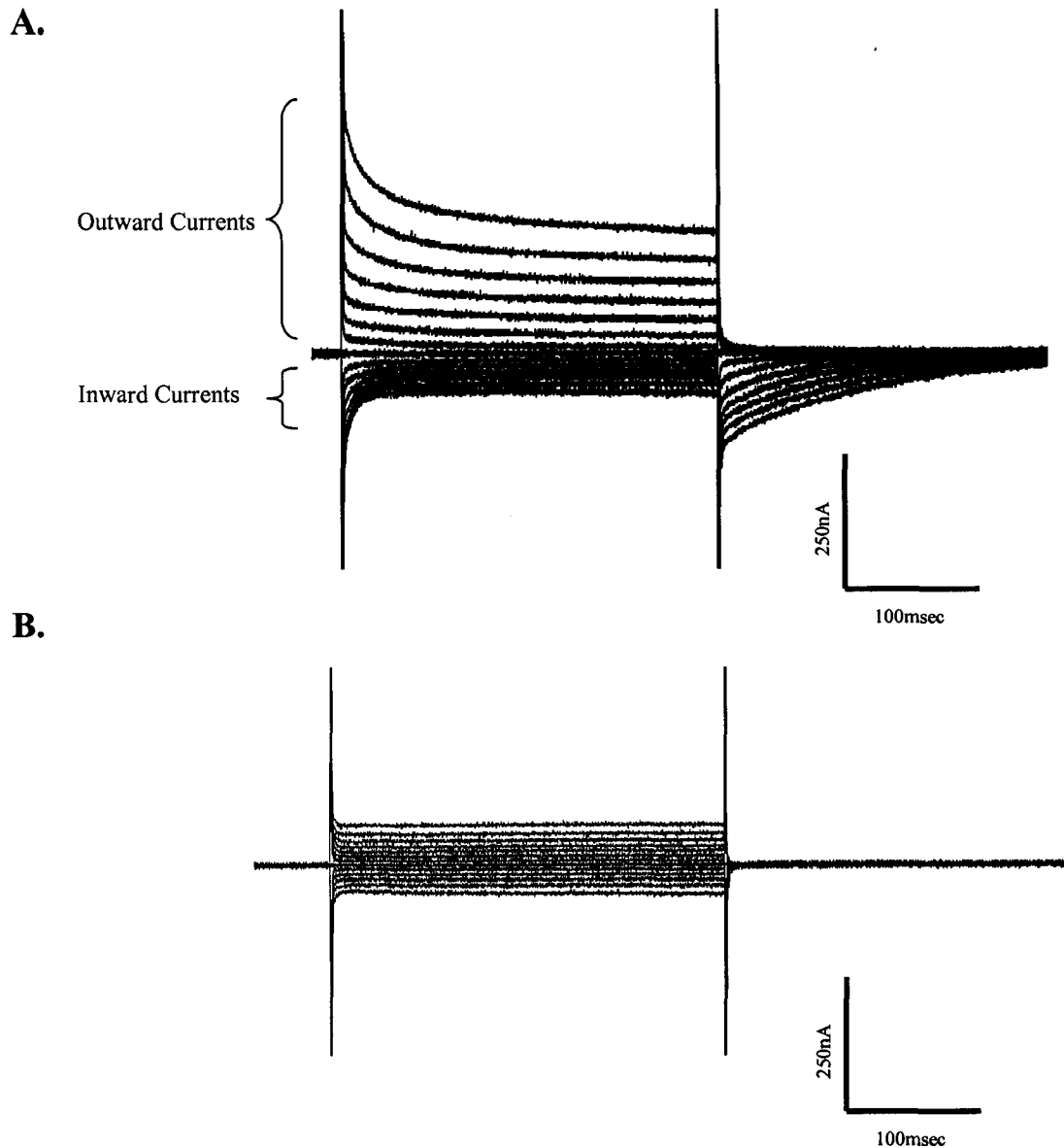


Figure 3-19. hCNT3 total currents in the presence of external Na^+ . **A.** Time course of transmembrane currents recorded in the presence of external Na^+ (100 mM NaCl; pH 8.5) upon voltage steps from a holding potential (V_h) of -50 mV to final potentials ranging between -170 and +90 mV, in 20 mV increments, in an hCNT3 producing oocyte. The capacitive transients have been truncated in order to clearly demonstrate the steady-state (leak) currents. The inward and outward currents are indicated. **B.** Time course of transmembrane currents in a control water-injected oocyte. The outward currents were not observed in the water-injected cell.

Bibliography

Acimovic Y and Coe IR. Molecular evolution of the equilibrative nucleoside transporter family: identification of novel family members in prokaryotes and eukaryotes. *Mol Biol Evol* 19(12): 2199-2210, 2002.

Baldwin SA, Mackey JR, Cass CE, and Young JD. Nucleoside transporters: molecular biology and implications for therapeutic development. *Mol Med Today* 5: 216-224, 1999.

Burckhardt B-C, Kroll B, and Frömter E. Proton transport mechanism in the cell membrane. *Pflügers Arch* 420: 78-82, 1992.

Cass CE. In: Drug transport in antimicrobial and anticancer chemotherapy, edited by Georgopapadakou NH. New York: Marcel Dekker, 1995.

Che M, Ortiz DF, and Arias IM. Primary structure and functional expression of a cDNA encoding the bile canalicular, purine-specific Na⁺ nucleoside cotransporter. *J Biol Chem* 270: 13596-13599, 1995.

Chen X-Z, Coady MJ, Jackson F, Bertleot A, and Lapointe J-Y. Thermodynamic determination of the Na⁺:glucose coupling ratio for the human SGLT1 cotransporter. *Biophys J* 69: 2405-2414, 1995.

Chen X-Z, Shayakul C, Berger UV, Tian W, and Hediger MA. Characterization of a rat Na⁺-dicarboxylate cotransporter. *J Biol Chem* 273: 20972-20981, 1998.

Chen X-Z, Zhu T, Smith DE, and Hediger MA. Stoichiometry and kinetics of the high-affinity H⁺-coupled peptide transporter PepT2. *J Biol Chem* 274: 2773-2779, 1999.

Craig JE, Zhang Y, and Gallagher MP. Cloning of the nupC gene of *Escherichia coli* encoding a nucleoside transport system, and identification of an adjacent insertion element, IS 186. *Mol Microbiol* 11(6): 1159-1168, 1997.

Crawford CR, Patel DH, Naeve C, and Belt JA. Cloning of the human equilibrative, nitrobenzylmercaptapurine riboside (NBMPR)-insensitive nucleoside transporter *ei* by functional expression in a transport-deficient cell line. *J Biol Chem* 273(9): 5288-5293, 1998.

Diez-Sampedro A, Eskandari S, Wright EM, and Hirayama BA. Na⁺-to-sugar stoichiometry of SGLT3. *Am J Physiol Renal Physiol* 49: F278-F282, 2001.

Griffiths DA and Jarvis SM. Nucleoside and nucleobase transport systems of mammalian cells. *Biochim Biophys Acta* 1286: 153-181, 1996.

Hamilton SR, Yao SYM, Ingram JC, Hadden DA, Ritzel MWL, Gallagher MP, Henderson PJF, Cass CE, Young JD, and Baldwin SA. Subcellular distribution and membrane topology of the mammalian concentrative Na⁺-nucleoside cotransporter rCNT1. *J Biol Chem* 276(30): 27981-27988, 2001.

Hirayama BA, Loo DDF, and Wright EM. Protons drive sugar transport through the Na⁺/glucose cotransporter (SGLT1). *J Biol Chem* 269(34): 21407-21410, 1994.

Hirayama BA, Loo DDF, and Wright EM. Cation effects on protein conformation and transport in the Na⁺/glucose cotransporter. *J Biol Chem* 272(4): 2110-2115, 1997.

Hong M, Schlichter L, and Bendayan R. A Na⁺-dependent nucleoside transporter in microglia. *J Pharmacol Exp Ther* 292(1): 366-374, 2000.

Huang Q-Q, Yao SYM, Ritzel MWL, Paterson ARP, Cass CE, and Young JD. Cloning and functional expression of a complementary DNA encoding a mammalian nucleoside transport protein. *J Biol Chem* 269: 17757-17760, 1994.

Hyde RJ, Cass CE, Young JD, and Baldwin SA. The ENT family of eukaryote nucleoside and nucleobase transporters: recent advances in the investigation of structure/function relationships and the identification of novel isoforms. *Mol Membr Biol* 18: 53-63, 2001.

Lee W-S, Kanai Y, Well RG, and Hediger MA. The high affinity Na⁺/glucose cotransporter: re-evaluation of function and distribution of expression. *J Biol Chem* 269(16): 12032-12039, 1994.

Loewen SK, Ng AML, Yao SYM, Cass CE, Baldwin SA, and Young JD. Identification of amino acid residues responsible for the pyrimidine and purine nucleoside specificities of human concentrative Na⁺ nucleoside cotransporters hCNT1 and hCNT2. *J Biol Chem* 274 (35): 24475-24484, 1999.

Loewen SK, Ng AML, Mohabir NN, Baldwin SA, Cass CE, and Young JD. Functional characterization of a H⁺/nucleoside cotransporter (CaCNT) from *Candida albicans*, the first fungal homolog of mammalian/bacterial concentrative nucleoside transporters. *Yeast* 2003a (*in press*).

Loewen SK, Yao SYM, Slugoski MD, Mohabir NN, Turner RJ, Weiner JH, Gallagher MP, Henderson PJF, Baldwin SA, Cass CE, and Young JD. Transport of antiviral and antineoplastic drugs by recombinant *Escherichia coli* nucleoside-H⁺ cotransporter (NupC) produced in *Xenopus laevis* oocytes. *Mol Membr Biol* 2003b (*in press*).

Mackenzie B, Loo DDF, Panayotova-Heiermann M, and Wright EM. Biophysical characteristics of the pig kidney Na⁺/glucose cotransporter SGLT2 reveal a common mechanism for SGLT1 and SGLT2. *J Biol Chem* 271 (51): 32678-32683, 1996.

Mackenzie B, Loo DDF, and Wright EM. Relationships between Na⁺/glucose cotransporter (SGLT1) currents and fluxes. *J Membr Biol* 162: 101-106, 1998.

Mackey JR, Baldwin SA, Young JD, and Cass CE. Nucleoside transport and its significance for anticancer drug resistance. *Drug Resist Updates* 1: 310-324, 1998.

Mackey JR, Yao SYM, Smith KM, Karpinski E, Baldwin SA, Cass CE, and Young JD. Gemcitabine transport in *Xenopus* oocytes expressing membrane mammalian nucleoside transporters. *J Natl Cancer Inst* 91(21): 1876-1881, 1999.

Pajor AM, Hirayama BA, and Loo DDF. Sodium and lithium interactions with the Na⁺/dicarboxylate cotransporter. *J Biol Chem* 273(30): 18923-18929, 1998.

Parent L, Supplisson S, Loo DF, and Wright EM. Electrogenic properties of the cloned Na⁺/glucose cotransporter: Part I. Voltage-clamp studies. *J Membr Biol* 125: 49-62, 1992a.

Parent L, Supplisson S, Loo DF, and Wright EM. Electrogenic properties of the cloned Na⁺/glucose cotransporter: Part II. A transport model under non rapid equilibrium conditions. *J Membr Biol* 125: 63-79, 1992b.

Pourcher T, Bassilana M, Sarkar HK, Kaback HR, and Leblanc G. The melibiose/Na⁺ symporter of *Escherichia coli*: kinetic and molecular properties. *Philos Trans R Soc Lond B Biol Sci* 326(1236): 411-423, 1990.

Quick M, Donald DDF, and Wright EM. Neutralization of a conserved amino acid residue in the human Na⁺/glucose transporter (hSGLT1) generates a glucose-gated H⁺ channel. *J Biol Chem* 276(3): 1728-1734, 2001.

Ritzel MWL, Yao SYM, Huang M-Y, Elliot JF, Cass CE, and Young JD. Molecular cloning and functional expression of cDNAs encoding a human Na⁺-nucleoside cotransporter (hCNT1). *Am J Physiol Cell Physiol* 272: C707-C714, 1997.

Ritzel MWL, Yao SYM, Ng AML, Mackey JR, Cass CE, and Young JD. Molecular cloning, functional expression and chromosomal localization of a cDNA encoding a human Na⁺ nucleoside cotransporter (hCNT2) selective for purine nucleosides and uridine. *Mol Membr Biol* 15: 203-211, 1998.

Ritzel MWL, Ng AML, Yao SYM, Graham K, Loewen SK, Smith KM, Ritzel GR, Mowles DA, Carpenter P, Chen X-Z, Karpinski E, Hyde RJ, Baldwin SA, Cass CE, and Young JD. Molecular identification and characterization of novel human and mouse concentrative Na⁺-nucleoside cotransporter proteins (hCNT3 and mCNT3) broadly selective for purine and pyrimidine nucleosides (system *cib*). *J Biol Chem* 276(4): 2914-2927, 2001.

Stein WD. In: Transport and diffusion across cell membranes, edited by Harcourt, Brace, and Jovanovich. Toronto: Academic Press, Inc., 1986.

Vickers MF, Young JD, Baldwin SA, Mackey JR, and Cass CE. Nucleoside transporter proteins: emerging targets for drug discovery. *Emerg Ther Targets* 4(4): 515-539, 2000.

Wang J, Su S-F, Dresser MJ, Schaner ME, Washington CB, and Giacomini KM. Na⁺-dependent purine nucleoside transporter from human kidney: cloning and functional characterization. *Am J Physiol Renal Physiol* 273(42): F1058-F1065, 1997.

Wu X, Yuan G, Brett CM, Hui AC, and Giacomini KM. Sodium-dependent nucleoside transport in choroid plexus from rabbit. Evidence for a single transporter for purine and pyrimidine nucleosides. *J Biol Chem* 267(13): 8813-8818, 1992.

Xiao G, Wang J, Tangen T, and Giacomini KM. A novel proton-dependent nucleoside transporter, CeCNT3 from *Caenorhabditis elegans*. *Mol Pharmacol* 59: 339-348, 2001.

Yao SYM, Ng AML, Ritzel MWL, Gati WP, Cass CE, and Young JD. Transport of adenosine by recombinant purine- and pyrimidine-selective sodium/nucleoside cotransporters from rat jejunum expressed in *Xenopus laevis* oocytes. *Mol Pharmacol* 50: 1529-1535, 1996.

Yao SYM, Ng AML, Muzyka WR, Griffiths M, Cass CE, Baldwin SA, and Young JD. Molecular cloning and functional characterization of nitrobenzylthioinosine (NBMPR)-sensitive (*es*) and NBMPR-insensitive (*ei*) equilibrative nucleoside transporter proteins (rENT1 and rENT2) from rat tissues. *J Biol Chem* 272: 28423-28430, 1997.

Yao SYM, Ng AML, Loewen SK, Cass CE, Baldwin SA, and Young JD. An ancient prevertebrate Na⁺-nucleoside cotransporter (hfCNT) from the Pacific hagfish (*Eptatretus stouti*). *Am J Physiol Cell Physiol* 283: C155-C168, 2002.

Young JD, Cheeseman C, Mackey JR, Cass CE, and Baldwin SA. Molecular mechanisms of nucleoside and nucleoside drug transport. *Curr Top Membr* 50: 329-378, 2001.

Chapter IV*:

**Presteady-state Currents of the Human Concentrative Na⁺-Nucleoside Cotransporter
hCNT3**

**A version of this chapter is in preparation for publication.*

Smith KM, Labeledz K, Cass CE, Baldwin SA, Chen XZ, Karpinski E, and Young JD.
Presteady-state currents of the human concentrative Na⁺-nucleoside cotransporter hCNT3. (*in preparation*).

Introduction

Most natural and synthetic nucleosides are hydrophilic and require specialized nucleoside transport proteins for permeation across the cell membrane. In human and other mammalian cells and tissues, five major nucleoside transport processes that differ in their cation dependence, permeant specificity, and inhibitor sensitivity have been described (Cass, 1995; Griffiths and Jarvis, 1996; Young *et al.*, 2001). Three are inwardly-directed concentrative mechanisms driven by the transmembrane sodium electrochemical gradient (systems *cit*, *cif*, and *cib*), and two are equilibrative bidirectional processes driven by the concentration gradient of the transported substrate (systems *es* and *ei*). System *cit* transports pyrimidine nucleosides and, to a lesser extent, adenosine, while system *cif* shows a permeant selectivity for purine nucleosides and uridine. System *cib*, in contrast, transports both pyrimidine and purine nucleosides. The equilibrative systems *es* and *ei* also transport both pyrimidine and purine nucleosides, with transporters of the *es*-type being sensitive to inhibition by the nucleoside analog nitrobenzylthioinosine (NBMPR). The NBMPR-insensitive *ei*-type systems also transport nucleobases.

Molecular cloning studies have isolated cDNAs encoding the rodent and human nucleoside transporter proteins responsible for each of these nucleoside transport processes. The relationships of these nucleoside transporter proteins to the systems defined by functional studies are as follows: CNT1 (*cit*), CNT2 (*cif*), CNT3 (*cib*), ENT1 (*es*), and ENT2 (*ei*) (Huang *et al.*, 1994; Che *et al.*, 1995; Yao *et al.*, 1996; Ritzel *et al.*, 1997; Yao *et al.*, 1997; Wang *et al.*, 1997; Crawford *et al.*, 1998; Ritzel *et al.*, 1998, 2001). Two further ENT isoforms (ENT3 and ENT4) of undetermined function have also been identified (Hyde *et al.*, 2001; Acimovic and Coe, 2002). Other identified CNTs include the H⁺/nucleoside cotransporter NupC from *Escherichia coli* (Craig *et al.*, 1997), hfCNT from an ancient marine prevertebrate, the Pacific hagfish (*Eptatretus stouti*) (Loewen *et al.*, 1999; Yao *et al.*, 2002), CeCNT3 from *Caenorhabditis elegans* (Xiao *et al.*, 2001), and CaCNT from *Candida albicans* (Loewen *et al.*, 2003).

Presteady-state currents analogous to the gating currents of ion channels are a general characteristic of cotransporters (Armstrong and Bezanilla, 1973), and have been observed for several gene families, including, but not limited to, transporters for sugars (glucose and *myo*-inositol) (Parent *et al.*, 1992a, b; Loo *et al.*, 1993; Chen *et al.*, 1996; Klamo *et al.*, 1996; Mackenzie *et al.*, 1996b; Hazama *et al.*, 1997), neurotransmitters and amino acids (norepinephrine, glutamate, GABA, taurine, and betaine) (Mager *et al.*, 1993; Galli *et al.*, 1995; Wadiche *et al.*, 1995), peptides (dipeptide) (Mackenzie *et al.*, 1996a; Chen *et al.*, 1999) and anions (iodide) (Eskandari *et al.*, 1997). Presteady-state currents (also referred to as transient currents) result when mobile charged residues of the channel or transporter move within the membrane to new equilibrium positions in response to changes in the voltage (also known as voltage steps or pulses) across the membrane. These currents are no longer observed when the new equilibrium (steady-state) is reached. Binding/dissociation of coupling ions or substrates is also often voltage-dependent and contributes to the observed presteady-state currents. Characterization of these currents provides kinetic and mechanistic information about cotransporter function.

In this thesis, electrophysiological experiments in *Xenopus* oocytes have examined the steady-state kinetic properties of the human Na⁺/dependent nucleoside transporter hCNT3, including the transport protein's permeant selectivity, cation specificity, kinetic parameters, voltage-dependence of transport, and cation/nucleoside coupling ratios (Ritzel *et al.*, 2001; *Chapter III*). Analysis of presteady-state currents provides information that cannot be obtained from experiments under steady-state conditions. In the present chapter, I have analyzed presteady-state currents exhibited by hCNT3 following step changes in membrane potential as a means to examine partial reactions in the CNT transport cycle and to estimate the number of hCNT3 proteins in the membrane and hence determine the turnover rate of the transporter.

Materials and Methods

Production of Recombinant hCNT3 in *Xenopus* Oocytes - hCNT3 plasmid DNA (pGEM-HE vector) was linearized with *NheI* and transcribed with T7 polymerase using the mMESSAGE mMACHINE™ (Ambion, Austin, TX) transcription system. The remaining template was removed by digestion with RNase-free DNase1. Stage V-VI oocytes extracted from the clawed frog *Xenopus laevis* were treated with collagenase (2 mg/ml) for 2 h and the remaining follicular layers removed manually (Huang *et al.*, 1994). Twenty-four hours after defolliculation, oocytes were injected with either 10 nl of water containing 10 ng of hCNT3 RNA transcript or 10 nl of water alone. Injected oocytes were then incubated for 4 days at 18 °C in modified Barth's solution (daily change) (88 mM NaCl, 1 mM KCl, 0.33 mM Ca(NO₃)₂, 0.41 mM CaCl₂, 0.82 mM MgSO₄, 2.4 mM NaHCO₃, 10 mM HEPES, 2.5 mM sodium pyruvate, 0.05 mg/ml penicillin, and 0.1 mg/ml gentamycin sulfate, pH 7.5) prior to measuring membrane currents.

Electrophysiological Studies - Presteady-state currents were measured using a GeneClamp 500B oocyte clamp amplifier (Axon Instruments, Inc., Foster City, California) in the two-electrode, voltage clamp mode. The GeneClamp 500B was interfaced to an IBM compatible PC *via* a Digidata 1200 A/D converter and controlled by pCLAMP 8.0 software (Axon Instruments, Inc., Foster City, California). All electrophysiological experiments were performed at room temperature. The microelectrodes were filled with 3 M KCl and had resistances ranging from 0.5 - 1.5 MΩ (megaohms). Oocytes were penetrated with the microelectrodes, and a 10 - 15 min period of membrane potential stabilization was allowed before voltage-clamping the oocyte. Oocytes were discarded if the membrane potential was unstable or more positive than -30 mV. The sodium-containing transport medium contained the following (in mM): NaCl, 100; KCl, 2; CaCl₂, 1; MgCl₂, 1; and HEPES, 10 (pH 8.5). The composition of the transport medium was varied by replacing NaCl (100 - 0 mM) with equimolar choline chloride (pH 8.5) ± nucleoside (uridine) at the appropriate concentration.

Presteady-state currents were studied using a voltage pulse protocol. Membrane voltage was stepped from the holding potential (V_h) of -50 mV to a series of test potentials (V_t) varying from -170 to +130 mV in 20 mV increments. The voltage rise time of the clamp was adjusted by use of an oscilloscope such that it varied between 200 and 500 μ sec (Fig. 4-1). In experiments determining the turnover rate of the transporter, membrane voltage was stepped from V_h of -50 mV to V_t from -170 to +150 mV in 40 mV increments, in order to ensure maximal charge displacement while reducing the number of voltage pulses to which the oocyte was subjected. The maximal steady-state inward Na^+ current (I_{max}) was measured at V_h of -50 mV with a saturating concentration of uridine (100 μ M). Currents were filtered at 2 kHz (four-pole Bessel filter) and sampled at a rate of 200 μ sec/point (corresponding to a sampling frequency of 5 kHz).

Data Analysis - For data analysis and presentation, the current at each test potential was averaged from 5 sweeps. If necessary, signals were further filtered at 750 Hz using the pCLAMP program suite. The presteady-state (transient) current was isolated from the oocyte capacitive current as well as from the steady-state (leak) current. Many transporters have inhibitors which block charge movements, such that recordings in the presence of the inhibitor can be subtracted from the total current in order to isolate the transient current (Mager *et al.*, 1998). Since no high-affinity inhibitors of the CNT transporter family have been identified, presteady-state currents of hCNT3 for the ON response (current response when membrane potential was stepped from V_h to V_t) and the OFF response (current response when V_t was stepped back to V_h) were obtained from the total current response without the use of an inhibitor. Steady-state leak currents were subtracted from total currents by zeroing the baseline using the pCLAMP program suite. The oocyte capacitive transient showed a single time constant ($\tau \sim 0.25$ msec) which was independent of membrane potential in the presence (Fig. 4-2A) or absence (Fig. 4-2B) of Na^+ . Presteady-state currents in the present study are therefore shown 1.5 msec after the onset of the voltage pulse. Presteady-state currents due to hCNT3 were fitted using the Simplex method (Nelder and Mead, 1965) with two exponential functions ($I(t) = A_1 \exp(-t/\tau_{\text{fast}}) + A_2 \exp(-t/\tau_{\text{slow}})$, where A_1 and A_2 are the amplitudes with time constants τ_{fast} and τ_{slow} , respectively) in order to calculate the current-time integral

(pCLAMP 8.0). Curve fits were considered successful only if the correlation was 0.95 or higher (Fig. 4-3). Charge movements (Q), obtained from the current-time integral of the curve fits, were plotted as a function of voltage and fitted to the Boltzmann function: $Q(V_t) = Q_{hyp} / (Q_{max} [1 + \exp((V_t - V_{0.5})z_d F / RT)])$, where the total charge $Q_{max} = Q_{dep} - Q_{hyp}$ (Q_{dep} and Q_{hyp} represent Q at depolarizing and hyperpolarizing limits, respectively), z_d is the product of the valence of the charge (z) and the apparent fraction of the field (δ) sensed by that charge, V_t is the membrane voltage during the pulse, $V_{0.5}$ is the membrane voltage at which half of the total charge has moved, F is Faraday's constant, R is the gas constant, and T is the absolute temperature. Each experiment was fitted to the Boltzmann function and the $V_{0.5}$ and z_d were determined. These parameters from the individual fits were then used to calculate the means \pm SEM of $V_{0.5}$ and z_d . The curves which are presented as figures were fitted to the mean \pm SEM of the charge displacements from 3 - 6 experiments.

Results

Presteady-state Currents of hCNT3 - Unless otherwise specified, presteady-state experiments were performed in the absence of nucleoside to eliminate steady-state inward currents of hCNT3 and to isolate partial reactions of the transport cycle. Since steady-state current studies described in *Chapter III* have shown that H^+ ions are capable of driving the uptake of nucleoside substrate mediated by hCNT3, presteady-state experiments were performed at pH 8.5 to minimize the H^+ driving force by maintaining the extracellular pH at a value greater than the intracellular oocyte pH of 7.3 - 7.6 (Burckhardt *et al.*, 1992; *Chapter III*). Oocytes were voltage clamped at a holding potential (V_h) of -50 mV and presteady-state currents were induced by a series of test voltages. In the representative experiment presented in Figure 4-4, V_t ranged from -170 to +90 mV in 20 mV increments (Fig. 4-4A). Figure 4-4B (*top current record*) shows total current recordings in an hCNT3-producing oocyte bathed in Na^+ -containing transport medium (100 mM NaCl; pH 8.5) in response to the voltage pulses. Current relaxations are apparent which persisted for tens of milliseconds after the time required to charge the membrane capacitance. These relaxations were not seen in control water-injected oocytes (Fig. 4-4B; *bottom current record*).

ON/OFF Current Responses - Figure 4-5 shows representative hCNT3 presteady-state currents (100 mM extracellular NaCl) isolated from the total current response by subtraction of both the steady-state (leak) and capacitive currents. For clarity, only current responses at final potentials of -170, -90, +10 and +90 mV are shown (Fig. 4-5A). Currents in Figure 4-4B are presented for both the ON response (*left current record*), when V_h is stepped to V_t , and for the OFF response (*right current record*), when the membrane potential is returned to the holding potential (V_t to V_h). The slow decay of the current, indicating the presence of presteady-state currents, is evident in both the ON and OFF current responses.

Effect of Na^+ on Presteady-state Currents - Figure 4-6A compares total current recordings for an hCNT3-producing oocyte in 100 *versus* 10 mM external Na^+ (*left and*

right current records, respectively) when the membrane voltage was stepped from V_h (-50 mV) to various V_t (V_t from -170 to +90 mV in 20 mV increments). Corresponding charge-voltage (Q-V) relationships for hCNT3-producing oocytes in 100 (n = 4; left graph) and 10 mM (n = 3; right graph) external Na^+ are shown in Figure 4-6B. At each clamped voltage, integration of the transporter-mediated currents with time yielded the charge (Q) moved by hCNT3 within the membrane electric field. The charge calculated for the OFF response was plotted as a function of membrane voltage. The curves were analyzed according to the Boltzmann equation to estimate the parameters Q_{\max} , z_d , and $V_{0.5}$. Since the maximal charge movement depends upon the level of transporter expression in the oocyte plasma membrane, the data were normalized to Q_{\max} in order to compare different oocytes with varying levels of expression. Q saturated with both hyperpolarization and depolarization and reversed at the holding potential ($V_h = -50$ mV). Q_{\max} was unaffected by reducing the external concentration of Na^+ ; in a representative experiment, Q_{\max} values of 102 and 95 nC were obtained for 100 and 10 mM external Na^+ , respectively (data not shown). The z_d value, obtained from the Boltzmann fit of charge movement in 6 different oocytes for both 100 and 10 mM Na^+ , was reduced as the concentration of Na^+ was lowered; z_d values of 0.92 ± 0.08 and 0.71 ± 0.07 were obtained in 100 and 10 mM external Na^+ , respectively. $V_{0.5}$, also obtained from the Boltzmann fit of charge movement in 6 different oocytes for both 100 and 10 mM Na^+ , shifted towards more negative values as the concentration of Na^+ was reduced; $V_{0.5}$ values of $+40.60 \pm 4.45$ and -44.90 ± 3.50 mV were obtained with 100 and 10 mM external Na^+ , respectively. The shift in $V_{0.5}$ in each oocyte can be used to calculate the effective fraction of the field, δ , sensed by Na^+ from $[\text{Na}^+]_1/[\text{Na}^+]_2 = \exp[\delta F(V_1 - V_2)/RT]$, where $[\text{Na}^+]_1$ and $[\text{Na}^+]_2$ are two different external concentrations of Na^+ (ie. 100 and 10 mM), V_1 and V_2 are the values of $V_{0.5}$ at $[\text{Na}^+]_1$ and $[\text{Na}^+]_2$, respectively, F is Faraday's constant, R is the gas constant, and T is the absolute temperature (Wadiche *et al.*, 1995). The δ obtained from 6 oocytes was 65.40 ± 4.10 %. This would imply the binding of sodium to site(s) that traverse 65.40 ± 4.10 % of the membrane electric field. The valence of the moveable charge (z), calculated from $z_d = \delta z$, was equal to -1.42 ± 0.15 .

ON/OFF Charge Movement - The total charge movement during a step change in the membrane potential in the absence of uridine was calculated for a range of test potentials ($V_t = -170$ to $+130$ mV in 20 mV increments). In the presence of external Na^+ (100 mM NaCl; pH 8.5), the charge movement at the onset of the voltage pulse (Q_{ON}) was found to be equal and opposite to the charge movement at the return to the pre-pulse potential (Q_{OFF}) (Fig. 4-7). Linear regression analysis yielded a slope of 1.02 ± 0.09 . These results indicate a conservation of charge during OFF and ON voltage steps.

Uridine Reversal of Presteady-state Currents - The effect of uridine on hCNT3 presteady-state currents and on Q_{max} (calculated for the OFF response) are shown in Figure 4-8. Transient and steady-state uridine-induced currents were measured in the presence of varying concentrations of uridine in the range 0 - 100 μM . Increasing the concentration of uridine reduced both the presteady-state current (Fig. 4-8A) and Q_{max} (Fig. 4-8B). At 25 μM uridine, a concentration close to the uridine apparent K_m^{uridine} (Ritzel *et al.*, 2001), Q_{max} was reduced by $\sim 50\%$.

Effect of V_h on Presteady-state Currents - The dependence of Q on the holding potential V_h is shown in Figure 4-9. Voltage pulses were performed with two different holding potentials, -30 and -50 mV, in the presence of external Na^+ (100 mM NaCl; pH 8.5), and the charge movement was normalized to maximal charge Q_{max} . The calculated z_d values were -1.50 ± 0.10 and -0.92 ± 0.08 at -30 and -50 mV, respectively, with $V_{0.5}$ values of $+4.50 \pm 3.96$ and $+40.60 \pm 4.45$ mV. In each case, the reversal potential of the charge movement was at the holding potential. There was therefore a decrease in z_d and a shift in $V_{0.5}$ to more positive potentials as the holding potential was made more negative.

Presteady-state Currents in the Absence of Na^+ - Figure 4-10A shows representative total current recordings in an hCNT3-producing oocyte induced by a series of test voltages (V_t from -170 to +90 mV in 20 mV increments) in the absence of external Na^+ (100 mM ChCl; pH 8.5). Presteady-state currents were observed in both the ON current response (Fig. 4-10B; *left current record*) and the OFF current response (Fig. 4-10B;

right current record). The charge-voltage (Q-V) relationship for hCNT3-producing oocytes under this condition is shown in Figure 4-11A (n = 4). The data were normalized to the maximal charge movement in order to compare oocytes with differing levels of expression. The charge movement at the onset of the voltage pulse (Q_{ON}) was found to be equal and opposite to the charge movement at the return to the pre-pulse potential (Q_{OFF}) (Fig. 4-11B). Linear regression analysis yielded a slope of 0.97 ± 0.04 , demonstrating that the system behaves according to conservation of charge in the absence of Na^+ .

Turnover Rate and Number of Transporters - Presteady-state current analysis has allowed the determination of the turnover rate (also known as turnover number) of a number of recombinant transporters expressed in the oocyte plasma membrane (Loo *et al.*, 1993; Panayotova-Heiermann *et al.*, 1995; Wadiche *et al.*, 1995). Linear regression of the steady-state transport current with saturating concentrations of uridine (100 μ M) at -50 mV (I_{max}) versus Q_{max} (calculated for the OFF response) in oocytes with differing levels of transporter expression yielded a straight line with a slope of $17.54 \pm 2.62 \text{ sec}^{-1}$ at a membrane potential of -50 mV, which corresponds to a charge transfer rate (Φ) of $16.14 \pm 3.13 \text{ sec}^{-1}$ (slope $\times z_d = 17.54 \times 0.92$) (Wadiche *et al.*, 1995). The turnover rate of the transporter is given by Φ/ν , where ν is the number of fundamental charges translocated per molecule of uridine at the corresponding potential (Wadiche *et al.*, 1995). As the Na^+ /uridine coupling ratio of hCNT3 is 1.66 ± 0.21 at -50 mV (*Chapter III*), the turnover rate of the transporter, reflecting the number of uridine molecules transported per hCNT3 protein per second, is $9.72 \pm 2.25 \text{ sec}^{-1}$ (Fig. 4-12).

Analysis of charge movements in the absence of uridine also allows estimation of the numbers of transporters (N) present in the oocyte plasma membrane, since $Q_{max} = Ne_0z_d$, where z_d is the magnitude of the charge valence associated with the electric field and e_0 is the elementary charge (Wright *et al.*, 1995; Klamo *et al.*, 1996; Eskandari *et al.*, 1997). Table 4-1 presents transporter numbers determined for 6 representative oocytes. Values were in the range 1.00 - 4.82×10^{10} hCNT3 transporters per oocyte, with a mean (\pm SEM) of $2.37 \times 10^{10} \pm 0.65 \times 10^{10}$.

Kinetics of Presteady-state Currents - The presteady-state currents of hCNT3 decayed exponentially over a range of voltages from -170 to +130 mV. Figure 4-3 shows that in the presence of extracellular Na⁺, two exponential components are required to adequately fit modeled curves to the presteady-state currents. The presteady-state currents of hCNT3 are therefore defined as the sum of two exponential functions ($I(t) = A_1 \exp(-t/\tau_{\text{fast}}) + A_2 \exp(-t/\tau_{\text{slow}})$, where A_1 and A_2 are the amplitudes with time constants τ_{fast} and τ_{slow} , respectively) (Chen *et al.*, 1996). Since the OFF response is always the return of the membrane potential to the holding potential (-50 mV), τ_{fast} and τ_{slow} do not vary. In order to determine the variation of τ_{fast} and τ_{slow} as a function of membrane voltage, the ON current responses were fitted to the sum of two exponentials at all test potentials. The faster component of the presteady-state current relaxation (τ_{fast}) is observed in both the presence and absence of extracellular Na⁺ and therefore must reflect movement of the empty carrier. τ_{fast} decayed with time constants ranging from 2 - 5 msec (ON response; data not shown). The slower component (τ_{slow}) of the presteady-state current relaxation is observed only in the presence of external Na⁺ and therefore must reflect Na⁺ binding/dissociation. τ_{slow} decayed with time constants between 80 - 100 msec (ON response; data not shown). The time constants, plotted as $1/\tau$ curves, which provide an indication of the rate for Na⁺ binding/dissociation and conformational changes of the empty carrier (*Chapter V*), are shown as a function of pulse potential in Figure 4-13. The rate for movement of the empty carrier ($1/\tau_{\text{fast}}$), in the complete absence of Na⁺ (100 mM ChCl; pH 8.5), showed a bell-shaped dependence on voltage (Fig. 4-13A), with the minimum rate occurring at approximately the midpoint of the corresponding Q-V relationship (Fig. 4-11A). With external Na⁺ present (100 mM NaCl; pH 8.5), the slow rate ($1/\tau_{\text{slow}}$) also displayed a voltage-dependence, while the fast rate ($1/\tau_{\text{fast}}$) was not strongly voltage-dependent (Fig. 4-13B). The minimum rate of $1/\tau_{\text{fast}}$ in the presence of external Na⁺ also occurred at approximately the midpoint of the corresponding Q-V curve (Fig. 4-6B). In the OFF response, both τ_{fast} and τ_{slow} were independent of voltage in both 2.5 and 100 mM Na⁺. τ_{fast} and τ_{slow} were equal to 4 - 5 and 15 - 20 msec in 2.5 mM Na⁺, respectively, and 8 - 10 and 94 - 132 msec in 100 mM Na⁺, respectively (Fig. 14-14).

Effect of Na⁺ on the Kinetics of the Presteady-state Currents - The effect of varying the external Na⁺ concentration on the slow time constant (τ_{slow}), plotted as $1/\tau$, was examined for the ON response in Figure 4-15. The Na⁺ concentrations tested were 100, 10, and 2.5 mM. For clarity, the $1/\tau$ curves are shown for 2.5 and 100 mM Na⁺. Similar to the effect of reducing the external Na⁺ concentration on the Q-V relationship, lowering the Na⁺ concentration from 100 to 10 mM (data not shown) and then to 2.5 mM shifted the rate *versus* voltage curve to more negative potentials and, in addition, raised its minimum.

DISCUSSION

In the absence of nucleoside and in response to step-changes in the membrane potential, oocytes producing hCNT3 exhibited slow current relaxations similar to those observed for several other cloned transporters produced in *Xenopus* oocytes, including the Na⁺/glucose cotransporter SGLT1 (Parent *et al.*, 1992a, b; Loo *et al.*, 1993; Chen *et al.*, 1996; Klamo *et al.*, 1996; Mackenzie *et al.*, 1996b; Hazama *et al.*, 1997), the thyroid Na⁺/I⁻ symporter NIS (Eskandari *et al.*, 1997), the oligopeptide transporter hPEPT1 (Mackenzie *et al.*, 1996a; Chen *et al.*, 1999), and the GABA transporter GAT1 (Mager *et al.*, 1993). These slow current relaxations, also known as presteady-state currents, reflect voltage-dependent processes in the cotransport cycle, such as conformational transitions of the empty transporter within the membrane and binding/dissociation of extracellular Na⁺ which has to cross a fraction of the membrane field to reach its binding site. The proposed model for Na⁺/nucleoside cotransport in Figure 4-16A shows the carrier states involved in the generation of the presteady-state currents. Presteady-state currents are used to estimate charge movements within the membrane and rate constants for partial reactions in the translocation cycle.

Several observations, which will be discussed subsequently, provide compelling evidence that the slow current relaxations observed in hCNT3-producing oocytes following voltage steps are indeed presteady-state currents and that these currents are the result of transporter expression. These observations include: (i) the absence of presteady-state currents in control oocytes; (ii) ON-charge movements (Q_{ON}) are equal and opposite to OFF-charge movements (Q_{OFF}); and (iii) presteady-state currents and maximal charge movements (Q_{max}) are reduced by uridine.

In hCNT3-producing oocytes, current relaxations observed during both the ON- and OFF-voltage pulses consist of two components, a fast component due to the oocyte membrane capacitance (Fig. 4-2), followed by a slower decay to a new steady-state. This slow decay, which is the presteady-state current of hCNT3, is not observed in control water-injected oocytes (Fig. 4-4B). Current relaxations following voltage steps are therefore due to expression of the transporter.

Charge movements induced by voltage steps from the holding potential to various test potentials were calculated from the transient current-time integral. Regardless of whether the membrane was stepped to hyperpolarizing or depolarizing potentials, the charge movement at the onset of the voltage pulse (Q_{ON}) was equal and opposite to the charge movement on return to the pre-pulse potential (Q_{OFF}) in both the presence (Fig. 4-7) and absence (Fig. 4-11B) of extracellular Na^+ , demonstrating conservation of charge. The transient relaxations therefore do not represent ionic currents flowing between the extracellular and intracellular compartments (ion permeation through the membrane), but instead represent the movement of charges between the extracellular medium and a point within the membrane field (ion binding/dissociation) or within the membrane (conformational change that moves charge(s) on the transporter within the membrane) (Mager *et al.*, 1993, 1996).

Presteady-state currents of hCNT3 were measured as a function of nucleoside concentrations (Fig. 4-8). Increasing concentrations of uridine reduced the slow current relaxation of hCNT3 (Fig. 4-8A). As a consequence, the maximal charge movement Q_{max} , calculated from Boltzmann fits to the current-time integral, was also reduced (Fig. 4-8B). These results are similar to those seen for other transporters, including the human and rabbit sodium glucose cotransporters hSGLT1 and rbSGLT1, respectively, in which presteady-state currents were blocked by the addition of saturating concentrations of glucose (Loo *et al.*, 1993; Hazama *et al.*, 1997). As the concentration of substrate is increased, there is an increase in the number of transporters partitioned into a non-voltage-dependent state, thus reducing the current relaxations and hence the maximal charge movement during voltage steps (Loo *et al.*, 1993; Nussberger *et al.*, 1997). Reference to the proposed model in Figure 4-16B shows that with both Na^+ and uridine present, the transporter binds substrate, moving it from the extracellular to cytosolic compartments of the membrane, thus reducing the proportion of transporters available for generation of the presteady-state currents.

Presteady-state currents are, in part, the result of Na^+ binding/dissociation to the transporter in response to changes in the membrane potential. Studies of several Na^+ -

and H⁺-coupled cotransporters have indicated that varying the extracellular concentration of the ion shifts the voltage-dependence of the presteady-state current (Loo *et al.*, 1993; Mager *et al.*, 1996; Hazama *et al.*, 1997; Nussberger *et al.*, 1997). Similar results were seen with hCNT3; as the concentration of Na⁺ was reduced, V_{0.5}, the voltage for 50 % Q_{max}, shifted to more hyperpolarized potentials (Fig. 4-6B). This shift in V_{0.5} is due to Na⁺ ions influencing the distribution of charge across the membrane and hence the proportioning of the different conformations of hCNT3 in the membrane (Loo *et al.*, 1993). At low Na⁺ concentrations, hyperpolarizing the membrane is required to generate the same maximal charge movement. In contrast, the maximal charge displacement (Q_{max}) was independent of the Na⁺ concentration; similar Q_{max} values were seen as the concentration of Na⁺ was reduced 10-fold (from 100 to 10 mM external NaCl) (data not shown). These results are similar to those seen with other cotransporters, such as the human glutamate transporter EAAT2 (Wadiche *et al.*, 1995), the potato H⁺/sucrose cotransporter StSUT1 (Boorer *et al.*, 1996), the human thyroid Na⁺/I⁻ symporter NIS (Eskandari *et al.*, 1997), the human intestinal oligopeptide transporter hPEPT1 (Mackenzie *et al.*, 1996a), and the rat GABA transporter GAT1 (Mager *et al.*, 1996), which found that reducing the concentration of the driving ion did not reduce Q_{max}. Q_{max} is therefore independent of the concentration of the driving ion, providing that the driving ion is present (Chen *et al.*, 1999). The reduction in z_d as the concentration of Na⁺ was lowered was similar to results seen with hSGLT1 in which lower z values were reported at reduced Na⁺ concentrations; these observations could not be explained either by the model presented by Chen *et al.* (1999) or that presented by Loo *et al.* (1993).

Conformational transitions of the ligand binding sites of the empty carrier from one side of the plasma membrane to the other also generate presteady-state currents (Parent *et al.*, 1992b; Loo *et al.*, 1993; Loo *et al.*, 1998; Lu and Hilegemann, 1999). Charge movements reflecting transitions of the empty carrier have been measured in oocytes producing the rabbit Na⁺/glucose cotransporter rbSGLT1 and the rat GABA transporter GAT1 under ion-free conditions (Parent *et al.*, 1992b; Hazama *et al.*, 1997; Lu and Hilegemann, 1999). Similarly, oocytes producing hCNT3 demonstrated presteady-state currents in the absence of external Na⁺ in addition to the capacitive transient (Fig. 4-10).

When plotted against voltage, the charge movements, corresponding to the integrals of the transient currents, were described by the Boltzmann function (Fig. 4-11A). The lack of effect of Na^+ concentration on Q_{max} , and the demonstration of presteady-state currents in the total absence of Na^+ suggests that charge movements are mostly due to movement of empty carrier in the membrane, while the effect of Na^+ concentration on $V_{0.5}$ (Fig. 4-6B) suggests that a secondary component of presteady-state current is due to Na^+ binding/dissociation from the transporter (Loo *et al.*, 1993).

Altering the external Na^+ concentration allows a determination of the fraction of the membrane field sensed by Na^+ and the valence of the movable charge. The observed effect of reducing the external Na^+ concentration on $V_{0.5}$ implies binding of sodium to site(s) that traverse 65.40 ± 4.10 % of the membrane electric field. Na^+ therefore binds to a site on the transporter that is ~ 35 % into the membrane bilayer. The valence of the moveable charge calculated from the Boltzmann parameters for 100 mM external Na^+ was equal to -1.42. Since two external Na^+ ions cross the membrane field during a complete cotransport cycle, as determined by the Na^+ /nucleoside coupling ratio of 2:1 (Ritzel *et al.*, 2001; *Chapter III*), this valence is consistent with the theoretical predicted valence of -2.

The number of hCNT3 transporters present in the oocyte plasma membrane and the turnover rate (turnover number) of the transporter may be estimated from the Boltzmann parameters of the charge movements (Mager *et al.*, 1993). The Q_{max} value is an index of the transporter density in the plasma membrane and is used to determine the number of transporters expressed in the plasma membrane through the equation $Q_{\text{max}} = Ne_0Z_d$ (Wright *et al.*, 1995; Klamo *et al.*, 1996; Eskandari *et al.*, 1997). By this approach, it was determined that the number of hCNT3 transporters present in the oocyte plasma membrane corresponded to $\sim 10^{10}$ copies per cell (Table 4-1). This value is within the range determined for other cotransporters: transporter numbers of 10^9 per oocyte have been reported for the human EAAT2 glutamate transporter (Wadiche *et al.*, 1995), 10^{10} for the human thyroid Na^+/I^- symporter NIS (Eskandari *et al.*, 1997), 10^{11} for the human intestinal H^+ coupled oligopeptide transporter hPEPT1 (Mackenzie *et al.*, 1996a), and

10^{12} for the rabbit Na^+ /glucose transporter rbSGLT1 (Wright *et al.*, 1994). The turnover rate (turnover number) of the transporter, which represents the number of transport events catalyzed by an individual transporter per unit time(s), may be estimated from the ratio of the uridine-evoked steady-state current (I_{max}) and the charge movement for the same individual oocyte (Q_{max}) (Wadiche *et al.*, 1995; Wright *et al.*, 1995; Klamo *et al.*, 1996; Eskandari *et al.*, 1997). For hCNT3, the number of uridine molecules transported per hCNT3 protein per second was ~ 9.72 at -50 mV, and is similar to that seen for other cotransporters such as the rat γ -amino-butyric acid transporter (GABA) GAT1 ($6 - 13 \text{ sec}^{-1}$) (Mager *et al.*, 1993) and rbSGLT1 (25 sec^{-1}) (Panayotova-Heiermann *et al.*, 1994) (Fig. 4-12).

The presteady-state currents of hCNT3 may be fitted by the sum of two exponential functions, giving a fast time constant (τ_{fast}) and a slow time constant (τ_{slow}). Since τ_{fast} is observed in both the presence and absence of extracellular Na^+ , it is likely that this fast time constant arises from movement of empty hCNT3 binding sites within the membrane field in response to voltage pulses, while the slow time constant (τ_{slow}), which is observed only in the presence of external Na^+ , is due to Na^+ binding/dissociation from the carrier. These results are similar to those seen with the rat GABA transporter GAT1; slow charge movements ($\tau \sim 100$ msec) are observed in the presence of extracellular Na^+ , while fast charge movements ($\tau < 10$ msec) are observed in the absence of Na^+ (Mager *et al.*, 1993, 1996; Lu and Hilgemann, 1999). The slow and fast charge movements were attributed to Na^+ binding and to movement of empty GAT1 binding sites, respectively (Mager *et al.*, 1996; Lu and Hilgemann, 1999). In the millimolar concentration range, rates of association of Na^+ with binding sites on the surface of a protein are generally less than microseconds (Mager *et al.*, 1993). The kinetics of charge movements associated with hCNT3 and GAT1 in external Na^+ occur on a time scale of ~ 100 msec (t_{slow}), suggesting that Na^+ binds to a presumed relatively inaccessible site within the membrane field (Mager *et al.*, 1993). $1/\tau$ curves for both movement of the empty transporter and Na^+ binding/dissociation for hCNT3 display a minimum with voltage which occurs at the midpoint of the charge-voltage curve (Fig. 4-13), similar to results seen with the GAT1

transporter (Mager *et al.*, 1996; Fesce *et al.*, 2002). The mathematical relationship between the time constants and the rate constants is discussed in *Chapter V*.

In conclusion, the transient currents observed in oocytes producing the human Na⁺/nucleoside cotransporter hCNT3 in response to step changes in the membrane potential are due to charge transfer by hCNT3. These charge movements are consistent with Na⁺ binding/dissociation from the transporter and conformational changes of the empty transporter within the membrane field. The fast time constant is likely to result from conformational transitions of the empty transporter, while the slow time constant is likely to result from Na⁺ binding/dissociation. This is the first time that information has been obtained concerning individual steps within the CNT translocation cycle.

Oocyte	Number of Transporters
1	4.82×10^{10}
2	3.58×10^{10}
3	1.47×10^{10}
4	1.54×10^{10}
5	1.02×10^{10}
6	1.00×10^{10}

Table 4-1. Numbers of Recombinant hCNT3 Transporters Present in the Oocyte Plasma Membrane. Maximum charge movement in the absence of uridine allows estimation of the number of hCNT3 transporters at the cell surface. Values for 6 individual representative oocytes are presented.

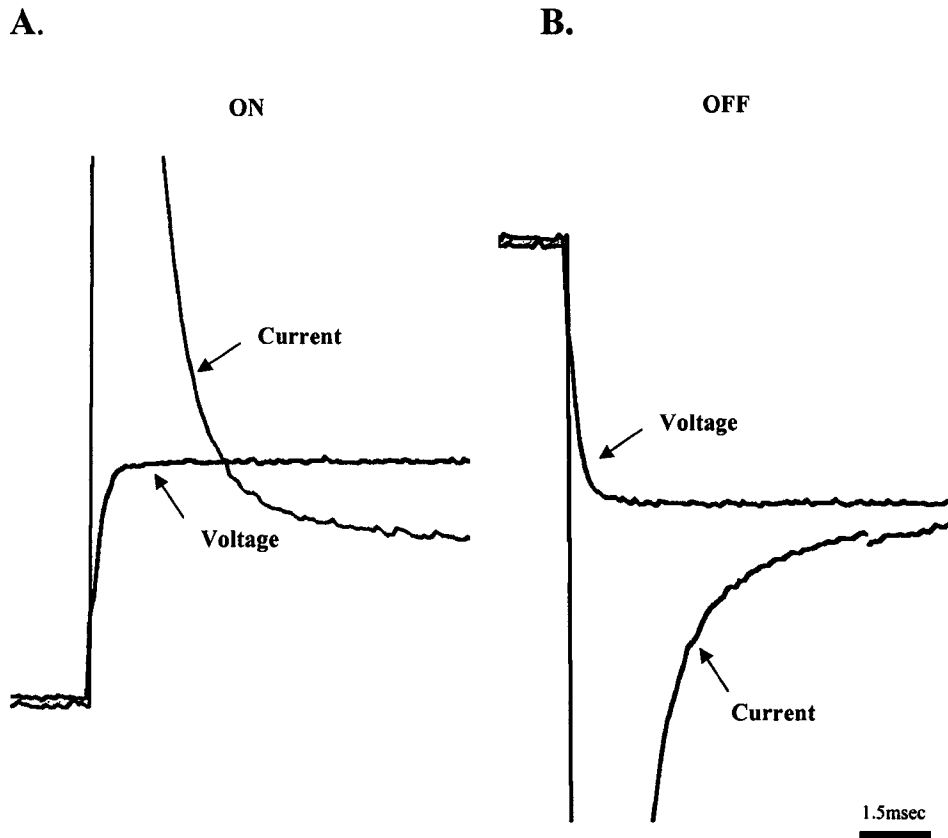


Figure 4-1. Time course of current and voltage records. Presteady-state current and voltage pulse for the ON response (A) when V_h was stepped to V_t and for the OFF response (B) when V_t was stepped back to V_h . The rise-time of the voltage clamp was $\sim 500 \mu\text{sec}$ in this experiment, which was performed with a representative hCNT3-producing oocyte.

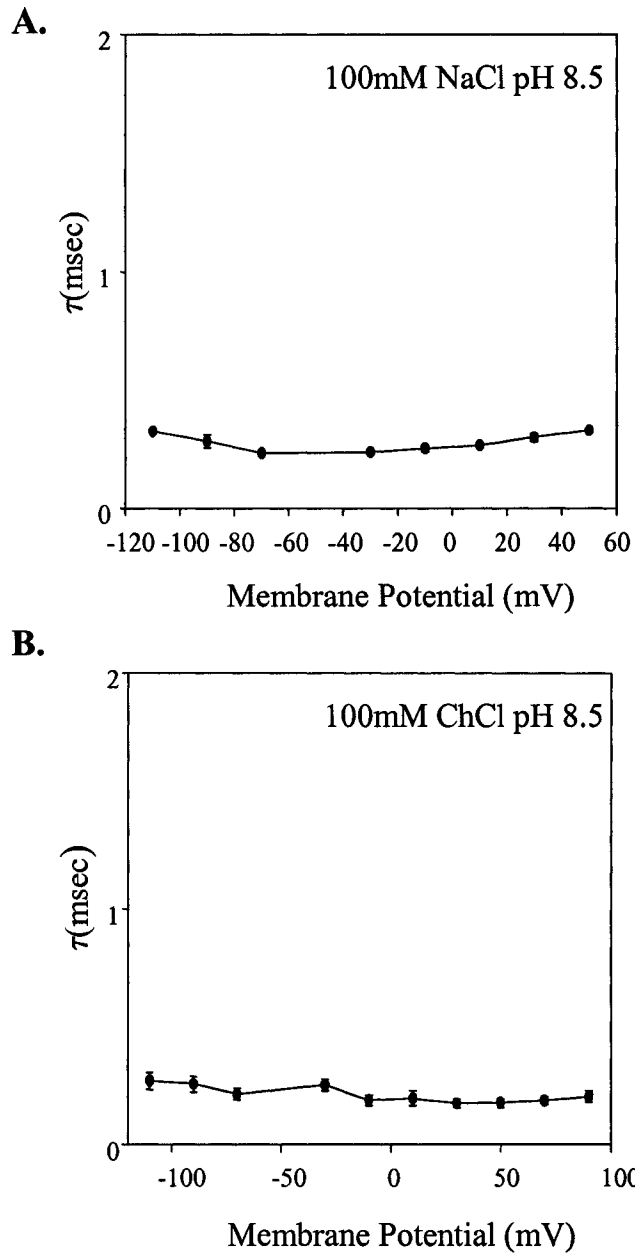
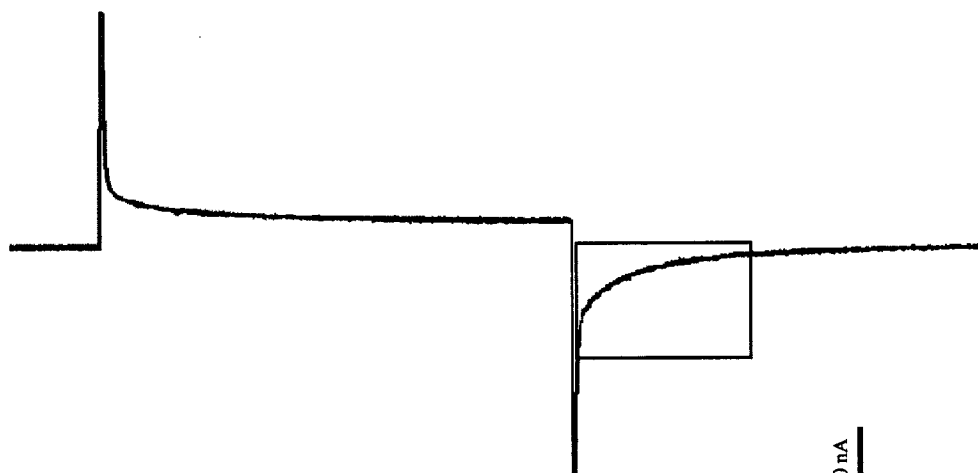


Figure 4-2. Time constants of *Xenopus* oocyte capacitive transients. The time constant for the oocyte membrane capacitance was measured in the presence (A; 100 mM NaCl; pH 8.5; n = 4) and absence (B; 100 mM ChCl; pH 8.5; n = 4) of external Na⁺ in hCNT3-producing oocytes.

A.



B.

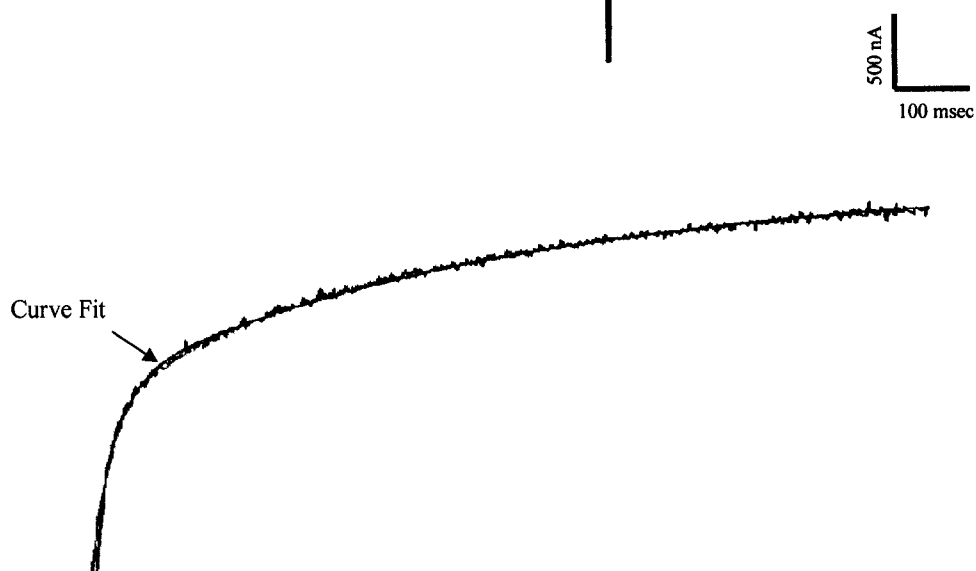


Figure 4-3. hCNT3 presteady-state curve fits. A. Representative current recording for an hCNT3-producing oocyte following a voltage pulse from $V_h = -50$ mV to $V_t = +90$ mV. Current relaxation for the OFF response (enclosed in the *solid box*) and the corresponding two-exponential fit are shown in B. The correlation coefficient of the fit was 0.965.

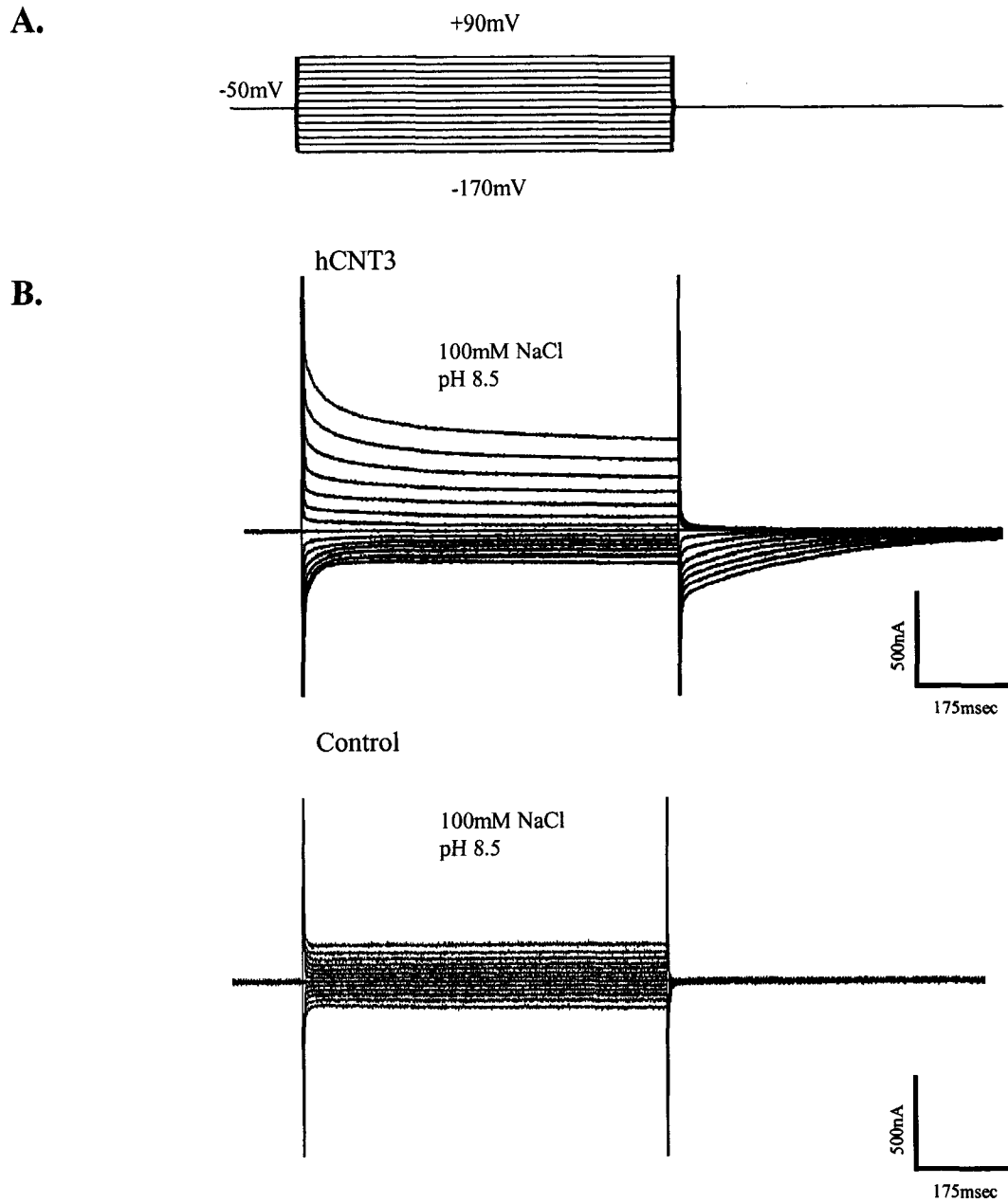
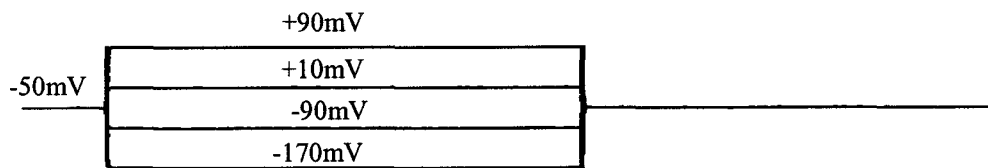


Figure 4-4. hCNT3 presteady-state currents elicited by voltage pulses. **A.** Voltage pulse protocol. The oocyte membrane was held at a holding potential (V_h) of -50 mV and stepped to a range of test potentials (V_t) between -170 and +90 mV in 20 mV increments. **B.** Representative membrane current records. An hCNT3-producing oocyte in Na^+ -containing transport medium (100 mM NaCl; pH 8.5) (*top current record*) displays slow current relaxations in response to voltage pulses not seen in a control water-injected oocyte (*bottom current record*).

A.



B.

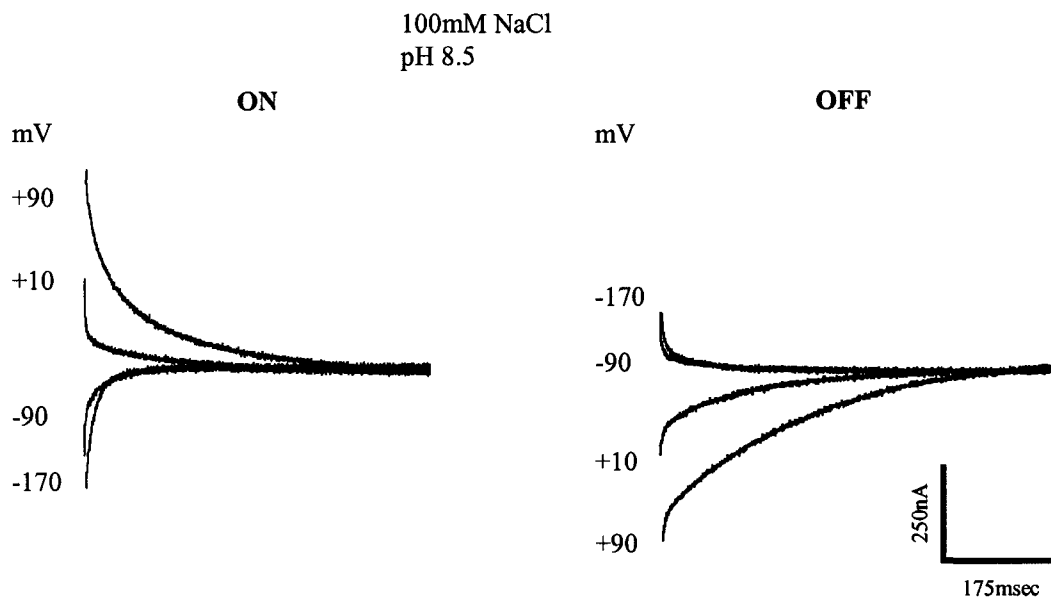


Figure 4-5. hCNT3 ON and OFF current relaxations. For clarity, presteady-state currents for the ON and OFF voltage steps are shown at four different test potentials only ($V_t = -170, -90, +10, \text{ and } +90 \text{ mV}$). The presteady-state current has been isolated from the oocyte capacitive current and steady-state (leak) currents. hCNT3 presteady-state currents are shown 1.5 msec after the onset of the voltage pulse. **A.** Voltage pulse protocol. **B.** Transient currents for the ON response when V_h was stepped to V_t (*left current record*) and for the OFF response when V_t was stepped back to V_h (*right current record*) in a representative hCNT3-producing oocyte in Na^+ transport medium (100 mM NaCl; pH 8.5).

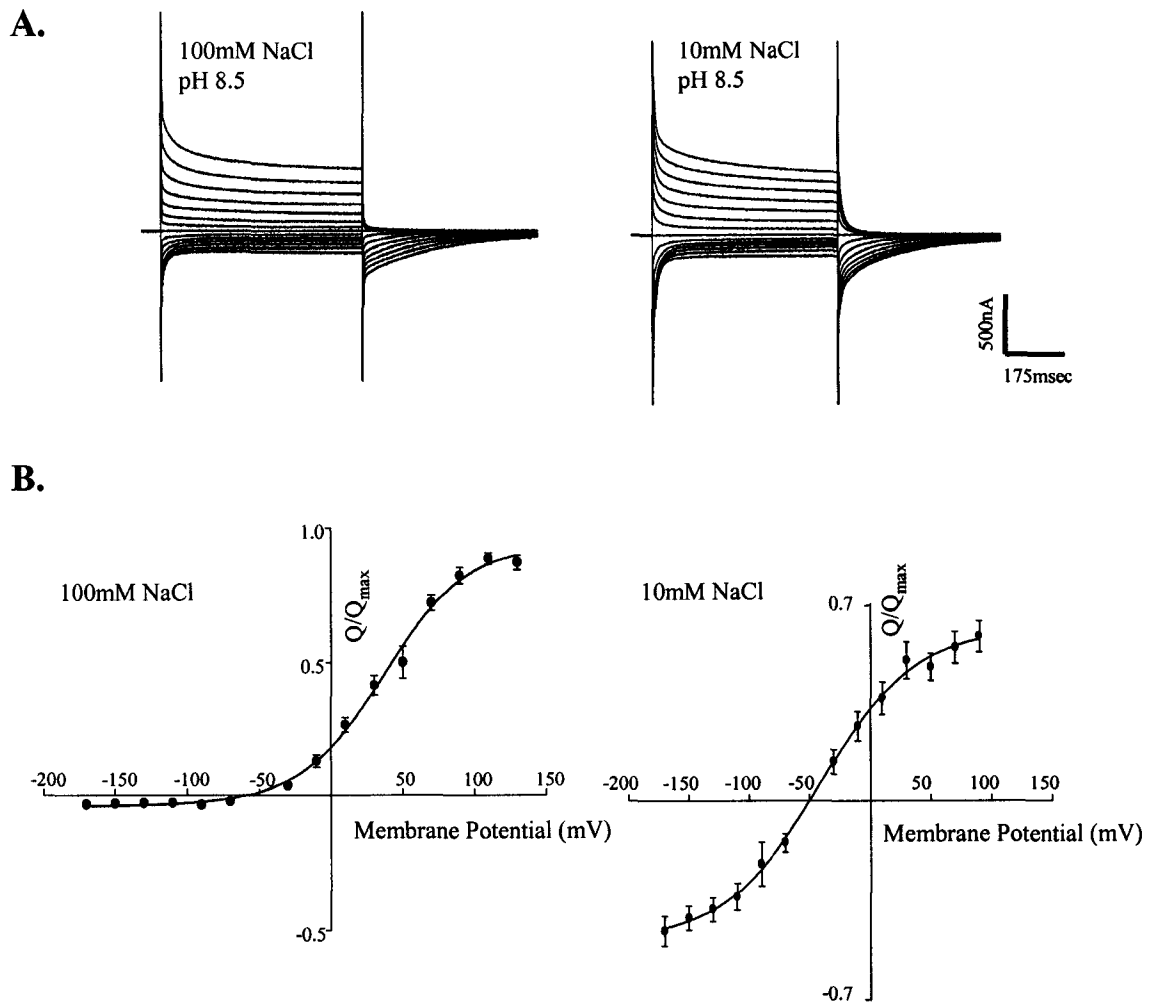


Figure 4-6. Dependence of hCNT3 presteady-state currents on external Na⁺. **A.** Membrane current records. A representative hCNT3-producing oocyte displays slow current relaxations in response to voltage pulses in both 100 mM NaCl (pH 8.5) (*left current record*) and 10 mM NaCl (pH 8.5) transport media (*right current record*). **B.** Q-V plots for hCNT3-producing oocytes in the presence of 100 and 10 mM external Na⁺ (pH 8.5). The data were fitted to the Boltzmann equation: $Q(V_t) = Q_{hyp}/(Q_{max}[1+\exp((V_t - V_{0.5})z_dF/RT)])$. Charge movements at each V_t were normalized to the maximal charge, and each point is the mean \pm SEM of n different oocytes (n = 4, 100 mM NaCl; n = 3, 10 mM NaCl).

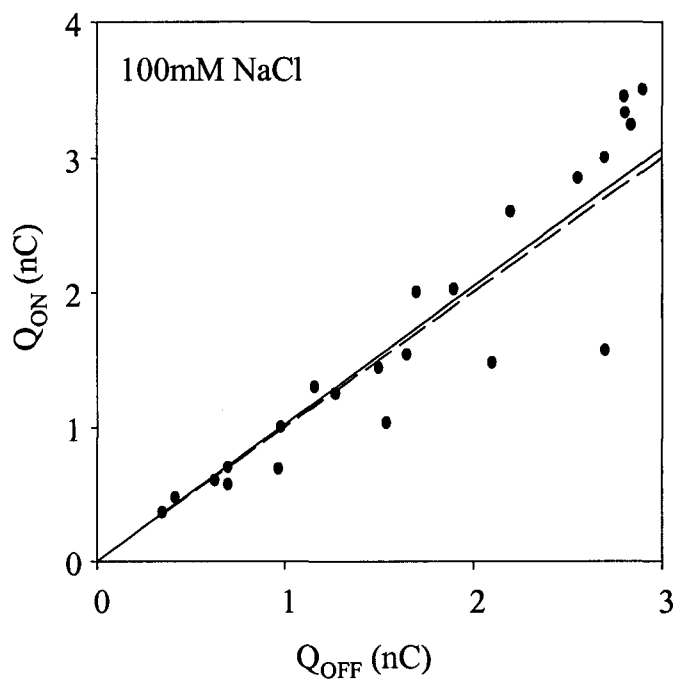


Figure 4-7. Relationship between hCNT3 ON and OFF charge movements. Correlation between charge movements in an hCNT3-producing oocyte (100 mM NaCl; pH 8.5) obtained from the time integral of transient currents following command pulses to a range of V_t between -170 and +90 mV and charge movements following return to V_h (-50 mV). Linear regression analysis of the data gave a slope (\pm SE) of 1.02 ± 0.09 (*solid line*) compared to a reference slope of unity (*broken line*).

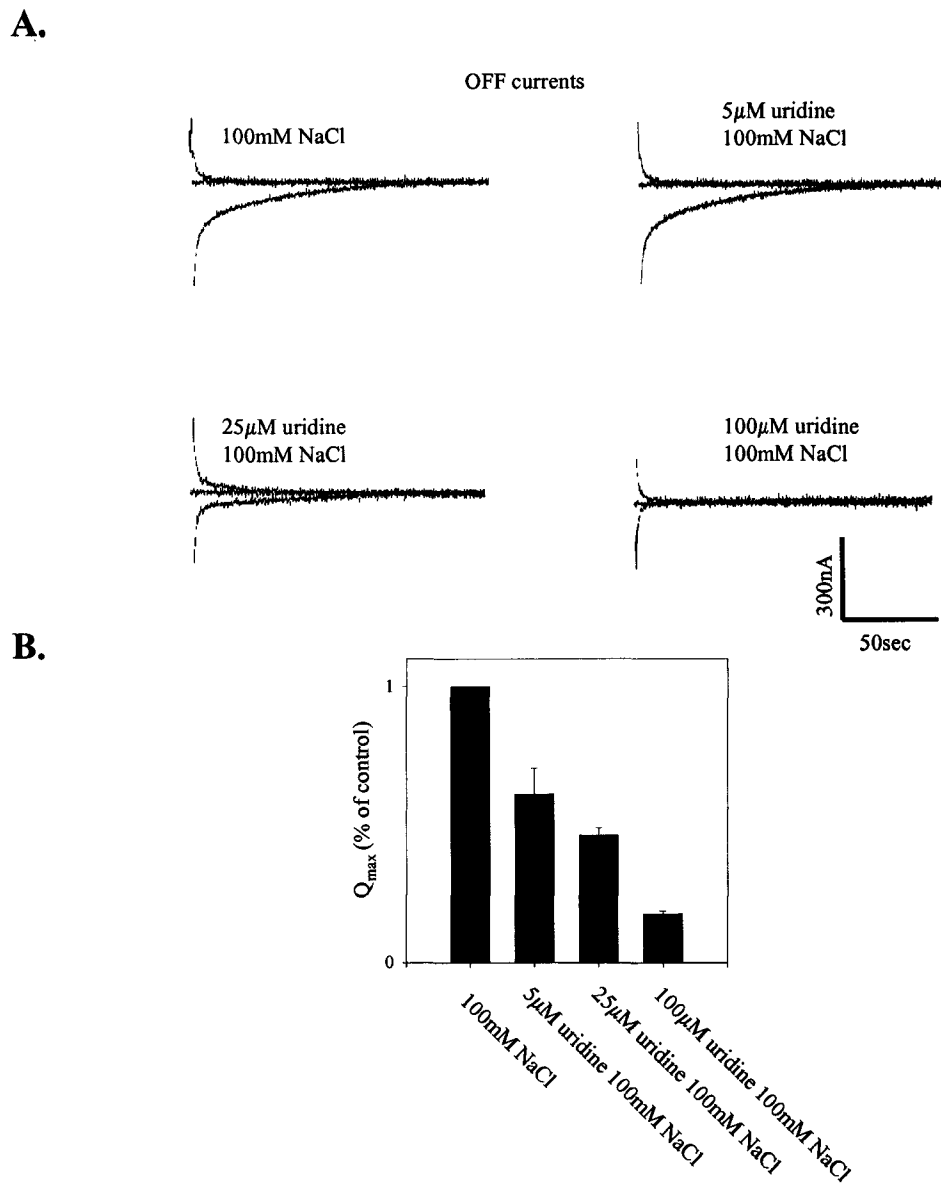


Figure 4-8. Effect of uridine on hCNT3 presteady-state currents. **A.** Representative presteady-state current records for the OFF response in an hCNT3-producing oocyte (100 mM NaCl; pH 8.5) when V_t was returned to V_h in the presence of 0 - 100 μ M uridine. The presteady-state currents have been isolated from the capacitive currents and the steady-state (leak) currents. **B.** Maximal charge moved (Q_{max}) as a function of uridine concentration. The charge movement with uridine present is plotted as a percentage of the charge movement with 100 mM NaCl present (control). Each bar represents the average charge (\pm SEM) of 4 different oocytes.

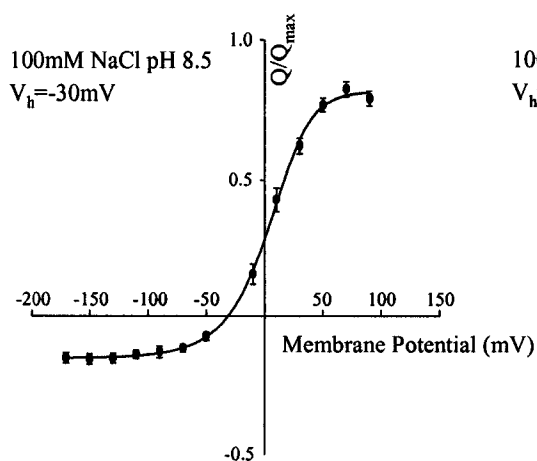
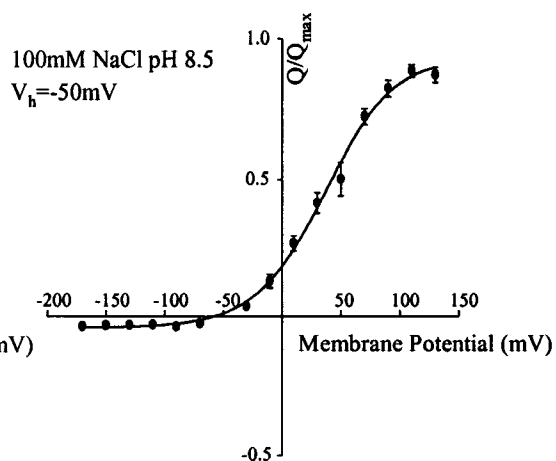
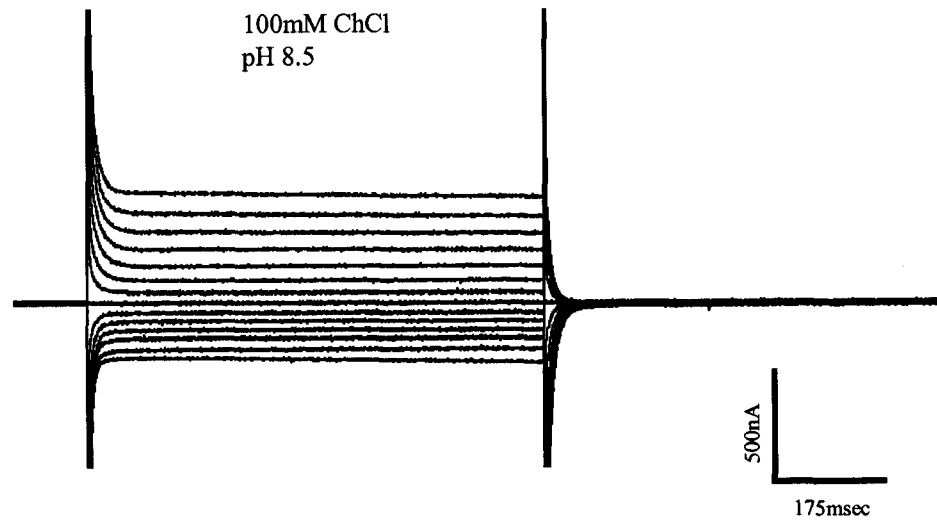
A.**B.**

Figure 4-9. Effect of holding potential on hCNT3 charge movements. Q-V plots for hCNT3-producing oocytes in the presence of external Na^+ (100 mM NaCl; pH 8.5) at holding potentials of -30 mV (A) and -50 mV (B). Charge movements at each V_t have been normalized to the maximal charge, and each point represents the mean (\pm SEM) of 3 different oocytes.

A.



B.

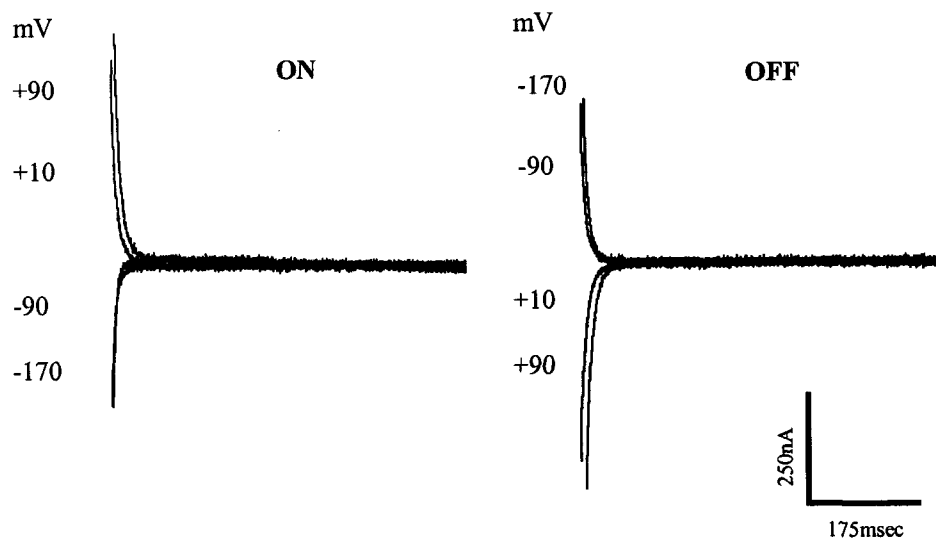
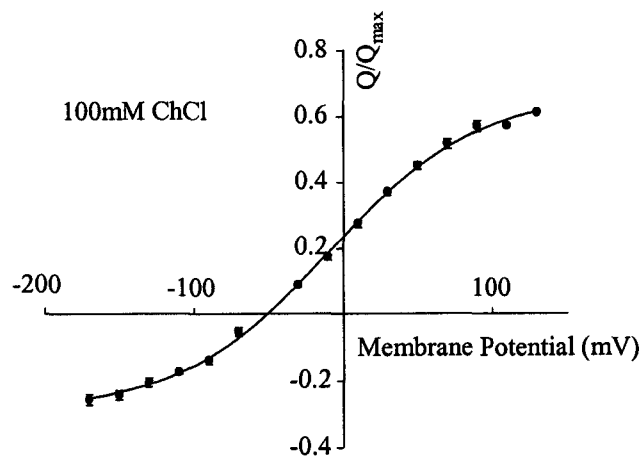


Figure 4-10. Charge movement of the hCNT3 empty carrier. A. Membrane current records. Presteady-state currents were measured in a representative hCNT3-producing oocyte in the absence of extracellular Na^+ (100 mM ChCl; pH 8.5). B. For clarity, transient currents for the ON (*left current record*) and OFF (*right current record*) responses are shown at four different test potentials only ($V_t = -170, -90, +10, \text{ and } +90$ mV).

A.



B.

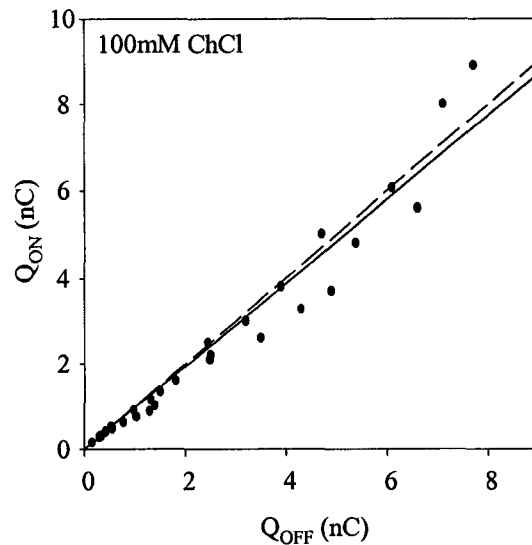


Figure 4-11. Analysis of hCNT3 charge movements due to the empty carrier.
A. Q-V plot for hCNT3-producing oocytes in the absence of external Na^+ (100 mM ChCl; pH 8.5). The data were fitted to the Boltzmann equation. Charge movements at each V_t were normalized to the maximal charge, and each point represents the mean (\pm SEM) of 4 different oocytes. **B.** Correlation between charge movements the absence of external Na^+ (100 mM ChCl; pH 8.5) obtained from the time integral of transient currents following command pulses to a range of V_t between -170 and +90 mV and charge movements following return to the holding potential ($V_h = -50$ mV). Linear regression analysis of the data gave a slope (\pm SE) of 0.97 ± 0.04 (*solid line*) compared to a reference slope of unity (*broken line*).

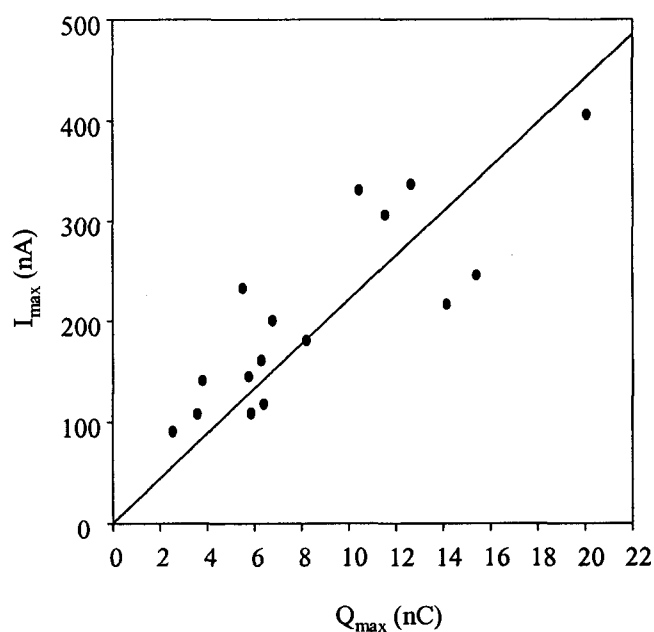


Figure 4-12. Turnover rate of recombinant hCNT3. Charge movements during voltage steps from $V_h = -50$ mV to V_t ranging from -170 to +150 mV (40 mV increments) were correlated with transporter expression level as determined by steady-state currents induced by 100 μ M uridine superfusion at $V_h = -50$ mV. Linear regression analysis of results for 16 individual oocytes gave a slope of $17.54 \pm 2.62 \text{ sec}^{-1}$ (*solid line*), corresponding to a turnover rate for the transporter of $9.72 \pm 2.25 \text{ sec}^{-1}$.

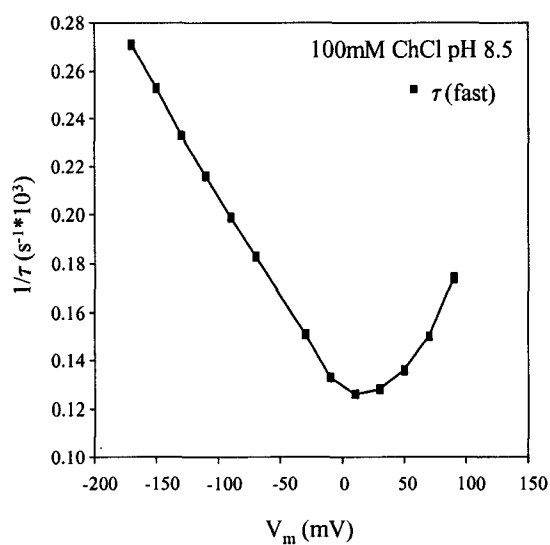
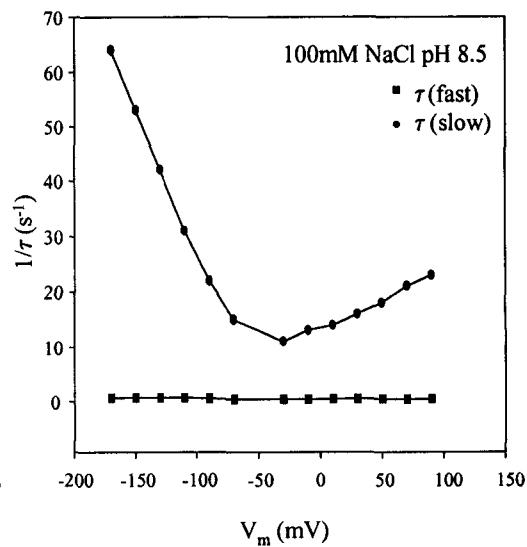
A.**B.**

Figure 4-13. Kinetics of hCNT3 current relaxations. Voltage-dependence of hCNT3 charge movement rates for the ON response in the absence (A) and presence (B) of external Na^+ (100 mM ChCl (pH 8.5) and 100 mM NaCl (pH 8.5) transport media, respectively). Results in the absence and presence of Na^+ are from the same representative hCNT3-producing oocyte.

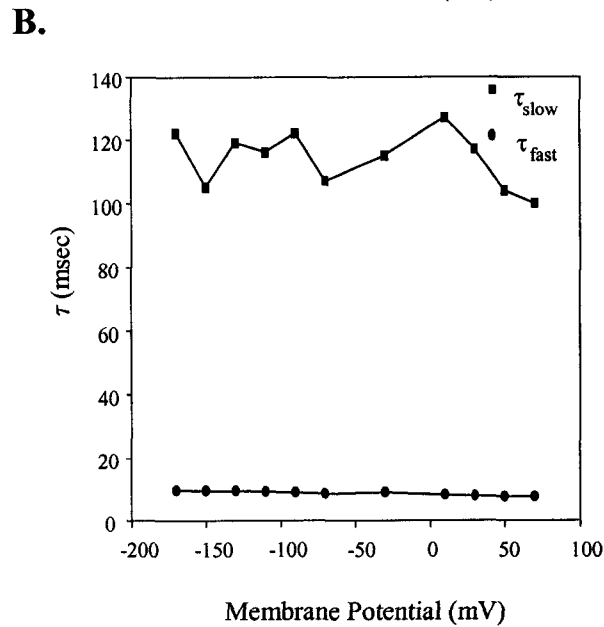
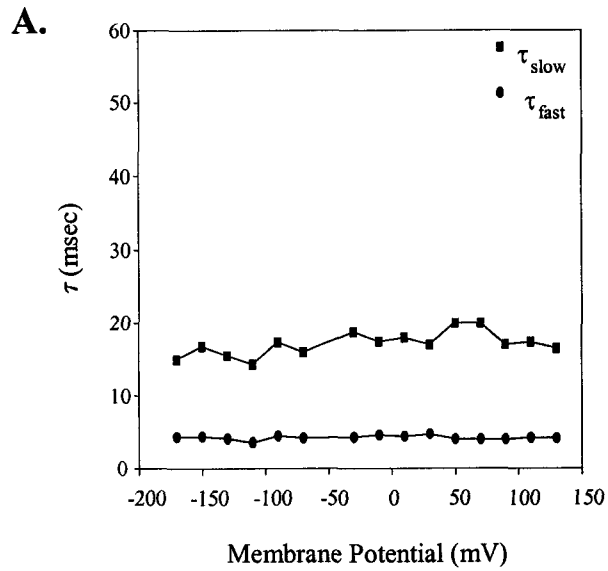


Figure 4-14. hCNT3 time constants for the OFF response. Relaxation OFF currents in Na⁺-containing media (NaCl; pH 8.5) were described by a slow time constant (τ_{slow}) and a fast time constant (τ_{fast}). **A.** Time constants in the presence of 2.5 mM extracellular Na⁺. **B.** Time constants in the presence of 100 mM extracellular Na⁺. Different hCNT3-producing oocytes were used in the two experiments.

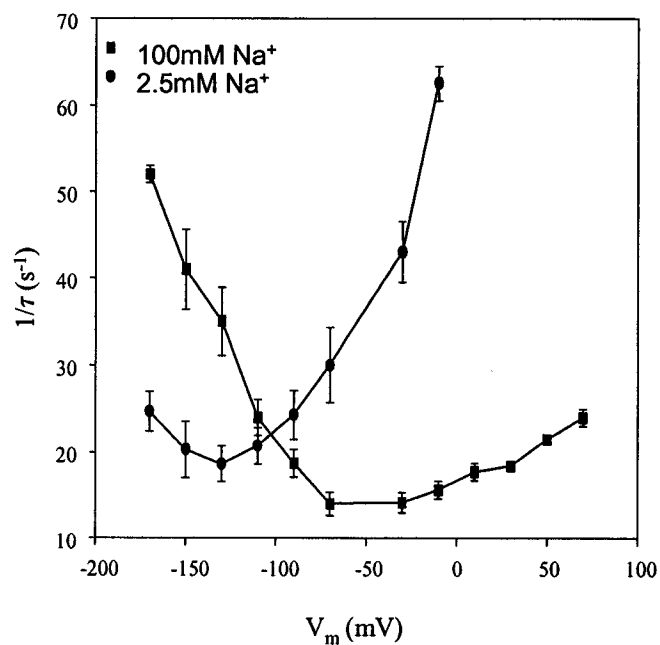


Figure 4-15. Na⁺-dependence of hCNT3 current relaxation kinetics. Na⁺-dependence of charge movement rates for the ON response. Kinetics of voltage pulse relaxations are shown for two different Na⁺ concentrations (2.5 and 100 mM NaCl; pH 8.5). Each point represents the mean (\pm SEM) for three different oocytes.

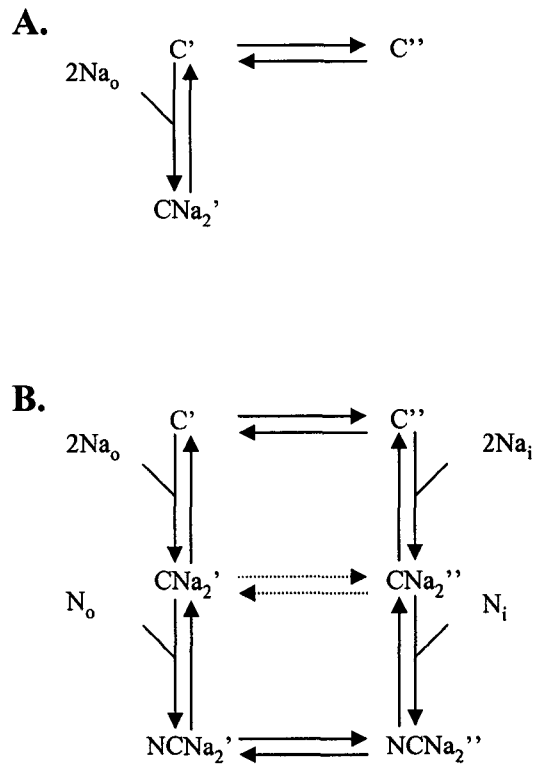


Figure 4-16. Proposed transport model for hCNT3 Na⁺/nucleoside cotransport. The carrier (C) possesses 2 binding sites for the driving ion Na⁺ and one binding site for the nucleoside (N). The carrier can face the outer (C') or inner (C'') face of the membrane. **A.** Progression of the transporter through carrier stages following step-changes in the membrane potential, yielding presteady-state currents. **B.** Na⁺/nucleoside cotransport by hCNT3.

Bibliography

Acimovic Y and Coe IR. Molecular evolution of the equilibrative nucleoside transporter family: identification of novel family members in prokaryotes and eukaryotes. *Mol Biol Evol* 19(12): 2199-2210, 2002.

Armstrong CM and Bezanilla F. Currents related to the movement of the gating particles of the sodium channels. *Nature* 242: 456-461, 1973.

Boorer KJ, Loo DDF, Frommer WB, and Wright EM. Transport mechanism of the cloned potato H⁺/sucrose cotransporter StSUT1. *J Biol Chem* 271(41): 25139-25144, 1996.

Burckhardt B-C, Kroll B, and Frömter E. Proton transport mechanism in the cell membrane. *Pflügers Arch* 420: 78-82, 1992.

Cass CE. In: Drug transport in antimicrobial and anticancer chemotherapy, edited by Georgopapadakou NH. New York: Marcel Dekker, 1995.

Che M, Ortiz DF, and Arias IM. Primary structure and functional expression of a cDNA encoding the bile canalicular, purine-specific Na⁺ nucleoside cotransporter. *J Biol Chem* 270: 13596-13599, 1995.

Chen X-Z, Coady MJ, and Lapointe JY. Fast voltage clamp discloses a new component of presteady-state currents from the Na(+)-glucose cotransporter. *Biophys J* 71(5): 2544-2552, 1996.

Chen X-Z, Zhu T, Smith DE, and Hediger MA. Stoichiometry and kinetics of the high-affinity H⁺-coupled peptide transporter PepT2. *J Biol Chem* 274(5): 2773-2779, 1999.

Craig JE, Zhang Y, and Gallagher MP. Cloning of the nupC gene of *Escherichia coli* encoding a nucleoside transport system, and identification of an adjacent insertion element, IS 186. *Mol Microbiol* 11(6): 1159-1168, 1997.

Crawford CR, Patel DH, Naeve C, and Belt JA. Cloning of the human equilibrative, nitrobenzylmercaptapurine riboside (NBMPR)-insensitive nucleoside transporter *ei* by functional expression in a transport-deficient cell line. *J Biol Chem* 273(9): 5288-5293, 1998.

Eskandari S, Loo DD, Dai G, Levy O, Wright EM, and Carrasco N. Thyroid Na⁺/I⁻ symporter. Mechanism, stoichiometry, and specificity. *J Biol Chem* 272(43): 27230-27238, 1997.

Fesce R, Giovannardi S, Bidna F, Bossi E, and Peres A. The relation between charge movement and transport-associated currents in the rat GABA cotransporter rGAT1. *J Physiol* 545(3): 739-750, 2002.

Galli A, DeFelice LJ, Duke BJ, Moore KR, and Blakely RD. Sodium-dependent norepinephrine-induced currents in norepinephrine-transporter-transfected HEK-293 cells blocked by cocaine and antidepressants. *J Exp Biol* 198: 2197-2212, 1995.

Griffiths DA and Jarvis SM. Nucleoside and nucleobase transport systems of mammalian cells. *Biochim Biophys Acta* 1286: 153-181, 1996.

Hazama A, Loo DDF, and Wright EM. Presteady-state currents of the rabbit Na⁺/glucose cotransporter (SGLT1). *J Membr Biol* 155: 175-186, 1997.

Huang Q-Q, Yao SYM, Ritzel MWL, Paterson ARP, Cass CE, and Young JD. Cloning and functional expression of a complementary DNA encoding a mammalian nucleoside transport protein. *J Biol Chem* 269: 17757-17760, 1994.

Hyde RJ, Cass CE, Young JD, and Baldwin SA. The ENT family of eukaryote nucleoside and nucleobase transporters: recent advances in the investigation of structure/function relationships and the identification of novel isoforms. *Mol Membr Biol* 18: 53-63, 2001.

Klamo EM, Drew ME, Landfear SM, and Kavanaugh MP. Kinetics and stoichiometry of a proton/*myo*-inositol cotransporter. *J Biol Chem* 271(25): 14937-14943, 1996.

Loewen SK, Ng AML, Yao SYM, Cass CE, Baldwin SA, and Young JD. Identification of amino acid residues responsible for the pyrimidine and purine nucleoside specificities of human concentrative Na⁺ nucleoside cotransporters hCNT1 and hCNT2. *J Biol Chem* 274 (35): 24475-24484, 1999.

Loewen SK, Ng AML, Mohabir NN, Baldwin SA, Cass CE, and Young JD. Functional characterization of a H⁺/nucleoside cotransporter (CaCNT) from *Candida albicans*, the first fungal homolog of mammalian/bacterial concentrative nucleoside transporters. *Yeast* 2003 (*in press*).

Loo DDF, Hazama A, Supplisson S, Turk E, and Wright EM. Relaxation kinetics of the Na⁺/glucose cotransporter. *Proc Natl Acad Sci* 90: 5767-5771, 1993.

Loo DDF, Hirayama BA, Gallardo EM, Lam JT, Turk E, and Wright EM. Conformational changes couple Na⁺ and glucose transport. *Proc Natl Acad Sci* 95: 7789-7794, 1998.

Lu C-C and Hilegemann DW. GAT1 (GABA: Na⁺:Cl⁻) cotransport function. Kinetic studies in giant *Xenopus* oocyte membrane patches. *J Gen Physiol* 114: 445-447; 1999.

Mackenzie B, Loo DDF, Fei Y-J, Liu W, Ganapathy V, Leibach FH, and Wright EM. Mechanisms of the human intestinal H⁺-coupled oligopeptide transporter hPEPT1. *J Biol Chem* 271(10): 5430-5437, 1996a.

Mackenzie B, Loo DDF, Panayotova-Heiermann M, and Wright EM. Biophysical characteristics of the pig kidney Na⁺/glucose cotransporter SGLT2 reveal a common mechanism for SGLT1 and SGLT2. *J Biol Chem* 271(51): 32678-32683, 1996b.

Mager S, Naeve J, Quick M, Labarca C, Davidson N, and Lester HA. Steady states, charge movements, and rates for a cloned GABA transporter expressed in *Xenopus* oocytes. *Neuron* 10: 177-188, 1993.

Mager S, Kleinberger-Doron N, Kehset GI, Davidson N, Kanner BI, and Lester HA. Ion binding and permeation at the GABA transporter GAT1. *J Neurosci* 16(17): 5405-5414, 1996.

Mager S, Cao Y, and Lester HA. Measurement of transient currents from neurotransmitter transporters expressed in *Xenopus* oocytes. *Methods Enzymol* 296: 551-566, 1998.

Nelder JA and Mead R. A simplex method for function minimization. *Comput J* 7: 308-313, 1965.

Nussberger S, Steel A, Trotti D, Romero MF, Boron WF, and Hediger MA. Symmetry of H⁺ binding to the intra- and extracellular side of the H⁺-coupled oligopeptide cotransporters PepT1. *J Biol Chem* 272(12): 7777-7785, 1997.

Panayotova-Heiermann M, Loo DDF, Lostao MP, and Wright EM. Sodium/D-glucose cotransporter charge movements involve polar residues. *J Biol Chem* 269(33): 21016-21020, 1994.

Panayotova-Heiermann M, Loo DDF, and Wright EM. Kinetics of steady-state currents and charge movements associated with the rat Na⁺/glucose cotransporters. *J Biol Chem* 270(45): 27099-27105, 1995.

Parent L, Supplisson S, Loo DF, and Wright EM. Electrogenic properties of the cloned Na⁺/glucose cotransporter: Part I. Voltage-clamp studies. *J Membr Biol* 125: 49-62, 1992a.

Parent L, Supplisson S, Loo DF, and Wright EM. Electrogenic properties of the cloned Na⁺/glucose cotransporter: Part II. A transport model under non-rapid equilibrium conditions. *J Membr Biol* 125: 63-79, 1992b.

Ritzel MWL, Yao SYM, Huang M-Y, Elliot JF, Cass CE, and Young JD. Molecular cloning and functional expression of cDNAs encoding a human Na⁺-nucleoside cotransporter (hCNT1). *Am J Physiol Cell Physiol* 272: C707-C714, 1997.

Ritzel MWL, Yao SYM, Ng AML, Mackey JR, Cass CE, and Young JD. Molecular cloning, functional expression and chromosomal localization of a cDNA encoding a human Na⁺/nucleoside cotransporter (hCNT2) selective for purine nucleosides and uridine. *Mol Membr Biol* 15(4): 203-211, 1998.

Ritzel MWL, Ng AML, Yao SYM, Graham K, Loewen SK, Smith KM, Ritzel RG, Mowles DA, Carpenter P, Chen X-Z, Karpinski E, Hyde RF, Baldwin SA, Cass CE, and Young JD. Molecular identification and characterization of novel human and mouse concentrative Na⁺-nucleoside cotransporter proteins (hCNT3 and mCNT3) broadly selective for purine and pyrimidine nucleosides (system *cib*). *J Biol Chem* 276: 2914-2927, 2001.

Wadiche JI, Arriza JL, Amara SG, and Kavanaugh MP. Kinetics of a human glutamate transporter. *Neuron* 14: 1019-1027, 1995.

Wang J, Su S-F, Dresser MJ, Schaner ME, Washington CB, and Giacomini KM. Na⁺-dependent purine nucleoside transporter from human kidney: cloning and functional characterization. *Am J Physiol Renal Physiol* 273(42): F1058-F1065, 1997.

Wright EM, Loo DF, Panayotova-Heiermann, Lostao MP, Hirayama BH, Mackenzie B, Boorer K, and Zampighi G. 'Active' sugar transport in eukaryotes. *J Exp Biol* 196: 197-212, 1994.

Wright EM, Loo M, Panayotova-Heiermann M, and Boorer KJ. Mechanisms of Na⁺-glucose cotransport. *Biochem Soc Trans* 22: 646-650, 1995.

Xiao G, Wang J, Tangen T, and Giacomini KM. A novel proton-dependent nucleoside transporter, CeCNT3 from *Caenorhabditis elegans*. *Mol Pharmacol* 59: 339-348, 2001.

Yao SYM, Ng AML, Ritzel MWL, Gati WP, Cass CE, and Young JD. Transport of adenosine by recombinant purine- and pyrimidine-selective sodium/nucleoside cotransporters from rat jejunum expressed in *Xenopus laevis* oocytes. *Mol Pharmacol* 50: 1529-1535, 1996.

Yao SYM, Ng AML, Muzyka WR, Griffiths M, Cass CE, Baldwin SA, and Young JD. Molecular cloning and functional characterization of nitrobenzylthioinosine (NBMPR)-sensitive (*es*) and NBMPR-insensitive (*ei*) equilibrative nucleoside transporter proteins (rENT1 and rENT2) from rat tissues. *J Biol Chem* 272: 28423-28430, 1997.

Yao SYM, Ng AML, Loewen SK, Cass CE, Baldwin SA, and Young JD. An ancient prevertebrate Na⁺-nucleoside cotransporter (hfCNT) from the Pacific hagfish (*Eptatretus stouti*). *Am J Physiol Cell Physiol* 283: C155-C168, 2002.

Young JD, Cheeseman C, Mackey JR, Cass CE, and Baldwin SA. Molecular mechanisms of nucleoside and nucleoside drug transport. *Curr Top Membr* 50: 329-378, 2001.

Chapter V:

General Discussion

The objective of my research presented in this thesis was to use the two-microelectrode voltage clamp in conjunction with heterologous expression in *Xenopus laevis* oocytes to study the electrophysiological properties of recombinant human members of the concentrative nucleoside transporter (CNT) family. Transport mediated by hCNT1 and h/mCNT3 was shown to be electrogenic, since inward currents were observed following addition of various physiological nucleosides and nucleoside analogs (*Chapter II-IV*). As described in *Chapter II*, I investigated the steady-state kinetic properties of hCNT1. Na⁺ currents measured in response to the addition of pyrimidine nucleosides, adenosine, and pyrimidine nucleoside analogs were consistent with results from radioisotope studies (Ritzel *et al.*, 1997). Using electrophysiology, I was also able to demonstrate hCNT1-mediated transport of two novel pyrimidine nucleoside mimics not available in radioisotope form. In kinetic experiments, Na⁺ was found to bind to the transporter first followed by nucleoside. Consistent with results from Na⁺ activation flux studies (Yao *et al.*, 1996), the hCNT1 Na⁺/nucleoside coupling ratio was determined to be 1:1. hCNT1 was strictly Na⁺-dependent, as no currents were detected with an inwardly-directed H⁺ ion gradient. As described in *Chapter III*, I participated in the functional characterization of the human and mouse proteins responsible for *cib*-type nucleoside transport activity (Ritzel *et al.*, 2001). This new CNT isoform, designated CNT3, along with the previously identified CNT1 (system *cit*) and CNT2 (system *cif*) transport proteins, correspond to the three major concentrative nucleoside transport processes identified in human and other mammalian cells and tissues. In *Xenopus* oocytes, human and mouse CNT3 (hCNT3 and mCNT3) were shown to mediate Na⁺ currents in response to both purine and pyrimidine nucleosides, demonstrating the broad permeant selectivity of this CNT isoform. In marked contrast to hCNT1 (*Chapter II*), the Na⁺/nucleoside coupling ratio of hCNT3 was 2:1 at negative membrane potentials (-90 mV), an observation consistent with the functional characteristics of *cib*-type transport activity reported in earlier flux studies in a number of cells and tissues (Wu *et al.*, 1992; Belt *et al.*, 1993; Huang *et al.*, 1993; Washington *et al.*, 1995; Redlak *et al.*, 1996). In a new finding, h/mCNT3 was also found to be H⁺- (and Li⁺)-dependent. In contrast to Na⁺-coupled hCNT3, H⁺-coupled hCNT3 had a H⁺/nucleoside coupling ratio of 1:1, and did not

mediate transport of antiviral pyrimidine nucleoside drugs. In *Chapter IV*, I investigated the presteady-state currents of hCNT3. Charge movements (Q) (the current-time integral of hCNT3 presteady-state currents), as a function of test potential, were described by the Boltzmann function. Q reversed at the holding potential, saturated at both hyperpolarizing or depolarizing potentials, and was decreased with increasing concentrations of uridine. The number of functional hCNT3 transport proteins expressed in the oocyte plasma membrane and the turnover number of the transporter were determined from Boltzmann parameters providing, for the first time, an estimate of CNT intrinsic catalytic activity. The presteady-state currents of hCNT3 were fitted by the sum of two exponential functions, giving a fast time constant (τ_{fast}) due to conformational changes of the empty transporter within the membrane field, and a slow time constant (τ_{slow}) due to Na^+ binding/dissociation from the transporter. The effect of Na^+ on the $V_{0.5}$ was used to calculate the effective fraction of the membrane field sensed by Na^+ . Binding of a single Na^+ ion (or independent binding of multiple ions) occurs at a site that traverses $\sim 65\%$ of the membrane electric field. The valence of the moveable charge was equal to -1.42.

Order of Substrate Binding

Analysis of steady-state kinetic parameters provides information about the binding order of substrates to the transporter (Klamo *et al.*, 1996). Results from steady-state transport experiments with hCNT1 demonstrated that Na^+ binds to the transporter first, followed by the nucleoside (*Chapter II*). Members of the CNT family of proteins therefore share a common transport mechanism with other cotransporters found in bacteria, plants, and animals, such as the SGLT1 Na^+ /glucose cotransporter and MIT H^+ /*myo*-inositol cotransporter, in which the cation binds first, increasing the affinity of the transporter for its co-substrate (Parent *et al.*, 1992a, b; Klamo *et al.*, 1996). These results are important in the development of a kinetic model for Na^+ /nucleoside cotransport. Phloridzin inhibition experiments also demonstrated ordered binding of substrates to the transporter; phloridzin bound to the transporter subsequent to Na^+ at a site possibly overlapping, in part, the translocation pore of the transporter. Although the

CNT and SGLT protein families are structurally unrelated, there were mechanistic similarities in the mode of phloridzin inhibition of Na⁺/nucleoside and Na⁺/glucose cotransport.

System-*cib* is a Member of the CNT Family

In 1992, a protein related to the rabbit intestinal Na⁺-dependent glucose transporter (SGLT1) was reported to possess low-level *cib*-type transport activity when produced in *Xenopus* oocytes (Pajor and Wright, 1992). This protein is now recognized as the rabbit ortholog of the human glucose transporter hSGLT2 (Wright, 2001).

Based on two observations, it was hypothesized instead that the protein responsible for *cib*-type nucleoside transport activity belongs to the CNT transporter family. First, hagfish CNT (hfCNT), cloned from the ancient marine prevertebrate *Eptatretus stouti*, was shown to possess *cib*-type transport activity (Yao *et al.*, 2002). Second, residue mutations in TM 7 of hCNT1 changed the substrate specificity of the transporter from pyrimidine nucleoside-selective (system *cit*) to one selective for both pyrimidine and purine nucleosides (system *cib*) (Loewen *et al.*, 1999). These findings led to the eventual isolation of two proteins from human and mouse, hCNT3 and mCNT3, respectively, that, when produced in *Xenopus* oocytes, demonstrated *cib*-type transport activity (Ritzel *et al.*, 2001). CNT3 represented the “missing” mammalian CNT isoform, CNT1 and CNT2 having been identified in earlier molecular cloning studies (Huang *et al.*, 1994; Che *et al.*, 1995; Yao *et al.*, 1996).

Novel Proton- and Lithium-coupled Nucleoside Transport Characteristics

It was shown in this thesis that h/mCNT3 exhibits novel cation coupling characteristics that have not previously been reported in studies of cells containing *cib*-type transport activity. Human and mouse CNT3 are able to utilize electrochemical gradients of H⁺ and Li⁺, in addition to Na⁺, to drive nucleoside influx into cells (*Chapter III*). In contrast, hCNT1 and hCNT2 (Ritzel *et al.*, 1998; Loewen *et al.*, 2003; *Chapter II*) are not H⁺- or Li⁺-dependent, but strictly rely on the electrochemical gradient of Na⁺. Human and

mouse CNT3 are more closely related structurally to the broadly selective hagfish transporter (hfCNT) than to mammalian CNT1/2 and, together with hfCNT, form a separate distinct CNT subfamily (Yao *et al.*, 2002). Initial functional characterization of recombinant hfCNT suggests that this transporter is not pH dependent, despite possessing a 2:1 Na⁺/nucleoside coupling ratio similar to h/mCNT3 (Yao *et al.*, 2002). Proton-driven CNT3 nucleoside uptake may be physiologically significant in the small intestine where a relatively low luminal pH provides a transmembrane proton gradient across the enterocyte brush border membrane (McEwan *et al.*, 1988). Examples of cotransporters present in intestine which are exclusively proton-linked include the human intestinal H⁺-dependent oligonucleotide transporter hPEPT1 (Liang *et al.*, 1995). The finding that h/mCNT3 did not transport the antiviral dideoxynucleoside drugs AZT and ddC with an inwardly-directed H⁺ ion gradient suggests that the binding of different cations to h/mCNT3 induces unique conformational changes in the substrate-binding pocket, which then determines the interaction of the transporter with the cotransported substrate. Future studies will explore structure/function relationships of transport-specific properties of CNT family members through chimeric constructs and site-directed mutagenesis to identify critical regions of the protein responsible for cation recognition and coupling. Initial chimeric studies between hCNT1 and hCNT3 suggest that the structural features determining H⁺-dependence reside in the carboxyl-terminal half of the protein (Loewen SK, Slugoski MD, Baldwin, SA, Cass CE, and Young JD, personal communication).

Cation/nucleoside Coupling Ratio

It was shown in *Chapter III* that human and mouse CNT3 have a 2:1 Na⁺/nucleoside coupling ratio, compared to a 1:1 coupling ratio for CNT1/CNT2 (Yao *et al.*, 1996; *Chapter II*). Information on the cation/nucleoside coupling ratio is of physiological significance since it indicates the concentrative capacity of the transporter; a two-Na⁺/one-nucleoside symporter will have a greater ability to transport nucleosides against a concentration gradient than will a one-Na⁺/one-nucleoside symporter.

Nucleoside Drug Transport

The difference in substrate selectivity between members of the CNT family for physiological pyrimidine and purine nucleosides is reflected in their ability to transport various nucleoside analog drugs used in the treatment of cancer and viral diseases as well as bacterial and fungal infections. CNT proteins are important in therapeutic drug delivery and chemoprotective strategies. The therapeutic efficacy of nucleoside analog drugs may be increased, while reducing toxicity, through manipulations based on knowledge of the various nucleoside transporter processes in normal and cancer cells (Mackey *et al.*, 1998). Treatments may soon be designed based on the number and types of functional nucleoside transporters, known as the nucleoside transport profile, of the target cell or tissue (Mackey *et al.*, 1998). Protection of normal cells from the toxic effects of nucleoside analog drugs may be obtained by co-administration of an inhibitor that blocks ENT but not CNT processes (Mackey *et al.*, 1998; Baldwin *et al.*, 1999). Such an inhibitor may also increase the cytotoxicity of the nucleoside analog drug towards cells that contain both ENT and CNT proteins by preventing ENT-mediated drug efflux (Mackey *et al.*, 1998; Baldwin *et al.*, 1999). Future work may allow the engineering of CNT proteins with a high affinity for a particular cytotoxic nucleoside drug and the introduction of a gene encoding that recombinant transporter to a particular tissue (Mackey *et al.*, 1998).

Presteady-state Currents of hCNT3

Recombinant human CNT3 produced in *Xenopus* oocytes exhibited presteady-state currents that reflect voltage-dependent processes, such as ion binding/dissociation from the transporter and conformational changes of the empty transporter within the membrane (*Chapter IV*). Presteady-state currents therefore provide information about individual steps in the transport cycle. Time constants for the carrier currents give estimates of the rate constants for the conformational changes, and the charge movements, integrals of the transient currents, give estimates of the number of hCNT3 proteins expressed in the plasma membrane as well as the turnover number of the transporter, transporter valence, and the depth within the membrane of cation binding site(s). The information obtained

from presteady-state current measurements of hCNT3, along with results from steady-state studies, will guide the development of detailed kinetic models for Na⁺/nucleoside cotransport and provide a framework for future structure/function experiments.

Presteady-state currents of cotransporters have characteristics in common with gating currents of voltage-dependent ion channels, such as relaxation time constants in the millisecond range, and charge movements which are described by the Boltzmann function (Panayotova-Heiermann *et al.*, 1994; Fesce *et al.*, 2002). In the case of channels, charge movements are due to the opening and closing of gate(s) controlling ion permeation, and as such, site-directed mutagenesis studies have identified charged residues involved in gating in the S4 region of the Na⁺ and K⁺ channels (Papazian *et al.*, 1991). Similarly, studies with cotransporters such as SGLT1 have attempted to identify residues responsible for charge movements (Panayotova-Heiermann *et al.*, 1994). My studies of hCNT3 suggest that the transporter carries two net negative charges, a valence consistent with the protein's 2:1 Na⁺/nucleoside coupling ratio. As an example of the direction that future site-directed mutagenesis studies may take, it will be of considerable interest and importance to identify the residue(s) responsible for hCNT3 charge movements (presumably aspartate/glutamate residues) to provide information on the molecular mechanism of CNT cation binding/coupling and the structural architecture of the translocation pore.

Kinetic Interpretation of τ_{slow} and τ_{fast}

Using the two-microelectrode voltage clamp, two time constants were observed in the presence of external Na⁺: τ_{fast} and τ_{slow} . For hCNT3, the data showed a decreased time constant at lower [Na⁺] (data not shown). A model that predicts such behaviour incorporates sequential binding of 2 Na⁺ (Fig. 5-1). For simplicity, the binding of the second Na⁺ is assumed to be instantaneous. τ_{fast} is associated with translocation of the free carrier between the inward-facing state (C'') and the outward-facing state (C'). τ_{slow} is associated with Na⁺ binding/dissociation. Although rates of association of Na⁺ with binding sites on the surface of a protein are generally less than microseconds (Mager *et*

al., 1993), the time constant of Na⁺ binding/dissociation to hCNT3 is slow due to presumed relative inaccessibility of Na⁺ to the cation binding site. Theoretically, the time constant (τ) associated with a rapid step is determined by the rate constants of that step (*ie.* it is equal to the inverse of the sum of the two rate constants) (Chen *et al.*, 1996). In contrast, the time constant associated with a slow step is also modified by rate constants from neighboring fast steps (Chen *et al.*, 1996). Therefore, the time constant of the empty carrier translocation (τ_{fast}) is given by Equation 1, while the time constant of Na⁺ binding/dissociation is determined by Equation 2. This model is similar to that of the rat GABA transporter GAT1 which incorporates sequential binding of two Na⁺ ions (Mager *et al.*, 1998) and is similar in mechanism to that proposed by Chen *et al.* (1996) for the human Na⁺/glucose cotransporter hSGLT1 which incorporates voltage-dependent modulation factors in the time constant for free carrier translocation between an intramembrane state and the outward facing carrier state. In order to determine the parameters in equations 1 and 2, the system must be modeled such that the parameters from the kinetic model fit the experimental data. Calculation of these parameters, which represent individual rate constants within the hCNT3 translocation cycle, will be an important goal of future studies.

$$\text{Equation 1: } \tau_{\text{fast}} = 1/(k_{12} + k_{21})$$

$$\text{Equation 2: } \tau_{\text{slow}} = 1/\{(k_{12}/(k_{12} + k_{21})) k_{23}[\text{Na}^+] + (k_{32}(k_{43}/(k_{43} + k_{34}[\text{Na}^+])))\}$$

Turnover Rate (Turnover Number)

The turnover rate (turnover number) of hCNT3, which indicates the number of nucleoside molecules translocated per transporter per second, may be estimated from the ratio of the uridine-evoked steady state current (I_{max}) and the charge movement for the same individual oocyte (Q_{max}). The calculated turnover rate for hCNT3 at room temperature was equal to $\sim 9.7 \text{ sec}^{-1}$ (*Chapter IV*) and is similar to that seen for other cotransporters such as the rat γ -amino-butyric acid transporter (GABA) GAT1 (6 - 13 sec^{-1}) (Mager *et al.*, 1993) and rbSGLT1 (25 sec^{-1}) (Panayotova-Heiermann *et al.*, 1994) expressed in *Xenopus* oocytes. For comparison, the calculated turnover rate for the

ENT transporters, determined from NBMPR-binding studies, was $\sim 10^4 \text{ sec}^{-1}$ (Jarvis and Young, 1986; Cass, 1995). The turnover rate of CNTs is therefore much lower than that for ENTs. However, the apparent substrate affinity (K_m) of the CNTs is higher than for ENTs and partly offsets this difference (Young *et al.*, 2001). Knowledge of the turnover rate of hCNT3 for uridine and, by extension, other nucleosides and nucleoside drugs will allow, for the first time, hCNT3 membrane abundance in different cells and tissues to be estimated based on experimentally determined rates of nucleoside transport. Assuming broadly similar turnover rates, such calculations may also be applied to hCNT1 and hCNT2.

Limitations of Electrophysiological studies of hCNT1/3 in *Xenopus* Oocytes

Electrophysiology provides a powerful technique for the functional characterization of transport proteins. There are, however, limitations, when studying the CNT proteins expressed in *Xenopus* oocytes using the two-microelectrode voltage-clamp, including the large size of the oocyte, inability to control the internal medium, relatively low levels of transporter expression, and the unavailability of an effective inhibitor of Na^+ /nucleoside transport. The *Xenopus* oocyte has a large diameter of 1.0 - 1.6 mm and, as such, has a long capacitive transient lasting up to 2 msec. Since the membrane potential is not at the desired test potential for about 500 μsec (Chapter IV) and the capacitive transient, which is part of the current record, lasts up to 1.5 msec, the resolution of fast events, such as activation or deactivation of Na^+ channels, can be obscured (Tagliatela *et al.*, 1992). It is possible to use oocytes with a smaller surface area, however, levels of transporter expression will be lower. Since the interior of the cell cannot be accessed in the two-microelectrode voltage clamp, the intracellular milieu cannot be controlled. The cut-open oocyte technique provides a solution to this problem, allowing internal perfusion of the oocyte. Transporter expression levels are important when studying both steady-state and presteady-state currents. However, steady-state current measurements can be performed with levels of transporter expression that are less than ideal. In contrast, presteady-state current measurements require much higher protein densities. In comparison with other cotransporters, levels of expression of the CNT transporters are quite low. Expression

levels of eukaryotic Na⁺/glucose transporters (SGLT) are in the order of 10¹² transporters per oocyte, compared to 10¹⁰ for hCNT3 (*Chapter IV*). The presteady-state currents are therefore smaller, making curve-fitting procedures during the analysis of presteady-state currents difficult. It will be of importance to focus future efforts to increase levels of expression of hCNT1/3 in oocytes as a means to facilitate further, in depth, studies of CNT presteady-state currents. During analysis, the hCNT3 presteady-state current must be isolated from the oocyte membrane capacitance as well as from steady-state leak currents. Charge movements may be blocked by nonsubstrate uptake inhibitors and records in the presence and absence of inhibitor can be subtracted to isolate the transporter-associated presteady-state current (Mager *et al.*, 1998). This is seen in studies of the human glutamate transporter EAAT2 and the rabbit Na⁺/glucose cotransporter SGLT1 which utilized the competitive inhibitors L-kainate and phloridzin, respectively, to isolate presteady-state currents (Wadiche *et al.*, 1995; Parent *et al.*, 1992a, b). The availability of an inhibitor would facilitate isolation of hCNT3 presteady-state currents.

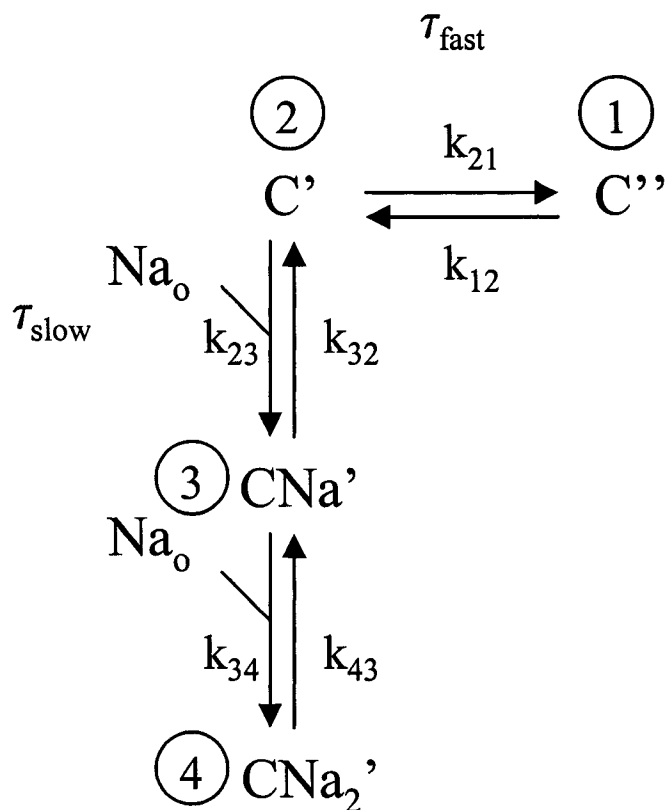


Figure 5-1. Three-state kinetic model for hCNT3 in the absence of substrates. Translocation of a free carrier across the membrane is described by the transitions between states 1 (C'' ; facing in) and 2 (C' ; facing out). The binding and dissociation of the first Na^+ to the carrier is described by transitions between 2 (C') and 3 (CNa'). The binding and dissociation of the second Na^+ to the carrier is described by transitions between 3 (CNa') and 4 (CNa_2'). The rate constants are given by k_{ij} , where i and j are two different states.

Bibliography

Baldwin SA, Mackey JR, Cass CE, and Young JD. Nucleoside transporters: molecular biology and implications for therapeutic development. *Mol Med Today* 5: 216-224, 1999.

Belt JA, Marina NM, Phelps DA, and Crawford CR. Nucleoside transport in normal and neoplastic cells. *Adv Enzyme Regul* 33: 235-252, 1993.

Cass CE. In: Drug transport in antimicrobial and anticancer chemotherapy, edited by Georgopapadakou NH. New York: Marcel Dekker, 1995.

Che M, Ortiz DF, and Arias IM. Primary structure and functional expression of a cDNA encoding the bile canalicular, purine-specific Na⁺-nucleoside cotransporter. *J Biol Chem* 270(23): 13596-13599, 1995.

Chen X-Z, Coady MJ, and Lapointe JY. Fast voltage clamp discloses a new component of presteady-state currents from the Na(+)-glucose cotransporter. *Biophys J* 71(5): 2544-2552, 1996.

Fesce R, Giovannardi S, Binda F, Bossi E, and Peres A. The relation between charge movement and transport-associated currents in the rat GABA cotransporter GAT1. *J Physiol* 545(3): 739-750, 2002.

Huang Q-Q, Harvey CM, Paterson ARP, Cass CE, and Young JD. Functional expression of Na⁺-dependent nucleoside transport systems of rat intestine in isolated oocytes of *Xenopus laevis*: Demonstration that rat jejunum expresses the purine-selective system N1 (*cif*) and a second, novel system N3 having broad specificity for purine and pyrimidine nucleosides. *J Biol Chem* 268(27): 20613-20619, 1993.

Huang Q-Q, Yao SYM, Ritzel MWL, Paterson ARP, Cass CE, and Young JD. Cloning and functional expression of a complementary DNA encoding a mammalian nucleoside transport protein. *J Biol Chem* 269(27): 17757-17760, 1994.

Jarvis SM and Young JD. Nucleoside transport in rat erythrocytes. Two components with differences in sensitivity to inhibition by nitrobenzylthioinosine and p-chloromercuriphenyl sulphonate. *J Membr Biol* 93:1-10, 1986.

Klamo EM, Drew ME, Landfear SM, and Kavanaugh MP. Kinetics and stoichiometry of a proton/*myo*-inositol cotransporter. *J Biol Chem* 271(25): 14937-14943, 1996.

Liang R, Fei YJ, Prasad PD, Ramamoorthy S, Han H, Yang-Feng TL, Hediger MA, Ganapathy V, and Leibach FH. Human intestinal H⁺/peptide cotransporter. Cloning, functional expression, and chromosomal localization. *J Biol Chem* 270(12): 6456-6463, 1995.

Loewen SK, Ng AML, Yao SYM, Cass CE, Baldwin SA, and Young JD. Identification of amino acid residues responsible for the pyrimidine and purine nucleoside specificities of human concentrative Na⁺ nucleoside cotransporters hCNT1 and hCNT2. *J Biol Chem* 274(35): 24475-24484, 1999.

Loewen SK, Yao SYM, Slugoski MD, Mohabir NN, Turner RJ, Weiner JH, Gallagher MP, Henderson PJF, Baldwin SA, Cass CE, and Young JD. Transport of antiviral and antineoplastic drugs by recombinant *Escherichia coli* nucleoside-H⁺ cotransporter (NupC) produced in *Xenopus laevis* oocytes. *Mol Membr Biol* 2003 (in press).

Mackey JR, Baldwin SA, Young JD, and Cass CE. Nucleoside transport and its significance for anticancer drug resistance. *Drug Resist Updates* 1: 310-324, 1998.

McEwan GTA, Daniel H, Fett C, Burgess MN, and Lucas ML. The effect of *Escherichia coli* STa enterotoxin and other secretagogues on mucosal surface pH of rat small intestine *in vivo*. *Proc R Soc Lond B Biol Sci* 234(1275): 219-237, 1988.

Mager S, Naeve J, Quick M, Labarca C, Davidson N, and Lester HA. Steady states, charge movements, and rates for a cloned GABA transporter expressed in *Xenopus* oocytes. *Neuron* 10: 177-188, 1993.

Mager S, Cao Y, and Lester H. Measurement of transient currents from neurotransmitter transporters expressed in *Xenopus* oocytes. *Methods Enzymol* 296: 551-566, 1998.

Pajor AM and Wright EM. Cloning and functional expression of a mammalian Na⁺/nucleoside cotransporter: A member of the SGLT family. *J Biol Chem* 267(6): 3557-3560, 1992.

Panayotova-Heiermann M, Loo DDF, Lostao MP, and Wright EM. Sodium/D-glucose cotransporter charge movements involve polar residues. *J Biol Chem* 269(33): 21016-21020, 1994.

Papazian DM, Timpe LC, Nung Jan Y, and Jan LY. Alteration of voltage-dependence of *Shaker* potassium channel by mutations in the S4 sequence. *Nature* 349: 305-310, 1991.

Parent L, Supplisson S, Loo DF, and Wright EM. Electrogenic properties of the cloned Na⁺/glucose cotransporter: Part I. Voltage-clamp studies. *J Membr Biol* 125: 49-62, 1992a.

Parent L, Supplisson S, Loo DF, and Wright EM. Electrogenic properties of the cloned Na⁺/glucose cotransporter: Part II. A transport model under non rapid equilibrium conditions. *J Membr Biol* 125: 63-79, 1992b.

Redlak MJ, Zehner ZE, and Betcher SL. Expression of rabbit ileal N3 Na⁺/nucleoside cotransport activity in *Xenopus laevis* oocytes. *Biochem Biophys Res Comm* 225: 106-111, 1996.

Ritzel MWL, Yao SYM, Huang MY, Elliot JF, Cass CE, and Young JD. Molecular cloning and functional expression of cDNAs encoding a human Na⁺-nucleoside cotransporter (hCNT1). *Am J Physiol* 272: C707-C714, 1997.

Ritzel MWL, Yao SYM, Ng AML, Mackey JR, Cass CE, and Young JD. Molecular cloning, functional expression and chromosomal localization of a cDNA encoding a human Na⁺/nucleoside cotransporter (hCNT2) selective for purine nucleosides and uridine. *Mol Membr Biol* 15(4): 203-211, 1998.

Ritzel MWL, Ng AML, Yao SYM, Graham K, Loewen SK, Smith KM, Ritzel GR, Mowles DA, Carpenter P, Chen X-Z, Karpinski E, Hyde RJ, Baldwin SA, Cass CE, and Young JD. Molecular identification and characterization of novel human and mouse concentrative Na⁺-nucleoside cotransporter proteins (hCNT3 and mCNT3) broadly selective for purine and pyrimidine nucleosides (system *cib*). *J Biol Chem* 276(4): 2914-2927, 2001.

Taglialatela M, Toro L, and Stefani E. Novel voltage clamp to record small, fast currents from ion channels expressed in *Xenopus* oocytes. *Biophys J* 61(1): 78-82, 1992.

Wadiche JI, Arriza JL, Amara SG, and Kavanaugh MP. Kinetics of a human glutamate transporter. *Neuron* 14: 1019-1027, 1995.

Washington CB, Brett CM, Wu X, and Giacomini KM. The effect of N-ethylmaleimide on the Na(+)-dependent nucleoside transporter (N3) in rabbit-choroid plexus. *J Pharmacol Exp Ther* 274 (1): 110-114, 1995.

Wright EM. Renal Na(+)-glucose cotransporters. *Am J Physiol Renal Physiol* 280: F10-F18, 2001.

Wu X, Yuan G, Brett CM, Hui AC, and Giacomini KM. Sodium-dependent nucleoside transport in choroid plexus from rabbit. Evidence for a single transporter for purine and pyrimidine nucleosides. *J Biol Chem* 267(13): 8813-8818, 1992.

Yao SYM, Ng AML, Ritzel MWL, Gati WP, Cass CE, and Young JD. Transport of adenosine by recombinant purine- and pyrimidine-selective sodium/nucleoside cotransporters from rat jejunum expressed in *Xenopus laevis* oocytes. *Mol Pharmacol* 50: 1529-1535, 1996.

Yao SYM, Ng AML, Loewen SK, Cass CE, Baldwin SA, and Young JD. An ancient prevertebrate Na⁺-nucleoside cotransporter (hfCNT) from the Pacific hagfish (*Eptatretus stouti*). *Am J Physiol Cell Physiol* 283: C155-C168, 2002.

Young JD, Cheeseman CI, Mackey JR, Cass CE, and Baldwin SA. Molecular mechanisms of nucleoside and nucleoside drug transport. *Current Topics Membr* 50: 329378, 2001.

Appendix A:

Gemcitabine Transport in *Xenopus* Oocytes Expressing Recombinant Plasma Membrane Mammalian Nucleoside Transporters

John R. Mackey, Sylvia Y. M. Yao, Kyla M. Smith, Edward Karpinski, Stephen A. Baldwin, Carol E. Cass, James D. Young

Background: Gemcitabine, a pyrimidine analogue of deoxycytidine, is an anticancer nucleoside drug that requires functional plasma membrane nucleoside transporter proteins to reach its intracellular targets and cause cytotoxicity. Because of technical difficulties inherent in studying nucleoside transport in human cells, we rigorously defined gemcitabine membrane transportability by producing each of the available human (h) and rat (r) recombinant nucleoside transporters (NTs) individually in *Xenopus laevis* oocytes. **Methods:** Oocytes were microinjected with *in vitro*-transcribed RNAs derived from complementary DNAs encoding (C = concentrative) rCNT1, rCNT2, hCNT1, hCNT2, (E = equilibrative) rENT1, rENT2, hENT1, and hENT2. Uptake of [³H]gemcitabine and [¹⁴C]uridine was measured 3 days after microinjection to determine kinetic constants. We also used the two-electrode, voltage-clamp technique to investigate the electrophysiology of hCNT1-mediated gemcitabine transport. **Results:** Gemcitabine was transported by most of the tested proteins (the exceptions being the purine-selective rCNT2 and hCNT2), with the greatest uptake occurring in oocytes producing recombinant rCNT1 and hCNT1. Influxes of gemcitabine mediated by hCNT1, hENT1, and hENT2 were saturable and conformed to Michaelis-Menten kinetics with apparent K_m values of 24, 160, and 740 μM , respectively. Gemcitabine had a limited ability to cross the lipid bilayer of oocyte membranes by simple diffusion. External application of gemcitabine to oocytes producing recombinant hCNT1 induced an inward current, which demonstrated that hCNT1 functions as a Na⁺/nucleoside co-transport protein and confirmed the

transporter's ability to transport gemcitabine. **Conclusions:** Mammalian nucleoside transporters vary widely in their affinity and capacity to transport gemcitabine. Variation in the tumor and tissue distribution of plasma membrane nucleoside transporter proteins may contribute to the solid tumor activities and schedule-dependent toxic effects of gemcitabine. [J Natl Cancer Inst 1999;91:1876-81]

Gemcitabine (2',2'-difluorodeoxycytidine, dFdC; Gemzar) is a pyrimidine analogue of deoxycytidine in which two fluorine atoms are present at the 28 position of the deoxyribose ring. Gemcitabine is unique among nucleoside drugs because it is active against epithelial cancers, including non-small-cell lung, breast, bladder, ovarian, and head and neck cancers (1). After intravenous administration, gemcitabine permeates the plasma membrane and is converted to 2',2'-difluorodeoxycytidine monophosphate (dFdCMP) by deoxycytidine kinase, and the latter is subsequently phosphorylated to the cytotoxic 5'-diphosphate and 5'-triphosphate derivatives by pyrimidine monophosphate and diphosphate kinases (2). 2',2'-difluorodeoxycytidine diphosphate inhibits ribonucleotide reductase, while 2',2'-difluorodeoxycytidine triphosphate is incorporated into DNA and RNA (3). Gemcitabine exhibits the properties of self-potential and masked chain termination. Among other mechanisms of self-potential, gemcitabine triphosphate inhibits deoxycytidine monophosphate deaminase, thereby decreasing triphosphate catabolism (2). In masked chain termination, an additional physiologic nucleotide is incorporated prior to inhibition of DNA polymerase, which conceals the incorporated gemcitabine nucleotide from exonuclease activity (4).

Because the molecular targets of gem-

Affiliations of authors: J. R. Mackey, C. E. Cass, Department of Oncology, University of Alberta, Canada, and Cross Cancer Institute, Edmonton, AB; S. Y. M. Yao, K. M. Smith, E. Karpinski, J. D. Young, Department of Physiology, University of Alberta; S. A. Baldwin, School of Biochemistry and Molecular Biology, University of Leeds, U.K.

Correspondence to: John R. Mackey, M.D., 11560 University Ave., Edmonton, AB T6C 1Z2, Canada (e-mail: johnmack@cancerboard.ab.ca).

See "Notes" following "References."

Oxford University Press

citabine are intracellular, permeation through the plasma membrane is the obligatory first step in cytotoxicity. Physiologic and therapeutic nucleosides are generally hydrophilic and require plasma membrane nucleoside transporter proteins for efficient cellular entry [reviewed in (5-7)]. Four major functionally distinct nucleoside transporter processes, each of which has been defined in molecular terms through isolation and functional expression of complementary DNAs (cDNAs) encoding the transporter proteins, have been described in human cells (8-13). These nucleoside transporters belong to two previously unrecognized families of membrane proteins and function either as equilibrative, bidirectional transporters (the equilibrative nucleoside transporter [ENT] family) or as concentrative, sodium/nucleoside cotransporters (the concentrative nucleoside transporter [CNT] family). The ENT proteins accept both pyrimidine and purine nucleosides as permeants but differ in their sensitivity to inhibition by nitrobenzylthioinosine (NBMPR): Human ENT1 (hENT1, an equilibrative sensitive, *es*-type transporter) is inhibited by nanomolar concentrations of NBMPR, whereas hENT2 (an equilibrative insensitive, *ei*-type transporter) is unaffected by low concentrations (<1 μ M) of NBMPR. One of the CNT proteins (hCNT1, a concentrative NBMPR-insensitive thymidine selective or *ct*-type transporter) is selective for pyrimidine nucleosides but also transports adenosine, albeit inefficiently. The other protein (hCNT2, a concentrative insensitive and formycin B-selective or *ci*-type transporter) is selective for purine nucleosides and uridine. The tissue and tumor distribution of the nucleoside transporters is not fully defined, but hENT1 is present in most human cells, while concentrative nucleoside transporters have been identified in liver (13), kidney (12-14), intestine (13,15,16), choroid plexus (17), and some cancer cell lines (18-21). Rat homologues of each of these proteins have also been identified and are designated rENT1, rENT2, rCNT1, and rCNT2 (22-25).

In cytotoxicity experiments performed *in vitro* (26), a deficiency in plasma membrane nucleoside transport, produced either pharmacologically or genetically, conferred two- to three-log protection from gemcitabine growth inhibition in human and murine cancer cell lines. By investigating gemcitabine cytotoxicity in a

panel of murine and human cell lines with defined nucleoside transporter activities, we concluded that gemcitabine uptake was apparently mediated by hENT1, hENT2, and hCNT1 but not by hCNT2. Studies with radiolabeled gemcitabine that were conducted in the same panel of cultured human cell lines with single nucleoside transport activities confirmed mediated uptake by the hENT1, hENT2, and hCNT1 transporters. Gemcitabine was most efficiently transported by hENT1 and hCNT1 but at rates approximately 10-fold lower than those of uridine. Plasma membrane diffusion of gemcitabine was much slower than mediated transport.

Because of the technical difficulties inherent in studying nucleoside transport in human cells (the presence of multiple endogenous nucleoside transport activities, variable transfection efficiencies when studying recombinant transporters, and characteristically rapid uptake rates requiring inhibitor-oil stop techniques), we have undertaken a definitive study of radiolabeled gemcitabine transportability by producing each of the available human and rat nucleoside transporter cDNAs individually in oocytes from the amphibian *Xenopus laevis*. In addition, by the use of whole-cell, two-electrode, voltage-clamp electrophysiology studies, we have studied hCNT1-mediated transport of uridine and gemcitabine without the requirement for radiolabeled permeants.

MATERIALS AND METHODS

CNT and ENT cDNAs

cDNAs encoding rCNT1 (GenBank accession No. U10279), rCNT2 (GenBank accession No. U66723), hCNT1 (GenBank accession No. U62966), hCNT2 (GenBank accession No. AF036109), rENT1 (GenBank accession No. AF015304), rENT2 (GenBank accession No. AF015305), hENT1 (GenBank accession No. U81375), and hENT2 (GenBank accession No. AF029358) in the plasmid expression vectors pGEM-3Z (Promega Corp., Madison, WI; rCNT1), pGEM-T (Promega Corp.; rCNT2, rENT1, and rENT2), or pBluescript II KS(+) (Stratagene, La Jolla, CA; hCNT1, hCNT2, hENT1, and hENT2) were obtained as described previously (8,9,11,13, 23-25).

Expression of cDNAs Encoding Recombinant Transporters in *Xenopus* Oocytes

Linearized plasmids were transcribed with T3 polymerase (hENT1 and hENT2), T7 polymerase (rCNT1, rCNT2, and hCNT1), or SP6 polymerase (rENT1 and rENT2) in the presence of the ^{mT}CpppG cap by use of the MEGAscript (Ambion, Austin,

TX) transcription system. The remaining template was removed by digestion with deoxyribonuclease 1. Defolliculated oocytes (23) were microinjected with either 10 nL of water containing 10 ng RNA transcript or 10 nL of water alone. *Xenopus* care was in accordance with institutional guidelines.

Radioisotope Flux Studies

Uptake of gemcitabine and uridine was measured 3 days after microinjection by use of high-performance liquid chromatography-repurified [³H]gemcitabine (Eli Lilly and Co., Indianapolis, IN) or [¹⁴C]uridine (Amersham Life Science Inc., Piscataway, NJ) at concentrations of 2 μ Ci/mL and 1 μ Ci/mL, respectively. Flux measurements were performed at room temperature (20°C) on groups of 10-12 oocytes in medium (0.2 mL) containing the following: 100 mM NaCl, 2 mM KCl, 1 mM CaCl₂, 1 mM MgCl₂, and 10 mM HEPES (pH 7.5). At the end of the incubation period, extracellular label was removed by six rapid washes in ice-cold medium. Individual oocytes were dissolved in 5% (wt/vol) sodium dodecyl sulfate for quantitation of oocyte-associated ³H or ¹⁴C by liquid scintillation counting (LS 6000 IC; Beckman Instruments, Inc., Fullerton, CA). Incubation periods for kinetic studies were selected to be within the initial linear phase of uptake curves to approximate zero-trans conditions and to measure initial rates of transport.

Results are presented as means with 95% confidence intervals (CIs) for 10-12 individual oocytes. Kinetic constants (apparent K_m and V_{max}) were determined by nonlinear regression analysis (ENZFITTER; Elsevier-Biosoft, Ferguson, MO). Each experiment was performed at least twice on different batches of oocytes.

Measurements of hENT1-Induced Sodium Currents

Oocyte membrane currents were measured by use of a CA-1B oocyte clamp (Dagan Corp., Minneapolis, MN) in the whole-cell, two-electrode, voltage clamp mode. The microelectrodes were filled with 3 M KCl and had resistances that ranged from 1 to 2.5 M Ω (mega ohm). The CA-1B was interfaced to a computer via a Digidata 1200B A/D converter and controlled by Axoscope software (Axon Instruments, Foster City, CA). Current signals were filtered at 20 Hz (four-pole Bessel filter) and sampled at a sampling interval of 50 msec. For data presentation, the current signals were further filtered at 0.5 Hz by use of pCLAMP software (Axon Instruments). All electrophysiologic experiments were performed at room temperature. The oocytes were penetrated and the membrane potential was observed for 15 minutes. If the membrane potential was unstable or less than -30 mV, these oocytes were not used. For measurements of hCNT1-generated currents, the oocyte membrane potential was clamped at -50 mV. Oocytes were then perfused with medium of the same composition used for radioisotope flux studies. For transport measurements, the medium was changed to one containing substrate, either gemcitabine (100 μ M) or uridine (100 μ M). In experiments examining Na⁺ dependence, sodium in the medium was replaced with equimolar choline.

RESULTS

In Fig. 1, we show a representative recombinant expression experiment in *Xenopus* oocytes that measured the uptake of gemcitabine or uridine (10 μ M, 20°C, 10-minute flux) in cells injected with water alone (control) or with water that contained transcripts for either rCNT1, rCNT2, hCNT1, hCNT2, eENT1, rENT2, hENT1, or hENT2. Gemcitabine, at the clinically achievable concentration of 10 μ M, was a permeant of six of the eight recombinant transporters tested, with the greatest uptake occurring in oocytes that produced recombinant rCNT1 and hCNT1. Gemcitabine was not a permeant of either rCNT2 or hCNT2, transporters that have been previously shown to be selective for purine nucleosides.

Subsequent experiments (Fig. 2) investigated the concentration dependence of gemcitabine transport by each of the four recombinant human transporters. Initial rates of transport (influx) were determined by use of an incubation period of 1 minute for hCNT1, 2 minutes for hENT2, 5 minutes for hENT1, and 60 minutes for hCNT2. Under these conditions, intracellular gemcitabine levels at the end of the incubation period were typically less than 15% of starting extracellular concentration, and uptake time courses were linear. To facilitate comparison between the different recombinant trans-

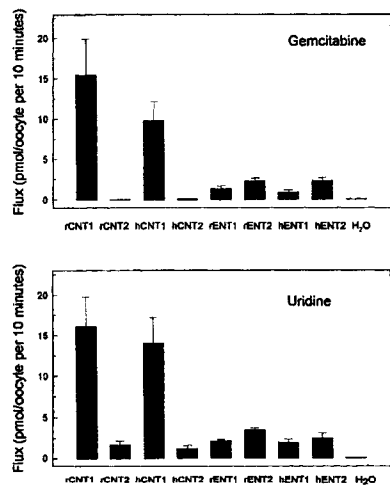
porters, influx values were calculated as pmol/oocyte · minute⁻¹. Kinetic parameters derived from the gemcitabine transport data in Fig. 2 are shown in Table 1 together with previously determined apparent K_m and V_{max} values for uridine influx.

Influxes of gemcitabine mediated by hCNT1, hENT1, and hENT2 were saturable and conformed to Michaelis-Menten kinetics with apparent K_m values of 24, 160, and 740 μ M, respectively. Except for recombinant hENT2, which exhibited a relatively low affinity for gemcitabine, the K_m values of the other recombinant transporters for gemcitabine influx were similar to the apparent K_m values of these transporters for uridine influx (45, 240, and 200 μ M, respectively, for hCNT1, hENT1, and hENT2) (8,9,11,13). In the case of hENT2 (uridine K_m 200 μ M), the recombinant transporter's relatively low affinity for gemcitabine (K_m value of 740 μ M) was compensated by a higher V_{max} value, so that the V_{max} : K_m ratio for hENT2-mediated gemcitabine transport was 0.059 compared with 0.032 for uridine transport (Table 1). Corresponding V_{max} : K_m ratios for gemcitabine and uridine influx by the other recombinant transporters were in good agreement with the 10- μ M-uptake data shown in Fig. 1. In contrast to the other recombinant transporters, no significant mediated transport of gemcitabine was

detected for hCNT2, even at high permeant concentrations (data not shown). Influx of gemcitabine in water-injected oocytes, like that in hCNT2-transcript-injected cells, was approximately linear over the concentration ranges studied (10 μ M-5 mM), suggesting a lack of endogenous-mediated transport of gemcitabine in oocytes. At a concentration of 1 mM, the magnitude of the gemcitabine flux (0.091 pmol/oocyte · minute⁻¹ [95% CI = 0.042-0.14]) was similar to that determined previously for uridine (0.102 pmol/oocyte · minute⁻¹ [95% CI = 0.010-0.104]) (24). Therefore, like uridine, gemcitabine has a limited ability to cross the lipid bilayer of cell membranes by simple diffusion.

Finally, we used whole-cell recording by the two-electrode, voltage-clamp technique to investigate the electrophysiology of hCNT1-mediated gemcitabine and uridine transport. In this technique, one microelectrode clamps the oocyte membrane to a predetermined potential (-50 mV in the case of the present experiments), while a second microelectrode delivers current to maintain that potential. The current (in nano-Amperes [nA]) needed to hold the membrane at the predetermined potential (-50 mV) is the measured parameter. As shown for the representative experiment in Fig. 3, external application of gemcitabine (100 μ M) to oocytes producing recombinant hCNT1 induced an inward current that returned to baseline on removal of the drug. The gemcitabine-induced current was not seen in control, water-injected oocytes and was abolished when extracellular Na⁺ was replaced by choline. In three separate experiments with different oocytes, the range of Na⁺ currents induced by 100 μ M gemcitabine was 10-15 nA compared with 55-68 nA for 100 μ M uridine. This 3.7-fold difference in gemcitabine-induced and uridine-induced Na⁺ currents was consistent with the estimates for fluxes of 100 μ M gemcitabine and uridine calculated from the hCNT1 kinetic parameters in Table 1 (4.7 and 17.9 pmol/oocyte · minute⁻¹ for 100 μ M gemcitabine and uridine, respectively). As was the case for gemcitabine, the uridine current was not seen in control, water-injected oocytes and was abolished when Na⁺ was replaced by choline. These studies demonstrated that hCNT1 functions as a Na⁺/nucleoside co-transport protein and confirmed the recombinant transporter's ability to transport gemcitabine.

Fig. 1. Transport of gemcitabine and uridine by recombinant human (h) and rat (r) concentrative (CNT) and equilibrative (ENT) nucleoside transporters expressed in *Xenopus laevis* oocytes. Oocytes were injected with either 10 nL of water alone or 10 nL water containing 10 ng of messenger RNA transcript. Uptake of [³H]gemcitabine and [¹⁴C]uridine (10 μ M, 20°C, 10-minute flux) was determined after 3 days in NaCl-containing transport medium. Each value represents the mean (with 95% confidence intervals) of 10-12 oocytes. Mediated fluxes of gemcitabine and uridine, defined as the difference in uptake values between RNA-injected and water-injected oocytes and given as pmol/oocyte per 10 minutes, were, respectively: 15.4 (10.9-19.9) and 16.1 (12.4-19.8) for rCNT1; 0 and 1.6 (1.0-2.2) for rCNT2; 9.8 (7.4-12.2) and 14.0 (10.9-17.1) for hCNT1; 0 and 1.1 (0.7-1.5) for hCNT2; 1.3 (0.9-1.7) and 2.1 (1.9-2.3) for rENT1; 2.2 (1.8-2.6) and 3.4 (3.2-3.6) for rENT2; 0.86 (0.56-1.2) and 1.9 (1.5-2.3) for hENT1; and 2.3 (1.9-2.7) and 2.5 (1.9-3.1) for hENT2.



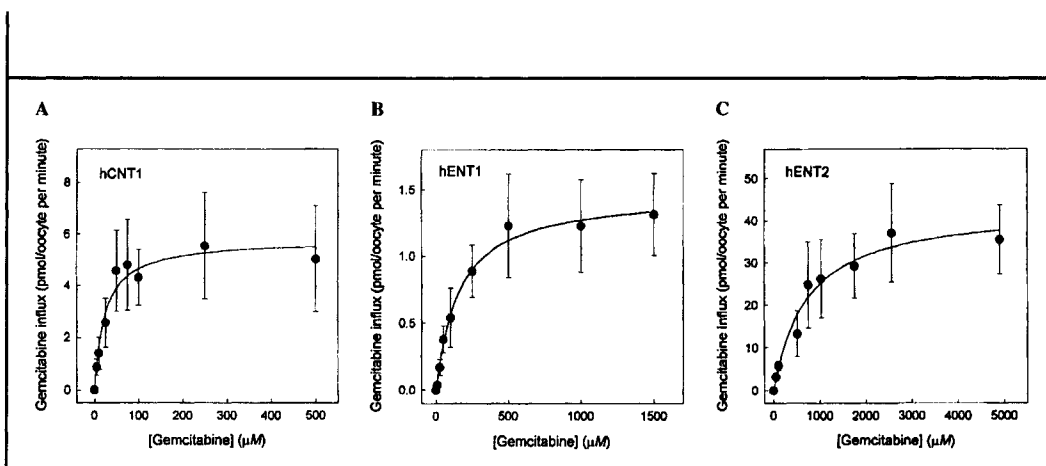


Fig. 2. Concentration dependence of gemcitabine influx. Oocytes were injected with either 10 nL of water alone or 10 nL of water containing 10 ng of messenger RNA transcripts encoding human nucleoside transporters hCNT1, hENT1, or hENT2. After 3 days, inward fluxes of [³H]gemcitabine by (panel A) hCNT1 (1 minute), (panel B) hENT1 (2 minutes), and (panel C) hENT2 (5 minutes) were determined at 20°C in NaCl-containing transport medium. Values represent influx in RNA-injected oocytes minus the corresponding influx in water-injected

cells and are the means with 95% confidence intervals of 10-12 oocytes for each group. Kinetic parameters of transporter-mediated gemcitabine influx are shown in Table 1. In a parallel study of gemcitabine fluxes induced by recombinant hCNT2 (60-minute flux), no mediated transport was detected. hCNT = human concentrative nucleoside transporter; hENT = human equilibrative nucleoside transporter.

Table 1. Kinetic parameters of gemcitabine and uridine influx mediated by human nucleoside transporters*

Nucleoside transporter	Substrate	Apparent K_m , μM (95% CI)	V_{max} , pmol/oocyte \cdot min ⁻¹ (95% CI)	Ratio, $V_{max} : K_m$	Reference No.
hCNT1	Gemcitabine	24 (12-36)	5.8 (5.0-5.4)	0.24	(9)
	Uridine	45 (29-61)	26 (24-28)	0.58	
hCNT2	Gemcitabine	-	-	-	(13)
	Uridine	40 (30-50)	0.74 (0.6-0.84)	0.02	
hENT1	Gemcitabine	160 (120-200)	1.5 (1.4-1.6)	0.010	(8)
	Uridine	240 (180-300)	3.6 (3.2-4.0)	0.015	
hENT2	Gemcitabine	740 (360-1100)	43 (35-51)	0.059	(11)
	Uridine	200 (140-260)	6.4 (6.0-6.8)	0.032	

*h = human; CNT = concentrative nucleoside transporter; ENT = equilibrative nucleoside transporter; CI = confidence interval; - = not observed. Apparent K_m and V_{max} values for gemcitabine influx were derived from the data presented in Fig. 2. For hCNT2, no mediated transport was detected.

DISCUSSION

Our results demonstrated that gemcitabine, like each of the physiologic nucleosides, diffuses only slowly through plasma membranes and requires protein-mediated transport for efficient cell entry. Mediated transport of gemcitabine by recombinant hCNT1, hENT1, and hENT2 was saturable and conformed to Michaelis-Menten kinetics with apparent K_m values of 24, 160, and 740 μM , respectively. These characteristics were similar to those observed previously (26) in human cell lines that produced only a single nucleoside transporter in isolation, in which we also found that diffusional uptake of gemcitabine was slow and that the influx of gemcitabine mediated by recom-

binant hCNT1, hENT1, and hENT2 was saturable with apparent K_m values of 18, 330, and 830 μM , respectively.

Although there have been few prior reports of differences in permeant selectivity or kinetics between ENT1- and ENT2-mediated transport processes, we report here marked differences in kinetics of gemcitabine transport by recombinant hENT1 and hENT2 in *Xenopus* oocytes. hENT1 transports gemcitabine with high affinity and low capacity, while hENT2 transports gemcitabine with low affinity and high capacity. These differences may, in part, explain why bolus infusion of gemcitabine has clinical efficacy against epithelial cancers, while it causes only modest degrees of myelotoxicity. Hematopoietic progenitor cells are believed to

possess predominantly hENT1 nucleoside transport capabilities based on the effectiveness of low concentrations of NBMPR in protecting such cells from the toxicity of cytotoxic nucleosides (27) and the enhancement of antifolate cytotoxicity to hematopoietic progenitor cells by nanomolar concentrations of NBMPR, which prevents nucleoside transporter-mediated thymidine uptake, thereby preventing thymidine rescue from inhibition of *de novo* synthesis of nucleotide precursors (28). In contrast, human epithelial cancer cell lines, including HeLa (26), MCF-7, and MDA-MB-435S (unpublished data), have substantial rates of hENT2-mediated gemcitabine uptake. These observations, taken together, suggest that human epithelial cancers may also possess hENT2 activity and might thereby take up gemcitabine more efficiently than hematopoietic precursors at the high (>50 μM) peak plasma concentrations achieved by 30-minute bolus gemcitabine (29).

Variation in the tissue and tumor distribution of the nucleoside transporters may also explain, in part, the different schedule-dependent toxic effects of bolus-infusion gemcitabine and prolonged-infusion gemcitabine. Gemcitabine is routinely administered on days 1, 8, and 15 of each 4-week cycle. When given as a 30-minute bolus infusion at doses of approximately 1200 mg/m², peak plasma levels exceeding 50 μM are achieved af-

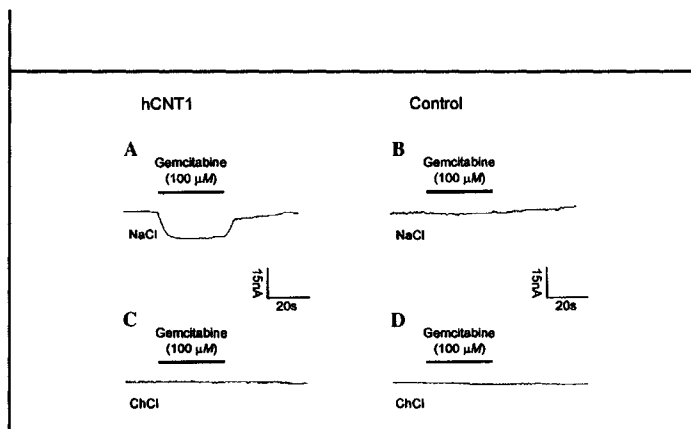


Fig. 3. Sodium currents induced by exposure of human concentrative nucleoside transporter (hCNT1)-producing oocytes to gemcitabine. Oocytes were injected with either 10 nL of water alone or 10 nL of water containing 10 ng of messenger RNA transcript encoding hCNT1. NaCl = Na⁺-containing transport medium; ChCl = choline-containing transport medium. Panel A: Inward current caused by perfusing an RNA-injected oocyte with 100 μM gemcitabine in Na⁺-containing transport medium. Panel B: The same oocyte perfused with 100 μM gemcitabine in transport medium with Na⁺ replaced by choline. No inward current was generated. Panels C and D show the same experiment described in panels A and B above but with a control, water-injected oocyte. No inward currents were generated.

ter 15 minutes (29,30); however, on completion of the infusion, gemcitabine is rapidly eliminated from the serum, with a half-life of 8 minutes (29). This gemcitabine administration schedule produces mild and noncumulative myelotoxicity and minimal hepatotoxicity. However, when given by weekly continuous infusion at doses of 10 mg/m² per minute for 120-280 minutes, median steady-state serum concentrations approach 25 μM, and cumulative myelotoxicity is dose limiting (31). Similarly, prolonging the duration of infusion to 1 hour of an otherwise standard gemcitabine dose causes hepatotoxicity as shown by elevated serum transaminases (32), possibly because of hCNT1-mediated accumulation of gemcitabine in hepatocytes. We have recently demonstrated the presence of hCNT1 transcript in human liver (13), and the rat homologue rCNT1 (33) has been identified functionally and molecularly in rat liver (34).

Although the accumulation of gemcitabine triphosphate by peripheral blood mononuclear cells and leukemic blasts is saturated by gemcitabine dose rates of 10 mg/m² per minute in large part due to saturation of deoxycytidine kinase (35,36), the relative importance of plasma membrane transport and metabolism is not known for other tissues or for solid tumors. Molecular and immunologic probes will be required to define the tissue and tumor distribution of the human

nucleoside transporters and may help guide clinical trials exploring rational scheduling and dosage regimens for the use of gemcitabine in cancer therapy (37).

In addition to using radioisotope flux measurements, we have investigated gemcitabine transportability by the two-electrode, voltage-clamp technique, a method that has not been used previously for the study of native or recombinant nucleoside transporters. These experiments provided a direct demonstration of the sodium dependence of hCNT1-mediated transport of gemcitabine and uridine. By confirming the protein-mediated nature of gemcitabine uptake by recombinant hCNT1 expressed in *Xenopus* oocytes, we have demonstrated that it is possible to use this technique to screen potential sodium-dependent permeants without the requirement for radiolabeling and to determine the relative efficiency of uptake among physiologic and therapeutic nucleosides. This result validates the utility of the *Xenopus* expression system as an appropriate method for kinetic determination of nucleoside drug transport by human nucleoside transport processes.

REFERENCES

- (1) Allegra CJ, Grem JL. Antimetabolites. In: DeVita VT Jr, editor. Cancer: principles and practice of oncology. Philadelphia (PA): Lippincott-Raven; 1997. p. 490-8.
- (2) Heinemann V, Xu YZ, Chubb S, Sen A, Hertel LW, Grindey GB, et al. Cellular elimination of 2',2'-difluorodeoxycytidine 5'-triphosphate: a

mechanism of self-potential. *Cancer Res* 1992;52:533-9.

- (3) Baker CH, Banzon J, Bollinger JM, Stubbe J, Samano V, Robins MJ, et al. 2'-Deoxy-2'-methylene-2'-methyl-5'-diphosphates: potent mechanism-based inhibitors of ribonucleotide reductase. *J Med Chem* 1991;34:1879-84.
- (4) Plunkett W, Huang P, Xu YZ, Heinemann V, Grunewald R, Gandhi V. Gemcitabine: metabolism, mechanisms of action, and self-potential. *Semin Oncol* 1995;22(Suppl 11):3-10.
- (5) Mackey JR, Baldwin SA, Young JD, Cass CE. The role of nucleoside transport in anticancer drug resistance. *Drug Resistance Updates* 1998;1:310-24.
- (6) Griffith DA, Jarvis SM. Nucleoside and nucleobase transport systems of mammalian cells. *Biochim Biophys Acta* 1996;1286:153-81.
- (7) Wang J, Schaner ME, Thomassen S, Su SF, Piquette-Miller M, Giacomini KM. Functional and molecular characteristics of Na⁺-dependent nucleoside transporters. *Pharm Res* 1997;14:1524-32.
- (8) Griffiths M, Beaumont N, Yao SY, Sundaram M, Boumah CE, Davies A, et al. Cloning of a human nucleoside transporter implicated in the cellular uptake of adenosine and chemotherapeutic drugs. *Nat Med* 1997;3:89-93.
- (9) Ritzel MW, Yao SY, Huang MY, Elliott JF, Cass CE, Young JD. Molecular cloning and functional expression of cDNAs encoding a human Na⁺-nucleoside cotransporter (hCNT1). *Am J Physiol* 1997;272:C707-14.
- (10) Crawford CR, Patel DH, Naeve C, Belt JA. Cloning of the human equilibrative, nitrobenzylmercaptapurine riboside (NBMPR)-insensitive nucleoside transporter ei by functional expression in a transport-deficient cell line. *J Biol Chem* 1998;273:5288-93.
- (11) Griffiths M, Yao SY, Abidi F, Phillips SE, Cass CE, Young JD, et al. Molecular cloning and characterization of a nitrobenzylthioinosine-insensitive (ei) equilibrative nucleoside transporter from human placenta. *Biochem J* 1997;328:739-43.
- (12) Wang J, Su SF, Dresser MJ, Schaner ME, Washington CB, Giacomini KM. Na⁺-dependent purine nucleoside transporter from human kidney: cloning and functional characterization. *Am J Physiol* 1997;273:F1058-65.
- (13) Ritzel MW, Yao SY, Ng AM, Mackey JR, Cass CE, Young JD. Molecular cloning, functional expression and chromosomal localization of a cDNA encoding a human Na⁺/nucleoside cotransporter (hCNT2) selective for purine nucleosides and uridine. *Mol Membr Biol* 1999;15:203-11.
- (14) Gutierrez MM, Brett CM, Ott RJ, Hui AC, Giacomini KM. Nucleoside transport in brush border membrane vesicles from human kidney. *Biochim Biophys Acta* 1992;1105:1-9.
- (15) Patil SD, Unadkat JD. Sodium-dependent nucleoside transport in the human intestinal brush-border membrane. *Am J Physiol* 1997;272:C1314-20.
- (16) Chandrasena C, Giltay R, Patil SD, Bakken A, Unadkat JD. Functional expression of human

- intestinal Na⁺-dependent and Na⁺-independent nucleoside transporters in *Xenopus laevis* oocytes. *Biochem Pharmacol* 1997;53:1909-18.
- (17) Washington CB, Giacomini KM, Brett CM. Nucleoside transport in isolated human and rhesus choroid plexus tissue slices. *Pharm Res* 1998;15:1145-7.
- (18) Roovers KI, Meckling-Gill KA. Characterization of equilibrative and concentrative Na⁺-dependent (cif) nucleoside transport in acute promyelocytic leukemia NB4 cells. *J Cell Physiol* 1996;166:593-600.
- (19) Flanagan SA, Meckling-Gill KA. Characterization of a novel Na⁺-dependent, guanosine-specific, nitrobenzylthioinosine-sensitive transporter in acute promyelocytic leukemia cells. *J Biol Chem* 1997;272:18026-32.
- (20) Belt JA, Harper EH, Byl JA, Noel LD. Sodium-dependent nucleoside transport in human myeloid leukemic cell lines and freshly isolated myeloblasts [abstract]. *Proc Am Assoc Cancer Res* 1992;33:20.
- (21) Belt JA, Marina NM, Phelps DA, Crawford CR. Nucleoside transport in normal and neoplastic cells. *Adv Enzyme Regul* 1993;33:235-52.
- (22) Che M, Ortiz DF, Arias IM. Primary structure and functional expression of a cDNA encoding the bile canalicular, purine-specific Na⁺-nucleoside cotransporter. *J Biol Chem* 1995;270:13596-9.
- (23) Huang QQ, Yao SY, Ritzel MW, Paterson AR, Cass CE, Young JD. Cloning and functional expression of a complementary DNA encoding a mammalian nucleoside transport protein. *J Biol Chem* 1994;269:17757-60.
- (24) Yao SY, Ng AM, Ritzel MW, Cass CE, Young JD. Transport of adenosine by recombinant purine- and pyrimidine-selective sodium/nucleoside cotransporters from rat jejunum expressed in *Xenopus laevis* oocytes. *Mol Pharmacol* 1996;50:1529-35.
- (25) Yao SY, Ng AM, Muzyka WR, Griffiths M, Cass CE, Baldwin SA, et al. Molecular cloning and functional characterization of nitrobenzylthioinosine (NBMPR)-sensitive (es) and NBMPR-insensitive (ei) equilibrative nucleoside transporter proteins (rENT1 and rENT2) from rat tissues. *J Biol Chem* 1997;272:28423-30.
- (26) Mackey JR, Mani RS, Selner M, Mowles D, Young JD, Belt JA, et al. Functional nucleoside transporters are required for gemcitabine influx and manifestation of toxicity in cancer cell lines. *Cancer Res* 1998;58:4349-57.
- (27) Cass CE, King KM, Montano JT, Janowska-Wieczorek A. A comparison of the abilities of nitrobenzylthioinosine, dilazep, and dipyrindamole to protect human hematopoietic cells from 7-deazaadenosine (tubercidin). *Cancer Res* 1992;52:5879-86.
- (28) Allay JA, Spencer HT, Wilkinson SL, Belt JA, Blakley RL, Sorrentino BP. Sensitization of hematopoietic stem and progenitor cells to trimetrexate using nucleoside transport inhibitors. *Blood* 1997;90:3546-54.
- (29) Abbruzzese JL, Grunewald R, Weeks EA, Gravel D, Adams T, Nowak B, et al. A phase I clinical, plasma, and cellular pharmacology study of gemcitabine. *J Clin Oncol* 1991;9:491-8.
- (30) Storniolo AM, Allerheiligen SR, Pearce HL. Preclinical, pharmacologic, and phase I studies of gemcitabine. *Semin Oncol* 1997;24(Suppl 7):S7-2-S7-7.
- (31) Touroutoglou N, Gravel D, Raber MN, Plunkett W, Abbruzzese JL. Clinical results of a pharmacodynamically-based strategy for higher dosing of gemcitabine in patients with solid tumors. *Ann Oncol* 1998;9:1003-8.
- (32) Pollera CF, Ceribelli A, Grecco M, Oliva C, Calabresi F. Prolonged infusion gemcitabine: a clinical phase I study at low- (300 mg/m²) and high-dose (875 mg/m²) levels. *Invest New Drugs* 1997;15:115-21.
- (33) Fang X, Parkinson FE, Mowles DA, Young JD, Cass CE. Functional characterization of a recombinant sodium-dependent nucleoside transporter with selectivity for pyrimidine nucleosides (cNT1rat) by transient expression in cultured mammalian cells. *Biochem J* 1996;317:457-65.
- (34) Felipe A, Ferrer-Martinez A, Casado FJ, Pastor-Anglada M. Expression of sodium-dependent purine nucleoside carrier (SPNT) mRNA correlates with nucleoside transport activity in rat liver. *Biochem Biophys Res Commun* 1997;233:572-5.
- (35) Grunewald R, Abbruzzese JL, Tarassoff P, Plunkett W. Saturation of 2828-difluorodeoxycytidine 58 triphosphate accumulation by mononuclear cells during a phase I trial of gemcitabine. *Cancer Chemother Pharmacol* 1991;27:258-62.
- (36) Grunewald R, Kantarjian H, Keating MJ, Abbruzzese J, Tarassoff P, Plunkett W. Pharmacologically directed design of the dose rate and schedule of 2828-difluorodeoxycytidine (Gemcitabine) administration in leukemia. *Cancer Res* 1990;50:6823-6.
- (37) Tempero M, Plunkett W, Ruiz van Haperen V, Hainsworth J, Hochster H, Lenzi R, et al. Randomized phase II trial of dose intense gemcitabine by standard infusion versus fixed dose rate in metastatic pancreatic adenocarcinoma [abstract]. *Proc ASCO* 1999;18:273.

NOTES

Supported by an Alberta Cancer Board New Investigators Award, the National Cancer Institute of Canada (NCIC), with funds from the Terry Fox Foundation, and by the Alberta Cancer Board and the Alberta Heritage Foundation for Medical Research (AHFMR). C. E. Cass is a Terry Fox Cancer Research Scientist of the NCIC. J. D. Young is a Heritage Medical Scientist of the AHFMR.

We thank Eli Lilly and Co. for the gift of gemcitabine and ³H-gemcitabine.

Manuscript received February 23, 1999; revised August 18, 1999; accepted September 3, 1999.

Appendix B:

Molecular Identification and Characterization of Novel Human and Mouse Concentrative Na⁺-Nucleoside Cotransporter Proteins (hCNT3 and mCNT3) Broadly Selective for Purine and Pyrimidine Nucleosides (System *cib*)*

Received for publication, August 24, 2000, and in revised form, October 5, 2000
Published, JBC Papers in Press, October 13, 2000, DOI 10.1074/jbc.M007746200

Mabel W. L. Ritzel[†], Amy M. L. Ng[†], Sylvia Y. M. Yao[†], Kathryn Graham[§], Shaun K. Loewen[¶],
Kyla M. Smith[†], R. Gary Ritzel[†], Delores A. Mowles[§], Pat Carpenter[§], Xing-Zhen Chen[†],
Edward Karpinski[†], Ralph J. Hyde^{**}, Stephen A. Baldwin^{**}, Carol E. Cass[§], and
James D. Young^{††}

From the Membrane Transport Research Group, Departments of [†]Physiology, [§]Oncology, and [¶]Biological Sciences,
University of Alberta, Edmonton, Alberta T6G 2H7, Canada and the ^{**}School of Biochemistry and Molecular Biology,
University of Leeds, Leeds LS2 9JT, United Kingdom

The human concentrative (Na⁺-linked) plasma membrane transport proteins hCNT1 and hCNT2 are selective for pyrimidine nucleosides (system *cit*) and purine nucleosides (system *cif*), respectively. Both have homologs in other mammalian species and belong to a gene family (CNT) that also includes hCNT, a newly identified broad specificity pyrimidine and purine Na⁺-nucleoside symporter (system *cib*) from the ancient marine vertebrate, the Pacific hagfish (*Eptatretus stouti*). We now report the cDNA cloning and characterization of *cib* homologs of hCNT from human mammary gland, differentiated human myeloid HL-60 cells, and mouse liver. The 691- and 703-residue human and mouse proteins, designated hCNT3 and mCNT3, respectively, were 79% identical in amino acid sequence and contained 13 putative transmembrane helices. hCNT3 was 48, 47, and 57% identical to hCNT1, hCNT2, and hCNT, respectively. When produced in *Xenopus* oocytes, both proteins exhibited Na⁺-dependent *cib*-type functional activities. hCNT3 was electrogenic, and a sigmoidal dependence of uridine influx on Na⁺ concentration indicated a Na⁺:uridine coupling ratio of at least 2:1 for both hCNT3 and mCNT3 (*cf* 1:1 for hCNT1/2). Phorbol myristate acetate-induced differentiation of HL-60 cells led to the parallel appearance of *cib*-type activity and hCNT3 mRNA. Tissues containing hCNT3 transcripts included pancreas, bone marrow, trachea, mammary gland, liver, prostate, and regions of intestine, brain, and heart. The hCNT3

gene mapped to chromosome 9q22.2 and included an upstream phorbol myristate acetate response element.

Most nucleosides, including those with antineoplastic and/or antiviral activities (1, 2), are hydrophilic, and specialized plasma membrane nucleoside transporter (NT)¹ proteins are required for uptake into or release from cells (3, 4). NT-mediated transport is therefore a critical determinant of metabolism and, for nucleoside drugs, their pharmacologic actions (5). NTs also regulate adenosine concentrations in the vicinity of cell surface receptors and have profound effects on neurotransmission, vascular tone, and other processes (6, 7).

Seven nucleoside transport processes² that differ in their cation dependence, permeant selectivities and inhibitor sensitivities have been observed in human and other mammalian cells and tissues. The major concentrative systems (*cit*, *cif*, and *cib*) are inwardly directed Na⁺-dependent processes and have been primarily described in specialized epithelia such as intestine, kidney, liver, and choroid plexus, in other regions of the brain, and in splenocytes, macrophages, and leukemic cells (3, 4). Concentrative NT transcripts have also been found in heart, skeletal muscle, placenta, and pancreas. The equilibrative (bidirectional) transport processes (*es* and *ei*) have generally lower substrate affinities and occur in most, possibly all, cell types (3, 4). Epithelia (*e.g.* intestine and kidney) and some nonpolarized cells (*e.g.* leukemic cells) coexpress both concentrative and equilibrative NTs, whereas other nonpolarized cells (*e.g.* erythrocytes) exhibit only equilibrative NTs (3, 4). Systems *cit* and *cif* are generally pyrimidine nucleoside selective and purine nucleoside selective, respectively, whereas systems *cib*, *es*, and *ei* transport both pyrimidine and purine nucleosides. System *ei* also transports nucleobases.

* This work was supported in part by the National Cancer Institute of Canada, with funds from the Canadian Cancer Society, the Alberta Cancer Board, the Natural Sciences and Engineering Research Council of Canada, the Wellcome Trust, and the Medical Research Council of the United Kingdom. Fluorescence *in situ* hybridization mapping and BAC library screening were performed at the Centre for Applied Genomics at the Hospital for Sick Children in Toronto. The costs of publication of this article were defrayed in part by the payment of page charges. This article must therefore be hereby marked "advertisement" in accordance with 18 U.S.C. Section 1734 solely to indicate this fact.

The nucleotide sequence(s) reported in this paper has been submitted to the GenBank™/EBI Data Bank with accession number(s) AF305210 and AF305211.

† Supported by a studentship from the Alberta Heritage Foundation for Medical Research.

†† Heritage Scientist of the Alberta Heritage Foundation for Medical Research. To whom correspondence and requests for reprints should be addressed: Dept. of Physiology, 7-55 Medical Sciences Bldg., University of Alberta, Edmonton, AB T6G 2H7, Canada. Tel.: 780-492-5895; Fax: 780-492-7566; E-mail: james.young@ualberta.ca.

¹ The abbreviations used are: NT, nucleoside transporter; AZT, 3'-azido-2'-deoxythymidine; BAC, bacterial artificial chromosome; CNT, concentrative nucleoside transporter; bp, base pair(s); ENT, equilibrative nucleoside transporter; kb, kilobase(s); NBMPR, nitrobenzylthioinosine (6-[(4-nitrobenzyl)thio]-9-β-D-ribofuranosylpurine); NMDG, N-methyl-D-glucamine; PCR, polymerase chain reaction; RT-PCR, reverse transcriptase-PCR; TM, putative transmembrane helix; EST, expressed sequence tag; contig, group of overlapping clones.

² The abbreviations used in transporter acronyms are: *c*, concentrative; *e*, equilibrative; *s* and *i*, sensitive and insensitive to inhibition by NBMPR, respectively; *f*, formycin B (nonmetabolized purine nucleoside); *t*, thymidine; *g*, guanosine; *b*, broad selectivity.

Molecular cloning studies have isolated cDNAs encoding the human and rat proteins responsible for four of these NT processes (*cit*, *cif*, *es*, and *el*) (8-17). These proteins and their homologs in other mammalian species comprise two previously unrecognized families of integral membrane proteins (CNT and ENT) with quite different predicted architectural designs (3, 4). The relationships of these NT proteins to the processes defined by functional studies are: CNT1 (*cit*), CNT2 (*cif*), ENT1 (*es*), and ENT2 (*el*). Although the NT protein(s) responsible for mammalian *cib* have remained elusive, we have recently identified a CNT protein with *cib*-type transport activity from the ancient marine vertebrate, the Pacific hagfish (*Eptatretus stouti*) (18).³ The CNT family also includes the *Escherichia coli* proton/nucleoside symporter NupC (19). Human and rat CNT1 (650 and 648 residues, 71 kDa), designated hCNT1 and rCNT1, respectively, are 83% identical in amino acid sequence (8, 11) and contain 13 putative TMs with an exofacial glycosylated tail at the carboxyl terminus (18).⁴ hCNT2 (658 residues) (12, 13) is 83% identical to rCNT2 (659 residues) (9, 10) and 72% identical to hCNT1 (11). The hagfish transporter hfCNT (683 residues) (18) is 50-52% identical to h/rCNT1/2 and has a similar predicted membrane topology. NupC (19), in contrast, is a smaller protein with 27% identity to mammalian CNTs, with the major difference being the absence of the equivalents of TM 1-3 and the amino- and carboxyl-terminal regions of the other proteins.

In structure/function studies, the characteristics of hCNT1/2 chimeras and sequence comparisons between h/rCNTs and hfCNT have identified two sets of adjacent residues in TMs 7 and 8 of hCNT1 that, when converted to the corresponding residues in hCNT2, changed the specificity of the transporter from *cit* to *cif* (18). Mutation of the two residues in TM 7 alone produced a protein with intermediate, *cib*-like activity. In this *cit/cib* conversion, mutation of hCNT1 Ser³¹⁹ to Gly was sufficient to enable transport of purine nucleosides, whereas mutation of the adjacent residue Gln³²⁰ to Met (which had no effect on its own) augmented this transport. TMs 7 and 8 have also been identified as potential determinants of substrate selectivity in rCNT1/2 (21), and mutation of rCNT1 Ser³¹⁸ (the rat counterpart of hCNT1 Ser³¹⁹) resulted in a *cib*-type phenotype similar to that seen with the hCNT1 Ser³¹⁹ mutation (22).

Although an earlier study had identified a member of the SGLT glucose transporter family, SNST1, as a candidate *cib*-type transporter (23), its nucleoside-transport activity is very low, and we hypothesized that the missing mammalian concentrative NT was more likely to be a CNT transporter. Following a search for additional mammalian CNT isoforms, we now report the cDNA cloning of new human and mouse members of the CNT transporter family. The encoded proteins, designated hCNT3 and mCNT3, respectively, exhibit strong *cib*-type functional activity when expressed in *Xenopus* oocytes and have primary structures that place them together with hfCNT in a CNT subfamily separate from h/rCNT1/2.

EXPERIMENTAL PROCEDURES

Molecular Cloning of hCNT3. BLAST searches of CNT sequences in the GenBankTM data base identified overlapping human ESTs from mammary gland (AI905993) and colon adenocarcinoma (AW083022) different from established members of the CNT transporter family. Together, they formed a composite cDNA fragment 807 bp in length with an open reading frame of 245 residues followed by 69 bp of 3'-untranslated sequence. The cDNA was 62% identical in nucleotide sequence to corresponding regions of the hCNT1 (U62968) and hCNT2 (AF036109) cDNAs and 68% identical to the hfCNT (AF132298) cDNA. The encoded amino acid sequence was 79% identical to the carboxyl

terminus of hfCNT and 58 and 62% identical, respectively, to hCNT1 and hCNT2.

These indications of a novel human CNT distinct from hCNT1 and hCNT2 were tested by RT-PCR in a panel of total RNA samples from human mammary gland, small intestine, kidney (CLONTECH, Palo Alto, CA), and liver (13). Because the close sequence similarity between the EST composite sequence and hfCNT suggested that the new CNT might correspond to system *cib*, we also performed RT-PCR on differentiated human myeloid HL-60 cells, a source of functional *cib*-type transport activity (see below). First strand cDNA was synthesized using the Superscript Preamplification system (Life Technologies, Inc.) and oligo(dT) as primer. The PCR reaction (30 μ l) contained 50 ng of template first-strand cDNA, 2.5 units of *Taq*-DeepVent DNA polymerase (100:1) and 10 pmol each of the 5'- and 3'-oligonucleotide primers 5'-GAAACATGTTTACTACCCACAG-3' and 5'-GTGGAGTTGAAGGCATTCTCTAAAACGT-3'. Amplification for one cycle at 94 °C for 55 s, 54 °C for 55 s, and 72 °C for 70 s, two cycles at 94 °C for 55 s, 55 °C for 55 s, and 72 °C for 70 s, and 30 cycles at 94 °C for 55 s, 58 °C for 55 s, and 72 °C for 70 s (RobocyclerTM40 Temperature Cycler, Stratagene, La Jolla, CA) generated visible PCR products of the predicted size (480 bp) from four of the samples (differentiated HL-60 cells, mammary gland, small intestine, and liver).

We extended the partial EST cDNA sequence by 5'-rapid amplification of cDNA ends amplification of mRNA from differentiated HL-60 cells using the FirstChoice RLM-RACE kit (Ambion, Austin, TX). Poly(A)⁺-selected RNA was treated with calf intestinal phosphatase to degrade 5'-truncated transcripts, followed by tobacco acid pyrophosphatase to remove cap from the remaining full-length mRNAs. A synthetic RNA adaptor from the kit was then ligated to the full-length 59-monophosphate transcript population using T4 RNA ligase, followed by first strand cDNA synthesis with oligo(dT) as primer. For the initial PCR, the 5'-primer was the outer adaptor primer provided by the kit and the gene-specific 3'-primer was 5'-GATATATATTGCTGCACACCGTTTACAA-3'. Amplification by *Taq*-DeepVent DNA polymerase (100:1) was for 40 cycles at 94 °C for 55 s, 65 °C for 55 s, and 72 °C for 3 min and 1 cycle at 72 °C for 10 min, the reaction mixture being heated to 94 °C for 1 min before addition of the *Taq*-DeepVent DNA polymerase mixture. The PCR reaction mixture was resolved on a 1% agarose gel, and faint bands between 1.5 and 2.0 kb in size were isolated and purified (QIAEX II Gel Extraction kit; Qiagen Inc.). This product was then reamplified by nested PCR (35 cycles at 94 °C for 55 s, 65 °C for 55 s, and 72 °C for 3 min and 1 cycle at 72 °C for 10 min) using an inner 5'-primer from the kit and the gene-specific 3'-primer 5'-TTAGCTCAAACACTCAGCTGTGGGTAGTC-3'. A defined band of ~1.7 kb was isolated, cloned into pGEM-T (Promega, Madison, WI), and sequenced by *Taq* DyeDeoxyterminator cycle sequencing using an automated model 373A DNA Sequencer (Applied Biosystems, Foster City, CA). The inset overlapped the 807-bp EST sequence by 114 bp and generated an additional 1633 bp of upstream sequence. The new composite 2440-bp sequence was 66% identical to the hfCNT cDNA and contained an open reading frame of 691 amino acids. cDNAs containing the complete coding sequence were then obtained by RT-PCR from differentiated HL-60 cells and mammary gland, as described previously, using 5'- and 39primers flanking the open reading frame (5'-CTAAATGAAGAGCCCTTGGGACCT-3' and 5'-AGCATCTGTACTTCAGAGTTCCTACTGG-3'). The resulting ~2.2-kb products were ligated into pGEM-T and sequenced in both directions to give identical 691-residue open reading frames flanked by 92 bp of 5'-untranslated nucleotide sequence and 41 bp of 3'-untranslated sequence.

As expected from their identical nucleotide and predicted amino acid sequences, there was no difference in hCNT3 transport function between cDNA clones isolated from HL-60 cells or mammary gland. Radioisotope transport studies reported in this paper were performed with the HL-60 clone in pGEM-T.

Molecular Cloning of mCNT3. BLAST searches of mouse ESTs in the GenBankTM data base identified 630- and 635-bp sequences from two mammary gland IMAGE clones with 73 and 83% sequence identity to parts of the hCNT3 cDNA sequence. IMAGE clone 1514965 aligned with the 5'-coding region, whereas 1515408 ended 54 bp short of the predicted stop codon. Both clones were obtained from the IMAGE Consortium through the American Type Culture Collection (Manassas, VA). PCR showed that they were incomplete, and sequencing of 1515408 gave an additional 85 bp of sequence to complete the 3'-end of the open reading frame. A cDNA with the complete coding sequence was then obtained by RT-PCR from mouse liver RNA (Jackson Laboratories, Bar Harbor, ME) with 59primer 5'-AGGATGTCCAGGCCAGACCCCGCAAAGA-3' and 3'-primer 5'-AGATCACAATTTATTAGGGATCCAAATTC-3'. First strand cDNA was synthesized using the Thermoscript

³ S. Y. M. Yao, A. M. L. Ng, S. K. Loewen, C. E. Cass, and J. D. Young, manuscript in preparation.

⁴ S. R. Hamilton, S. Y. M. Yao, M. P. Gallagher, P. J. F. Henderson, C. E. Cass, J. D. Young, and S. A. Baldwin, manuscript in preparation.

RT-PCR System (Life Technologies, Inc.), and amplification by *Taq* DeepVent DNA polymerase (100:1) was for 2 cycles at 94 °C for 2 min, 64 °C for 1 min, and 72 °C for 2.5 min, 2 cycles at 94 °C for 1 min, 62 °C for 1 min, and 72 °C for 2.5 min, 30 cycles at 94 °C for 1 min, 60 °C for 1 min, and 72 °C for 2.5 min, and one final extension cycle for 10 min at 72 °C. The resulting ~2.0-kb product was ligated into pGEM-T and subcloned into the enhanced *Xenopus* expression vector pGEM-HE (24). Each was sequenced in both directions, giving identical 703-amino acid residue open reading frames flanked by short 3-bp regions of 5'-untranslated or 3'-nucleotide sequence. By providing additional 5'- and 3'-untranslated sequences from a *Xenopus* β -globin gene, the pGEM-HE construct gave greater functional activity and was used in subsequent transport characterization of the mouse protein. pGEM-HE was also used for electrophysiological studies of hCNT3.

Expression of Recombinant hCNT3 and mCNT3 in *Xenopus* Oocytes. hCNT3 and mCNT3 plasmid DNAs were linearized with *NcoI* (pGEM-T) or *NheI* (pGEM-HE) and transcribed with T7 polymerase mMMESSAGE mMACHINE™ (Ambion). Stage VI oocytes of *Xenopus laevis* (8) were microinjected with 20 nl of water or 20 nl of water containing capped RNA transcripts (20 ng) and incubated in modified Barth's medium (changed daily) at 18 °C for 72 h prior to the assay of transport activity.

hCNT3 and mCNT3 Radioligand Flux Studies. Transport was traced using the appropriate $^{14}\text{C}/^3\text{H}$ -labeled nucleoside, nucleoside drug, or nucleobase (Moravsek Biochemicals, Brea, CA or Amersham Pharmacia Biotech) at a concentration of 1 and 2 $\mu\text{Ci}/\text{ml}$ for ^{14}C - and ^3H -labeled compounds, respectively. [^3H]Cimetidine (2',3'-difluoro-oxoecytidine) was a gift from Eli Lilly Inc. (Indianapolis, IN). Radiochemicals were 98-99% pure (see HL-60 transport studies). Flux measurements were performed at room temperature (20 °C) as described previously (8, 11) on groups of 12 oocytes in 200 μl of transport medium containing 100 mM NaCl, 2 mM KCl, 1 mM CaCl_2 , 1 mM MgCl_2 , and 10 mM HEPES, pH 7.5. Except where otherwise indicated, the nucleoside concentration was 20 μM . At the end of the incubation period, extracellular label was removed by six rapid washes in ice-cold transport medium, and individual oocytes were dissolved in 5% (w/v) SDS for quantitation of oocyte-associated radioactivity by liquid scintillation counting (LS 6000 IC; Beckman). Initial rates of transport (influx) were determined using an incubation period of 5 min (8). Choline replaced sodium in Na^+ dependence experiments, and the transport medium for adenosine uptake contained 1 μM deoxycoformycin to inhibit adenosine deaminase activity. The flux values shown are the means \pm S.E. of 10-12 oocytes, and each experiment was performed at least twice on different batches of cells. Kinetic ($K_{0.5}$ and V_{max}) and Na^+ activation parameters ($K_{0.5}$ and Hill coefficient) \pm S.E. were determined using ENZFITTER (Elsevier-Biosoft, Cambridge, UK) and SigmaPlot (SPSS Inc., Chicago, IL) software, respectively.

Measurement of hCNT3-induced Sodium Currents. Oocytes were voltage clamped using the two-electrode voltage clamp. Membrane currents were measured at room temperature by use of a GeneClamp 500B oocyte clamp (Axon Instruments, Foster City, CA). The microelectrodes were filled with 3 M KCl and had resistances that ranged from 1-2.5 M Ω . The GeneClamp 500B was interfaced to a computer via a Digidata 1200 A/D converter and controlled by Axoscope software (Axon Instruments, Foster City, CA). Current signals were filtered at 20 Hz (four-pole Bessel filter) and sampled at intervals of 20 ms. For data presentation, the signals were further filtered at 0.5 Hz by use of pCLAMP software (Axon Instruments). Cells were not used if resting membrane potentials were unstable or less than -30 mV. For measurements of hCNT3-generated currents, oocyte membrane potentials were clamped at -50 mV. Oocytes were perfused with the same medium used for radioligand flux studies, and transport assays were initiated by changing the substrate-free solution to one containing nucleoside (200 μM). In experiments examining Na^+ dependence, sodium in the medium was replaced by choline.

HL-60 Cell Culture and Differentiation. The human promyelocytic cell line, HL-60, obtained from the American Type Culture Collection, was propagated as suspension cultures in RPMI 1640 medium, supplemented with 10% fetal calf serum using reagents purchased from Life Technologies, Inc. Stock cultures were maintained in 5% CO_2 without antibiotics at 37 °C, subcultured every 3-4 days and demonstrated to be mycoplasma-free. Cell numbers were determined using a Coulter Counter model Z2 (Coulter Electronics Inc., Luton, UK).

To induce differentiation, HL-60 cells (3×10^6) growing in logarithmic phase were placed in 10-cm Falcon Primaria tissue culture plates (Becton Dickinson) in the presence of phorbol 12-myristate 13-acetate (200 ng/ml) (Sigma) freshly dissolved in acetone. After 48 h, the plates were washed once with transport buffer (see below) to remove nonad-

herent cells and then incubated for 15 min in the presence or absence of 100 μM dilazep. Transport assays were performed on the remaining adherent cells. Total RNA and mRNA were prepared from exponentially growing parent and adherent HL-60 cells using the RNeasy Mini Protocol (Qiagen) and Fast Track 2.0 Isolation kit (Invitrogen, Carlsbad, CA), respectively.

HL-60 Radioligand Flux Studies. Nucleoside uptake by differentiated HL-60 cells was measured as described previously (25) by exposing replicate cultures at room temperature to ^3H -labeled permeant (10 μM , 1 $\mu\text{Ci}/\text{ml}$) in sodium or sodium-free transport medium (130 mM NaCl or 130 mM NMDG/HCl and 3 mM K_2HPO_4 , 2 mM CaCl_2 , 1 mM MgCl_2 , 20 mM Tris/HCl, and 5 mM glucose, pH 7.4). Radiochemicals (Moravsek Biochemicals) were 98-99% pure as assessed by high performance liquid chromatography using water-methanol gradients on a C18 reverse phase column, and transport for timed intervals of 1-6 min was terminated by immersion of the culture dish in an excess volume of ice-cold transport solution. Assays to detect concentrative transport were performed in the presence of 100 μM dilazep (a gift from Hoffman La Roche & Co., Basel, Switzerland) to block equilibrative transport of the test nucleoside. Transport by nonadherent parental HL-60 cells was performed as described previously (26) using the inhibitor oil stop method. Values are presented as the means of triplicate measurements \pm S.D.

Tissue and Cell Distribution of hCNT3 mRNA. A human multiple tissue expression (MTE™) RNA array (CLONTECH) and dot blots of mRNA (0.5 μg) from parent and differentiated HL-60 cells on BrightStar-Plus nylon transfer membrane (Ambion) were incubated with a cDNA probe corresponding to hCNT3 amino acid residues 359-549 labeled with ^{32}P using the ^{32}P QuickPrime kit (Amersham Pharmacia Biotech). Hybridization at high stringency (68 °C) was performed using ExpressHyb hybridization solution (CLONTECH) and 100 $\mu\text{g}/\text{ml}$ of sheared herring sperm DNA. Wash conditions were as described in the CLONTECH ExpressHyb user manual. Signals on exposed blots were converted to a high resolution *tiff* image (Hewlett Packard ScanJet 4C) and quantified using the public domain NIH Image program, version 1.60. For Northern analysis, 5- μg samples of mRNA from human pancreas, bone marrow, trachea, intestine, liver, brain, heart, and kidney (CLONTECH) were separated on a 0.8% formaldehyde-agarose gel, blotted on to BrightStar-Plus nylon transfer membrane, and hybridized with the same hCNT3 probe (residues 359-549) under identical high stringency conditions.

Possible cross-hybridization between CNT family members was tested on dot blots of dilutions (0.5 μg -5 ng RNA) of hCNT1, hCNT2, and hCNT3 *in vitro* transcripts. Three identical series of blots were incubated either with hCNT3 probe or with equivalent probes for hCNT1 or hCNT2. The hCNT3 probe, which was 63 and 58% identical in nucleotide sequence to the corresponding regions of hCNT1 and hCNT2, respectively, showed no cross-hybridization with hCNT1 or hCNT2 transcripts. Similarly, there was no cross-reactivity between the hCNT1 and hCNT2 probes and hCNT3 RNA. Some cross-hybridization was seen between the hCNT1 and hCNT2 probes (73% nucleotide sequence identity) and their respective transcripts at RNA loadings \leq 50 ng. Under the conditions of high stringency used in our experiments, the hCNT3 probe was therefore specific.

Quantitative Real Time RT-PCR. In TaqMan™ quantitative RT-PCR (Applied Biosystems), an oligonucleotide probe, labeled with a fluorescent tag at the 5'-end and a quenching molecule at the 3'-end, is located between two PCR primers. The 5'-nucleotidase activity of *Taq* polymerase cleaves the fluorescent dye from the probe during each PCR cycle. The fluorescent signal generated is monitored in real time and is proportional to the amount of starting template in the sample.

RNA from parent or differentiated HL-60 cells was reverse transcribed using the TaqMan™ Gold RT-PCR kit (Applied Biosystems) and subjected to real time PCR using an Applied Biosystems PRISM 7700 Sequence Detection System and TaqMan™ Universal PCR Master Mix kit. Amplification conditions were a single cycle at 50 °C for 2 min and 95 °C for 10 min, followed by 40 cycles at 95 °C for 15 s and 1 min at 60 °C using hCNT3 probe and primers designed using Primer Express software (Applied Biosystems). The hCNT3 probe 5'-6-carboxy-fluorescein-CGGACTACATCCATGCTCCITC-6-carboxy-tetramethylrhodamine-3' was purchased from Applied Biosystems, whereas the 5'- and 3'-primers were 5'-GGGTCCCTAGGAATCGTGATC-3' and 5'-CGAGGGCATATACGCTTTC-3', respectively. GAPDH and 18 S ribosomal RNA probes and primers, used as internal controls, were purchased as a TaqMan™ RNA Control Reagent kit. Relative quantification of hCNT3 message was determined as described previously (27).

Chromosomal Fluorescence *In Situ* Hybridization. Analysis of normal human lymphocyte metaphase chromosomes was performed by

methods described previously (28) using a PCR probe corresponding to hCNT3 amino acid residues 86-685. Chromosomal localization of the gene was also determined by screening an RPCI-11 human male BAC library (29).

RESULTS AND DISCUSSION

Membrane transport studies in various human and other mammalian cell and tissue preparations have produced evidence that concentrative (Na^+ -linked) cellular uptake of nucleosides and nucleoside drugs is mediated by at least three distinct mechanisms (3, 4). Systems *cit* and *cif* are found primarily in specialized epithelia such as intestine, liver, and kidney and have characteristic, overlapping substrate specificities for pyrimidine and purine nucleosides, respectively. As well, a broadly selective transport activity for both pyrimidine and purine nucleosides (system *cib*) has been described (3, 4). Expression cloning and other recombinant DNA strategies have recently established that systems *cit* and *cif* are mediated by isoforms of the CNT transporter family, designated in humans as hCNT1 and hCNT2, respectively (8-13). In the present study, we report the molecular identification and characterization of the human and mouse *cib* transporters and demonstrate that they represent a new mammalian isoform of the CNT transporter family (hCNT3 and mCNT3, respectively).

Molecular Identification of hCNT3 and mCNT3 The possibility that *cib* might be a CNT transporter (18) led to identification of ESTs encoding partially overlapping regions at the carboxyl terminus of a new, previously unrecognized human CNT distinct from hCNT1 or hCNT2. The full-length cDNA obtained by 5'-rapid amplification of cDNA ends/RT-PCR amplification of phorbol 12-myristate 13-acetate-differentiated human myeloid HL-60 cells and by RT-PCR of human mammary gland encoded a 691-residue protein (77 kDa), designated here as hCNT3.⁵ Differentiated HL-60 cells represent a functionally defined source of *cib* transport activity (see below), whereas human mammary gland was the origin of one of the carboxyl terminus ESTs. The hCNT3 sequence enabled us, in turn, to identify ESTs from mouse mammary gland encoding the amino- and carboxyl terminus ends of a mouse homolog. The corresponding full-length mouse cDNA, obtained by RT-PCR from liver (also a source of hCNT3 transcript), encoded a 703-residue protein designated here as mCNT3.⁵

hCNT3 and mCNT3 Amino Acid Sequences hCNT3 was 57% identical in amino acid sequence to hCNT and 48 and 47% identical to hCNT1 and hCNT2, respectively (Fig. 1A). Protein structure algorithms predicted a topology for hCNT3 similar to that of hCNT and hCNT1/2 (20), with relatively large extramembrane amino and carboxyl termini (carboxyl terminus external) linked by 13 TMs and short hydrophilic sequences (≤ 22 residues), with the exception of larger extracellular loops between TMs 5-6, 9-10, and 11-12 (Fig. 1B). Residues within TMs 4-13 were particularly highly conserved between hCNT3 and hCNT (67% sequence identity), whereas TMs 1-3 and the amino and carboxyl termini were much more divergent. The conserved TM 4-13 domains of hCNT3 and hCNT corresponded closely to the predicted membrane architecture of the shorter *E. coli* CNT proton/nucleoside cotransporter NupC (19), suggesting that these regions represent the functionally important core structure of the proteins. We engineered an amino-terminal truncated form of rCNT1 and established that the TM 1-3 region is not required for transport activity.⁶ mCNT3 contained additional amino acids at the amino terminus (Fig. 1A) and was 78% identical in

sequence to hCNT3, 57% identical to hCNT, and 48% identical to mCNT2 (AF079853), the other known mouse CNT.

Since we first identified rCNT1 from rat Jejunum by expression selection in *Xenopus* oocytes in 1994, more than 40 members of the CNT protein family have been identified from mammals, lower vertebrates, insects, nematodes, pathogenic yeast, and bacteria. As shown in Fig. 1C, phylogenetic analysis identified discrete clusters of proteins, including two for bacteria and one for vertebrate transporters. hCNT3 and mCNT3 were placed together with hCNT in a different vertebrate CNT subfamily from the human and other mammalian CNT1 and CNT2 proteins. Characteristically conserved motifs of the CNT transporter family present in hCNT3 and mCNT3 included $\text{G}_2\text{X}_2\text{G}_2\text{X}_2\text{XFC}$ between TMs 5 and 6, $(\text{G/A})\text{KKX}_3(\text{N/T})\text{E}(\text{F/Y})$ $(\text{V/F/T})(\text{A/G/S})(\text{Y/M/F})$ between TMs 11 and 12, and $(\text{G/S})\text{F}(\text{A/S})\text{N}(\text{F/I/P})(\text{S/G})(\text{S/T})\text{X}(\text{G/A})$ in TM 12. In common with other CNTs, hCNT3 and mCNT3 also contained multiple consensus sites for *N*-linked glycosylation, grouped at the carboxyl terminus (hCNT3 Asn⁶³⁶ and Asn⁶⁶⁴, mCNT3 Asn⁶⁴⁸ and Asn⁶⁷⁶). The extracellular location of this region has been confirmed by mutagenesis of rCNT1, which is glycosylated at Asn⁶⁰⁵ and Asn⁶⁴³ (20).

Previously (18), we have identified two adjacent pairs of residues (Ser³¹⁹/Gln³²⁰ and Ser³⁵³/Leu³⁵⁴) in the TM 7-9 region of hCNT1 that, when mutated together to the corresponding residues in hCNT2 (Gly³¹³/Met³¹⁴ and Thr³⁴⁷/Val³⁴⁸), converted hCNT1 (*cib*) into a transporter with *cif*-type functional characteristics. An intermediate broad specificity *cib*-like transport activity was produced by mutation of the two TM 7 residues alone; mutation of Ser³¹⁹ to Gly allowed for transport of purine nucleosides, and this was augmented by mutation of Gln³²⁰ to Met. Mutation of Ser³⁵³ in TM 8 to Thr converted the *cib*-like transport of the TM 7 double mutant into one with *cif*-like characteristics but with relatively low adenosine transport activity. Mutation of Leu³⁵⁴ to Val increased the adenosine transport capability of the TM 7/8 triple mutant, producing a full *cif* transport phenotype. On its own, mutation of Ser³⁵³ converted hCNT1 into a transporter with novel uridine-selective transport properties. The sequences of hCNT3 and mCNT3 at these positions were intermediate between hCNT1 and hCNT2, one member of each pair of residues being identical to the corresponding residue in hCNT1 and the other to that in hCNT2. These sequences in hCNT3 and mCNT3 were identical to hCNT (Gly³⁴⁰/Gln³⁴¹ and Ser³⁷⁴/Val³⁷⁵ in the case of hCNT3).

Functional Expression and Substrate Specificity of Recombinant hCNT3 and mCNT3 hCNT1 and hCNT2 display *cit*- and *cif*-type Na^+ -dependent nucleoside transport activities (11, 13). Therefore, although both hCNT1 and hCNT2 transport uridine and certain uridine analogs, they are otherwise selective for pyrimidine (hCNT1) and purine (hCNT2) nucleosides (except for modest transport of adenosine by hCNT1). hCNT, in contrast, exhibits *cib*-type Na^+ -dependent nucleoside transport activity and is broadly selective for both pyrimidine and purine nucleosides.

Fig. 2A shows a representative transport experiment in *Xenopus* oocytes measuring uptake of uridine and a panel of other radiolabeled pyrimidine and purine nucleosides (cytidine, thymidine, adenosine, guanosine, and inosine) and nucleobases (uracil and hypoxanthine) in cells injected with water alone (control) or with water containing hCNT3 transcripts. Uptake of uridine (20 μM , 30-min flux) by hCNT3-expressing oocytes was Na^+ -dependent (60.7 ± 4.5 and 6.1 ± 0.7 pmol/oocyte in

⁵ GenBank™ /EBI Data Bank accession numbers AF305210 and AF305211.

⁶ M. W. L. Ritzel, A. M. L. Ng, S. Y. M. Yao, K. Graham, S. K. Loewen, K. M. Smith, R. G. Ritzel, D. A. Mowles, P. Carpenter, X.-Z. Chen, E.

Karpinski, R. J. Hyde, S. A. Baldwin, C. E. Cass, and J. D. Young, unpublished observation.

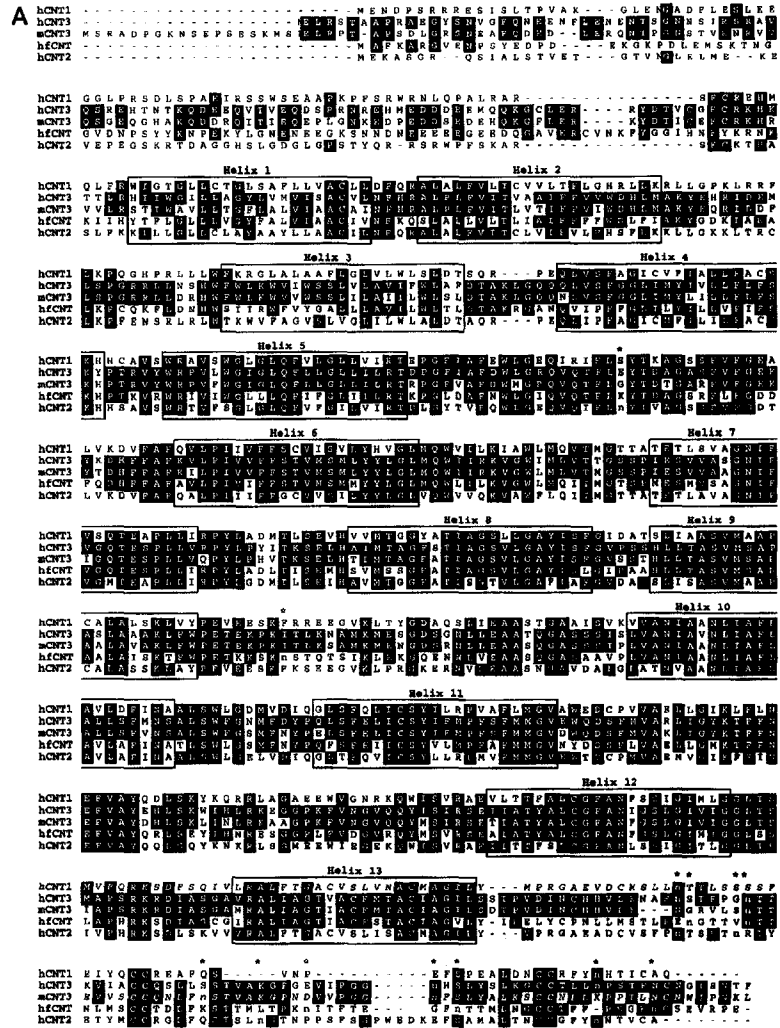


FIG. 1. hCNT3 and mCNT3 are members of the CNT family of nucleoside transporters. *A*, alignment of the predicted amino acid sequences of hCNT3 (GenBank™ accession number AF305210) and mCNT3 (GenBank™ accession number AF305211) with those of hCNT1 (GenBank™ accession number U62968), hCNT2 (GenBank™ accession number AF036109), and hCNT (GenBank™ accession number AF132298) using the GCG FILEUP program. Potential membrane-spanning α -helices are numbered. Putative glycosylation sites in predicted extracellular domains of hCNT3, mCNT3, hCNT1, hCNT2, and hCNT are shown in lowercase (*n*), and their positions are highlighted by an asterisk above the aligned sequences. Residues in hCNT3 identical to one or more of the other transporters are indicated by black boxes. *B*, topological model of hCNT3 and hCNT. Potential membrane-spanning α -helices are numbered, and putative glycosylation sites in predicted extracellular domains in hCNT3 and hCNT are indicated by solid and open stars, respectively. Residues identical in the two proteins are shown as solid circles. Residues corresponding to insertions in the sequence of hCNT3 or hCNT are indicated by circles containing + and - signs, respectively. *C*, phylogenetic tree showing relationships between hCNT3 and mCNT3 and other eukaryotic and prokaryotic members of the CNT transporter family. In addition to those listed in *A*, these are: rCNT1 (rat CNT1, GenBank™ accession number U10279); pkCNT1 (pig kidney CNT1, GenBank™ accession number AF009673); rCNT2 (rat CNT2, GenBank™ accession number U25055); mCNT2 (mouse CNT2, GenBank™ accession number AF079853); rbcCNT2 (rabbit CNT2, GenBank™ accession number AF161716); F27E11.1 (*Caenorhabditis elegans*, GenBank™ accession number AF016413); CG11778_DROME (*Drosophila melanogaster*, GenBank™ accession number AAF58996); CG8083_DROME (*D. melanogaster*, GenBank™ accession number AAF58997); F27E11.2 (*C. elegans*, GenBank™ accession number AF016413); YEIM_HAEIN (*Hemophilus influenzae*, Swissprot accession number P42312); NUPC_ECOLI (*E. coli*, Swissprot accession number P33031); YXJA_BACSU (*Bacillus subtilis*, Swissprot accession number P39141); HI0519_HAEIN (*H. influenzae*, GenBank™ accession number U32734); YUTK_BACSU (*B. subtilis*, GenBank™ accession number Z99120); VC2352_VIBCH (*Vibrio cholerae*, GenBank™ accession number AAF95495); VC1953_VIBCH (*V. cholerae*, GenBank™ accession number AAF95101); VCA0179_VIBCH (*V. cholerae*, GenBank™ accession number AAF96092); UNKNOWN_STREP (*Streptococcus pyogenes*, open reading frame (284) present in contig0001 from the *S. pyogenes* genome sequencing project, Oklahoma University); UNKNOWN_YERPE (*Yersinia pestis*,

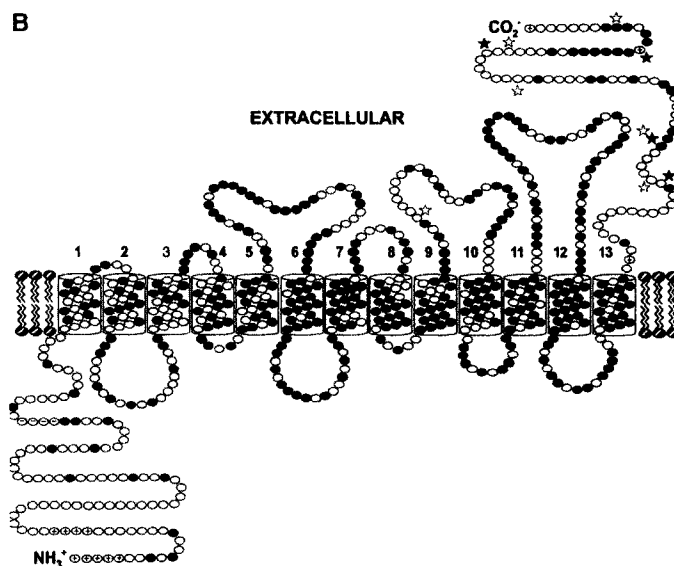


FIG. 1D continued

Na^+ and choline medium, respectively) and concentrative (60.7 pmol/oocyte corresponds to an in-to-out concentration ratio of ~3:1, calculated assuming an oocyte water content of 1 μl). In Na^+ medium, uridine uptake in control water-injected oocytes was only 0.5 ± 0.1 pmol/oocyte, giving a mediated flux (uptake by RNA-injected oocytes minus uptake in water-injected oocytes) of 60.2 pmol/oocyte and a mediated-to-basal flux ratio of 120:1. Consistent with *cib*-type functional activity, each of the other pyrimidine and purine nucleosides tested (cytidine, thymidine, adenosine, guanosine, and inosine) gave similar mediated fluxes. mCNT3 (Fig. 2B) exhibited a similar pattern of Na^+ -dependent *cib*-type functional activity, and neither protein transported uracil or hypoxanthine.

Fig. 3 compares the differences in substrate specificity between hCNT3, mCNT3, hCNT, hCNT1, and hCNT2 by measuring the mediated uptake of three diagnostic nucleoside permeants (uridine, thymidine, and inosine). All five proteins transported uridine. However, hCNT1 (*cit*) exhibited pyrimidine nucleoside selective characteristics (marked thymidine uptake, low inosine transport), whereas hCNT2 (*cif*) was purine nucleoside selective (low thymidine uptake, marked in-

osine transport). hCNT3, mCNT3, and hCNT exhibited similar *cib*-type profiles, with marked transport of both thymidine and inosine. Subsequent in depth transport experiments focussed on the human transporter hCNT3.

Kinetic Properties and Inhibitor Sensitivity of Recombinant hCNT3- Fig. 4 shows representative concentration dependence curves for uridine, cytidine, thymidine, adenosine, guanosine, and inosine, measured as initial rates of transport (5-min flux) in hCNT3-expressing oocytes and in control water-injected cells. Kinetic constants for the hCNT3-mediated component of influx are presented in Table I. K_m values varied between 15 and 53 μM (cytidine, adenosine, uridine, thymidine, guanosine, inosine) and were within the range expected for native *cib*-type transporters (30-32) and for hCNT in oocytes (17-54 μM).³ They were also similar to K_m values obtained previously for permeants of recombinant mammalian CNT1/2 transporters. For example, the hCNT3 K_m for uridine was 22 μM compared with 37-45 μM for hCNT1, rCNT1, and hCNT2 (8, 11, 13). hCNT3 K_m values for thymidine and inosine were 21 and 53 μM , respectively, compared with 13 μM for thymidine transport by rCNT1 (33) and 20 μM for inosine

open reading frame present in contig971 from the *Y. pestis* genome sequencing project, Sanger Center); UNKNOWN_YERPE (*Y. pestis*, open reading frame present in contig976 from the *Y. pestis* genome sequencing project, Sanger Center); UNKNOWN_SALTY (*Salmonella typhi*, open reading frame present in contig18 (CT18) from the *S. typhi* genome sequencing project, Sanger Center); UNKNOWN_BACAN (*Bacillus anthracis*, open reading frame present in contig1985 from the *B. anthracis* genome sequencing project, TIGR); UNKNOWN_BACAN (*B. anthracis*, open reading frame present in contig1745 from the *B. anthracis* genome sequencing project, TIGR); UNKNOWN_CAUCR (*Caulobacter crescentus*, open reading frame present in contig12574 from the *C. crescentus* genome sequencing project, TIGR); UNKNOWN_STAAU (*Staphylococcus aureus*, open reading frame present in contig6185 from the *S. aureus* genome sequencing project, TIGR); UNKNOWN_STAAU (*S. aureus*, open reading frame present in contig6213 from the *S. aureus* genome sequencing project, TIGR); UNKNOWN_STAAU (*S. aureus*, open reading frame present in contig6186 from the *S. aureus* genome sequencing project, TIGR); UNKNOWN_SHEPU (*Shewanella putrefaciens*, open reading frame present in contig6401 from the *S. putrefaciens* genome sequencing project, TIGR); UNKNOWN_SHEPU (*S. putrefaciens*, open reading frame present in contig6410 from the *S. putrefaciens* genome sequencing project, TIGR); UNKNOWN_SHEPU (*S. putrefaciens*, open reading frame present in contig6413 from the *S. putrefaciens* genome sequencing project, TIGR); UNKNOWN_SHEPU (*S. putrefaciens*, open reading frame present in contig6438 from the *S. putrefaciens* genome sequencing project, TIGR); UNKNOWN_SHEPU (*S. putrefaciens*, open reading frame present in contig6438 from the *S. putrefaciens* genome sequencing project, TIGR); PM1292_SHEPU (*Pasteurella multocida*, open reading frame gene product PM1292 from the *P. multocida* genome sequencing project, University of Minnesota); UNKNOWN_CANAL (*Candida albicans*, open reading frame present in contig5-2704 from the *C. albicans* genome sequencing project, Stanford); and UNKNOWN_HAEDU (*Hemophilus ducreyi*, open reading frame present in contig730 from the *H. ducreyi* genome sequencing project, University of Washington). The phylogenetic tree was constructed from a multiple alignment of the 43 CNT sequences using ClustalX version 1.81 for Windows (50) and KITSCH, PHYLIP version 3.57c (51) software (20, 53). The CNT3/hCNT and CNT1/2 subfamilies are highlighted.

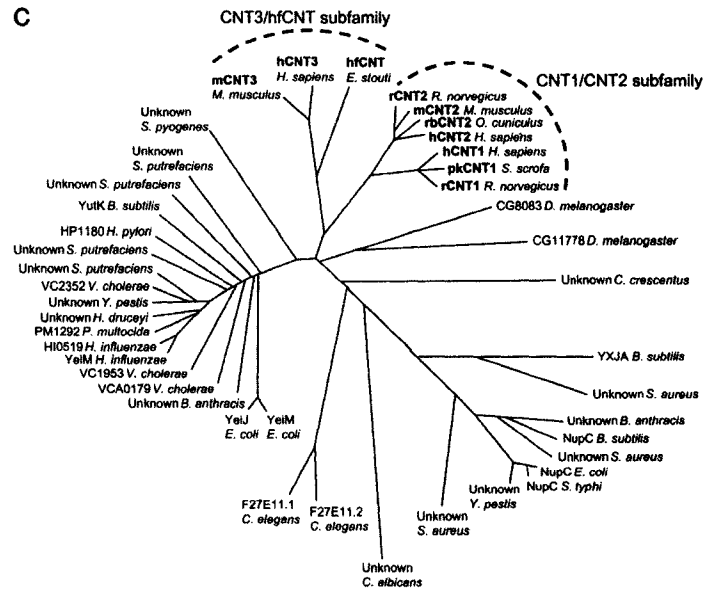


FIG. 1- continued

transport by rCNT2 (21). hCNT3 V_{max} values were in the range 24 and 51 pmol/oocyte.5 min⁻¹ (uridine, thymidine, cytidine, adenosine, guanosine, inosine), giving $V_{max}:K_m$ ratios of 0.9-2.1 (Table I). These data support the *cib*-type specificity profile of hCNT3 shown in Fig. 2A and demonstrate that hCNT3 transports different pyrimidine and purine nucleosides with very similar efficiencies. For all of the nucleosides tested (Fig. 4), influx in water-injected oocytes was linear with concentration, consistent with nonmediated simple diffusion through the lipid bilayer.

In addition to the three major mammalian concentrative nucleoside transport systems *cit*, *cif*, and *cib*, there are two minor Na⁺-dependent nucleoside transport processes, *cs* and *cs*, which have been described only in leukemic cells (34, 35). Although their permeant preferences have not been well defined, the *cs* process (34) accepts guanosine, and the *cs* process (35) accepts adenosine analogs as permeants. In contrast to *cit*, *cif*, and *cib*, both are inhibited by nanomolar concentrations of NBMPR (34, 35). hCNT3 was unaffected by NBMPR or other equilibrative nucleoside transport inhibitors, dipyrindamole and dilazep, at concentrations up to 10 μ M (100 μ M for dilazep, which is more soluble), eliminating hCNT3 as a possible contributor to *cs* or *cs* transport activity (Fig. 5).

hCNT3 Na⁺:Nucleoside Cotransport. Na⁺/nucleoside coupling ratios of 1:1 have been described for various *cit* and *cif* transport activities in different mammalian cells and tissues (reviewed in Ref. 3). In contrast, a coupling ratio of 2:1 has been reported for system *cib* in choroid plexus and microglia (30, 31). In Fig. 6 (A and C), we show for both hCNT3 and mCNT3 that the relationship between uridine influx (10 μ M) and Na⁺ concentration was sigmoidal. Fitting the data to the Hill equation, $v = V_{max} [Na^+]^n / (K_{50}^n + [Na^+]^n)$, gave Hill coefficients (n) of 2.2 ± 0.2 (hCNT3) and 2.3 ± 0.1 (mCNT3), indicating a Na⁺/nucleoside coupling ratio of at least 2:1. Similar values of n (2.0 ± 0.2 and 2.0 ± 0.1 , respectively) were determined from the slopes of Hill plots of the data (Fig. 6, B and D), and in five

independent experiments, Hill plot transformations gave a mean hCNT3 Hill coefficient of 2.1 ± 0.3 . Because rCNT1 exhibited a Hill coefficient of 1 in similar experiments (10), our data establish, for the first time, that the stoichiometry of Na⁺/nucleoside coupling is different in different CNT family members. In this respect, the CNTs resemble the SGLT glucose transporter family, where examples of proteins with 2:1 and 1:1 Na⁺/sugar coupling ratios (SGLT1 and SGLT2, respectively) have been described (36-39). Similarly, the PepT2 and PepT1 proton-linked peptide transporters have 2:1 and 1:1 H⁺/peptide coupling ratios, respectively (40). There was an interesting difference in K_{50} values for Na⁺ activation between hCNT3 and mCNT3 (16 ± 1 and 7 ± 1 mM, respectively), although both transporters were fully saturated with Na⁺ at cation concentrations approaching the physiological concentration range (Fig. 6, A and C).

In addition to radioisotope flux studies, we also used the two-electrode voltage clamp technique to investigate the Na⁺ dependence of hCNT3-mediated nucleoside transport. As shown in Fig. 7, external application of uridine, thymidine, and inosine (200 μ M) to oocytes expressing recombinant hCNT3 induced inward currents for all three nucleosides that returned to baseline upon removal of permeant. No currents were seen in water-injected oocytes or when Na⁺ in the extracellular medium was replaced by choline, demonstrating that hCNT3 functions as a broad specificity electrogenic Na⁺/nucleoside symporter. In parallel with the radioisotope transport data shown in Fig. 6 (A and C), there was a sigmoid relationship between uridine-evoked current and Na⁺ concentration (data not shown). In preliminary experiments to determine directly the Na⁺/nucleoside coupling ratio by simultaneous measurement of Na⁺ currents and [¹⁴C]uridine influx under voltage clamp conditions, as described previously for the SDCT1 rat kidney dicarboxylate transporter (41), we have confirmed that hCNT3 has a Na⁺/nucleoside coupling ratio $\geq 2:1$, whereas for hCNT1 the ratio is 1:1.⁶ A two-Na⁺/one-nucleoside symporter

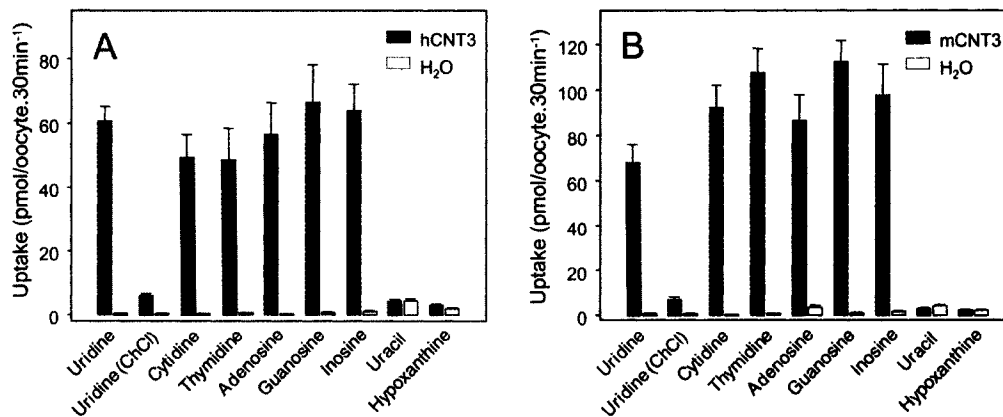


FIG. 2. Uptake of $^{14}\text{C}/^3\text{H}$ -labeled nucleosides and nucleobases by recombinant hCNT3 and mCNT3 expressed in *Xenopus* oocytes. Uptake of nucleosides and nucleobases ($20\ \mu\text{M}$, 20°C , 30 min) in oocytes injected with RNA transcripts or water alone was measured in transport medium containing 100 mM NaCl or 100 mM choline chloride (ChCl).

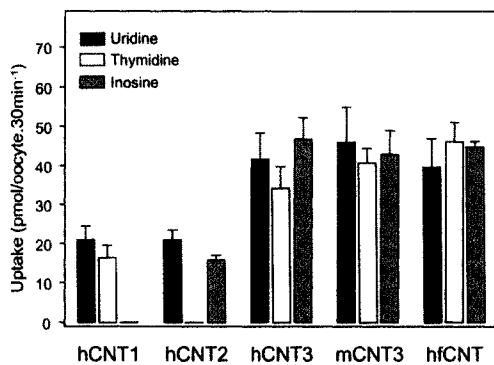


FIG. 3. Nucleoside selectivity of recombinant hCNT3, mCNT3, hCNT1, hCNT2, and hCNT. Transporter-mediated nucleoside uptake ($20\ \mu\text{M}$, 20°C , 30 min) was measured in transport medium containing 100 mM NaCl. Mediated transport was calculated as uptake in RNA-injected oocytes minus uptake in water-injected oocytes.

will have a greater ability to transport permeant against its concentration gradient than a one- Na^+ /one-nucleoside symporter, and they may have evolved to transport nucleosides under different conditions. Experiments are in progress with hCNT, mCNT3, and other CNTs to determine whether the 2:1 stoichiometry is limited to members of the CNT3/hCNT subfamily (Fig. 2A) or has a more widespread distribution.

hCNT3-mediated Transport of Anticancer and Antiviral Nucleoside Drugs- The difference in substrate specificity between CNT1 and CNT2 for physiological pyrimidine and purine nucleosides is reflected in their complementary roles for transport of pyrimidine and purine antiviral and anticancer nucleoside drugs. For example, we have used *Xenopus* oocyte expression to establish that mammalian CNT1/2 proteins transport antiviral dideoxynucleosides: h/rCNT1 transports the AIDS drugs 3'-azido-3'-deoxythymidine (AZT) and 2',3'-dideoxycytidine but not 2',3'-dideoxyinosine whereas hCNT2 transports only 2',3'-dideoxyinosine (8, 11, 13, 42). Gemcitabine, a cytidine analog used in therapy of solid tumors, is a good hCNT1 permeant but is not transported by hCNT2 either in oocytes (43) or in transfected HeLa cells (44). As shown in Fig. 8,

hCNT3, a *cib*-type NT, efficiently transported both pyrimidine (5-fluorouridine, 5-fluoro-2'-deoxyuridine, zebularine, and gemcitabine) and purine (cladribine and fludarabine) anticancer nucleoside drugs. Lower, but still significant, uptake was observed for pyrimidine (AZT and 2',3'-dideoxycytidine) and purine (2',3'-dideoxyinosine) antiviral nucleoside drugs, the magnitudes of the fluxes being similar to those found previously for hCNT1 (AZT and 2',3'-dideoxycytidine) and hCNT2 (2',3'-dideoxyinosine) (11, 13). Only ganciclovir, an antiviral drug with an acyclic ribose moiety, was not transported. Therefore, by virtue of its ability to transport both pyrimidine and purine nucleosides, hCNT3 is capable of transporting a broader range of therapeutic nucleosides than either hCNT1 or hCNT2. Consistent with the present results, thymidine transport by the microglial *cib* transporter was inhibited by AZT (31).

Tissue and Cell Distribution- The *cib* process has been described functionally in rabbit choroid plexus (30), rat MSL-9 microglia cells (31), *Xenopus* oocytes injected with rat jejunal mRNA (32), human leukemic (45) and colorectal carcinoma CaCo cells (46) and, after induction of differentiation, in human HL-60 cells (see below). The human and mouse ESTs that led to the identification of h/mCNT3 were from human/mouse mammary gland and human colon adenocarcinoma, whereas the full-length transporter cDNAs were isolated from differentiated HL-60 cells and mammary gland (hCNT3) and liver (mCNT3). Fig. 9 shows a multiple tissue expression RNA array for 76 human tissues and cells probed with hCNT3 cDNA (a second commercial RNA array from the same supplier gave essentially identical results). As described under "Experimental Procedures," this analysis was performed under conditions of high stringency where there was no cross-hybridization between hCNT3 and hCNT1 or hCNT2. The distribution pattern of hCNT3 transcripts, although selective, was surprisingly widespread. Highest levels were found in a number of normal tissues, including mammary gland, pancreas, bone marrow, and trachea, with substantial levels in various regions of the intestine (but very much less in kidney) and more modest levels in liver, lung, placenta, prostate, testis, and other tissues, including some regions of the brain and heart. hCNT3 transcripts were generally present in fetal tissues but were low in various cultured cell lines, including K562, HeLa, and undifferentiated HL-60 (see also below). In contrast, h/rCNT1 and h/rCNT2 transcripts are found primarily in specialized epithe-

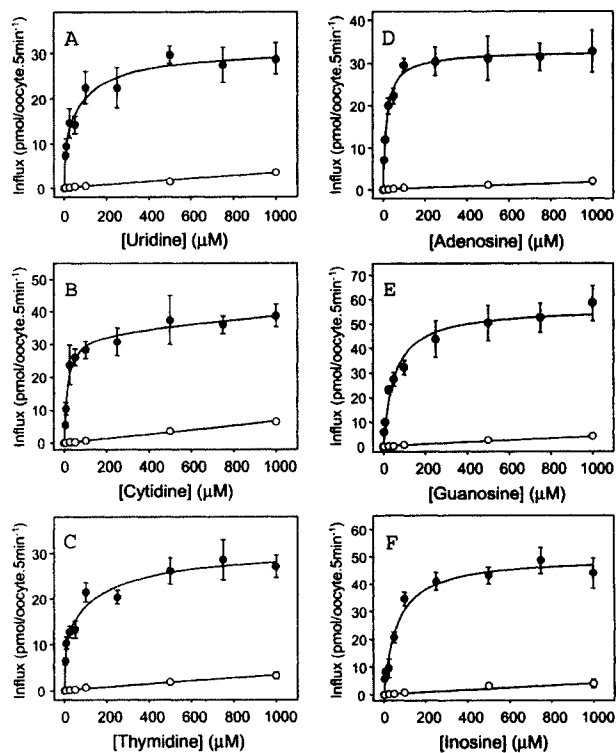


FIG. 4. Kinetic properties of recombinant hCNT3. A-F, initial rates of nucleoside uptake (5-min fluxes, 20°C) in oocytes injected with RNA transcripts (solid circles) or water alone (open circles) were measured in transport medium containing 100 mM NaCl. Kinetic parameters calculated from the mediated component of transport (uptake in RNA-injected oocytes minus uptake in water-injected oocytes) are presented in Table I.

TABLE I
Kinetic properties of hCNT3

Substrate	Apparent K_m^a		V_{max}^a		$V_{max}:K_m$
	μM		$(pmol/oocyte\ min^{-1})$		
Uridine	21.6	5.4	25.8	1.3	1.19
Cytidine	15.4	2.7	32.8	1.0	2.13
Thymidine	21.2	6.3	24.2	1.4	1.14
Adenosine	15.1	1.8	30.4	0.7	2.01
Guanosine	43.0	6.6	51.4	1.8	1.20
Inosine	52.5	12.6	44.8	2.5	0.85

^a From Fig. 4.

lia, including small intestine, kidney, and liver (8±13). Other reported sources of h/rCNT1 and h/rCNT2 transcripts include brain, spleen, heart, pancreas, and skeletal muscle (9, 12, 47). A systematic analysis of CNT1/2 transcript distribution similar to that shown in Fig. 9 for hCNT3 would be helpful to more fully characterize the different expression patterns of the three transporters.

In parallel with the multiple tissue expression RNA array, we also investigated the distribution of hCNT3 transcript in selected tissues by Northern blotting. This less sensitive technique detected hCNT3 transcripts in pancreas, bone marrow, and trachea but not in intestine, liver, brain, or heart (Fig. 10). Kidney, as expected from Fig. 9, was also negative. In pancreas, bone marrow, and trachea, three bands were apparent: a major 5.3-kb transcript and secondary bands at 6.5 and 4.8 kb. Although two of the bands were similar in size to the major transcripts of hCNT1 (3.4 kb) and hCNT2 (4.5-kb) (13), the blot was probed at high stringency under conditions where there

was no cross-reactivity with hCNT1/2 (see "Experimental Procedures"). It is likely, therefore, that they represent alternate hCNT3 gene transcripts rather than cross-hybridization with other CNT family members. The absence of bands in kidney, which contains transcripts for both hCNT1 and hCNT2 (13), is further evidence of the specificity of the hCNT3 probe. The same tissues (plus mammary gland) were also analyzed by TaqMan™ quantitative RT-PCR using hCNT3-specific primers as described below for HL-60 cells. Relative levels of hCNT3 transcript by this method were pancreas > bone marrow, trachea, intestine > mammary gland >> liver, brain, heart > kidney (data not shown).

HL-60 Cells (Functional Studies)- The human promyelocytic leukemia cell line HL-60 can be induced to differentiate into adherent monocyte/macrophage-like cells treatment with phorbol esters (48, 49). Upon differentiation, the cells exhibit a decrease in equilibrative, Na⁺-independent nucleoside transport that is accompanied by an increase in concentrative, Na⁺-dependent transport of both pyrimidine and purine nucleosides (50). To rigorously identify the concentrative transport process(es) contributing to this uptake, we first determined the uridine transport profile of parent and phorbol 12-myristate 13-acetate-treated HL-60 cells under conditions previously shown to be optimal for induction of the concentrative transport activity (50). Equilibrative transport was measured by replacing Na⁺ in the transport medium with NMDG, and concentrative transport was determined in the presence of Na⁺ but with the addition of dilazep (100 μM) to inhibit equilibrative transport activity. We have shown that this concentration of dilazep has no effect on hCNT3 transport activity (Fig. 5). Although previ-

Fig. 5. Recombinant hCNT3 is not inhibited by NBMPR, dipyridamole, or dilazep. Initial rates of transporter-mediated uridine uptake ($20 \mu\text{M}$, 20°C , 5 min) were measured in transport medium containing 100 mM NaCl in the absence or presence of $1\text{--}10 \mu\text{M}$ NBMPR and dipyridamole or $1\text{--}100 \mu\text{M}$ dilazep. Oocytes were incubated with inhibitor for 30 min before the addition of permeant. Mediated transport was calculated as uptake in RNA-injected oocytes minus uptake in water-injected oocytes (uptake of uridine by water-injected oocytes was unaffected by NBMPR, dipyridamole, or dilazep).

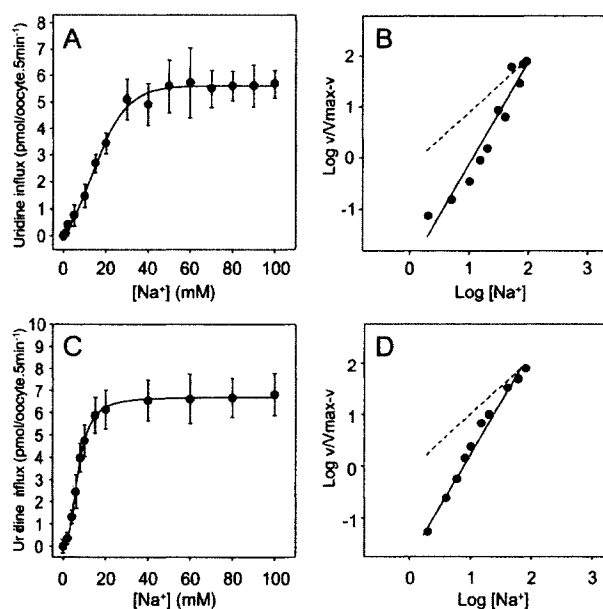
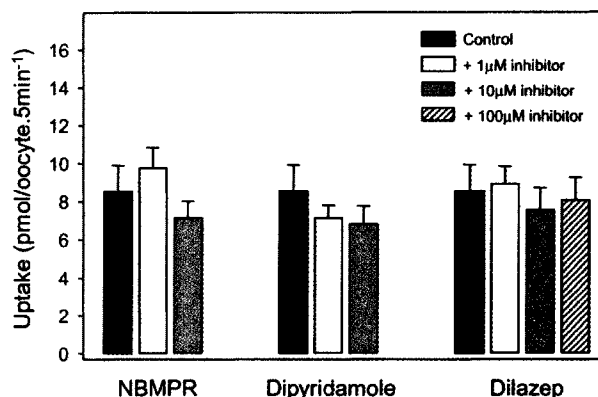


Fig. 6. Sodium dependence of influx of uridine mediated by recombinant hCNT3 and mCNT3. Initial rates of transporter-mediated uptake of uridine ($10 \mu\text{M}$, 20°C , 5 min) by hCNT3 (A) and mCNT3 (C) were measured in transport medium containing $0\text{--}100 \text{ mM}$ NaCl using choline chloride to maintain isosmolality. Mediated transport was calculated as uptake in RNA-injected oocytes minus uptake in water-injected oocytes (uptake of uridine by water-injected oocytes was not Na⁺-dependent). B and D are Hill plots of the hCNT3 and mCNT3 data, respectively. K_{50} values and Hill coefficients (n) are given in the text. Broken lines in B and D correspond to n values of 1.

ous studies have reported a small amount of Na⁺-dependent transport activity in untreated HL-60 cells (50, 51), our assays did not detect any concentrative transport in the parent cell line, which exhibited only equilibrative uptake of 10 mM uridine (Fig. 11A). However, there was a notable increase in Na⁺-dependent uridine transport in differentiated, adherent HL-60 cells (Fig. 11B). Uptake of thymidine and formycin B (a non-metabolized analog of inosine) was then used to define which of the concentrative transport processes (*cit*, *cif*, *cib*) was active in differentiated HL-60 cells (Fig. 11, C and D). Both nucleosides were taken up by the concentrative process(es) of differentiated HL-60 cells. Transport of thymidine was totally inhibited by unlabeled thymidine, inosine, and uridine, whereas formycin B uptake was reciprocally inhibited by thymidine. Thus, *cib* (rather than *cit* + *cif*) was the dominant concentrative transport activity in differentiated HL-60 cells. Consistent with this result, concentrative uridine transport was inhibited by uri-

dine, thymidine, and inosine (data not shown). Dot blot analysis (Fig. 9A) and nonquantitative RT-PCR (Fig. 12A) established that the appearance of *cib* functional activity correlated with substantially increased levels of hCNT3 transcripts in differentiated versus parent HL-60 cells, the latter exhibiting only small amounts of hCNT3 mRNA. In RT-PCR experiments, parent and differentiated HL-60 cells were negative for hCNT2 mRNA and expressed only very small amounts of hCNT1 mRNA, most likely as a consequence of bleed-through transcription (data not shown). These results provided further evidence that the concentrative nucleoside transport activity seen in differentiated HL-60 cells was mediated by *cib* and not by (*cit* + *cif*).

HL-60 Cells (TaqManTM Quantitative Real Time RT-PCR)—The relative levels of hCNT3 transcripts in HL-60 parent and differentiated cells were determined by quantitative real time RT-PCR (Fig. 12B). Glyceraldehyde-3-phosphate dehydrogen-

FIG. 7. Sodium currents induced by exposure of recombinant hCNT3 to nucleoside permeants. Upper left panel, inward currents caused by perfusing an hCNT3-expressing oocyte at room temperature with 200 μ M inosine, uridine, or thymidine in Na⁺-containing transport medium (NaCl). Upper right panel, the same oocyte perfused with 200 μ M inosine, uridine, or thymidine in transport medium with Na⁺ replaced by choline (ChCl). No inward currents were generated. Lower panels, the same experiments described for upper panels above but with a control water-injected oocyte. No inward currents were generated.

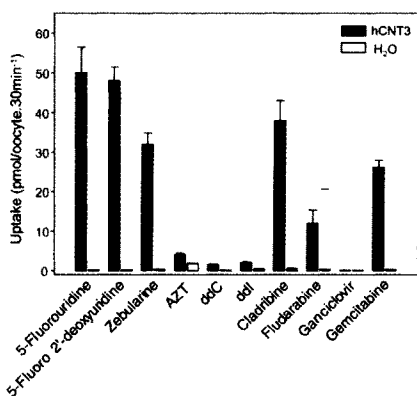
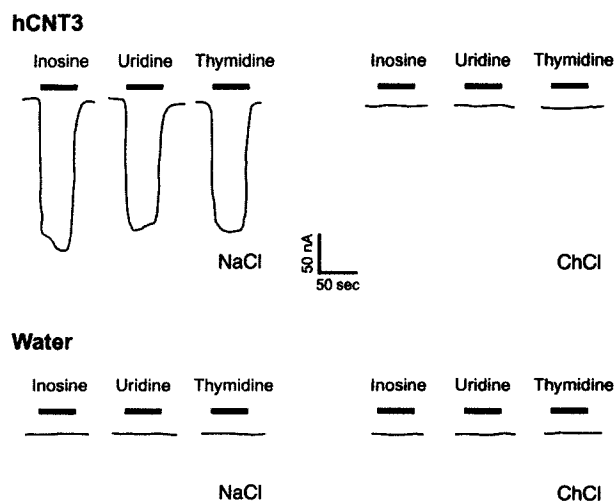


FIG. 8. Uptake of ³H-labeled anticancer and antiviral nucleoside drugs by recombinant hCNT3 expressed in *Xenopus* oocytes. Uptake of nucleoside drugs (20 μ M, 20°C, 30 min) in oocytes injected with RNA transcripts or water alone was measured in transport medium containing 100 mM NaCl. ddC, 2',3'-dideoxycytidine; ddI, 2',3'-dideoxyinosine.

ase and hCNT3 were demonstrated to amplify with equal efficiency, and glyceraldehyde-3-phosphate dehydrogenase was therefore used as the internal control to normalize levels of expression of hCNT3 mRNA between samples. To compare samples, a threshold line was set at the phase of the PCR reaction during which the fluorescent signal accumulated exponentially. As shown in Fig. 12B, there was a substantial difference between the HL-60 parent and differentiated samples in the PCR cycle numbers at the threshold line, and three independent experiments gave a mean (\pm S.E.) ratio of 4.08 ± 0.09 , indicating (because PCR amplification is an exponential process) that there was 16.9 ± 1.05 more hCNT3 mRNA in differentiated versus parent HL-60 cells. Similar results were obtained when the data were normalized to 18 S gene expression (data not shown). The human tumor cell lines K562 (erythrocytosis) and HeLa (cervical carcinoma) were also tested in this assay (data not shown) and gave signals that were close to

background levels (see also Fig. 9A). These results, taken with those of the transport experiments, indicated that the small amount of hCNT3 transcription in the HL-60 parent cells did not result in enough protein to be functionally detected, whereas the differentiated cells that expressed 16-fold more hCNT3 mRNA had a readily measurable *cib* transport process. Because the analyses were performed on exponentially growing parent and differentiated cells, the difference in transcript levels between parent and differentiated HL-60 cells could not be attributed to cell proliferation.

Chromosomal Localization of the hCNT3 Gene- Although the genes encoding hCNT1 and hCNT2 have both been mapped to chromosome 15 (15q25-26 (11) and 15q15 (13), respectively), fluorescence *in situ* hybridization analysis localized the hCNT3 gene to 9q22.2. The same chromosomal band location was determined by screening a human BAC library. Searches of the Sanger Center human genomic sequence data base, and the Unfinished High Throughput Genomic Sequence GenBank™ data base identified two chromosome 9 clones (GenBank™ accession numbers AL356134 and AL353787) containing multiple hCNT3 genomic fragments that, when aligned, revealed 27.3-kb of composite hCNT3 gene sequence containing 74% of the hCNT3 coding sequence. The coding sequence that was obtained was an exact match with corresponding regions of the hCNT3 cDNA sequence.⁵ Analysis of hCNT3 5'-genomic sequence in the potential upstream promoter region of the gene revealed the presence of a eukaryotic phorbol myristate acetate (ester) response element (52) with the sequence 5'-TGAGTCA-3' that may potentially contribute to the transcriptional regulation of hCNT3 seen in HL-60 cells. Studies are in progress to compare the organization of the hCNT3 gene with that for hCNT1 (32 kb), which has been determined to contain 18 exons separated by 17 introns (GenBank™ accession numbers 187967-187978).

Conclusions- The CNT protein family in humans is represented by three members, hCNT1, hCNT2, and the presently described hCNT3. Searches of the Unfinished High Throughput Genomic Sequence GenBank™ data base have so far revealed no other closely related members of this family in humans.⁶ hCNT3 is a transcriptionally regulated electrogenic transport protein that, unlike hCNT1 and hCNT2, has a broad permeant selectivity for pyrimidine and purine nucleosides and

FIG. 9. Tissue distribution of hCNT3 mRNA. A and B, a commercial human multiple tissue expression RNA array probed with a ^{32}P -labeled cDNA corresponding to hCNT3 amino acid residues 359-549. The *inset* in A is a dot blot of mRNA (0.5 μg) from suspension parent and adherent differentiated HL-60 cells probed with the same cDNA. The numbered samples are: 1, leukemia (undifferentiated HL-60); 2, HeLa S3; 3, leukemia (K-562); 4, leukemia (MOLT-4); 5, Burkitt's lymphoma (Raji); 6, Burkitt's lymphoma (Daudi); 7, colorectal adenocarcinoma (SW480); 8, lung carcinoma (A549); 9, whole brain; 10, cerebral cortex; 11, frontal lobe; 12, parietal lobe; 13, occipital lobe; 14, temporal lobe; 15, paracentral gyrus of cerebral cortex; 16, pons; 17, cerebellum (left); 18, cerebellum (right); 19, corpus callosum; 20, amygdala; 21, caudate nucleus; 22, hippocampus; 23, medulla oblongata; 24, putamen; 25, substantia nigra; 26, accumbens nucleus; 27, thalamus; 28, pituitary gland; 29, spinal cord; 30, esophagus; 31, stomach; 32, duodenum; 33, jejunum; 34, ileum; 35, ileocecum; 36, appendix; 37, colon (ascending); 38, colon (transverse); 39, colon (descending); 40, rectum; 41, heart; 42, aorta; 43, atrium (left); 44, atrium (right); 45, ventricle (left); 46, ventricle (right); 47, interventricular septum; 48, apex of the heart; 49, kidney; 50, skeletal muscle; 51, spleen; 52, thymus; 53, peripheral blood leukocyte; 54, lymph node; 55, bone marrow; 56, trachea; 57, lung; 58, placenta; 59, bladder; 60, uterus; 61, prostate; 62, testis; 63, ovary; 64, liver; 65, pancreas; 66, adrenal gland; 67, thyroid gland; 68, salivary gland; 69, mammary gland; 70, fetal brain; 71, fetal heart; 72, fetal kidney; 73, fetal liver; 74, fetal spleen; 75, fetal thymus; 76, fetal lung; 77, human DNA (100 ng); 78, human DNA (500 ng).

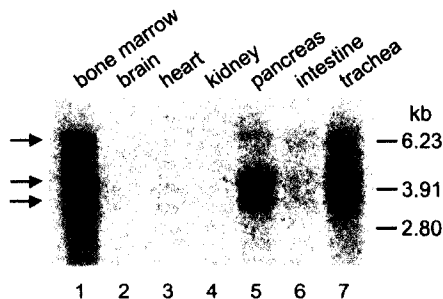
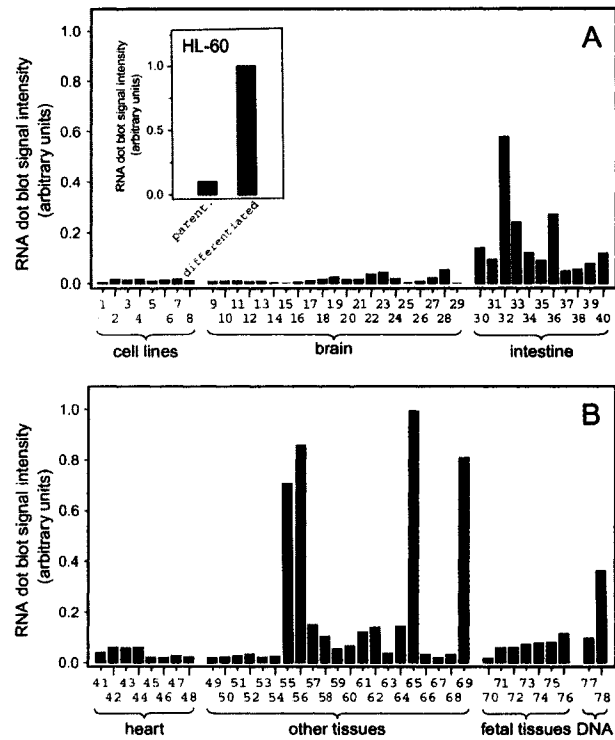


FIG. 10. High stringency Northern analysis of mRNA from human tissues probed with ^{32}P -labeled hCNT3 cDNA. Samples of human tissue mRNA (5 μg) were separated on a 0.8% formaldehyde-agarose gel and blotted on to BrightStar-Plus nylon transfer membrane. Hybridization with a radiolabeled cDNA probe for the coding sequence of hCNT3 amino acid residues 359-549 was performed under high stringency conditions where there was no cross-reactivity with hCNT1 or hCNT2. Arrows indicate the positions of three bands in pancreas, bone marrow with sizes of 3.5, 4.2, and 6.5 kb.

nucleoside drugs. Hill-type analysis of the relationship between uridine influx and Na^+ concentration indicated a Na^+ :uridine coupling ratio of at least 2:1, compared with 1:1 for hCNT1/2. These characteristics and the induction of hCNT3 mRNA in HL-60 cells following phorbol ester treatment identified hCNT3 as the physiological human *cib* transporter. A mouse homolog of hCNT3 (mCNT3) was also cloned, suggesting

that CNT3 is widely distributed in mammals.

A candidate *cib*-type transporter SNST1 that is related to the Na^+ -dependent glucose transporter SGLT1 was identified in 1992 in rabbit kidney (23). There is no sequence similarity between SNST1 and either the CNT or ENT protein families. Although recombinant SNST1, when expressed in oocytes, stimulated low levels of Na^+ -dependent uptake of uridine that was inhibited by pyrimidine and purine nucleosides (*i.e.* *cib*-type pattern), the function of this protein remains unclear because the rate of uridine transport in oocytes was only 2-fold above endogenous (background) levels, whereas a > 100-fold stimulation was observed with h/mCNT3. It is likely that the true physiological substrate of SNST1 is a low molecular weight metabolite for which there is overlapping permeant recognition with nucleosides.

hCNT3 and mCNT3 are more closely related to the hagfish transporter hCNT than to mammalian CNT1/2 and thus form a separate CNT subfamily. Hagfish diverged from the main line of vertebrate evolution about 550 million years ago and represent the most ancient class of extant vertebrates. The high degree of amino acid sequence similarity between h/mCNT3 and hCNT in the TM 4-13 region (67% sequence identity) may indicate functional constraints on the primary structure of this domain and suggests that *cib*-type concentrative NTs fulfill important physiological functions. The tissue distribution of hCNT3 transcripts was more widespread than anticipated from previous studies of *cib* functional activity and is different from that of either CNT1 or CNT2. Although transcripts for mammalian CNT1 and CNT2 have been described in jejunum, kidney, liver, and brain (CNT1) and jejunum, kidney,

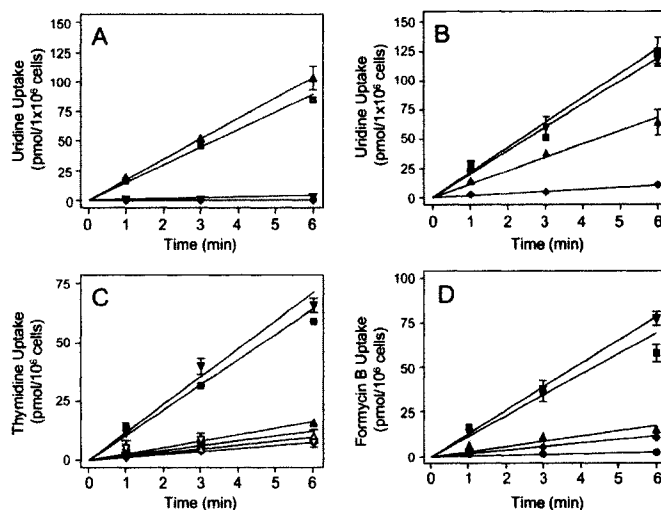


FIG. 11. Time courses of ^3H -labeled uridine, thymidine, and formycin B uptake by HL-60 cells. *A* and *B*, uptake of $10\ \mu\text{M}$ uridine (20°C) by suspension parent (*A*) and adherent differentiated (*B*) HL-60 cells. Total transport (square, no inhibitor, Na^+ -containing medium) was compared with equilibrative transport (upward triangle, no inhibitor, NMDG-containing medium), concentrative transport (downward triangle, $100\ \mu\text{M}$ dilazep, Na^+ -containing medium), and diffusion (diamond, $100\ \mu\text{M}$ dilazep, NMDG-containing medium). *C* and *D*, uptake of $10\ \mu\text{M}$ thymidine (*C*) and formycin B (*D*) by the concentrative transport process in adherent differentiated HL-60 cells. Uptake of each permeant was measured at 20°C to demonstrate total transport (square, no inhibitor, Na^+ -containing medium), equilibrative transport (upward triangle, no inhibitor, NMDG-containing medium), concentrative transport (downward triangle, $100\ \mu\text{M}$ dilazep, Na^+ -containing medium), and diffusion (diamond, $100\ \mu\text{M}$ dilazep, Na^+ -containing medium). In addition, concentrative transport, in the presence of Na^+ and $100\ \mu\text{M}$ dilazep, of each permeant was assessed in the presence of competing unlabeled nucleosides including $1\ \text{mM}$ thymidine (circle), $1\ \text{mM}$ inosine (open downward triangle), and $1\ \text{mM}$ uridine (open upward triangle).

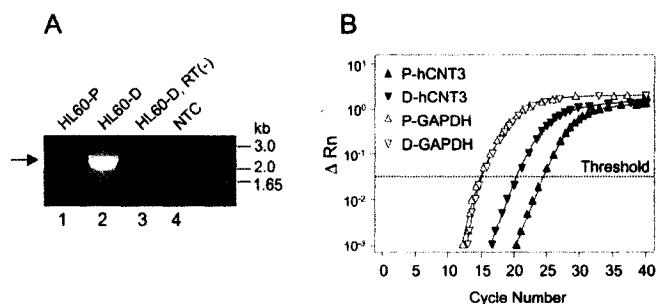


FIG. 12. Nonquantitative RT-PCR and TaqManTM quantitative RT-PCR of hCNT3 transcripts in HL-60 cells. *A*, RNA from suspension parent (HL60-P, lane 1) and adherent differentiated (HL60-D, lane 2) cells in exponential growth was subjected to RT followed by PCR using hCNT3 primers flanking the hCNT3 open reading frame (see "Experimental Procedures"), and the products were run on an ethidium bromide-stained agarose gel. hCNT3-specific PCR products migrated at the expected size of $\sim 2.2\ \text{kb}$ (arrow). The negative controls were RNA preparations from differentiated HL-60 cells that were subjected to PCR but not RT (RT(-), lane 3) and that did not contain template (NTC, lane 4). A predominant band was amplified from the HL-60 differentiated cells (lane 2), whereas a faint band of the same size was amplified from the HL-60 parent sample (lane 1). The RT-free (lane 3) and template-free (lane 4) preparations were both negative. *B*, real time quantitative PCR was performed on cDNA from HL-60 parent (P, upward triangles) or differentiated (D, downward triangles) cells in exponential growth using primers and probes specific for either hCNT3 (solid symbols) or glyceraldehyde-3-phosphate dehydrogenase (open symbols). The ΔR_n , or change in reporter fluorescence normalized to the cycle-to-cycle signal from a passive reference dye, is plotted against the PCR cycle number. The cycle threshold, C_t , values were assessed at the point at which ΔR_n values crossed the threshold value, which was above background and within the exponential phase of the reaction. The values plotted are from representative samples. The results of three experiments, each with duplicate samples, were used to calculate the difference in hCNT3 transcript expression between the two cell populations (see "Results and Discussion"). The template-free control values were at background levels.

liver, spleen, heart, skeletal muscle, and pancreas (CNT2), the highest levels of hCNT3 transcripts were found in pancreas, bone marrow, trachea, mammary gland, and duodenum. Clinically, hCNT3 may be expected to contribute to the concentrative cellular uptake of both anticancer and antiviral nucleoside drugs. Future studies of the transcriptional regulation of the

hCNT3 gene will enhance our understanding of its physiological function(s) and therapeutic potential.

REFERENCES

- Perigaud, C., Gosselin, G., and Imbach, J. L. (1992) *Nucleosides Nucleotides* 11, 903-945
- Handschumacher, R. E., and Cheng, C. Y. (1993) in *Cancer Metabolism*

- (Holland, E., Fret, E., Bast, R. C., Kufe, D. W., Morton, D. L., and Weichselbaum, R. R., eds) pp. 712-732, Lea & Febiger, Philadelphia, PA
3. Cass, C. E. (1995) in *Drug Transport in Antimicrobial and Anticancer Chemotherapy* (Georgopapadakou, N. H., ed) pp. 404-451, Marcel Dekker, New York
 4. Baldwin, S. A., Mackey, J. R., Cass, C. E., and Young, J. D. (1998) *Mol. Med. Today* **5**, 216-224
 5. Mackey, J. R., Baldwin, S. A., Young, J. D., and Cass, C. E. (1998) *Drug Resistance Updates* **1**, 310-324
 6. Fredholm, B. B. (1997) *Curr. Med. Chem.* **4**, 35-66
 7. Shryock, J. C., and Belardinelli, L. (1997) *Am. J. Cardiol.* **79**, 2-10
 8. Huang, Q. Q., Yao, S. Y. M., Ritzel, M. W. L., Paterson, A. R.-P., Cass, C. E., and Young, J. D. (1994) *J. Biol. Chem.* **269**, 17757-17760
 9. Che, M., Ortiz, D. F., and Arias, I. M. (1995) *J. Biol. Chem.* **270**, 13596-13599
 10. Yao, S. Y. M., Ng, A. M. L., Ritzel, M. W. L., Gati, W. P., Cass, C. E., and Young, J. D. (1996) *Mol. Pharmacol.* **50**, 1529-1535
 11. Ritzel, M. W. L., Yao, S. Y. M., Huang, M. Y., Elliot, J. F., Cass, C. E., and Young, J. D. (1997) *Am. J. Physiol.* **272**, C707-C714
 12. Wang, J., Su, S. F., Dresser, M. J., Schaner, M. E., Washington, C. B., and Giacomini, K. M. (1997) *Am. J. Physiol.* **273**, F1058-F1065
 13. Ritzel, M. W. L., Yao, S. Y. M., Ng, A. M. L., Mackey, J. R., Cass, C. E., and Young, J. D. (1998) *Mol. Membr. Biol.* **15**, 203-211
 14. Griffiths, M., Beaumont, N., Yao, S. Y. M., Sundaram, M., Bouman, C. E., Davies, A., Kwong, F. Y. P., Coe, I. R., Cass, C. E., Young, J. D., and Baldwin, S. A. (1997) *Nat. Med.* **3**, 89-93
 15. Yao, S. Y. M., Ng, A. M. L., Muzyka, W. R., Griffiths, M., Cass, C. E., Baldwin, S. A., and Young, J. D. (1997) *J. Biol. Chem.* **272**, 28423-28430
 16. Griffiths, M., Yao, S. Y. M., Abidi, F., Phillips, S. E. V., Cass, C. E., Young, J. D., and Baldwin, S. A. (1997) *Biochem. J.* **328**, 739-743
 17. Crawford, C. R., Patel, D. H., Naeve, C., and Belt, J. A. (1998) *J. Biol. Chem.* **273**, 5288-5293
 18. Loewen, S. K., Ng, A. M. L., Yao, S. Y. M., Cass, C. E., Baldwin, S. A., and Young, J. D. (1999) *J. Biol. Chem.* **274**, 24475-24484
 19. Craig, J. E., Zhang, Y., and Gallagher, M. P. (1994) *Mol. Microbiol.* **11**, 1159-1168
 20. Thompson, J. D., Gibson, T. J., Plewniak, F., Jeanmougin, F., and Higgins, D. G. (1997) *Nucleic Acids Res.* **24**, 4876-4882
 21. Wang, J., and Giacomini, K. M. (1997) *J. Biol. Chem.* **272**, 28845-28848
 22. Wang, J., and Giacomini, K. M. (1999) *J. Biol. Chem.* **274**, 2298-2302
 23. Pajor, A. M., and Wright, E. M. (1992) *J. Biol. Chem.* **267**, 3557-3560
 24. Liman, E. R., Tytgat, J., and Hess, P. (1992) *Neuron* **9**, 861-871
 25. Graham, K. A., Leithoff, J., Coe, I. R., Mowles, D., Mackey, J. R., Young, J. D., and Cass, C. E. (2000) *Nucleosides Nucleotides Nucleic Acids* **19**, 415-434
 26. Boleti, H., Coe, I. R., Baldwin, S. A., Young, J. D., and Cass, C. E. (1997) *Neuropharmacology* **38**, 1167-1179
 27. Pink, L., Seeger, W., Ermert, L., Hanze, J., Stahl, U., Grimmlinger, F., Kummer, W., Bohle, R. M. (1998) *Nat. Med.* **4**, 1329-1333
 28. Roy, L., Sorokine-Durrin, I., and Voisin, P. (1996) *Int. J. Radiat. Biol.* **70**, 665-669
 29. Plass, C., Weichenhan, D., Catanese, J., Costello, J. F., Yu, F., Yu, L., Smiraglia, D., Cavenee, W. K., Caligiuri, M. A., deJong, P., and Held, W. A. (1997) *DNA Res.* **4**, 253-255
 30. Wu, X., Yuan, G., Breit, C. M., Hui, A. C., and Giacomini, K. M. (1992) *J. Biol. Chem.* **267**, 8813-8818
 31. Hong, M., Schlichter, L. and Bendayan, R. (2000) *J. Pharmacol. Exp. Ther.* **292**, 366-374
 32. Huang, Q. Q., Harvey, C. M., Paterson, A. R. P., Cass, C. E., and Young, J. D. (1993) *J. Biol. Chem.* **268**, 20613-20619
 33. Fang, X., Parkinson, F. E., Mowles, D. A., Young, J. D., and Cass, C. E. (1996) *Biochem. J.* **317**, 457-465
 34. Planagan, S. A., and Meckling-Gill, K. A. (1997) *J. Biol. Chem.* **272**, 18026-18032
 35. Paterson, A. R. P., Gati, W. P., Vijayalakshmi, D., Cass, C. E., Mant, M. J., Young, J. D., and Belch, A. R. (1993) *Proc. Am. Assoc. Cancer Res.* **34**, A84
 36. Kanai, Y., Lee, W. S., You, G., Brown, D., and Hediger, M. A. (1994) *J. Clin. Invest.* **93**, 397-404
 37. Chen, X. Z., Coady, M. J., Jackson, F., Berteloot, A., and Lapointe, J. Y. (1995) *Biophys. J.* **69**, 2405-2414
 38. Mackenzie, B., Loo, D. D. F., Panayotova-Heiermann, M., and Wright, E. M. *J. Biol. Chem.* **271**, 32678-32683
 39. Mackenzie, B., Loo, D. D., and Wright, E. M. (1998) *J. Membr. Biol.* **162**, 101-106
 40. Chen, X. Z., Zhu, T., Smith, D. E., and Hediger, M. A. (1999) *J. Biol. Chem.* **274**, 2773-2779
 41. Chen, X. Z., Shayakul, C., Berger, U. V., Tian, W., and Hediger, M. (1998) *J. Biol. Chem.* **273**, 20972-20981
 42. Yao, S. Y. M., Cass, C. E., and Young, J. D. (1996) *Mol. Pharmacol.* **50**, 388-393
 43. Mackey, J. R., Yao, S. Y. M., Smith, K. M., Karpinski, E., Baldwin, S. A., Cass, C. E., and Young, J. D. (1999) *J. Natl. Cancer Inst. U. S. A.* **91**, 1876-1881
 44. Mackey, J. R., Mani, R. S., Selner, M., Molwes, D., Young, J. D., Belt, J. A., Crawford, C. R., and Cass, C. E. (1998) *Cancer Res.* **58**, 4349-4357
 45. Belt, J. A., Harper, E., and Byl, J. (1992) *Proc. Am. Assoc. Cancer Res.* **33**, 20
 46. Belt, J. A., Marina, N. M., Phelps, D. A., and Crawford, C. R. (1993) *Adv. Enzyme Regul.* **33**, 235-252
 47. Anderson, C. M., Xiong, W., Young, J. D., Cass, C. E., and Young, J. D. (1996) *Mol. Brain Res.* **42**, 358-361
 48. Rovera, G., Santoli, D., and Damsky, C. (1979) *Proc. Natl. Acad. Sci. U. S. A.* **76**, 2779-2783
 49. Lotem, J., and Sachs, L. (1976) *Proc. Natl. Acad. Sci. U. S. A.* **76**, 5158-5162
 50. Lee, C. W., Sokoloski, J. A., Sartorelli, A. C., and Handschumacher, R. E. (1991) *Biochem. J.* **274**, 85-90
 51. Lee, C. W., Sokoloski, J. A., Sartorelli, A. C., and Handschumacher, R. E. (1994) *In Vivo* **8**, 795-801
 52. Deutsch, P. J. (1988) *Proc. Natl. Acad. Sci. U. S. A.* **85**, 7922-7926
 53. Felsenstein, J. (1989) *Cladistics* **5**, 164-166